

1 **Development of a multi-disciplinary**
2 **toolkit to study time cells in the**
3 **hippocampus**

5 A Thesis

6

7

8 Submitted to the
9 Tata Institute of Fundamental Research,
10 Mumbai

11 for the degree of Doctor of Philosophy
12 in Biology

13

14 by
15 Kambadur Gundu Ananthamurthy

16

17

18 Tata Institute of Fundamental Research
19 Mumbai
20 July, 2023

21

22

DECLARATION

23

24 This thesis is a presentation of my original research work.
25 Wherever contributions of others are involved, every effort is
26 made to indicate this clearly, with due reference to the
27 literature, and acknowledgment of collaborative research and
28 discussions.

29

30 The work was done under the guidance of Professor Upinder
31 S. Bhalla, at the Tata Institute of Fundamental Research,
32 Mumbai.

33



Kambadur Gundu Ananthamurthy

35

36 In my capacity as supervisor of the candidate's thesis, I certify
37 that the above statements are true to the best of my
38 knowledge.

39



Prof. Upinder S. Bhalla

41 Date: 28th July, 2023

42 Acknowledgments

43

44 Projects like the ones described in this thesis cannot be accomplished
45 without good, strong leadership. I thank Upi for the opportunity to learn
46 and grow in his lab, and his patience to see me through tough
47 moments.

48 I thank Shona and Mukund for advice and help over the past decade.
49 I thank my seniors Mehrab, Ashesh, Partha, and Subha. I hope I can
50 make them proud, someday.

51 I thank my colleagues Sahil, Dilawar, Oliver, and Aditya for helping me
52 whenever I asked.

53 I thank Sriram, Manoj, Krishna, and Amit for everything I learnt in CIFF.
54 I thank Mohini, Mugdha, Sebastien, Arnab, and Terence, for being my
55 friends for as long as they could.

56 I thank Supriya, Harini, Anupratap, Sohail, and Prabahan, my well-
57 wishers from Shona lab.

58 I thank KS Krishnan for help and advice, in the early days of the
59 programme. His absence cannot be filled with anything else.

60 I thank Sanjay, Axel, Panic, Vatsala, Uma, Madan, and Jitu, for always
61 bringing a breath of inspiration to my life and my work.

62 I thank Dr. Shane Heiney for showing me the way with trace eye-blink
63 conditioning, and Dr. Daniel Dombeck for the chronic hippocampus
64 preparation.

65 I'm indebted to the Animal Care and Resource Center (ACRC), the
66 Central Imaging and Flow Facility (CIFF), Dorababu & the Electronics
67 Workshop, Devakumar & the Mechanical Workshop, for anything and
68 everything I have been able to make or create.

69 I thank Swarna and Nikhila for teaching me Tennis. I also thank the
70 Football group, the Badminton group, the Music group, the Theater
71 group, and the Improv group, for always giving me a chance to
72 explore.

73 I thank Neha Panwar for being there in the end.

74 "Very little" is what I'd have achieved without my parents. I hope to be
75 a good person and live up to the values they have taught me.
76 I thank the canteen, the sports facility and gym, hospitality,
77 instrumentation, and admin, for helping me with everything else.

78

for Archana && Bujju,

Index of Tables

79	Table 1: Summary table of behaviour protocols attempted and essential results.....	108
82	Table 2: Recipe for ready-to-use cortex buffer. The buffer is typically prepared and stored in aliquots to be used each week. The correct pH range of the buffer was often a crucial factor ensuring the success of the hippocampal preparation.....	118

Table of Figures

87	Figure 1: A schematic representation of the Trisynaptic Pathway as observed with coronal slices, along the longitudinal axis of the hippocampus. Image adapted from the webpage for the Neural Circuits and Memory Lab, University of Wisconsin (Milwaukee) [https://sites.lsa.umich.edu/diba-lab/neural-circuits-of-the-hippocampus/]	33
93	Figure 2: Water delivery calibration to reward the animal consistently with the same volume of water.....	74
95	Figure 3: Optoisolator circuit to amplify +5V DC input to +12V DC output	76
97	Figure 4: Lick detector circuit based on a MOSFET design. Whenever the animal performed a lick, a +5V DC Output would be read out.....	77
99	Figure 5: Typical trial structure with the various phases. Each trial was followed by a randomized Inter-Trial Interval (ITI).....	79
101	Figure 6: Performance evaluation for two example mice trained to Protocol 1.1 and 1.2. Percentage of total licks in the various trial phases (Pre-Tone, Tone, CT, and ITI), across all sessions of training (coloured bar plots) for A) Mouse 3, and B) Mouse	80
105	Figure 7: Performance evaluation for two example mice trained to Protocol 2. Percentage of total licks in the various trial phases (Pre-Tone, Tone, CT, and ITI), across all sessions of training (coloured bar plots), for (A) Mouse S1, and (B) Mouse S2	85
109	Figure 8: Schematic representation of the experimental setup for a simple detection task where the animal must perform a lick upon correctly detecting the presence of the conditioned stimulus (CS; from a range of modalities).....	88
113	Figure 9: Typical trial structure with the various phases and lick dependent relationships.....	89
115	Figure 10: (A) Performance traces for all the animals individually shown in dashed grey lines. Mean + SEM in black. (B) Mean Performance (%) and Mean Go Tone Lick Percentage (%) with Session for the Go/No-Go Task, plotted in black and green,	

119	respectively.	90
120	Figure 11: The number of licks in the pre-tone (blue), no-go tone (red),	
121	and go tone (green) phases, in a representative animal, in a session	
122	with maximum Performance (%).	91
123	Figure 12: Schematic representation to showcase the two main	
124	subtypes of Classical Conditioning (Eye-Blink Conditioning, for our	
125	experiments) based on the relative timing and presentation of the CS	
126	and US.	94
127	Figure 13: Trial-by-trial (left) and trial-averaged running speed (right)	
128	for two example animals, (A) M2 Session 12, and (B) M5 Session 12.	
129	97
130	Figure 14: Schematic representation of (A) the behaviour rig with 2-	
131	Photon imaging, to train head-fixed mice on a Trace Eye-Blink	
132	Conditioning (TEC) task, and (B) relative time intervals between the	
133	CS and US.	99
134	Figure 15: A picture of a head-fixed mouse clamped on the behaviour	
135	rig, with key components: 1) Red LED Illumination, 2) Blue LED CS, 3)	
136	Air-puff port directed to the left eye, and 4) Height-adjustable Treadmill.	
137	100
138	Figure 16: Steps from behaviour video frame to Fraction of Eye-	
139	Closed (FEC) analysis	101
140	Figure 17: Conditioned Responses (CRs) are small amplitude eye-	
141	blinks triggered by the CS, and develop with multiple training sessions,	
142	while Unconditioned Responses (URs) are large eye-blanks to the US,	
143	typically consistent across sessions. (A,B) Trial-by-trial FEC traces for	
144	M11 (A) Session 2, and (B) Session 4. (C,D) Trial-averaged FEC	
145	traces for M11 (C) Session 2, and (D) Session 4, with paired (red) and	
146	probe (green) trials.	103
147	Figure 18: Performance in terms of the percentage of Hit Trials to total	
148	trials across sessions, including an ISI switch from 250 ms to 350 ms.	
149	Here, M2 is a strong learner (>60% hit trials/session) and M5 is a weak	
150	learner (30-60 % hit trials/session). M1, M3, and M4 did not learn the	
151	task.....	104
152	Figure 19: Conditioned Responses (CRs) are preserved for previously	
153	learnt ISIs, and switching the ISI to longer intervals results in Complex	
154	(multi-CR) eye-blink responses. (A,B) Trial-by-trial FEC scores for (A)	
155	250 ms ISI (left) and (B) 500 ms ISI. (C,D) Trial-averaged FEC traces	
156	for (C) 250 ms ISI, and (D) 500 ms ISI, with paired (red) and probe	
157	(green) trials.	105
158	Figure 20: Conditioned Response (CR) onset timing is maintained	
159	across ISI switches. Representative examples from a short ISI switch	
160	from (A) 250 ms to (B) 350 ms (right).	106
161	Figure 21: Bar plots for Conditioned Response (CR) onset across	

162	multiple sessions of training after ISI switch from 250 ms to 350 ms,	
163	irrespective of how strongly the animals learnt the task. (A) red, strong	
164	learner, and (B) blue, weak learner.....	106
165	Figure 22: Representative example of mice trained to 550 ms ISI	
166	(Session 6) and 750 ms (Session 4). (A,B) Trial-by-trial FEC responses	
167	for (A) 550 ms ISI (M17 Session 6), and (B) 750 ms ISI (M22 Session	
168	4). (C,D) Trial-averaged FEC responses for (C) 550 ms ISI (M17	
169	Session 6), and (D) 750 ms ISI (M22 Session 4), with paired (red) and	
170	probe trials (green).	107
171	Figure 23: (A) A schematic of the rodent brain, showcasing the two	
172	hippocampi, one in each hemisphere. The hippocampi lie ~1 mm	
173	(mice) below the cortical surface. (B) The hippocampal preparation	
174	allows optical access to the deep lying hippocampal CA1 cells, relative	
175	to the skull/cortex. The CA1 cell bodies arrange in a laminar fashion as	
176	a tight cell body layer that can be visualized by fluorescence (using	
177	either OGB-1 or GCaMP).	115
178	Figure 24: Figure 24: Schematic representation for stereotaxic viral	
179	injection.	121
180	Figure 25: (A) Representative Two-Photon Calcium Image of a plane	
181	of Hippocampal CA1 cells, bolus loaded with Oregon Green Bapta-1	
182	(OGB-1), at an instant in time. Example cells marked out post-hoc as	
183	pink, green, blue and red. Scale bar 20 μ m. (B) Representative dF/F	
184	(%) traces for the calcium activity. Recorded in a single 10s video for	
185	example cells – pink, green, blue, and red. Scale bar 1 sec; 10% dF/F.	
186	123
187	Figure 26: Tissue Degradation over time. Representative Two-Photon	
188	Calcium images of a snapshot in time of the Hippocampal CA1 cell	
189	body layer on (A) Day 1 after the surgery and (B) Day 3, after the	
190	surgery. Scale bar 30 μ m.	125
191	Figure 27: Chronic calcium imaging of the same Hippocampal CA1	
192	cells over weeks. Representative 2-Photon images from (A) Day 20,	
193	and (B) Day 21, after surgery. Landmarks have been marked and were	
194	used to confirm frame registration and identify cells. Scale bar 100 μ m.	
195	126
196	Figure 28: (A) Representative Two-Photon Calcium Image of a plane	
197	of Hippocampal CA1 cells expressing GCaMP6f at an instant in time.	
198	Example cells marked out post-hoc in pink, blue, and green, with no-	
199	cell background in red. Scale bar 20 μ m. (B) Representative dF/F (%)	
200	traces for the calcium activity recorded in a single 10s video for	
201	example cells – pink, blue, and green, with no-cell background in red.	
202	Scale bar 2 sec; 10% dF/F.	127
203	Figure 29: (A) Correlation Coefficients for cell pairs from an example	
204	two-photon recording. (B) Meta-K Means clustering with cell pairs	

205	using the heuristic that within group pairs would be more similar than	
206	between group pairs. In this example, the cells were clustered into two	
207	groups, I (red) and II (yellow). (C) Two-Photon image of the field of	
208	view of cells; same as Figure 25A. (D) Spatial organization of	
209	correlated cell pair groups during spontaneous activity (Modi et al.,	
210	2014).	129
211	Figure 30: (A) Trial-averaged (25 trials) calcium activity from ~100	
212	CA1 cells in trials where a 5000 Hz tone was presented (red bar). (B)	
213	Trial-averaged (18 trials) calcium activity from the same cells in trials	
214	where a 5 LPM air-puff to the ipsilateral whiskers was presented (red	
215	bar). Scale bar 1 sec (black bar).	130
216	Figure 31: (A) Correlation Coefficients for cell pairs from post whisker-	
217	puff stimulation periods. (B) Meta-K Means clustering with cell pairs	
218	using the heuristic that within group pairs would be more similar than	
219	between group pairs. In this example, the cells were clustered into	
220	three groups I (red), II (orange), and III (yellow). (D) No clear spatial	
221	organization of correlated cell pair groups post whisker stimulation.	131
222	Figure 32: (A) Correlation Coefficients for cell pairs from a trial-shuffle	
223	control dataset (B) Meta-K Means clustering revealed that there were	
224	no cell pair groups identified.	132
225	Figure 33: Example Time Cells visualized as event raster plots (A, B,	
226	C), along with the trial-summed activity profiles (D, E, F) suggesting	
227	~50% hit trials, for cells 29 and 72 from Session 1 (session type 5) with	
228	mouse M26, and slightly lower reliability (~25% hit trials) from cell 105.	
229	The Conditioned Stimulus (CS; blue LED) is presented at time 0 ms.	
230	136
231	Figure 34: Example Other Cells visualized as event raster plots (A, B,	
232	C), along with the trial-summed activity profiles (D, E, F) for cells 10,	
233	25, and 120 from Session 1 (session type 5) with mouse M26. The	
234	Conditioned Stimulus (CS; blue LED) is presented at time 0 ms.....	137
235	Figure 35: Event Time Histograms or tuning curves for Identified Time-	
236	Locked Cells with trial-summed peaks in session 4 of training (session	
237	type 5) with mouse M26. (A) Unsorted list of Time cells. (B) Peak-	
238	sorted list of the same cells. Here, 1 bin = 3 frames = ~210 ms	
239	(sampling rate 14.5 Hz without binning; ~5 Hz with binning). As per the	
240	(legacy) session type 5 protocol, the CS (50 ms Blue LED flash) was	
241	presented in frame bin 39, followed by a stimulus-free trace interval	
242	during frame bins 40 and 41, and then the US (50 ms airpuff to	
243	ipsilateral eye) was presented in frame bin 42.....	138
244	Figure 36: Temporal Information (bits) vs Sorted time cell number from	
245	the analytically identified Time Cells in Session 4 (session type 5) with	
246	mouse M26. No clear trend was observed.....	139
247	Figure 37: More time cells observed to attain tuning as training	

248	sessions. Event Time Histograms of the identified set of time cells	
249	between A) Sessions 1 and (B) Session 2, with mouse M26 (session	
250	type 5).	141
251	Figure 38: Sorted Time Cells form Sequences that develop with	
252	learning. Trial-Averaged calcium activity traces for all recorded cells	
253	across A) Session 1, B) Session 2, and C) Session 4, with mouse M26	
254	(sessiontype 5). Time 0 ms was aligned to the CS. The CS + Trace +	
255	US interval lasted from 0-600 ms, here.....	142
256	Figure 39: Same/similar tuning across session 1 and session 2 for this	
257	example time cell. Blue Event Time Histograms represent the tuning	
258	curve for the cell for session 1 (date: 20180508) and Red represent the	
259	same but for session 2 (date: 20180509). Pearson's correlation	
260	coefficient between the two session pairs was 0.7011.	143
261	Figure 40: Three example chronically tracked cell pairs with tuning	
262	peaks arriving earlier with training sessions (rows). Blue Event Time	
263	Histograms represent the tuning curve for any cell for session 1 (date:	
264	20180508) and Red represent the same but for session 2 (date:	
265	20180509). Pearson's correlation coefficient between the session pairs	
266	was 0.6.348, 0.5872 and 0.7027 for A) cell pair 1, B) cell pair 2, and C)	
267	cell pair3, respectively.	144
268	Figure 41: Example chronically tracked cell pair with de-tuning	
269	between session 1 and 4. Blue Event Time Histograms represent the	
270	tuning curve for the example cell for session 1 (date: 20180508) and	
271	Red represent the same but for session 4 (date: 20180514). Pearson's	
272	correlation coefficient between the two curves was -0.0606.	145
273	Figure 42: Comparing chronically tracked time cells across sessions	
274	for all matched cell pairs by (A) Correlation Analysis, and (B) Timing of	
275	peaks.....	146

276 **Table of Contents**

277	DECLARATION	2
278	Acknowledgments	3
279	Index of Tables	6
280	Table of Figures	6
281	Table of Contents	10
282	Abstract	13
283	Chapter 1 – Introduction	15
284	Projects and overall goals	15

285	A toolkit to study time cells: Thesis Objectives	16
286	Engrams associated with Learning and Memory	18
287	Dynamics in the neural code for engrams	20
288	Theories on the function of the hippocampus.....	24
289	A brief introduction to associative learning	29
290	Space and time in the hippocampus	32
291	“Single-cell, multi-trial” vs. “multi-cell, single-trial” approaches in Neuroscience	38
293	Dimensionality reduction in the analysis of physiology.....	41
294	Synthetic benchmarks for pre-hoc development of analytical procedures	42
295	Single-Unit Electrophysiology vs 2-Photon Calcium Imaging to study the	
296	Hippocampus	45
297	Calcium imaging by 2-Photon Microscopy	47
298	Automated ROI detection for large-scale Calcium Imaging datasets	51
299	Short Summaries of the 3 projects.....	51
300	Project I - How do sensory representations transform with learning?.....	51
301	Project II - How does the timing of cellular activity adjust to behavioural task variables?	
302	53
303	Project III - What is the best way to detect and score time-tuned cellular activity?	54
304	Code Availability	56
305	Bibliography	56
306	Chapter 2 – Behaviour.....	70
307	Towards understanding brain activity in a reproducible context.....	70
308	Operant conditioning [Project I]	72
309	Required features	72
310	Water delivery and calibration	74
311	Opto-isolator circuit for solenoid control	75
312	Lick detection circuit.....	76
313	Controlling task details and protocol information.....	77
314	Head-bar implant, Animal Handling, and Water deprivation	78
315	PROTOCOL 1.1: Stimulus Detection Task.....	78
316	PROTOCOL 1.2: Stimulus Detection Task with aversive punishment	79
317	Results – Protocols 1.1 and 1.2.....	81
318	Protocol 2: Stimulus Detection task with timeout box	81
319	Results – Protocol 2	83
320	Protocol 3: Delayed Non-Match to Sample (DNMS).....	86
321	Results – Protocol 3	87
322	Protocol 4: Go/No-Go Task	87
323	Results – Protocol 4	89

324	Operant conditioning experiments failed to match behavioural requirements.....	92
325	Trace Eye-Blink Conditioning [Project II]	93
326	Tracking eye-blink responses.....	95
327	Treadmill and tracking running speed	96
328	Behaviour rig and protocol control - Software	98
329	Analysis - TEC	101
330	Results - TEC.....	102
331	Bibliography	109
332	Chapter 3 – Imaging.....	111
333	Physiology in the hippocampus	112
334	Methodology – Acute and chronic imaging [Projects I & II]	114
335	Preparation of Cortex Buffer	116
336	Oregon Green Bapta-1 injections for acute imaging.....	118
337	GCaMP and chronic imaging	120
338	Results - Imaging	122
339	2-Photon calcium imaging of hippocampal CA1, <i>in vivo</i>	122
340	Acute Imaging of OGB-1 loaded hippocampal CA1, <i>in vivo</i>	122
341	Chronic imaging of hippocampal CA1 using GCaMP.....	124
342	Spontaneous activity during non-stimulus periods	127
343	Spatial organization of activity correlated cells during spontaneous activity.....	128
344	Stimulus evoked responses	129
345	Spatial organization of activity correlated cells post whisker-puff stimulation.....	131
346	Chronic imaging now possible for weeks with the same mouse	133
347	Preliminary analysis to identify time cells	134
348	Tuning, re-tuning, and de-tuning of time cells across sessions	140
349	Bibliography	148
350	Chapter 4 – Analysis.....	152
351	Chapter 5 – Discussion	159
352	The study of hippocampal CA1 sequences	159
353	Standardizing combined behaviour and recording experiments.....	162
354	Mapping sequences to abstract variables	163
355	Better temporal resolution requires new techniques.....	165
356	Does the brain create or predict?	166
357	Bibliography	168
358	All Bibliography	171

359 **Abstract**

360

361 The mammalian Hippocampus is considered important for the
362 formation of several kinds of memory, one of which is the association
363 between stimuli occurring separately in time. Several studies have
364 shown that small populations of Hippocampal CA1 cells fire in time-
365 locked sequences, "bridging" the time gap in temporal tasks (B. Kraus
366 et al., 2013; MacDonald et al., 2011, 2013; Pastalkova et al., 2008),
367 including a single-session version of Trace Eye-Blink Conditioning or
368 TEC (Modi et al., 2014). Such cells are commonly termed time cells
369 (Eichenbaum, 2017; MacDonald et al., 2011).

370 The main goal of the Thesis was to be able to study time cells under a
371 variety of behavioural tasks and conditions and elucidate several
372 physiological properties. We standardised a multi-day Trace Eye-Blink
373 Conditioning (TEC) protocol to train head-fixed C57Bl6 mice (Siegel et
374 al., 2015). TEC involves an association between a previously neutral
375 Conditioned Stimulus (CS) with an eye-blink inducing Unconditioned
376 Stimulus (US), across an intervening, stimulus-free, Trace Interval. We
377 were able to observe stable, adaptive learning with our protocol. We
378 also standardized an *in vivo* imaging preparation to record calcium
379 activity from Hippocampal CA1 cells, adapted from previously
380 published methods (Dombeck et al., 2010; Modi et al., 2014). We used
381 a custom-built two photon laser-scanning microscope and performed
382 galvo-scans through the imaging window, during TEC acquisition. The
383 behaviour and imaging was conducted simultaneously to record
384 calcium activity as the animal learnt the task. Chronic Calcium Imaging
385 allowed us to track and record the activity of the same cells, confirmed
386 morphologically. We could then identify time cells across sessions, and

387 look for adaptations in tuning curves, along multiple sessions.
388 Furthermore, numerous approaches have been developed to analyse
389 time cells and neuronal activity sequences, but it is not clear if their
390 classifications match, nor how sensitive they are to various sources of
391 data variability. We provide two main contributions to address this: A
392 resource of synthetic 2-photon calcium activity data, and a survey of
393 several methods for analyzing time cell data using our synthetic data
394 as ground truth. The synthetic dataset and its generation code are
395 useful for profiling future methods, testing analysis tool-chains, and as
396 input to computational and experimental models of sequence
397 detection. We characterized strengths and weaknesses of several
398 time-cell analysis methods. Finally, we benchmark how computational
399 requirements scale with large datasets typical of recent recording
400 technologies.

401

402 Chapter 1 – Introduction

403

404 The vertebrate Central Nervous System (CNS), consisting primarily of
405 the central ganglia (brain) and the spinal cord, samples and receives
406 information from the external world offering top-down control over the
407 activity of all parts of the body. Functions like exploration, food
408 acquisition, and danger aversion, all involve complex coordination
409 between,

- 410 ● the Sensory Systems (that integrate information from the
411 environment),
412 ● the Memory Systems (that integrate sensory information with
413 prior experience), and
414 ● the Motor Systems (that integrate motor plans and execute
415 movement).

416

417 Projects and overall goals

418

419 The overall focus of the work and experiments described in this Thesis
420 was to study Memory Systems, specifically, in terms of,

421

422 **Project I:** How do sensory representations transform with
423 learning?

424

425 **Project II:** How does the timing of cellular activity adjust to
426 behavioural task variables?

427

428 **Project III:** What is the best way to detect and score time-tuned
429 cellular activity?

430

431 Narrowing down, we as a lab were interested in the mammalian
432 hippocampus, a brain structure which is important for consolidating
433 information (from Sensory and other Memory Systems) to enable
434 certain kinds of short-term memory and the translation of short-term
435 memory to long-term.

436

437 **A toolkit to study time cells: Thesis 438 Objectives**

439

440 Ramón y Cajal, one of the pioneers of neuroscience around 1900,
441 utilized Camillo Golgi's staining method to conclusively describe
442 neurons in the brain as independent functional units connected to each
443 other in intricate networks made up of many nodes ($\sim 10^6 - 10^9$). These
444 neurons have since been described not just anatomically, but also on
445 the basis of genetics, development, and neurophysiology.

446

447 In the sub-discipline of Learning and Memory an often studied neuron
448 type is the pyramidal neuron, an example of which is the hippocampal
449 CA1 pyramidal neuron. **It has been an important goal to study memory**
450 **and the neural code in terms of finer temporal order, viz., behavioural**
451 **time scales (~ms to s).** Combining

- 452 • stable, adaptable trace eye-blink conditioning behaviour, and,
453 • cellular resolution 2-photon calcium imaging of hippocampal
454 CA1, *in vivo*,
455 • with the goal to study time cell physiology,

456 was the core objective of the toolkit and the thesis as a whole.
457
458 Development in circuit manipulation tools using light-mediated
459 activation or suppression of neuronal excitability (Luo et al., 2018),
460 afford experimenters the ability to control circuits at ms time scales.
461 Concomitant progress in effective physiological models of network
462 activity during bouts of recall of the learnt behavioural trace require
463 standardized behaviour and recording. For us, this mandated the
464 design of a relatively low-cost, end-to-end configurable, combined
465 behavioural and recording technology, to reliably study the neural code
466 at the ms time scale, *in vivo*.
467
468 This thesis describes a toolkit of techniques ranging in a wide, multi-
469 disciplinary scope, assembled with standardized hardware and
470 software routines studying animal behaviour, network neurophysiology,
471 and statistical analyses. The aim of the toolkit was to support the
472 experimental ability to study the hippocampal CA1 pyramidal neuron
473 network, under strictly controlled behavioural contexts designed to train
474 experimental mice on temporal or episodic memory tasks. Specifically,
475 these tasks such as trace eye-blink conditioning (TEC) have previously
476 been described to elicit hippocampal CA1 sequences (B. Kraus et al.,
477 2013; B. J. Kraus et al., 2015; MacDonald et al., 2011, 2013; Modi et
478 al., 2014; Pastalkova et al., 2008). This spatiotemporal network activity
479 sequence is dynamic and built from individual hippocampal CA1
480 pyramidal neurons showcasing time tuned activity through spiking.
481 These cells are called time cells (Eichenbaum, 2017; MacDonald et al.,
482 2011).
483

484 More generally, sequential activity is hypothesized to be involved even
485 in the retrieval of evidence from memory, during more complex
486 behavioural decisions that are not directly informed by the sequences
487 of stimuli presented (see Shadlen & Shohamy, 2016 for review). It is
488 still uncertain if sequential activity comprehensively describes the
489 dynamic, physiological substrate of the neural code for memory and
490 learning, *i.e.* – the engram, at behavioural time scales, or that other
491 mechanisms may also be applicable, depending on the requirements
492 of the task. We now discuss engrams and the temporal limitations of
493 identifying engram cells using activity based molecular techniques.

494 **Engrams associated with Learning and**
495 **Memory**

496

497 The term "engram" (coined by Richard Semon) refers to the physical
498 substrate of memory in the organism, used for storing and recalling
499 memories (Josselyn & Tonegawa, 2020). Donald Hebb's theory of
500 Hebbian Plasticity (Hebb, 1949) postulated that memory formation was
501 correlated to modulations in synaptic strength and connectivity. The
502 theory critically emphasized that the pair of neurons connected through
503 the synapse undergoing plasticity to strengthen efficacy, required the
504 spiking activity of both neurons. In subsequent decades, research into
505 the idea led to the theory of spike-timing-dependent plasticity
506 (Caporale & Dan, 2008), a mechanism of synaptic plasticity based on
507 the relative timing of activity of the neurons. It is still a matter of debate
508 whether the biophysical manifestation of the engram is the synapse,
509 the activity of the neurons, biophysical or chemical processes, but it is

510 likely that the engram is distributed across several computational
511 scales in the brain.

512

513 An important first step in early neuroscience research attempted to
514 identify specific functions for specific brain regions. Experimenters
515 would train a variety of model systems to specific behavioural tasks
516 and attempt to delineate specific brain regions crucial (or not) to the
517 task using targeted lesion or ablation studies (see Vaidya et al., 2019
518 for review).

519

520 Eric Kandel's experiments with the Aplysia sensory neurons studied gill
521 withdrawal - an aversive but stable, adaptive behaviour (Carew et al.,
522 1971). The reliability of this learned response allowed the experiments
523 to include crucial electrophysiological and neurochemical circuit
524 dissections that ultimately lead to the discovery of the entire neural
525 circuit orchestrating the task, even to the level of cellular signaling.
526 This led to decades of research focused on the plasticity of synapses
527 across nervous systems in the animal kingdom.

528

529 With the development of more sophisticated recording and molecular
530 techniques, further details on mechanism within specific brain regions
531 and circuits could be described. Specifically, technological
532 advancements in molecular neuroscience led to the development of a
533 number of fluorescent sensors, conditional tagging, activators and
534 inhibitors that allowed cellular resolution tracing of the engram (Luo et
535 al., 2018).

536

537 Experiments by Sheena Josselyn, Alcino Silva, and colleagues led to
538 the discovery that the intrinsic excitability of a pyramidal neuron in any

539 network positively biased the probability of recruitment to the engram
540 (Han et al., 2009; Rogerson et al., 2014; Silva et al., 2009; Yiu et al.,
541 2014; Y. Zhou et al., 2009), *viz.*, the tagged set of cells were active
542 when memory was learnt and recalled. The engram seemed to be
543 described in terms of the cellular sub-population involved but the
544 experiment could only identify the same over a relatively longer
545 window of time (~mins.). This could lead to only a static list of cells
546 which may even have included False Positives (Type I error).
547 Importantly, any dynamics in the spatiotemporal patterns of activity of
548 the pyramidal neurons were not amenable to study at shorter
549 timescales (~ms.). On the other hand, physiological recordings could
550 describe these dynamics at short timescales, but were rarely translated
551 to chronic measurements of the activity of the same cells across days
552 and sessions, given technical limitations at the time.

553 **Dynamics in the neural code for engrams**

554
555 We first discuss some important results that help motivate the study of
556 physiological recordings in the context of engrams, *i.e.*, the dynamical
557 nature of the neural code (~ms to s). In later sections we will describe
558 these dynamics in more detail.

559
560 Place cells and their role in spatial navigation have been studied in
561 great detail through decades of research ever since they were first
562 described by John O'Keefe (O'Keefe & Dostrovsky, 1971). We did not
563 explicitly study place cells in this thesis but some key discoveries in
564 literature require mention, with the goal to build a case for a theory of
565 CA1 ensemble sequences (Modi et al., 2014). Briefly, place cells are

566 pyramidal neurons that showcased a higher than baseline probability
567 of firing action potentials whenever animals navigating spatial
568 environments visited specific locations. The tuning curves or firing
569 fields for these cells often map to the real spatial trajectory of the
570 animal and is thought to be an assimilation of both brain external
571 stimuli such as visual cues, as well as brain internal variables such as
572 motivation, goal orientation, memory, and experience(Ferbinteanu et
573 al., 2011; Ferbinteanu & Shapiro, 2003; Foster, 2017; Frank et al.,
574 2000; Wood et al., 2000).

575

576 As the animal enters these landmark locations in any spatial context,
577 these place cells showcase Phase Precession, firing earlier in phase to
578 cycles of Theta a network rhythm clocked at ~4-10 Hz, as the animal's
579 position changes relative to the landmark. These navigation mapped
580 place cell sequences are called Theta Sequences (Foster & Wilson,
581 2007), typically mapped to a few active neurons at a time.

582

583 In very specific contexts, these place cells express activity sequences
584 synchronized to Sharp Wave Ripples, a different network activity
585 phenomenon clocked at ~10-30 Hz, often not tied to the animal's
586 location, called Replay Sequences (Csicsvari et al., 2007; Foster &
587 Wilson, 2006). These sequences have been described to play out
588 typically in reverse temporal order to models of place cell sequences
589 describing known trajectories in space.

590

591 There is variability in the firing of place cells in any spatial context, and
592 studies have mapped specific sequences to very specific trajectory
593 goals (going towards or away from locations) with modulation by both
594 egocentric and allocentric orientations cues(Davidson et al., 2009;

595 Ferbinteanu et al., 2011; Ferbinteanu & Shapiro, 2003; Frank et al.,
596 2000; Wood et al., 2000) and movement speed based estimates of
597 distance (Kropff et al., 2015).

598

599 Place cell and time cell sequences have many similarities and
600 differences in descriptive neurophysiology, but may emerge from the
601 same memory organization principles (Buzsáki & Llinás, 2017). It is
602 argued that there is significance to the exact phrasing of the CA1
603 sequence in any given context. Furthermore, a very interesting feature
604 observed is Time-stamping, *viz.*, time dependent overlap of ensemble
605 responses to different contexts and behavioural parameters (Cai et al.,
606 2016; Mau et al., 2018).

607

608 We developed and standardized a multi-session, adaptable Trace Eye-
609 Blink Conditioning (TEC) paradigm in which head-fixed mice learn to
610 form associations between neutral and high-valence stimuli. We
611 describe associative learning in later sections as well in Chapter 2 –
612 “Behaviour”. TEC has been previously observed to elicit CA1 activity
613 sequences even in a single session of training (Modi et al., 2014). The
614 functional involvement of the hippocampus in the acquisition of
615 Conditioned Responses (CRs) has been studied and implicated by
616 studying acquisition rates to multiple trace intervals. It was found that
617 memory load, inferred in terms of task difficulty with longer trace
618 intervals (300 ms vs 500 ms), was crucial to observing an effect of
619 hippocampal lesions on the behavioural expression of CRs (Moyer et
620 al., 1990).

621

622 Several stimulus modalities have been used as the Unconditioned
623 Stimulus (US) such as periorbital air-puffs and electrical shocks (see

624 Disterhoft & Weiss, 2017 for review). Throughout all our TEC
625 experiments, we chose to use the mildly aversive air-puff to elicit the
626 Unconditioned Response (UR) to the US. Further, we use a flash of a
627 blue LED as the Conditioned Stimulus (CS), expecting to observe
628 reliable Conditioned Responses (CRs) to the CS within 3-7 days, for
629 trace intervals of ~250 ms (Siegel et al., 2015). CRs are observed as a
630 preemptive eye-blink response elicited reliably before the presentation
631 of the US – a reproducible attempt to avoid the discomfort of the
632 aversive air-puff. This is in accordance with the Rescorla-Wagner
633 model of Classical Conditioning, which assumes that association of the
634 CS and US based on repeated pairing depends on how well the
635 presence of the CS predicts the future occurrence of the US, along
636 with other variables such as the relative intensities and modalities of
637 the presented stimuli (Rescorla & Wagner, 1972). Extensions to this
638 model have suggested that there could be negative effects to the
639 associative learning when other CS (CS1, CS2, etc.) are also paired
640 together in within-compound-association tasks such as “backward
641 blocking” (Hamme & Wasserman, 1993). For our experiments we used
642 only one CS for any training session, typically a 50 ms flash of a blue
643 LED. However, our behavioural setup allows for multiple CS types,
644 e.g., CS1 = Blue LED flash and CS2 = auditory tone, to be presented
645 based on the experiment.

646

647 Transient increases in CA1 excitability post acquisition of the task were
648 described up to 4-5 days (Moyer et al., 1996) and could be important to
649 the forging of the task specific spatiotemporal sequences during
650 learning. In an *in vitro* assay, coronal sections of the hippocampus
651 (Figure 1) were stimulated at the Perforant Path to the cells of the
652 Dentate Gyrus in patterns that could be mnemonically mapped to

653 stereotypic, temporal sequences of Excitatory Postsynaptic Potentials
654 (EPSPs) read out at the hilar mossy cell layer ~400-500 ms later (Hyde
655 & Strowbridge, 2012). This suggested the presence of temporal
656 sequences even at the Dentate Granule cell layer, many synapses
657 before the hippocampal CA1.

658

659 On a longer timescale, hippocampal lesion-based experiments on mice
660 have been used to describe the role of the hippocampus to within 4
661 weeks of TEC, with deficits in Conditioned Responses (CRs) as a
662 readout of the effect of the lesion (Takehara et al., 2002). We aimed to
663 examine the processes that underlie this time-dependent role of the
664 hippocampus by chronically tracking the same cohort of hippocampal
665 CA1 cells across the sessions of TEC, at cellular resolution, using
666 galvo-scanning 2-photon calcium imaging. We were specifically
667 interested in studying the emergence and long-term activity dynamics
668 of time cells, touted to be the behavioural time scale ($\sim 10\text{-}10^3$ ms)
669 expression of the memory engram during associative learning, as
670 described in later sections. Preliminary results and additional details on
671 our TEC paradigm may be found in Chapter 2 – “Behaviour”.

672 **Theories on the function of the 673 hippocampus**

674

675 We now provide a very brief outline of the four main ideas of
676 hippocampal function studied over the past few decades. These are,
677 A) Response Inhibition - Studied mostly in the 1960's, this
678 perspective described the Hippocampus as important to the
679 ability of animals to inhibit their impulses and natural, habitual,

680 or dominant behavioral responses to stimuli, in order to select
681 more appropriate responses. This perspective was justified by
682 two observations with regard to animals with hippocampal
683 damage - 1) these animals tended to be hyperactive, and 2)
684 were unable to withhold previously learnt responses. British
685 psychologist Jeffrey Alan Gray developed this perspective to
686 link hippocampal activity with anxiety (McNaughton & Gray,
687 2000). Studies have now implicated the hippocampus in the
688 facilitation of correct responses and inhibition of incorrect
689 responses during contextual memory tasks, though not for
690 visual discrimination of contexts (Kim & Lee, 2012). Response
691 Inhibition is considered an executive function and the brain
692 circuitry involved, also includes (other than the hippocampus)
693 the prefrontal cortex, subthalamic nucleus, and caudate nucleus
694 (Diamond, 2013). Inhibitory control is typically impaired in
695 patients with drug addiction, attention deficit hyperactivity
696 disorder (ADHD), obsessive compulsive disorder (OCD), and
697 Tourette's syndrome, among many others, and is an active area
698 of research (Diamond, 2013; Nestler et al., 2015). Typical
699 neuropsychological tests used to measure inhibitory control
700 include the Stroop task, Go/No-Go task, Simon task, Flanker
701 task, anti-saccade tasks, delay of gratification tasks, and stop-
702 signal tasks (Diamond, 2013).

703

704 B) Episodic Memory – a form of declarative or explicit memory that
705 refers to the ability and mechanistic paradigms that allow for the
706 behavioural recall of a collection of past personal experiences,
707 occurring at particular places and times to the subject. The term
708 was coined by Endel Tulving in 1972 (see Clayton et al., 2007),

709 although the perspective was popularized many decades prior,
710 by the psychological studies on Patient H. M. (Henry Molaison),
711 who had been suffering from epileptic seizures and had to
712 undergo extensive hippocampectomy (surgical destruction of
713 the hippocampi), as treatment. American neurosurgeon William
714 Beecher Scoville and British-Canadian neuropsychologist
715 Brenda Milner were pioneers of this study and were able to
716 describe severe anterograde and partial retrograde amnesia in
717 the patient post surgery (Scoville & Milner, 1957). Since the late
718 2000's, the discovery and description of time cells (B. Kraus et
719 al., 2013; B. J. Kraus et al., 2015; MacDonald et al., 2011, 2013;
720 Modi et al., 2014; Pastalkova et al., 2008), has reinvigorated this
721 perspective. **Nine important, collective properties of episodic**
722 **memory distinguish it from other types of memory** (see Conway,
723 2009 for review) *viz.*, episodic memory
724 i) is a summary record of sensory-perceptual-conceptual-
725 affective processing,
726 ii) retains patterns of activation/inhibition over long periods,
727 iii) is often represented in the form of visual images,
728 iv) is perspective centered (subjective),
729 v) is a representation of short time slices of experience,
730 vi) is represented on a temporal dimension roughly in order
731 of occurrence,
732 vii) subject to rapid forgetting (extinction),
733 viii) helps make autobiographical remembering specific, and,
734 ix) is recollectively experienced when accessed.
735 The study of episodic memory and time cells forms the core of
736 this thesis, and further details, experiments, and preliminary
737 results are discussed in subsequent sections and chapters.

- 738
- 739 C) Spatial Cognition – is the ability of experimental animals to
- 740 locate and ascribe valence to points in space, during the
- 741 navigation of environments (see Hartley et al., 2014 for review).
- 742 Originally popularized by the remarkable work of American-
- 743 British neuroscientist John O’Keefe and American psychologist
- 744 Lynn Nadel, the link between hippocampal function and spatial
- 745 navigation was solidified with the discovery and subsequent
- 746 descriptions of place cells (Morris et al., 1982; O’Keefe &
- 747 Dostrovsky, 1971; O’Keefe & Recce, 1993). This perspective is
- 748 the most popular amongst the known and studied functions of
- 749 the Hippocampus and has been the subject of a large body of
- 750 work. Indeed, the Nobel Prize in Physiology or Medicine 2014
- 751 was awarded to John O’Keefe, May-Britt Moser, and Edvard I.
- 752 Moser, for “The Brain’s Navigational Place and Grid Cell
- 753 System”. Both egocentric as well as allocentric cues are
- 754 assimilated in an individual’s ability to navigate space, creating
- 755 a mental representation of the environment or cognitive map
- 756 (see “Focus on Spatial Cognition,” 2017 for review). There is
- 757 evidence that the hippocampus and striatal circuits process
- 758 different aspects of the environment, using very different
- 759 learning rules, i.e., incidental learning and associative
- 760 reinforcement, respectively (Burgess, 2008). Spatial Cognition
- 761 and place cells will be discussed to a limited extent in
- 762 subsequent sections though these topics were not explicitly
- 763 studied in the experiments for this thesis.
- 764
- 765 D) Contextual Mapping – An emerging consensus in the field is
- 766 that the hippocampus actually builds contextual maps of the

environment or perceived events, with expansions to the neural activity code along any relevant dimension of stimuli. Stimuli or events cuing any modality, e.g., spatial, temporal, frequency, etc., may be assimilated, along with more brain internal variables such as (but not limited to) motivation, expected reward status, prior experience in related tasks, and goal-orientation (task specific). Furthermore, this allows the hippocampus to make predictive models that bind new information streams to collectively update predictions (M. R. Cohen & Kohn, 2011; Eichenbaum, 2017; Miller et al., 2023; O'Keefe & Nadel, 1978). **Pattern separation and conjunctive representation of the combined multi-modal experience in the hippocampus, has been implicated in reinforcement learning** (Ballard et al., 2019). **Contextual mapping** considers the hippocampal-entorhinal circuit as a Tolman-Eichenbaum machine (TEM) with the medial entorhinal cortex (MEC) cells thought to describe important aspects of past experience and the hippocampal cells implicated in binding the current sensory experience with prior experience (Ballard et al., 2019; Eichenbaum, 2017), with the goal to develop a functional model of the subjective experience of animals and flexibly selecting appropriate responses. To complement studies on place and time cells, the mapping of auditory tone frequencies in a frequency sweep (a relatively abstract external concept) has also been reported in the hippocampus-entorhinal circuit (Aronov et al., 2017).

Episodic memory forms the central function of study for all the hippocampus related experiments described in the thesis. Trace Eye-

796 Blink Conditioning (TEC) is an example of a task used to study
797 episodic recall (Thompson, 2004). The behavioural acquisition and
798 expression of CRs correlate well with the neuronal expression of
799 spatiotemporal sequences of time cells (Modi et al., 2014). Our
800 experiments aimed to describe finer details such as how the animals
801 assign valence to the neutral Conditioned Stimulus (CS) and how time
802 cell population codes adapt to changes in the trace interval. Some
803 characteristic features of the engram at behavioural time scales, *viz.*,
804 time cell activation sequences, have been described as preliminary
805 results (Chapter 3 – “Imaging”), under the behavioural context of TEC,
806 an associative learning task.
807

808 **A brief introduction to associative learning**

809
810 The ability to physiologically record cells is insufficient without placing
811 the experimental animals in precisely defined, stable behavioural
812 contexts. Only in this way can neural activity be checked for
813 correlations or mapping to distinct changes in external behaviour
814 variables and the decisions that the animal makes, accordingly.
815 Combining behaviour and recording was considered an important
816 guiding principle in all our experiments. **Associative learning** is the
817 overall process by which animals develop behavioural valence to
818 neutral stimuli that occur in temporal conjunction to other potent,
819 behaviour eliciting stimuli. We wished to study the network level
820 responses in the hippocampus, *in vivo*, especially during early learning
821 of associated stimuli, *i.e.*, behavioural acquisition, combining stable,
822 adaptable associative learning paradigms such as Trace Eye-Blink

823 Conditioning (TEC) with cellular resolution, behaviour time scale, high-
824 yield recordings of neurophysiology.

825

826 Prior to the early 20th century, Structuralism was a dominant
827 perspective in Psychology, insisting on introspection - the observation
828 and report of one's own mind and thoughts. Experiments and
829 discoveries by Ivan Pavlov at the Military Medical Academy in
830 Petrograd (St. Petersburg), eventually led to a dramatic shift in
831 perspective, with the birth of Classical Conditioning, a type of
832 associative learning. Following the very same methodology advocated
833 by Francis Bacon (early 17th century), quantitative data from carefully
834 conducted animal experiments were recorded, with the idea to narrow
835 down on a small number of hypotheses that could explain experimental
836 observations.

837

838 Ivan Pavlov provided essential demonstrations of anticipation and
839 made tremendous progress in understanding the circumstances on
840 which anticipation depends, and this is why Classical Conditioning is
841 also often referred to as Pavlovian Conditioning. Following Pavlov's
842 studies (Pavlov, 1927), it was proposed that Classical Conditioning
843 was a prototypical example of Association. While it does have caveats
844 such as covert learning when observable behaviour may be blocked
845 (Dickinson et al., 1983; Krupa & Thompson, 2003), Associative
846 learning is rich with a variety of animals and association tasks that
847 have been crucial to study memory and learning over the past century.

848

849 Typically, animals require no prior training to elicit a behavioural or
850 motor movement to biologically potent stimulus (appetitive or aversive),
851 called an Unconditioned Stimulus (US). Examples include food, water,

852 electrical shock, temperature shock, etc.. Without pairing with a US, a
853 neutral stimulus elicits no observable response from an animal, and
854 such a stimulus is called a Conditioned Stimulus (CS). Examples
855 include simple auditory tones, flashes of light, among others.

856
857 Classical Conditioning is both the behavioural procedure as well as the
858 learning process that results from the pairing of a previously neutral
859 stimulus (CS) with a biologically potent stimulus (US). Repeated
860 pairing allows animals to make implicit associations between the CS
861 and US, and essentially anticipate the occurrence of the US, once the
862 CS is observed. Animals report this forecasting feat by producing the
863 same response that they would to a US, albeit often a milder version.

864 Typical protocols for Classical Conditioning, follow the regime of
865 Forward pairing, *viz.*, - the CS is presented before the US, and this
866 temporal structure will be followed unanimously across all behaviour
867 experiments described in this thesis.

868
869 The standardization of the behavioural task, physiological recording
870 (imaging) preparation, as well as the custom analysis routines to look
871 for various physiological features are described in this thesis.
872 Combining these multi-disciplinary approaches allowed us to develop a
873 toolkit to study time cells in the hippocampus, under strict behavioural
874 contexts. It is important to note, however, that spatiotemporal
875 sequences of activity as measured by calcium imaging based
876 simultaneous recordings of a large number of cells, are not limited to
877 the hippocampus, being studied even in the visual cortex (Pachitariu et
878 al., 2017; Poort et al., 2015), somatosensory cortex (Petersen, 2019),
879 entorhinal cortex (Heys et al., 2014), and even in the cerebellum
880 (Giovannucci et al., 2017). Essentially, the analytical methods

881 developed (Ananthamurthy & Bhalla, 2023) can easily be adapted to
882 other neuronal network recordings where time-tuning may be
883 applicable. Experimental protocols for associative learning have been
884 standardized for a variety of animals, in a variety of experimental
885 conditions. The specific issue is of developing an experimental system
886 that can run simultaneous TEC behaviour and 2-photon imaging, in
887 concert, and provide the context for time cell physiology to be studied,
888 *in vivo*. It was important to design both aspects of the experiments
889 (behaviour and imaging) since these were the most suitable conditions
890 for studies on time cells.

891 Space and time in the hippocampus

892
893 Damage to the hippocampal system has been shown to cause the
894 impairment of long-term memory or amnesia, in human patients,
895 rodents, and non-human primates. Interestingly, such damage to the
896 Hippocampus seems to have no observable effect on the capacity for
897 acquisition and expression of skilled performance. These two results
898 suggest the role of the Hippocampus in certain kinds of memory, but
899 not all.

900
901 Anatomically, the hippocampal system receives input from, and in turn,
902 projects to the neocortical brain regions that serve as the site to
903 process higher order categories and modalities of information. The
904 hippocampal circuit is anatomically >3-4 synapses away from the
905 peripheral nervous system, and information typically arrives after many
906 layers of intervening processing and computation. It is thus suggested
907 that the hippocampus holds a privileged position in the brain, receiving

908 the outcomes of the computation of the brain's various modules, and
909 relating to them (Baudry & Lynch, 1981; Ekstrom & Ranganath, 2018;
910 Moscovitch et al., 2016; Poppenk et al., 2013; Tao et al., 2021). A
911 large majority of the cortical information is sent to the Hippocampus via
912 the Entorhinal Cortex (EC). This information is processed in roughly
913 three stereotactically and molecularly separable layers of cells in the
914 following order: EC → Dentate Gyrus → CA3 → CA1. This pathway
915 from the EC to the CA1 has three separate synaptic connections
916 (across the layers) and is also known as the Trisynaptic Pathway
917 (Figure 1). The output of the CA1 is then sent to other cortical areas.
918

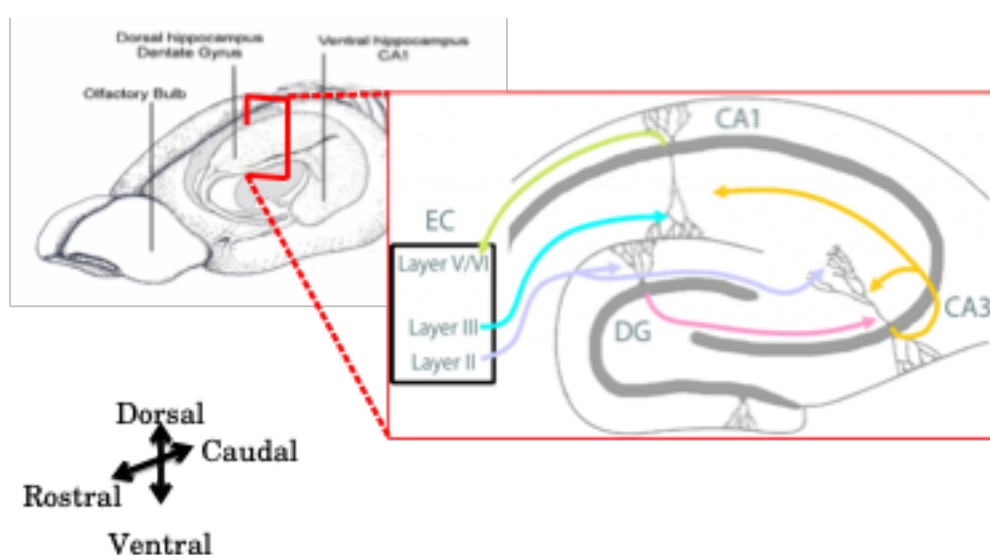


Figure 1: A schematic representation of the Trisynaptic Pathway as observed with coronal slices, along the longitudinal axis of the hippocampus. Image adapted from the webpage for the Neural Circuits and Memory Lab, University of Wisconsin (Milwaukee) [<https://sites.lsa.umich.edu/diba-lab/neural-circuits-of-the-hippocampus/>].

919 One of the most significant discoveries in the hippocampal system and
920 surrounding brain structures was the role played in spatial cognition.
921 An enormous corpus of research has conclusively described,
922 • head-direction cells: with tuning curves tied to the direction that
923 experimental animals were oriented to. These cells respond to
924 egocentric vestibular cues as well as allocentric sensory cues
925 (Ranck, 1973; Taube et al., 1990), in the dorsal presubiculum,
926 retrosplenial cortex, entorhinal cortex, thalamus, and striatum,
927 among others.
928 • grid cells: with multi-modal tuning curves at regular spatial
929 positions as a lattice, across the environment being navigated.
930 These cells assimilate information about location, distance, and
931 direction, and are typically found in the entorhinal cortex (Fyhn
932 et al., 2004; Hafting et al., 2005).
933 • boundary vector cells: with tuning curves to the edges of the
934 environment being navigated. These cells are typically found in
935 the subiculum, pre- and para-subiculum, and entorhinal cortex
936 (Bjerknes et al., 2014; Lever et al., 2009; O’Keefe & Burgess,
937 1996; Savelli et al., 2008; Solstad et al., 2008).
938 • speed cells: with modulated firing rates based on the actual
939 running or movement speed of the animals. These cells are
940 typically found in the entorhinal cortex (Kropff et al., 2015).
941 • place cells: with tuning curves to specific locations in the
942 environment (O’Keefe & Dostrovsky, 1971; O’Keefe & Recce,
943 1993). These cells may be found in several hippocampal sub-
944 layers but often studied in the CA1.
945
946 The activity of neurons in the hippocampus of awake, behaving
947 animals is modulated by significant stimuli or objects in the

948 environment as well as relationships between temporally discontiguous
949 but relevant, paired stimuli. With the discovery of place cells, it was
950 clear that the CA1 of animals navigating a spatial environment,
951 showcased location specific firing fields. With the discovery of time
952 cells, it was noted that the CA1 of animals could elicit spatiotemporal
953 sequences of activity whenever the animal was required to make a link
954 between stimuli or events, even with a stimulus-free period in between.
955 Together, these results provided an important physiological parallel
956 between the spatial learning and episode learning deficit seen with
957 damage to the Hippocampus. Curiously, both place cells and time
958 cells, as well as the sequences built up with them were non-
959 topographically mapped, *i.e.*, they may be located anywhere in the
960 hippocampus, with no obvious spatial order (Dombeck et al., 2010;
961 Modi et al., 2014)(Dombeck et al., 2010; Modi et al., 2014), in contrast
962 to results from the cortex (Dombeck et al., 2009; Ozden et al., 2008).
963
964 In an experiment published in 2008, Eva Pastalkova and colleagues
965 from Gyorgy Buzsaki's lab had rats navigate a figure 8 maze, with the
966 animal being rewarded with water, in between trials, if they managed to
967 alternate between the left and right arms (Pastalkova et al., 2008). As
968 an added nuance in the task, just before launching into the left or right
969 arms, the animal had to spend a fixed amount of time running a
970 treadmill, held in place. This would allow self-motion cues, but with the
971 absence of any other external stimuli. Impressively, single-units
972 recorded from the hippocampal CA1 cells revealed strong correlation
973 with the time spent on the treadmill, despite the absence of external
974 cues, and that different cells tuned to different time points, forming a
975 spatiotemporal sequence of activation (Pastalkova et al., 2008). In a
976 different experiment published in 2011, Christopher J. MacDonald and

977 colleagues from Howard Eichenbaum's lab had rats had to go around
978 a maze and perform a olfactory task (MacDonald et al., 2011). The
979 animals were first presented with an odour, then made to wait for a
980 delay period in a cordoned off section of the maze, before being
981 allowed to either dig for a reward or continue on the maze, depending
982 on the odour presented. As trials progressed, Hippocampal CA1 cells
983 were recorded (single-units) and found to not only be modulated by the
984 decision to be taken, but also to the amount of time spent in the delay
985 period. Experimentally, the delay period could be elongated or
986 shortened, each having an effect on remapping of the tuning fields of
987 the various CA1 cells, but to different extents (MacDonald et al., 2011).

988

989 In 2013, the Eichenbaum group published their findings with head-fixed
990 rats (no movement in space) performing a Delayed Match-To Sample
991 (DMS) task with pairs of odours, where again time tuned activity could
992 be observed with a sequence of Hippocampal CA1 cell activations, that
993 depended on the identity of the first odour (MacDonald et al., 2013). In
994 2014, Mehrab Modi, Ashesh Dhawale, and Upinder Bhalla published
995 their results with head-fixed mice learning and performing a Trace Eye-
996 Blink Conditioning (TEC), wherein it was observed that Hippocampal
997 CA1 cell activity sequences emerged in close relation to the acquisition
998 of behavioural performance, thus cementing the idea that sub-
999 populations of Hippocampal CA1 cells could bridge temporal gaps
1000 between relevant, paired stimuli, and that they did so with the activity
1001 of time-tuned cells (Modi et al., 2014).

1002

1003 Finally, it was important to study if these apparently time-tuned cells
1004 were tuned to the actual duration of time in a delay period, or whether
1005 it was more important for these cells to track the distance run. In an

1006 experiment published in 2013, Benjamin Kraus and colleagues from
1007 Howard Eichenbaum's lab again had their rats navigate a figure 8
1008 maze, but with a motorized treadmill in the central arm, to
1009 experimentally regulate the running speed. With this setup, the study
1010 was successful at delineating that both time spent running and
1011 distance run were important features, and that different cells could tune
1012 to either of the features (B. Kraus et al., 2013; B. J. Kraus et al., 2015).
1013 Whenever hippocampal CA1 cells showcased time-tuned activity (as
1014 opposed to space/location-tuned activity), such cells were dubbed
1015 "Time Cells" (Eichenbaum, 2017; MacDonald et al., 2011).
1016
1017 Other interesting physiological parallels between the CA1 place cells
1018 and time cells are,
1019 1. Phase Precession: In relation to theta oscillations (6-10 Hz)
1020 measured as local field potentials (LFP), individual cells tended
1021 to fire action potentials at progressively earlier phases with each
1022 successive cycle, described first for place cells (O'Keefe &
1023 Recce, 1993), and then also for time cells (Pastalkova et al.,
1024 2008).
1025 2. Temporal Compression: Sequences of place or time cells could
1026 be elicited at significantly shorter time scales, with fidelity in the
1027 participating cells (Dragoi & Buzsáki, 2006; Foster, 2017).
1028 Indeed, with regard to the typically studied regime of ~100-200
1029 ms or behaviour time scales, the same sequence may be
1030 elicited at ~10 ms as short segments during Sharp Wave
1031 Ripples (Dragoi et al., 1999; V. Itskov et al., 2008; Jadhav et al.,
1032 2012; O'Keefe & Recce, 1993; Valero et al., 2015) or even as
1033 the whole sequences during Replay (Csicsvari et al., 2007; Diba
1034 & Buzsáki, 2007; Foster, 2017; Foster & Wilson, 2006; Gupta et

1035 al., 2010; Pfeiffer & Foster, 2013) or Pre-play (Dragoi, 2013;
1036 Dragoi & Tonegawa, 2011).

1037 3. Remapping: Systematic changes in the experimental paradigm,
1038 such as those to the size of the experimental arena or in the
1039 time interval between stimuli or events, would result in
1040 systematic changes in the firing fields of place (Muller & Kubie,
1041 1989) and time cells (MacDonald et al., 2011).

1042 4. Variable Firing Fields: The width of the firing fields for a set of
1043 place or time cells, respectively, may be variable. However, an
1044 important distinction here is that there is as yet no clearly
1045 identified predictor of the widths for place cells to spatial
1046 directions, while time cells tuned to later time points in the inter-
1047 stimulus or delay periods usually exhibit a widening of firing
1048 fields (B. Kraus et al., 2013; B. J. Kraus et al., 2015; MacDonald
1049 et al., 2011, 2013; Mau et al., 2018; Pastalkova et al., 2008).
1050 The significance of firing field density and tuning widths is as yet
1051 an open line of inquiry.

1052

1053 Single-units recorded from the medial entorhinal cortex (MEC) as well
1054 as the hippocampal CA1 that were found tuned to specific frequency
1055 “landmarks” during frequency sweeps self-initiated by rats (Aronov et
1056 al., 2017), suggesting that the CA1 could tune to variables other than
1057 space and time. This added even more weight to “Contextual Mapping”
1058 as an important function of the hippocampus.

1059 **“Single-cell, multi-trial” vs. “multi-cell,
1060 single-trial” approaches in Neuroscience**

1061

1062 A dominant, early perspective in neurophysiology had been to record
1063 activity from a single cell, over many trials, under a variety of
1064 conditions (bath applications in slice physiology, different physiological
1065 conditions like stress and genetic background, etc.). For more than one
1066 recorded cell, the process would be repeated, till the dataset was
1067 complete.

1068

1069 An intermediate perspective was to record from multiple cells
1070 simultaneously, yet treat each cell independently for analysis towards
1071 correlation and mechanism studies, across many repeats of
1072 experimental conditions or trials (same as above).

1073

1074 An important and more modern perspective is to record from multiple
1075 cells simultaneously, and use this network or population activity to
1076 decode single-trial characteristics (position, time, stimulus presence,
1077 etc.) using very powerful numerical and mathematical algorithms
1078 involving (but not limited to) Bayesian Decoding and Information
1079 Theory. The essential idea is that the neuronal code of the brain is not
1080 defined just by the activity of single neurons since they may only
1081 encode very specific fractions of the experience, but rather that the
1082 population encodes the full experience, using a number of distributed
1083 and redundant strategies.

1084 • Bayesian Decoding: Using the activity of multiple,
1085 simultaneously recorded neurons to develop a likelihood
1086 estimate of the evidence (firing rate combinations) to the
1087 experimental parameter (spatial position, relative time, etc.)
1088 and combine this with the experimentally determined prior
1089 (probability), to obtain estimates of the conditional or

1090 posterior probability of a parameter value, given evidence.
1091 Bayes' Rule describes
1092
$$P(A|B) = P(B|A).P(A)/P(B)$$

1093 ... where,
1094 A: Parameter value (position, time, etc.)
1095 B: Evidence (cellular firing rate)
1096 $P(A)$: Prior Probability (experimentally defined)
1097 $P(B)$: Probability of evidence (Firing Rate)
1098 $P(A|B)$: Posterior probability of parameter value given
1099 evidence
1100 $P(B|A)$: Likelihood estimate of evidence given parameter
1101 value (based on recordings)
1102 This methodology has been used to not only successfully
1103 predict specific time points in a trial from population activity, but
1104 has also been used to observe that the population activity from
1105 a session of recording is able to predict time points in trials
1106 conducted on subsequent sessions of recording, up unto 3-4
1107 sessions (Mau et al., 2018).
1108 • Information Theory: Using recorded cellular activity to
1109 estimate how much information this activity carries about
1110 experimental parameters (position, time, stimuli, etc.) in a
1111 trial-by-trial fashion. Three essential metrics have been
1112 used,
1113 1. Information per activity spike (I_{spike}), in bits/spike
1114 2. Information per unit time (I_{sec}), in bits/sec
1115 3. Mutual Information (MI) between evidence and
1116 parameter value, in bits
1117 William Skaggs, Bruce McNaughton and colleagues published a
1118 series of experiments working out the value of Information Theory

1119 based approaches to deciphering the hippocampal code, reviewed
1120 previously (Skaggs et al., 1996). This idea was later adapted strongly
1121 by the field but focus throughout, remained on place cells.

1122

1123 A major step forward with “multi-cell, single-trial” approaches is the
1124 benefit of resolving how each cell and inter-cell interactions contribute
1125 to stimulus representation, behavioural task variables, and other brain-
1126 intrinsic computation. Technological advances in large-scale
1127 neurophysiology recordings such as the increased density of tetrode
1128 drives, Neuropixels, Optical sectioning and microscopy, Resonant
1129 scanning, etc., have enabled the discovery of well coordinated
1130 sequences of cellular activity such as Sharp Wave Ripples (SWRs),
1131 Replay, and behavioural timescale spatio-temporal sequences, *in vivo*,
1132 among others. This is primarily due to a radical improvement in an
1133 experimenter’s ability to simultaneously record from multiple cells
1134 (Foster, 2017), going from yields of ~10 cells to even ~10⁴ cells, per
1135 animal.

1136

1137 **Dimensionality reduction in the analysis of** 1138 **physiology**

1139

1140 Bayesian and Information theoretic approaches as well as methods
1141 like Principal Component Analysis (PCA) afford the experimenter a
1142 variety of mathematical procedures to examine dimensionality
1143 reduction, viz., the transformation of high-dimensional
1144 neurophysiological activity from recorded cells into low-dimensional
1145 representations that still retain meaningful properties of the original
1146 data (Pudil & Novovičová, 1998; van der Maaten et al., 2009). Such

1147 pre-processing steps in analysis often help delineate the contributions
1148 of test variables to function. Claude Shannon is often credited with
1149 development of Information Theory (Shannon, 1948), yet the field has
1150 evolved to also describing how relevance is assigned to a signal,
1151 based on statistical associations between multiple signals or stimuli in
1152 a sensory experience (Bialek et al., 1996, 2001; Chigirev & Bialek,
1153 2004; Tishby et al., 1999).

1154

1155 In the final version of the paper (Ananthamurthy & Bhalla, 2023;
1156 attached as Chapter 4 – “Analysis”), we reoriented focus on the most
1157 popular of the algorithms, and provide very well performing
1158 Python/C++ implementations, especially of the Ridge-to-background
1159 ratio (Mau et al., 2018) and Temporal Information (Mau et al., 2018)
1160 calculations, each of which consider cellular physiology and estimate a
1161 score for time cell-like behaviour.

1162 **Synthetic benchmarks for pre-hoc 1163 development of analytical procedures**

1164

1165 An interesting study published in 2018 used synthetic test datasets to
1166 go to the extent of estimating place cell detection algorithm
1167 performance on the basis of I_{spike} , I_{sec} and MI (Souza et al., 2018). They
1168 found,

- 1169 1. MI could outperform the other two in a variety of scenarios.
- 1170 2. I_{spike} and I_{sec} may still be useful in identifying unique
1171 subpopulations of place cells.
- 1172 3. Important algorithmic adjustments could be made to the
1173 calculations of I_{spike} and I_{sec} , to equalize performance between
1174 them and MI.

1175 There is clear nuance in the population code that required such a
1176 perspective during analysis. Eichenbaum and colleagues popularized
1177 the use of such metrics in the context of time cells (Mau et al., 2018),
1178 yet a systematic approach to identifying the best algorithms for time
1179 cells was requisite. We resorted to the use of such surrogate synthetic
1180 datasets acting as a large cohort of user-configurable test datasets to
1181 benchmark and characterize the predictive performance of a variety of
1182 time cell detection algorithms (Ananthamurthy & Bhalla, 2023; attached
1183 as Chapter 4 – “Analysis”). Analysis on real physiology datasets where
1184 categorical labels must be assessed is expected to benefit from this
1185 comparative analysis. Our Python/C++ implementations were
1186 rigorously tested and developed to the extent of excellent predictive
1187 performance. These algorithmic procedures may be used to study the
1188 nuances of time cell sequences with more statistical confidence.
1189

1190 Correlation analysis between pairs of recorded cells is one of the most
1191 important analytical directions taken by neurophysiologists
1192 understanding brain function, and has been reviewed previously (M. R.
1193 Cohen & Kohn, 2011). However, such analysis can be subject to False
1194 Positives, without appropriate significance studies. Specifically, it is
1195 important to look at whether the activity profile or tuning curves for cells
1196 (in relation to task variables) is significant above chance or other
1197 clearly defined cutoffs, using a large number of randomized surrogates
1198 of the recorded activity, generated by adding random timing shifts or
1199 bootstraps. Multiple pairwise correlations may not be sufficient to
1200 identify synchronous sequential activity in the network, without looking
1201 at higher orders of correlation across recorded cells. Ultimately, such
1202 studies benefit from simultaneous high-yield recordings, updated
1203 analytical procedures utilizing surrogate data for significance analysis,

1204 examining repetitions across trials (or trial-to-trial variability), and even
1205 the use of multiple analytical strategies, as reviewed previously
1206 (Foster, 2017; Grün, 2009).

1207

1208 Internally driven as opposed to externally driven network models of
1209 activity sequences have been proposed as the mechanism driving
1210 hippocampal CA1 sequences (Buzsáki & Llinás, 2017; Eichenbaum,
1211 2017). The CA1 neurons participating in any sequence may represent
1212 physiologically mappable attractors in temporally specific contexts. Our
1213 2-photon calcium recordings are expected to shed light on important
1214 correlations between task variables and the spatiotemporal sequence
1215 of activity, measured chronically, at cellular resolution.

1216

1217 Synfire chains (Abeles, 1982, 1991, 2004, 2009; Abeles et al., 2004)
1218 as sequential neuronal activity patterns or motifs have been described
1219 in cortical slices *in vitro* (Reyes, 2003), as well as *in vivo* (Ikegaya et
1220 al., 2004). The 2004 study described these sequences as songs
1221 (Ikegaya et al., 2004) that can incorporate new information as
1222 extensions of the motifs by combining multiple synfire chains
1223 (Bienenstock, 1995). However, an important consideration is that the
1224 original theoretical ideas behind synfire chains assumed feed-forward
1225 connections between layers of neurons, with recognition by
1226 subsequent neurons looking only at waves of synchrony, rather than
1227 specific individual neuronal identities (Abeles, 2004). Another important
1228 perspective is that these cortical sequences could be artifacts elicited
1229 just by chance, given the nature of membrane voltage fluctuations
1230 (McLelland & Paulsen, 2007; Mokeichev et al., 2007). There is thus
1231 some speculation over the significance of “cortical songs”, *in vivo*. **The**

1232 use of properly developed and benchmarked analytical procedures,
1233 tested and verified on physiology-equivalent test datasets (synthetic),
1234 is expected to help alleviate potential doubts in published physiology
1235 results (real recordings). For proper testing of our time cell detection
1236 algorithms, we incorporated many important user-controllable
1237 parameters for the generation of synthetic datasets, such as (but not
1238 limited to) Noise, Event Widths, Hit Trial Ratio, Trial-pair Imprecision,
1239 and Background Activity. Furthermore, reported but not popularly
1240 accepted physiological sequences such as synfire chains (Ikegaya et
1241 al., 2004) and preplay (Dragoi & Tonegawa, 2011), may now be more
1242 rigorously tested using the time cell analysis and detection algorithms
1243 provided (Ananthamurthy & Bhalla, 2023; attached as Chapter 4 –
1244 “Analysis”).
1245

1246 **Single-Unit Electrophysiology vs 2-Photon 1247 Calcium Imaging to study the Hippocampus**

1248
1249 The most well characterized and studied function of the hippocampus
1250 and surrounding tissue (Entorhinal Cortex, Parasubiculum, etc.) was
1251 the role these tissue systems played in Spatial Navigation and Coding.
1252 Single-Unit Electrophysiology was paramount to being able to isolate
1253 the activity from individual cells, and eventually was used to discover
1254 and describe properties of place cells (O’Keefe & Dostrovsky, 1971),
1255 grid cells (Fyhn et al., 2004; Hafting et al., 2005)(Fyhn et al., 2004;
1256 Hafting et al., 2005), head-direction cells (Taube et al., 1990), along
1257 with numerous other important physiological discoveries, as detailed
1258 previously. However, even with advances in the density of tetrode

1259 recordings, the yield of recorded cells from any given animal was often
1260 limited to <50 cells. It was only with the invention of Neuropixels (Jun
1261 et al., 2017) that this yield could be expanded to ~1000 cells. We had
1262 opted to utilize calcium imaging by 2-Photon Microscopy (Denk et al.,
1263 1990; Stosiek et al., 2003). This methodology, allowed us to record
1264 ~100-150 cells per session with our mice, albeit with significant cost to
1265 the recording frame rate on account of the limitations of the technique.
1266 Electrical recordings may be sampled even >20 kHz, while imaging
1267 based techniques typically cannot be used to record wide fields of
1268 view, sampled at >100 Hz (1-2 orders of magnitude, comparing
1269 sampling rates). Many spike sorting algorithms (see Buccino et al.,
1270 2022 for review) as well as automated ROI detection (see Robbins et
1271 al., 2021 for review) have been suggested for automated cell source
1272 identification, yet challenges remain, such as,
1273 1) scalability - more sources to identify from ever larger datasets force
1274 longer analysis runs.
1275 2) reproducibility – pre-processing analytical steps require manual
1276 curation to clean up the raw datasets, and this often affects the final
1277 result. We discuss details of our technique along with challenges and
1278 preliminary results, in Chapter 3 – “Imaging”.
1279
1280 The hippocampi (one in each hemisphere) of the mouse brain lie ~1
1281 mm below the most superficial layers of cortex (just inside the
1282 cranium), a barrier typically too wide for typical 1-photon fluorescence
1283 imaging systems (Confocal, Spinning Disk, etc.). This poses a very
1284 difficult challenge for imaging preparations since there are hardware
1285 and other technical limits to how long the working distance of
1286 microscope objectives can be made. The use of 2-photon microscopy
1287 combined with combinations of cortical excavations (to aid physical

1288 access), microendoscopes, as well as prisms to guide emitted
1289 fluorescence, have all been used to achieve deep brain imaging based
1290 recordings at cellular resolution, in rodents (Andermann et al., 2013;
1291 Attardo et al., 2015; Barreto et al., 2009; Barreto & Schnitzer, 2012;
1292 Dombeck et al., 2010; Heys et al., 2014; Murray & Levene, 2012;
1293 Velasco & Levene, 2014; Ziv et al., 2013).

1294

1295 All imaging preparation standardizations described in this thesis invoke
1296 2-Photon calcium imaging of hippocampal CA1 cells at cellular
1297 resolution (1 pix = ~1 μ m), following cortical excavations just above the
1298 left hippocampus (Dombeck et al., 2010).

1299 **Calcium imaging by 2-Photon Microscopy**

1300

1301 Typically, as cells become activated and elicit action potentials, there is
1302 often a large concomitant influx of Ca^{2+} ions through voltage gated
1303 calcium channels all around the perisomatic membrane, amongst other
1304 cellular compartments. Several organic dyes have been developed that
1305 reversibly bind Ca^{2+} ions in the cytosol and either become fluorescent
1306 or emit greater fluorescence (often with a red shift) when in this Ca^{2+} -
1307 bound state (Paredes et al., 2008). Additionally tremendous advances
1308 in molecular biology has seen the deployment of Genetically Encoded
1309 Calcium Indicators (GECIs) that may be exogenously incorporated into
1310 the genome of target cells. These GECIs serve the same function as
1311 organic calcium dyes, but may easily be replenished in the cytosol
1312 given the cell's natural machinery for transcription and translation, and
1313 whose Fluorescence properties can be engineered for brightness,
1314 responsivity, Ca^{2+} binding K_d , and fluorescence emission wavelengths.

1315 The number of cells that may be recorded by fluorescence is often only
1316 limited to either the spread of the organic dye or the imaging
1317 magnification settings, allowing for yields of 100-1000 cells.

1318

1319 With any Imaging based neurophysiology, there is always a trade-off
1320 between yield (number of cells recorded simultaneously) and temporal
1321 resolution. Increasing the yield by recording over a larger area of tissue
1322 requires many more pixels per imaging frame, resulting in a loss of
1323 temporal resolution (frame rate). On the other hand, increasing the
1324 frame rate necessitates capturing fewer pixels per frame, decreasing
1325 yield. There is even a limitation of simply zooming out, since stable
1326 fluorescence intensity fluctuations can only be identified when each
1327 cell is defined at least by a certain number of pixels, to allow proper
1328 isolation.

1329

1330 Specifically with calcium imaging, the signal to be recorded
1331 corresponds to Ca^{2+} flux in the cytoplasm as measured by the change
1332 in emitted fluorescence of reporters such as GCaMP, with a $\tau_{\text{rise}} = 10-$
1333 100 ms and $\tau_{\text{fall}} = 100-300$ ms (Chen et al., 2013). This signal is one or
1334 two orders of magnitude slower than the action potential ($\sim 2-5$ ms).
1335 However, this may not necessarily be a limitation since a dominant
1336 idea in the field is to simply consider rate coding, or time-averaged
1337 spiking activity (Abeles, 2004), bringing down the effective temporal
1338 resolution of the electrical record.

1339

1340 Genetically Encoded Voltage Indicators (GEVIs) that fluoresce with
1341 higher emission during membrane voltage dynamics have also been
1342 developed. However, their localization onto the membrane of the cell,
1343 instead of the cytoplasm, diminishes the total emitted photon flux per

1344 unit time, and requires longer bin times to achieve reasonable signal-
1345 to-noise, as reviewed previously (Mollinedo-Gajate et al., 2021). This
1346 unfortunately brings down the frame rate even more than what can be
1347 achieved with GECIs. We avoided GEVIs in the projects described in
1348 this thesis.

1349

1350 A major advancement in Fluorescence Imaging was the invention of
1351 Confocal and Multiphoton (typically 2-Photon) Microscopes, which
1352 allowed for unprecedented recording signal-to-noise by optical
1353 sectioning. 2-Photon Imaging itself was an important development for
1354 the neurophysiology of tissue greater than 300 μm in thickness, typical
1355 of rodent brain tissue, because it avoids wasteful excitation of imaging
1356 planes that are not in focus (out-of-plane). The 2-Photon effect
1357 requires two photons of longer wavelength (lower energy per photon),
1358 to near instantaneously excite a fluorophore. The photon flux is highest
1359 at the focal plane (with an N-squared dependence) of the microscope
1360 so only the section of the tissue corresponding to the focal place is
1361 allowed to achieve fluorescence. Additionally, longer wavelengths of
1362 excitation light can more easily penetrate deeper layers of tissue, due
1363 to comparatively lower scattering or Rayleigh effect (Denk et al., 1990;
1364 Helmchen & Denk, 2005).

1365

1366 The hippocampus (specifically the hippocampal CA1) was the main
1367 brain structure of interest for all our physiology experiments, and lies
1368 under about 1 mm of cortical tissue for mice. This is a depth that is
1369 difficult to image even with 2-Photon Microscopy. The typical
1370 methodology employed in such cases is to perform a cortical
1371 excavation just above the Hippocampus filling the crevice with optically
1372 clearer agarose or silicone elastomer. Even so, the hippocampal CA1

1373 cell body layer (*Stratum Pyramidale*) still lies about 150-300 μm below
1374 the external capsule and corpus callosum fibers (left intact for chronic
1375 imaging). Accordingly, we combined cortical excavation with 2-Photon
1376 microscopy, using a long working distance objective with a wide field of
1377 view, imaging cytosolic Ca^{2+} activity with the help of either an organic
1378 dye (OGB-1; acute imaging) or a GECI (GCaMP6f; chronic imaging).

1379

1380 An important perspective that has motivated the use of Imaging based
1381 physiology recordings (as opposed to Electrophysiological methods)
1382 other than potential yield, is that imaging provides anatomical
1383 confirmation of any particular recorded cell, and this in turn allows for,
1384 A) Unambiguous isolation of the same cell across multiple imaging
1385 sessions (across days and weeks). Single-Units are ultimately
1386 only algorithmically resolved and this can be done only for cells
1387 that are active and are represented in multiple spatially
1388 separated electrodes. However, very recently, Ashesh Dhawale
1389 and colleagues from Bence Olveczky's lab have devised a
1390 solution to track the movement of electrodes in tissue over time
1391 and use this information to ensure chronic recording of the
1392 same units (Dhawale et al., 2017). This technique was not
1393 available at the time when experiments for this thesis were
1394 started.

1395 B) Unambiguous detection of the lack of activity in an otherwise
1396 recorded cell. Since the cell can be anatomically identified
1397 independent of activity, it is possible to observe the absence of
1398 Ca^{2+} activity. Automated cell ROI detection (Francis et al., 2012;
1399 Maruyama et al., 2014; Mukamel et al., 2009; Pachitariu et al.,
1400 2017; Pnevmatikakis et al., 2016) simplifies the pre-processing
1401 step of cell isolation even over large batch sizes. These

1402 procedures inherently require the use of the calcium activity
1403 profiles of recorded cells, viz., inactive cells (though
1404 anatomically visible), may not be isolated.

1405 **Automated ROI detection for large-scale** 1406 **Calcium Imaging datasets**

1407
1408 A number of automated ROI detection algorithms have been cited in
1409 literature that require minimal user intervention, perform relatively fast
1410 identification for a large number of identified sources (putative cells).
1411 Some popular algorithms include PCA/ICA (Mukamel et al., 2009),
1412 Suite2p (Pachitariu et al., 2017), and Non-Negative Matrix
1413 Factorization or NNMF (Pnevmatikakis et al., 2016), which all have
1414 been developed to the extent where comparable or oftentimes much
1415 better ROI detection is achieved than as compared to the more tedious
1416 hand-drawn ROIs which scales very poorly with orders of cells
1417 recorded.
1418 We have strictly followed Suite2p (Pachitariu et al., 2017) for all
1419 physiological ROI (cell sources) described in this thesis.
1420

1421 **Short Summaries of the 3 projects**

1422 **Project I - How do sensory representations transform** 1423 **with learning?**

1424 Sensory Systems Neuroscience is a very popular field spanning
1425 studies looking at numerous brain regions and sub-regions in the

1426 cortex and hippocampus, *in vivo* (R. A. Andersen et al., 1993; Fassihi
1427 et al., 2017; Khan et al., 2010; Meeks et al., 2010; Petersen, 2019;
1428 Poort et al., 2015; Voelcker et al., 2022), among several others. Many
1429 if not most of these studies describe neural activity in animals with
1430 expert levels of behavioural learning and performance to the presented
1431 stimuli. Lacunae still remain as to mechanisms deployed during active
1432 or online learning especially in the early stages of behavioural training.
1433 There are not many published physiological readouts from large CA1
1434 populations, *in vivo*, under behavioural contexts for time cell activation,
1435 during the early, acquisition phases (Sessions 1-7, etc.) in associative
1436 learning. It is unclear what the spatiotemporal pattern of activity would
1437 reveal with a systematic, longitudinal survey.

1438

1439 We deployed our experiments with the intention to study how Calcium
1440 Imaging by 2-Photon could reveal finer population level details of
1441 network activity as the animals were tested on the learning of an
1442 operant conditioning or lick behaviour task. We were able to,
1443 1. Prototype OGB-1 based calcium imaging *in vivo*, from head-
1444 fixed mice in a manner suited to combined behaviour and
1445 recording experiments, and
1446 2. Study preliminary data from animals that correlation based
1447 functional activity clusters of recorded CA1 cells have spatial
1448 organization during bouts of spontaneous activity.

1449

1450 However, we were not satisfied with the level and rate of learning in
1451 our test animals eventually leading to a search for more stable
1452 behaviour paradigms in mice. Additionally, the use of OGB-1 as the
1453 Calcium Indicator also had to be abandoned since this fundamentally
1454 disallowed multi-day tracking of the same cells. We discuss our

1455 prototyping efforts and preliminary data for this project in detail, in the
1456 first few sections each of Chapters 2 (“Behaviour”) and 3 (“Imaging”).

1457

1458 **Project II - How does the timing of cellular activity adjust**
1459 **to behavioural task variables?**

1460

1461 Research on the cerebellum has made substantial progress in the
1462 elucidation of network mechanisms correlating well with external
1463 stimulus timing based variables, as animals learn Trace Eye-Blink
1464 Conditioning and Delay Conditioning (Kalmbach, Davis, et al., 2010;
1465 Kalmbach, Ohyama, et al., 2010; Medina et al., 2000; Ohyama et al.,
1466 2003; Siegel & Mauk, 2013). The preeminent studies on time cells in
1467 the hippocampus have focused on the context of appetitive reinforcing
1468 stimuli (Eichenbaum, 2004, 2017; B. Kraus et al., 2013; B. J. Kraus et
1469 al., 2015; MacDonald et al., 2011, 2013; Mau et al., 2018; Pastalkova
1470 et al., 2008). Time cells in the behavioural context of Trace Eye-Blink
1471 conditioning, an aversive learning paradigm, have been explored (Modi
1472 et al., 2014), but details such as correlations with rates of behavioural
1473 learning, tuning adaptability, and long-term stability (~weeks) of the
1474 time sequences are yet to be studied. **The degree of variability in time**
1475 **cell responses under these conditions is likely to inform mechanistic**
1476 **models of spatiotemporal sequences as observed in the hippocampus.**

1477

1478 We prototyped a GCaMP6f based *in vivo* hippocampal preparation that
1479 allowed for chronic, longitudinal recordings of hippocampal CA1, by 2-
1480 Photon Calcium Imaging (Dombeck et al., 2010) that could be

1481 combined with a stable and adaptable learning protocols of Trace Eye-
1482 Blink Conditioning (Siegel et al., 2015).

1483 From our preliminary set of recordings we were able to,

- 1484 1. Detect time cells in our population recordings,
- 1485 2. Observe signs of expansion of the time cell sub-population over
1486 early stages of learning, and
- 1487 3. Observe shifts in the timing of peak for known, chronically
1488 tracked time cells, typically moving away from the US and
1489 towards the CS.

1490

1491 Technical difficulties prevented us from expanding our experimental
1492 recording datasets to the point where these results could be looked at
1493 more critically and the results may be sufficient for publication. We
1494 discuss our prototyping efforts and preliminary data for this project in
1495 detail, in the last few sections each of Chapters 2 (“Behaviour”) and 3
1496 (“Imaging”).

1497

1498 **Project III - What is the best way to detect and score
1499 time-tuned cellular activity?**

1500

1501 Given that we had collected a reasonable sample of multi-day tracked
1502 cells while head-fixed mice were being trained to a Trace Eye-Blink
1503 Conditioning (TEC) task, we wished to move forward to identifying time
1504 cells in the most reliable way, with the aim to drawing quality
1505 conclusions from the physiology recordings.

1506

1507 The paper entitled “Synthetic Data Resource and Benchmarks for Time
1508 Cell Analysis and Detection Algorithms” (Ananthamurthy & Bhalla,
1509 2023) was a consolidation of our progress to analyse physiology data
1510 from real and synthetic cells expressed as calcium activity trials and
1511 sessions.

1512

1513 Here, we used a computational approach and developed categorically
1514 labelled, user definable, large scale synthetic datasets, as a test bed to
1515 compare and benchmark the predictions made by popular time cell
1516 detection algorithms. We were able to test the sensitivity of these
1517 computational algorithms across a wide array of experimental
1518 recording parameters, and could ultimately conclude the best
1519 operational regimes for each of them. All of the code base for this
1520 project is freely available online

1521 (<https://github.com/bhallalab/TimeCellAnalysis>) and is intended to be a
1522 resource to researchers.

1523 The paper is attached as Chapter 4 (“Analysis”).

1524 **Code Availability**

1525

1526 All our code for Synthetic Data generation and time cell Analysis is
1527 available at <https://www.github.com/bhallalab/TimeCellAnalysis>.

1528

1529 All our code for conducting Trace Eye-Blink Conditioning (TEC)
1530 behaviour is available at
<https://www.github.com/ananthamurthy/eyeBlinkBehaviour>.

1532

1533 Analysis scripts for evaluating TEC performance are available at
1534 <https://github.com/ananthamurthy/MATLAB/tree/master/TECAnalysis>.

1535 **Bibliography**

1536

1537 Abeles, M. (1982). *Local Cortical Circuits: An Electrophysiological Study*. Springer-Verlag.

1539 <https://books.google.co.in/books?id=s25lwwEACAAJ>

1540 Abeles, M. (1991). *Corticonics: Neural Circuits of the Cerebral Cortex*. Cambridge University Press. <https://doi.org/DOI:10.1017/CBO9780511574566>

1543 Abeles, M. (2004). Time Is Precious. *Science*, 304(5670), 523–524.
1544 <https://doi.org/10.1126/science.1097725>

1545 Abeles, M. (2009). *Synfire Chains* (L. R. B. T.-E. of N. Squire, Ed.; pp. 829–832). Academic Press.

1547 <https://doi.org/https://doi.org/10.1016/B978-008045046-9.01437-6>

1548 Abeles, M., Hayon, G., & Lehmann, D. (2004). Modeling compositionality by dynamic binding of synfire chains. *Journal of Computational Neuroscience*, 17(2), 179–201.
1551 <https://doi.org/10.1023/B:JCNS.0000037682.18051.5f>

1552 Ananthamurthy, K. G., & Bhalla, U. S. (2023). Synthetic Data Resource and Benchmarks for Time Cell Analysis and Detection Algorithms. *ENeuro*, ENEURO.0007-22.2023.

1555 <https://doi.org/10.1523/ENEURO.0007-22.2023>

1556 Andermann, M. L., Gilfoy, N. B., Goldey, G. J., Sachdev, R. N. S.,
1557 Wölfel, M., McCormick, D. A., Reid, R. C., & Levene, M. J. (2013). Chronic Cellular Imaging of Entire Cortical Columns in Awake

- 1559 Mice Using Microprisms. *Neuron*, 80(4), 900–913.
1560 <https://doi.org/10.1016/j.neuron.2013.07.052>
- 1561 Andersen, R. A., Snyder, L. H., Li, C.-S., & Stricanne, B. (1993).
1562 Coordinate transformations in the representation of spatial
1563 information. *Current Opinion in Neurobiology*, 3(2), 171–176.
1564 [https://doi.org/https://doi.org/10.1016/0959-4388\(93\)90206-E](https://doi.org/https://doi.org/10.1016/0959-4388(93)90206-E)
- 1565 Aronov, D., Nevers, R., & Tank, D. W. (2017). Mapping of a non-spatial
1566 dimension by the hippocampal-entorhinal circuit. *Nature*,
1567 543(7647), 719–722. <https://doi.org/10.1038/nature21692>
- 1568 Attardo, A., Fitzgerald, J. E., & Schnitzer, M. J. (2015). Impermanence
1569 of dendritic spines in live adult CA1 hippocampus. *Nature*,
1570 523(7562), 592–596. <https://doi.org/10.1038/nature14467>
- 1571 Ballard, I. C., Wagner, A. D., & McClure, S. M. (2019). Hippocampal
1572 pattern separation supports reinforcement learning. *Nature
1573 Communications*, 10(1), 1073. <https://doi.org/10.1038/s41467-019-08998-1>
- 1575 Barretto, R. P. J., Messerschmidt, B., & Schnitzer, M. J. (2009). In vivo
1576 fluorescence imaging with high-resolution microlenses. *Nature
1577 Methods*, 6(7), 511–512. <https://doi.org/10.1038/nmeth.1339>
- 1578 Barretto, R. P. J., & Schnitzer, M. J. (2012). In vivo optical
1579 microendoscopy for imaging cells lying deep within live tissue.
1580 *Cold Spring Harbor Protocols*, 2012(10), 1029–1034.
1581 <https://doi.org/10.1101/pdb.top071464>
- 1582 Baudry, M., & Lynch, G. (1981). Hippocampal glutamate receptors.
1583 *Molecular and Cellular Biochemistry*, 38(1), 5–18.
1584 <https://doi.org/10.1007/BF00235685>
- 1585 Bialek, W., Callan, C. G., & Strong, S. P. (1996). Field Theories for
1586 Learning Probability Distributions. *Physical Review Letters*,
1587 77(23), 4693–4697. <https://doi.org/10.1103/physrevlett.77.4693>
- 1588 Bialek, W., Nemenman, I., & Tishby, N. (2001). Predictability,
1589 Complexity, and Learning. *Neural Comput.*, 13(11), 2409–2463.
1590 <https://doi.org/10.1162/089976601753195969>
- 1591 Bienenstock, E. (1995). A model of neocortex. *Network: Computation
1592 in Neural Systems*, 6(2), 179–224. https://doi.org/10.1088/0954-898X_6_2_004
- 1594 Bjerknes, T. L., Moser, E. I., & Moser, M.-B. (2014). Representation of
1595 Geometric Borders in the Developing Rat. *Neuron*, 82(1), 71–78.
1596 <https://doi.org/10.1016/j.neuron.2014.02.014>
- 1597 Buccino, A. P., Garcia, S., & Yger, P. (2022). Spike sorting: new trends
1598 and challenges of the era of high-density probes. *Progress in
1599 Biomedical Engineering*, 4(2), 022005.
1600 <https://doi.org/10.1088/2516-1091/ac6b96>
- 1601 Burgess, N. (2008). Spatial Cognition and the Brain. *Annals of the New*

- 1602 *York Academy of Sciences*, 1124(1), 77–97.
1603 <https://doi.org/https://doi.org/10.1196/annals.1440.002>
1604 Buzsáki, G., & Llinás, R. (2017). Space and time in the brain. *Science*
1605 (*New York, N.Y.*), 358(6362), 482–485.
1606 <https://doi.org/10.1126/science.aan8869>
1607 Cai, D. J., Aharoni, D., Shuman, T., Shobe, J., Biane, J., Song, W.,
1608 Wei, B., Veshkini, M., La-Vu, M., Lou, J., Flores, S. E., Kim, I.,
1609 Sano, Y., Zhou, M., Baumgaertel, K., Lavi, A., Kamata, M.,
1610 Tuszyński, M., Mayford, M., ... Silva, A. J. (2016). A shared neural
1611 ensemble links distinct contextual memories encoded close in
1612 time. *Nature*, 534(7605), 115–118.
1613 <https://doi.org/10.1038/nature17955>
1614 Caporale, N., & Dan, Y. (2008). Spike timing-dependent plasticity: a
1615 Hebbian learning rule. *Annual Review of Neuroscience*, 31, 25–
1616 46. <https://doi.org/10.1146/annurev.neuro.31.060407.125639>
1617 Carew, T. J., Castellucci, V. F., & Kandel, E. R. (1971). An Analysis of
1618 Dishabituation and Sensitization of The Gill-Withdrawal Reflex In
1619 Aplysia. *International Journal of Neuroscience*, 2(2), 79–98.
1620 <https://doi.org/10.3109/00207457109146995>
1621 Chen, T.-W., Wardill, T. J., Sun, Y., Pulver, S. R., Renninger, S. L.,
1622 Baohan, A., Schreiter, E. R., Kerr, R. A., Orger, M. B., Jayaraman,
1623 V., Looger, L. L., Svoboda, K., & Kim, D. S. (2013). Ultrasensitive
1624 fluorescent proteins for imaging neuronal activity. *Nature*,
1625 499(7458), 295–300. <https://doi.org/10.1038/nature12354>
1626 Chigirev, D., & Bialek, W. (2004, January). Optimal manifold
1627 representation of data: An information theoretic approach.
1628 *Advances in Neural Information Processing Systems 16 -*
1629 *Proceedings of the 2003 Conference, NIPS 2003*.
1630 Clayton, N. S., Salwiczek, L. H., & Dickinson, A. (2007). Episodic
1631 memory. *Current Biology*, 17(6), R189–R191.
1632 <https://doi.org/10.1016/j.cub.2007.01.011>
1633 Cohen, M. R., & Kohn, A. (2011). Measuring and interpreting neuronal
1634 correlations. *Nature Neuroscience*, 14(7), 811–819.
1635 <https://doi.org/10.1038/nn.2842>
1636 Conway, M. A. (2009). Episodic memories. *Neuropsychologia*, 47(11),
1637 2305–2313.
1638 <https://doi.org/https://doi.org/10.1016/j.neuropsychologia.2009.02.003>
1639 Csicsvari, J., O'Neill, J., Allen, K., & Senior, T. (2007). Place-selective
1640 firing contributes to the reverse-order reactivation of
1641 CA1 pyramidal cells during sharp waves in open-field exploration.
1642 *The European Journal of Neuroscience*, 26(3), 704–716.
1643 <https://doi.org/10.1111/j.1460-9568.2007.05684.x>

- 1645 Davidson, T. J., Kloosterman, F., & Wilson, M. A. (2009). Hippocampal
1646 replay of extended experience. *Neuron*, 63(4), 497–507.
1647 <https://doi.org/10.1016/j.neuron.2009.07.027>
- 1648 Denk, W., Strickler, J. H., & Webb, W. W. (1990). Two-photon laser
1649 scanning fluorescence microscopy. *Science (New York, N.Y.)*,
1650 248(4951), 73–76. <https://doi.org/10.1126/science.2321027>
- 1651 Dhawale, A. K., Poddar, R., Wolff, S. B. E., Normand, V. A.,
1652 Kopelowitz, E., & Ölveczky, B. P. (2017). Automated long-term
1653 recording and analysis of neural activity in behaving animals.
1654 *ELife*, 6, e27702. <https://doi.org/10.7554/eLife.27702>
- 1655 Diamond, A. (2013). Executive Functions. *Annual Review of
1656 Psychology*, 64(1), 135–168. <https://doi.org/10.1146/annurev-psych-113011-143750>
- 1658 Diba, K., & Buzsáki, G. (2007). Forward and reverse hippocampal
1659 place-cell sequences during ripples. *Nature Neuroscience*, 10(10),
1660 1241–1242. <https://doi.org/10.1038/nn1961>
- 1661 Dickinson, A., Nicholas, D. J., & Mackintosh, N. J. (1983). A re-
1662 examination of one-trial blocking in conditioned suppression. *The
1663 Quarterly Journal of Experimental Psychology B: Comparative and
1664 Physiological Psychology*, 35, 67–79.
1665 <https://doi.org/10.1080/14640748308400914>
- 1666 Disterhoft, J. F., & Weiss, C. (2017). Eyeblink Conditioning – A
1667 Behavioral Model of Procedural and Declarative Learning. In J. H.
1668 Byrne (Ed.), *Learning and Memory: A Comprehensive Reference
1669 (Second Edition)* (pp. 327–355). Academic Press.
1670 <https://doi.org/https://doi.org/10.1016/B978-0-12-809324-5.21087-0>
- 1672 Dombeck, D. A., Graziano, M. S., & Tank, D. W. (2009). Functional
1673 Clustering of Neurons in Motor Cortex Determined by Cellular
1674 Resolution Imaging in Awake Behaving Mice. *The Journal of
1675 Neuroscience*, 29(44), 13751 LP – 13760.
1676 <https://doi.org/10.1523/JNEUROSCI.2985-09.2009>
- 1677 Dombeck, D. A., Harvey, C. D., Tian, L., Looger, L. L., & Tank, D. W.
1678 (2010). Functional imaging of hippocampal place cells at cellular
1679 resolution during virtual navigation. *Nature Neuroscience*, 13(11),
1680 1433–1440. <https://doi.org/10.1038/nn.2648>
- 1681 Dragoi, G. (2013). Internal operations in the hippocampus: single cell
1682 and ensemble temporal coding. *Frontiers in Systems
1683 Neuroscience*, 7, 46. <https://doi.org/10.3389/fnsys.2013.00046>
- 1684 Dragoi, G., & Buzsáki, G. (2006). Temporal encoding of place
1685 sequences by hippocampal cell assemblies. *Neuron*, 50(1), 145–
1686 157. <https://doi.org/10.1016/j.neuron.2006.02.023>
- 1687 Dragoi, G., Carpi, D., Recce, M., Csicsvari, J., & Buzsáki, G. (1999).

- 1688 Interactions between hippocampus and medial septum during
1689 sharp waves and theta oscillation in the behaving rat. *The Journal*
1690 *of Neuroscience : The Official Journal of the Society for*
1691 *Neuroscience*, 19(14), 6191–6199.
1692 <http://www.ncbi.nlm.nih.gov/pubmed/10407055>
- 1693 Dragoi, G., & Tonegawa, S. (2011). Preplay of future place cell
1694 sequences by hippocampal cellular assemblies. *Nature*,
1695 469(7330), 397–401. <https://doi.org/10.1038/nature09633>
- 1696 Eichenbaum, H. (2004). Hippocampus: Cognitive processes and
1697 neural representations that underlie declarative memory. *Neuron*,
1698 44(1), 109–120. <https://doi.org/10.1016/j.neuron.2004.08.028>
- 1699 Eichenbaum, H. (2017). On the Integration of Space, Time, and
1700 Memory. *Neuron*, 95(5), 1007–1018.
1701 <https://doi.org/10.1016/j.neuron.2017.06.036>
- 1702 Ekstrom, A. D., & Ranganath, C. (2018). Space, time, and episodic
1703 memory: The hippocampus is all over the cognitive map.
1704 *Hippocampus*, 28(9), 680–687.
1705 <https://doi.org/https://doi.org/10.1002/hipo.22750>
- 1706 Fassihi, A., Akrami, A., Pulecchi, F., Schönfelder, V., & Diamond, M. E.
1707 (2017). Transformation of Perception from Sensory to Motor
1708 Cortex. *Current Biology : CB*, 27(11), 1585-1596.e6.
1709 <https://doi.org/10.1016/j.cub.2017.05.011>
- 1710 Ferbinteanu, J., & Shapiro, M. L. (2003). Prospective and retrospective
1711 memory coding in the hippocampus. *Neuron*, 40(6), 1227–1239.
1712 [https://doi.org/10.1016/s0896-6273\(03\)00752-9](https://doi.org/10.1016/s0896-6273(03)00752-9)
- 1713 Ferbinteanu, J., Shirvalkar, P., & Shapiro, M. L. (2011). Memory
1714 Modulates Journey-Dependent Coding in the Rat Hippocampus.
1715 *The Journal of Neuroscience*, 31(25), 9135 LP – 9146.
1716 <https://doi.org/10.1523/JNEUROSCI.1241-11.2011>
- 1717 Focus on spatial cognition. (2017). *Nature Neuroscience*, 20(11), 1431.
1718 <https://doi.org/10.1038/nn.4666>
- 1719 Foster, D. J. (2017). Replay Comes of Age. *Annual Review of*
1720 *Neuroscience*, 40, 581–602. <https://doi.org/10.1146/annurev-neuro-072116-031538>
- 1722 Foster, D. J., & Wilson, M. A. (2006). Reverse replay of behavioural
1723 sequences in hippocampal place cells during the awake state.
1724 *Nature*, 440(7084), 680–683. <https://doi.org/10.1038/nature04587>
- 1725 Foster, D. J., & Wilson, M. A. (2007). Hippocampal theta sequences.
1726 *Hippocampus*, 17(11), 1093–1099.
1727 <https://doi.org/10.1002/hipo.20345>
- 1728 Francis, M., Qian, X., Charbel, C., Ledoux, J., Parker, J. C., & Taylor,
1729 M. S. (2012). Automated region of interest analysis of dynamic
1730 Ca²⁺ signals in image sequences. *American Journal of*

- 1731 *Physiology. Cell Physiology*, 303(3), C236-43.
1732 <https://doi.org/10.1152/ajpcell.00016.2012>
- 1733 Frank, L. M., Brown, E. N., & Wilson, M. (2000). Trajectory encoding in
1734 the hippocampus and entorhinal cortex. *Neuron*, 27(1), 169–178.
1735 [https://doi.org/10.1016/s0896-6273\(00\)00018-0](https://doi.org/10.1016/s0896-6273(00)00018-0)
- 1736 Fyhn, M., Molden, S., Witter, M. P., Moser, E. I., & Moser, M.-B.
1737 (2004). Spatial representation in the entorhinal cortex. *Science*
1738 (*New York, N.Y.*), 305(5688), 1258–1264.
1739 <https://doi.org/10.1126/science.1099901>
- 1740 Giovannucci, A., Badura, A., Deverett, B., Najafi, F., Pereira, T. D.,
1741 Gao, Z., Ozden, I., Kloth, A. D., Pnevmatikakis, E., Paninski, L.,
1742 De Zeeuw, C. I., Medina, J. F., & Wang, S. S.-H. (2017).
1743 Cerebellar granule cells acquire a widespread predictive feedback
1744 signal during motor learning. *Nature Neuroscience*, 20(5), 727–
1745 734. <https://doi.org/10.1038/nn.4531>
- 1746 Grün, S. (2009). Data-Driven Significance Estimation for Precise Spike
1747 Correlation. *Journal of Neurophysiology*, 101(3), 1126–1140.
1748 <https://doi.org/10.1152/jn.00093.2008>
- 1749 Gupta, A. S., van der Meer, M. A. A., Touretzky, D. S., & Redish, A. D.
1750 (2010). Hippocampal Replay Is Not a Simple Function of
1751 Experience. *Neuron*, 65(5), 695–705.
1752 <https://doi.org/https://doi.org/10.1016/j.neuron.2010.01.034>
- 1753 Hafting, T., Fyhn, M., Molden, S., Moser, M.-B., & Moser, E. I. (2005).
1754 Microstructure of a spatial map in the entorhinal cortex. *Nature*,
1755 436(7052), 801–806. <https://doi.org/10.1038/nature03721>
- 1756 Hamme, L. J. Van, & Wasserman, E. A. (1993). Cue Competition in
1757 Causality Judgments: The Role of Manner of Information
1758 Presentation. *Bulletin of the Psychonomic Society*, 31(5), 457–
1759 460. <https://doi.org/10.3758/bf03334962>
- 1760 Han, J.-H., Kushner, S. A., Yiu, A. P., Hsiang, H.-L. L., Buch, T.,
1761 Waisman, A., Bontempi, B., Neve, R. L., Frankland, P. W., &
1762 Josselyn, S. A. (2009). Selective erasure of a fear memory.
1763 *Science (New York, N.Y.)*, 323(5920), 1492–1496.
1764 <https://doi.org/10.1126/science.1164139>
- 1765 Hartley, T., Lever, C., Burgess, N., & O'Keefe, J. (2014). Space in the
1766 brain: how the hippocampal formation supports spatial cognition.
1767 *Philosophical Transactions of the Royal Society B: Biological*
1768 *Sciences*, 369(1635), 20120510.
1769 <https://doi.org/10.1098/rstb.2012.0510>
- 1770 Hebb, D. O. (1949). The organization of behavior; a
1771 neuropsychological theory. In *The organization of behavior; a*
1772 *neuropsychological theory*. Wiley.
- 1773 Helmchen, F., & Denk, W. (2005). *Deep tissue two-photon microscopy*.

- 1774 2(12), 9. <https://doi.org/10.1038/nmeth818>
- 1775 Heys, J. G., Rangarajan, K. V., & Dombeck, D. A. (2014). The
1776 Functional Micro-organization of Grid Cells Revealed by Cellular-
1777 Resolution Imaging. *Neuron*, 84(5), 1079–1090.
1778 <https://doi.org/10.1016/j.neuron.2014.10.048>
- 1779 Hyde, R. A., & Strowbridge, B. W. (2012). Mnemonic representations
1780 of transient stimuli and temporal sequences in the rodent
1781 hippocampus in vitro. *Nature Neuroscience*, 15(10), 1430–1438.
1782 <https://doi.org/10.1038/nn.3208>
- 1783 Ikegaya, Y., Aaron, G., Cossart, R., Aronov, D., Lampl, I., Ferster, D.,
1784 & Yuste, R. (2004). Synfire chains and cortical songs: temporal
1785 modules of cortical activity. *Science (New York, N.Y.)*, 304(5670),
1786 559–564. <https://doi.org/10.1126/science.1093173>
- 1787 Itskov, V., Pastalkova, E., Mizuseki, K., Buzsaki, G., & Harris, K. D.
1788 (2008). Theta-mediated dynamics of spatial information in
1789 hippocampus. *The Journal of Neuroscience : The Official Journal
1790 of the Society for Neuroscience*, 28(23), 5959–5964.
1791 <https://doi.org/10.1523/JNEUROSCI.5262-07.2008>
- 1792 Jadhav, S. P., Kemere, C., German, P. W., & Frank, L. M. (2012).
1793 Awake hippocampal sharp-wave ripples support spatial memory.
1794 *Science (New York, N.Y.)*, 336(6087), 1454–1458.
1795 <https://doi.org/10.1126/science.1217230>
- 1796 Josselyn, S. A., & Tonegawa, S. (2020). Memory engrams: Recalling
1797 the past and imagining the future. *Science (New York, N.Y.)*,
1798 367(6473). <https://doi.org/10.1126/science.aaw4325>
- 1799 Jun, J. J., Steinmetz, N. A., Siegle, J. H., Denman, D. J., Bauza, M.,
1800 Barbarits, B., Lee, A. K., Anastassiou, C. A., Andrei, A., Aydin, Ç.,
1801 Barbic, M., Blanche, T. J., Bonin, V., Couto, J., Dutta, B., Gratiy,
1802 S. L., Gutnisky, D. A., Häusser, M., Karsh, B., ... Harris, T. D.
1803 (2017). Fully integrated silicon probes for high-density recording of
1804 neural activity. *Nature*, 551(7679), 232–236.
1805 <https://doi.org/10.1038/nature24636>
- 1806 Kalmbach, B. E., Davis, T., Ohyama, T., Riusech, F., Nores, W. L., &
1807 Mauk, M. D. (2010). Cerebellar Cortex Contributions to the
1808 Expression and Timing of Conditioned Eyelid Responses. *Journal
1809 of Neurophysiology*, 103(4), 2039–2049.
1810 <https://doi.org/10.1152/jn.00033.2010>
- 1811 Kalmbach, B. E., Ohyama, T., & Mauk, M. D. (2010). Temporal
1812 Patterns of Inputs to Cerebellum Necessary and Sufficient for
1813 Trace Eyelid Conditioning. *Journal of Neurophysiology*, 104(2),
1814 627–640. <https://doi.org/10.1152/jn.00169.2010>
- 1815 Khan, A. G., Parthasarathy, K., & Bhalla, U. S. (2010). Odor
1816 representations in the mammalian olfactory bulb. *Wiley*

- 1817 *Interdisciplinary Reviews. Systems Biology and Medicine*, 2(5),
1818 603–611. <https://doi.org/10.1002/wsbm.85>
- 1819 Kim, S., & Lee, I. (2012). The hippocampus is required for visually
1820 cued contextual response selection, but not for visual
1821 discrimination of contexts. *Frontiers in Behavioral Neuroscience*,
1822 6. <https://doi.org/10.3389/fnbeh.2012.00066>
- 1823 Kraus, B. J., Brandon, M. P., Robinson, R. J., Connerney, M. A.,
1824 Hasselmo, M. E., & Eichenbaum, H. (2015). During Running in
1825 Place, Grid Cells Integrate Elapsed Time and Distance Run.
1826 *Neuron*, 88(3), 578–589.
1827 <https://doi.org/10.1016/j.neuron.2015.09.031>
- 1828 Kraus, B., Robinson, R., White, J., Eichenbaum, H., & Hasselmo, M.
1829 (2013). Hippocampal “Time Cells”: Time versus Path Integration.
1830 *Neuron*, 78(6), 1090–1101.
1831 <https://doi.org/10.1016/j.neuron.2013.04.015>
- 1832 Kropff, E., Carmichael, J. E., Moser, M.-B., & Moser, E. I. (2015).
1833 Speed cells in the medial entorhinal cortex. *Nature*, 523(7561),
1834 419–424. <https://doi.org/10.1038/nature14622>
- 1835 Krupa, D., & Thompson, R. (2003). Inhibiting the Expression of a
1836 Classically Conditioned Behavior Prevents Its Extinction. *The
1837 Journal of Neuroscience : The Official Journal of the Society for
1838 Neuroscience*, 23, 10577–10584.
1839 <https://doi.org/10.1523/JNEUROSCI.23-33-10577.2003>
- 1840 Lever, C., Burton, S., Jeewajee, A., O'Keefe, J., & Burgess, N.
1841 (2009). Boundary Vector Cells in the Subiculum of the
1842 Hippocampal Formation. *The Journal of Neuroscience*, 29(31),
1843 9771 LP – 9777. <https://doi.org/10.1523/JNEUROSCI.1319-09.2009>
- 1845 Luo, L., Callaway, E. M., & Svoboda, K. (2018). Genetic Dissection of
1846 Neural Circuits: A Decade of Progress. *Neuron*, 98(2), 256–281.
1847 <https://doi.org/https://doi.org/10.1016/j.neuron.2018.03.040>
- 1848 MacDonald, C. J., Carrow, S., Place, R., & Eichenbaum, H. (2013).
1849 Distinct hippocampal time cell sequences represent odor
1850 memories in immobilized rats. *The Journal of Neuroscience : The
1851 Official Journal of the Society for Neuroscience*, 33(36), 14607–
1852 14616. <https://doi.org/10.1523/JNEUROSCI.1537-13.2013>
- 1853 MacDonald, C. J., Lepage, K. Q., Eden, U. T., & Eichenbaum, H.
1854 (2011). Hippocampal “time cells” bridge the gap in memory for
1855 discontiguous events. *Neuron*, 71(4), 737–749.
1856 <https://doi.org/10.1016/j.neuron.2011.07.012>
- 1857 Maruyama, R., Maeda, K., Moroda, H., Kato, I., Inoue, M., Miyakawa,
1858 H., & Aonishi, T. (2014). Detecting cells using non-negative matrix
1859 factorization on calcium imaging data. *Neural Networks : The*

- 1860 *Official Journal of the International Neural Network Society*, 55,
1861 11–19. <https://doi.org/10.1016/j.neunet.2014.03.007>
- 1862 Mau, W., Sullivan, D. W., Kinsky, N. R., Hasselmo, M. E., Howard, M.
1863 W., & Eichenbaum, H. (2018). The Same Hippocampal CA1
1864 Population Simultaneously Codes Temporal Information over
1865 Multiple Timescales. *Current Biology*, 28(10), 1499–1508.e4.
1866 <https://doi.org/10.1016/j.cub.2018.03.051>
- 1867 McLelland, D., & Paulsen, O. (2007). Cortical Songs Revisited: A
1868 Lesson in Statistics. *Neuron*, 53(3), 319–321.
1869 <https://doi.org/https://doi.org/10.1016/j.neuron.2007.01.020>
- 1870 McNaughton, N., & Gray, J. A. (2000). Anxiolytic action on the
1871 behavioural inhibition system implies multiple types of arousal
1872 contribute to anxiety. *Journal of Affective Disorders*, 61(3), 161–
1873 176. [https://doi.org/10.1016/s0165-0327\(00\)00344-x](https://doi.org/10.1016/s0165-0327(00)00344-x)
- 1874 Medina, J. F., Garcia, K. S., Nores, W. L., Taylor, N. M., & Mauk, M. D.
1875 (2000). Timing mechanisms in the cerebellum: testing predictions
1876 of a large-scale computer simulation. *The Journal of
1877 Neuroscience : The Official Journal of the Society
1878 for Neuroscience*, 20(14), 5516–5525.
1879 <https://doi.org/10.1523/JNEUROSCI.20-14-05516.2000>
- 1880 Meeks, J. P., Arnson, H. A., & Holy, T. E. (2010). Representation and
1881 transformation of sensory information in the mouse
1882 accessory olfactory system. *Nature Neuroscience*, 13(6), 723–
1883 730. <https://doi.org/10.1038/nn.2546>
- 1884 Miller, A. M. P., Jacob, A. D., Ramsaran, A. I., De Snoo, M. L.,
1885 Josselyn, S. A., & Frankland, P. W. (2023). Emergence of a
1886 predictive model in the hippocampus. *Neuron*.
1887 <https://doi.org/10.1016/j.neuron.2023.03.011>
- 1888 Modi, M. N., Dhawale, A. K., & Bhalla, U. S. (2014). CA1 cell activity
1889 sequences emerge after reorganization of network correlation
1890 structure during associative learning. *eLife*, 3, e01982–e01982.
1891 <https://doi.org/10.7554/eLife.01982>
- 1892 Mokeichev, A., Okun, M., Barak, O., Katz, Y., Ben-Shahar, O., &
1893 Lampl, I. (2007). Stochastic Emergence of Repeating Cortical
1894 Motifs in Spontaneous Membrane Potential Fluctuations In Vivo.
1895 *Neuron*, 53, 413–425.
1896 <https://doi.org/10.1016/j.neuron.2007.01.017>
- 1897 Mollinedo-Gajate, I., Song, C., & Knöpfel, T. (2021). Genetically
1898 Encoded Voltage Indicators. *Advances in Experimental Medicine
1899 and Biology*, 1293, 209–224. https://doi.org/10.1007/978-981-15-8763-4_12
- 1900 Morris, R. G. M., Garrud, P., Rawlins, J. N. P., & O'Keefe, J. (1982).
1901 Place navigation impaired in rats with hippocampal lesions.

- 1903 *Nature*, 297(5868), 681–683. <https://doi.org/10.1038/297681a0>
- 1904 Moscovitch, M., Cabeza, R., Winocur, G., & Nadel, L. (2016). Episodic
1905 Memory and Beyond: The Hippocampus and Neocortex in
1906 Transformation. *Annual Review of Psychology*, 67(1), 105–134.
1907 <https://doi.org/10.1146/annurev-psych-113011-143733>
- 1908 Moyer, J. R. J., Thompson, L. T., & Disterhoft, J. F. (1996). Trace
1909 eyeblink conditioning increases CA1 excitability in a transient
1910 and learning-specific manner. *The Journal of Neuroscience : The
1911 Official Journal of the Society for Neuroscience*, 16(17), 5536–
1912 5546. <https://doi.org/10.1523/JNEUROSCI.16-17-05536.1996>
- 1913 Mukamel, E. A., Nimmerjahn, A., & Schnitzer, M. J. (2009). Automated
1914 analysis of cellular signals from large-scale calcium imaging data.
1915 *Neuron*, 63(6), 747–760.
1916 <https://doi.org/10.1016/j.neuron.2009.08.009>
- 1917 Muller, R. U., & Kubie, J. L. (1989). The firing of hippocampal place
1918 cells predicts the future position of freely moving rats. *The Journal
1919 of Neuroscience : The Official Journal of the Society
1920 for Neuroscience*, 9(12), 4101–4110.
1921 <https://doi.org/10.1523/JNEUROSCI.09-12-04101.1989>
- 1922 Murray, T. A., & Levene, M. J. (2012). Singlet gradient index lens for
1923 deep in vivo multiphoton microscopy. *Journal of Biomedical
1924 Optics*, 17(2), 021106. <https://doi.org/10.1117/1.JBO.17.2.021106>
- 1925 Nestler, E. J., Hyman, S. E., Holtzman, D. M., & Malenka, R. C. (2015).
1926 Higher Cognitive Function and Behavioral Control. In *Molecular
1927 Neuropharmacology: A Foundation for Clinical Neuroscience*, 3e.
1928 McGraw-Hill Education.
1929 <neurology.mhmedical.com/content.aspx?aid=1105916482>
- 1930 Ohyama, T., Nores, W. L., Murphy, M., & Mauk, M. D. (2003). What
1931 the cerebellum computes. *Trends in Neurosciences*, 26(4), 222–
1932 227. [https://doi.org/10.1016/S0166-2236\(03\)00054-7](https://doi.org/10.1016/S0166-2236(03)00054-7)
- 1933 O'Keefe, J., & Burgess, N. (1996). Geometric determinants of the
1934 place fields of hippocampal neurons. *Nature*, 381(6581), 425–428.
1935 <https://doi.org/10.1038/381425a0>
- 1936 O'Keefe, J., & Dostrovsky, J. (1971). The hippocampus as a spatial
1937 map. Preliminary evidence from unit activity in the freely-moving
1938 rat. *Brain Research*, 34(1), 171–175. [https://doi.org/10.1016/0006-8993\(71\)90358-1](https://doi.org/10.1016/0006-8993(71)90358-1)
- 1940 O'Keefe, J., & Nadel, L. (1978). The Hippocampus as a Cognitive Map.
1941 In *Philosophical Studies* (Vol. 27).
1942 <https://doi.org/10.5840/philstudies19802725>
- 1943 O'Keefe, J., & Recce, M. L. (1993). Phase relationship between
1944 hippocampal place units and the EEG theta rhythm.
1945 *Hippocampus*, 3(3), 317–330.

- 1946 https://doi.org/10.1002/hipo.450030307
- 1947 Ozden, I., Lee, H. M., Sullivan, M. R., & Wang, S. S.-H. (2008). Identification and Clustering of Event Patterns From In Vivo Multiphoton Optical Recordings of Neuronal Ensembles. *Journal of Neurophysiology*, 100(1), 495–503.
- 1948
1949
1950
1951 https://doi.org/10.1152/jn.01310.2007
- 1952 Pachitariu, M., Stringer, C., Dipoppa, M., Schröder, S., Rossi, L. F., Dalgleish, H., Carandini, M., & Harris, K. D. (2017). Suite2p: beyond 10,000 neurons with standard two-photon microscopy. *BioRxiv*, 61507. https://doi.org/10.1101/061507
- 1953
1954
1955
1956 Paredes, R. M., Etzler, J. C., Watts, L. T., Zheng, W., & Lechleiter, J. D. (2008). Chemical calcium indicators. *Methods (San Diego, Calif.)*, 46(3), 143–151.
- 1957
1958 https://doi.org/10.1016/j.ymeth.2008.09.025
- 1959 Pastalkova, E., Itskov, V., Amarasingham, A., & Buzsaki, G. (2008). Internally Generated Cell Assembly Sequences in the Rat Hippocampus. *Science*, 321(5894), 1322–1327.
- 1960
1961
1962
1963 https://doi.org/10.1126/science.1159775
- 1964 Pavlov, I. P. (1927). Conditioned reflexes: an investigation of the physiological activity of the cerebral cortex. In *Conditioned reflexes: an investigation of the physiological activity of the cerebral cortex*. Oxford Univ. Press.
- 1965
1966
1967
1968 Petersen, C. C. H. (2019). Sensorimotor processing in the rodent barrel cortex. *Nature Reviews. Neuroscience*, 20(9), 533–546.
- 1969
1970 https://doi.org/10.1038/s41583-019-0200-y
- 1971 Pfeiffer, B. E., & Foster, D. J. (2013). Hippocampal place-cell sequences depict future paths to remembered goals. *Nature*, 497(7447), 74–79. https://doi.org/10.1038/nature12112
- 1972
1973
1974 Pnevmatikakis, E. A., Soudry, D., Gao, Y., Machado, T. A., Merel, J., Pfau, D., Reardon, T., Mu, Y., Lacefield, C., Yang, W., Ahrens, M., Bruno, R., Jessell, T. M., Peterka, D. S., Yuste, R., & Paninski, L. (2016). Simultaneous Denoising, Deconvolution, and Demixing of Calcium Imaging Data. *Neuron*, 89(2), 285–299.
- 1975
1976
1977
1978
1979 https://doi.org/https://doi.org/10.1016/j.neuron.2015.11.037
- 1980 Poort, J., Khan, A. G., Pachitariu, M., Nemri, A., Orsolic, I., Krupic, J., Bauza, M., Sahani, M., Keller, G. B., Mrsic-Flogel, T. D., & Hofer, S. B. (2015). Learning Enhances Sensory and Multiple Non-sensory Representations in Primary Visual Cortex. *Neuron*, 86(6), 1478–1490. https://doi.org/10.1016/j.neuron.2015.05.037
- 1981
1982
1983
1984
1985 Poppenk, J., Evensmoen, H. R., Moscovitch, M., & Nadel, L. (2013). Long-axis specialization of the human hippocampus. *Trends in Cognitive Sciences*, 17(5), 230–240.
- 1986
1987
1988 https://doi.org/10.1016/j.tics.2013.03.005

- 1989 Pudil, P., & Novovičová, J. (1998). Novel Methods for Feature Subset
 1990 Selection with Respect to Problem Knowledge. In H. Liu & H.
 1991 Motoda (Eds.), *Feature Extraction, Construction and Selection: A*
 1992 *Data Mining Perspective* (pp. 101–116). Springer US.
 1993 https://doi.org/10.1007/978-1-4615-5725-8_7
- 1994 Ranck, J. B. (1973). Studies on single neurons in dorsal hippocampal
 1995 formation and septum in unrestrained rats: Part I. Behavioral
 1996 correlates and firing repertoires. *Experimental Neurology*, 41(2),
 1997 462–531. [https://doi.org/https://doi.org/10.1016/0014-4886\(73\)90290-2](https://doi.org/https://doi.org/10.1016/0014-4886(73)90290-2)
- 1999 Rescorla, R. A., & Wagner, A. (1972). A theory of Pavlovian
 2000 conditioning: Variations in the effectiveness of reinforcement and
 2001 nonreinforcement. In *Classical Conditioning II: Current Research*
 2002 and Theory: Vol. Vol. 2.
- 2003 Reyes, A. D. (2003). Synchrony-dependent propagation of firing rate in
 2004 iteratively constructed networks in vitro. *Nature Neuroscience*,
 2005 6(6), 593–599. <https://doi.org/10.1038/nn1056>
- 2006 Robbins, M., Christensen, C. N., Kaminski, C. F., & Zlatic, M. (2021).
 2007 Calcium imaging analysis - how far have we come?
 2008 *F1000Research*, 10, 258.
- 2009 Rogerson, T., Cai, D. J., Frank, A., Sano, Y., Shobe, J., Lopez-Aranda,
 2010 M. F., & Silva, A. J. (2014). Synaptic tagging during memory
 2011 allocation. *Nature Reviews Neuroscience*, 15(3), 157–169.
 2012 <https://doi.org/10.1038/nrn3667>
- 2013 Savelli, F., Yoganarasimha, D., & Knierim, J. J. (2008). Influence of
 2014 boundary removal on the spatial representations of the
 2015 medial entorhinal cortex. *Hippocampus*, 18(12), 1270–1282.
 2016 <https://doi.org/10.1002/hipo.20511>
- 2017 Scoville, W. B., & Milner, B. (1957). Loss of recent memory after
 2018 bilateral hippocampal lesions. In *Journal of Neurology,*
 2019 *Neurosurgery & Psychiatry* (Vol. 20, pp. 11–21). BMJ Publishing
 2020 Group. <https://doi.org/10.1136/jnnp.20.1.11>
- 2021 Shadlen, M. N., & Shohamy, D. (2016). Decision making and
 2022 sequential sampling from memory. *Neuron*, 90(5), 927–939.
- 2023 Shannon, C. E. (1948). A Mathematical Theory of Communication. *Bell*
 2024 *System Technical Journal*, 27(3), 379–423.
 2025 <https://doi.org/https://doi.org/10.1002/j.1538-7305.1948.tb01338.x>
- 2026 Siegel, J. J., & Mauk, M. D. (2013). Persistent Activity in Prefrontal
 2027 Cortex during Trace Eyelid Conditioning: Dissociating Responses
 2028 That Reflect Cerebellar Output from Those That Do Not. *The*
 2029 *Journal of Neuroscience*, 33(38), 15272 LP – 15284.
 2030 <https://doi.org/10.1523/JNEUROSCI.1238-13.2013>
- 2031 Siegel, J. J., Taylor, W., Gray, R., Kalmbach, B., Zemelman, B. V.,

- 2032 Desai, N. S., Johnston, D., & Chitwood, R. A. (2015). Trace
2033 Eyeblink Conditioning in Mice Is Dependent upon the Dorsal
2034 Medial Prefrontal Cortex, Cerebellum, and Amygdala: Behavioral
2035 Characterization and Functional Circuitry. *ENeuro*, 2(4),
2036 ENEURO.0051-14.2015. <https://doi.org/10.1523/ENEURO.0051-14.2015>
- 2037 Silva, A. J., Zhou, Y., Rogerson, T., Shobe, J., & Balaji, J. (2009).
2038 Molecular and cellular approaches to memory allocation in neural
2039 circuits. *Science (New York, N.Y.)*, 326(5951), 391–395.
2040 <https://doi.org/10.1126/science.1174519>
- 2041 Skaggs, W., McNaughton, B., Gothard, K., & Markus, E. (1996). An
2042 Information-Theoretic Approach to Deciphering the Hippocampal
2043 Code. *Neural Inf. Process Syst.*, 5.
- 2044 Solstad, T., Boccara, C. N., Kropff, E., Moser, M.-B., & Moser, E. I.
2045 (2008). Representation of Geometric Borders in the Entorhinal
2046 Cortex. *Science*, 322(5909), 1865–1868.
2047 <https://doi.org/10.1126/science.1166466>
- 2048 Souza, B. C., Pavão, R., Belchior, H., & Tort, A. B. L. (2018). On
2049 Information Metrics for Spatial Coding. *Neuroscience*, 375, 62–73.
2050 <https://doi.org/10.1016/j.neuroscience.2018.01.066>
- 2051 Stosiek, C., Garaschuk, O., Holthoff, K., & Konnerth, A. (2003). In vivo
2052 two-photon calcium imaging of neuronal networks. *Proceedings of
2053 the National Academy of Sciences of the United States of
2054 America*, 100(12), 7319–7324.
2055 <https://doi.org/10.1073/pnas.1232232100>
- 2056 Takehara, K., Kawahara, S., Takatsuki, K., & Kirino, Y. (2002). Time-
2057 limited role of the hippocampus in the memory for trace eyeblink
2058 conditioning in mice. *Brain Research*, 951(2), 183–190.
2059 [https://doi.org/10.1016/s0006-8993\(02\)03159-1](https://doi.org/10.1016/s0006-8993(02)03159-1)
- 2060 Tao, S., Wang, Y., Peng, J., Zhao, Y., He, X., Yu, X., Liu, Q., Jin, S., &
2061 Xu, F. (2021). Whole-Brain Mapping the Direct Inputs of Dorsal
2062 and Ventral CA1 Projection Neurons. *Frontiers in Neural Circuits*,
2063 15. <https://doi.org/10.3389/fncir.2021.643230>
- 2064 Taube, J. S., Muller, R. U., & Ranck, J. B. J. (1990). Head-direction
2065 cells recorded from the postsubiculum in freely moving rats.
2066 I. Description and quantitative analysis. *The Journal of
2067 Neuroscience : The Official Journal of the Society
2068 for Neuroscience*, 10(2), 420–435.
2069 <https://doi.org/10.1523/JNEUROSCI.10-02-00420.1990>
- 2070 Thompson, R. F. (2004). In Search of Memory Traces. *Annual Review
2071 of Psychology*, 56(1), 1–23.
2072 <https://doi.org/10.1146/annurev.psych.56.091103.070239>
- 2073 Tishby, N., Pereira, F. C., & Bialek, W. (1999). The information

- 2075 bottleneck method. *Proc. of the 37-Th Annual Allerton Conference*
2076 *on Communication, Control and Computing*, 368–377.
2077 <https://arxiv.org/abs/physics/0004057>
- 2078 Vaidya, A. R., Pujara, M. S., Petrides, M., Murray, E. A., & Fellows, L.
2079 K. (2019). Lesion Studies in Contemporary Neuroscience. *Trends*
2080 *in Cognitive Sciences*, 23(8), 653–671.
2081 <https://doi.org/https://doi.org/10.1016/j.tics.2019.05.009>
- 2082 Valero, M., Cid, E., Averkin, R. G., Aguilar, J., Sanchez-Aguilera, A.,
2083 Viney, T. J., Gomez-Dominguez, D., Bellistri, E., & de la Prida, L.
2084 M. (2015). Determinants of different deep and superficial CA1
2085 pyramidal cell dynamics during sharp-wave ripples. *Nature*
2086 *Neuroscience*. <https://doi.org/10.1038/nn.4074>
- 2087 van der Maaten, L., Postma, E., & van den Herik, H. (2009).
2088 Dimensionality reduction: a comparative review. *Journal of*
2089 *Machine Learning Research*, 66–71.
- 2090 Velasco, M. G. M., & Levene, M. J. (2014). In vivo two-photon
2091 microscopy of the hippocampus using glass plugs. *Biomedical*
2092 *Optics Express*, 5(6), 1700–1708.
2093 <https://doi.org/10.1364/BOE.5.001700>
- 2094 Voelcker, B., Pancholi, R., & Peron, S. (2022). Transformation of
2095 primary sensory cortical representations from layer 4 to layer 2.
2096 *Nature Communications*, 13(1), 5484.
2097 <https://doi.org/10.1038/s41467-022-33249-1>
- 2098 Wood, E. R., Dudchenko, P. A., Robitsek, R. J., & Eichenbaum, H.
2099 (2000). Hippocampal Neurons Encode Information about Different
2100 Types of Memory Episodes Occurring in the Same Location.
2101 *Neuron*, 27(3), 623–633.
2102 [https://doi.org/https://doi.org/10.1016/S0896-6273\(00\)00071-4](https://doi.org/https://doi.org/10.1016/S0896-6273(00)00071-4)
- 2103 Yiu, A. P., Mercaldo, V., Yan, C., Richards, B., Rashid, A. J., Hsiang,
2104 H.-L. L., Pressey, J., Mahadevan, V., Tran, M. M., Kushner, S. A.,
2105 Woodin, M. A., Frankland, P. W., & Josselyn, S. A. (2014).
2106 Neurons are recruited to a memory trace based on relative
2107 neuronal excitability immediately before training. *Neuron*, 83(3),
2108 722–735. <https://doi.org/10.1016/j.neuron.2014.07.017>
- 2109 Zhou, Y., Won, J., Karlsson, M. G., Zhou, M., Rogerson, T., Balaji, J.,
2110 Neve, R., Poirazi, P., & Silva, A. J. (2009). CREB regulates
2111 excitability and the allocation of memory to subsets of neurons
2112 in the amygdala. *Nature Neuroscience*, 12(11), 1438–1443.
2113 <https://doi.org/10.1038/nn.2405>
- 2114 Ziv, Y., Burns, L. D., Cocker, E. D., Hamel, E. O., Ghosh, K. K., Kitch,
2115 L. J., El Gamal, A., & Schnitzer, M. J. (2013). Long-term dynamics
2116 of CA1 hippocampal place codes. *Nature Neuroscience*, 16(3),
2117 264–266. <https://doi.org/10.1038/nn.3329>

2118 **Chapter 2 – Behaviour**

2119

2120 **Towards understanding brain activity in a**
2121 **reproducible context**

2122

2123 Our understanding of memory and learning depends upon the type of
2124 learning that is studied (Schreurs, 1989). Two important categories of
2125 memory and learning experiments are,

- 2126 1. Non-associative (Habituation and Sensitization), and
2127 2. Associative learning (Classical and Operant Conditioning).

2128

2129 Non-associative learning paradigms provide information about how an
2130 organism responds to repeated presentations of a single stimulus
2131 (Brown, 1998). However, it was of interest to us to study how animals
2132 responded to a number of events and stimuli being associated, and
2133 how the activity of the brain relates to this. **Multi-modal stimulus**
2134 **integration is typical of the sensory experience. We felt it interesting to**
2135 **study how animals learnt to associate each stimulus modality,**
2136 **individually, given no clear *a priori* reason to assume that the**
2137 **physiological response would be identical for each.** Hence, we chose
2138 to design our experiments to incorporate associative learning, which is
2139 a relatively permanent change in behaviour that results from the
2140 temporal conjunction of two or more events or stimuli.

2141

2142 Empirically, reproducible behaviour depends on strong associations
2143 between the events or stimuli being paired, and may often require

2144 many repeated pairings or trials. Additionally, having the animal
2145 engage in the behavioural task and pay attention to the stimuli being
2146 presented, is crucial to look for important correlations between the
2147 experiment conditions (external) and brain activity (internal).
2148

2149 Anaesthetized animals have been previously used to study brain
2150 activity and led to important discoveries, e.g. - visual representation of
2151 moving bars in the visual cortex (Hubel & Wiesel, 1962), habituation in
2152 the Hippocampus (Deshmukh & Bhalla, 2003). However, it was clear
2153 that similar experiments repeated in awake animals did not result in the
2154 same observations. Indeed, animals needed to navigate a known
2155 environment before the discovery of place cells (O'Keefe &
2156 Dostrovsky, 1971), grid cells (Fyhn et al., 2004; Hafting et al., 2005),
2157 and head-direction cells (Ranck, 1973; Taube et al., 1990), among
2158 others, could be made. **We chose to avoid anaesthetized animals for**
2159 **the experiments described in this thesis. It is unclear if deep states of**
2160 **anaesthesia are also conducive to time cell sequence activation.**
2161 **Additionally, even if some form of sequential activity may be in effect**
2162 **during anaesthetic states, it would be very difficult to implicate**
2163 **physiological relevance without appropriate experimental modulations**
2164 **in a behavioural context.**

2165

2166 The reliability of the overt behavioural responses of the experiment
2167 animals then sets the conditions and parameter list to study physiology
2168 within the confines of reproducible behavioural contexts, and was
2169 considered an important mandate for the standardization of any of the
2170 behavioural tasks described in this chapter. Under the umbrella of
2171 associative learning, we began our experiments with various protocols
2172 related to operant conditioning wherein the reinforcing signal for

2173 learning was a water reward to correctly timed licks. As will be
2174 discussed in the next few sections, we later switched to aversive
2175 conditioning with Trace Eye-Blink Conditioning.

2176 **Operant conditioning [Project I]**

2177

2178 Operant conditioning is both the procedure and a type of associative
2179 learning process through which the strength of a voluntarily performed
2180 behaviour is modified positively (appetitively) by reward (water,
2181 sucrose, food, etc.), or negatively (aversively) by punishment (air-puff
2182 to the eye, electrical shocks, etc.). For example, if the animal responds
2183 to a presented stimulus by performing a lick onto a water spout, then a
2184 water reward would strengthen the behaviour while Lithium Chloride
2185 solution (which is aversive) would weaken it.

2186

2187 We now describe our experiments and results with regard to operant
2188 conditioning, in more detail.

2189

2190 **Required features**

2191

2192 For Project I, the goal was to study how the association of a neutral
2193 stimulus with a water reward modified the neurophysiological activity of
2194 the hippocampal CA1. **We aimed to more systematically study time**
2195 cells with the granularity of well-defined associative learning and ms
2196 resolution, high-yield (~100-150) CA1 recordings using 2-photon
2197 imaging. We believe this is why there is still insufficient clarity on the
2198 network level responses in the CA1, *in vivo*, especially during early

2199 learning of associated stimuli, *i.e.*, behavioural acquisition. We outline
2200 our set of core objectives required as features for the behavioural task:
2201 1. An assortment of different stimuli and modalities (light, tone, etc.)
2202 to be presented to the animal.
2203 2. The animal must withhold any motor movement during the
2204 presentation of the stimuli, to study pure stimulus responses.
2205 3. The animal must perform a lick for a water reward after the end of
2206 the stimulus presentation.
2207 4. The animal must be able to make the association between stimuli
2208 and water reward within 7-14 days of training (given technical
2209 limitations of chronic recording from tissue).

2210

2211 The behavioural state of the animal, in terms of anxiety, motivation,
2212 attention, etc., may be variable when a naïve animal is presented with
2213 different stimuli. This may cause a large variability in the activity of
2214 cells, since the animal may not be paying attention to it. Also, if the
2215 animal were rewarded for performing the task it is expected that there
2216 would be motivation to pay attention to the stimuli presented. Finally,
2217 such a task would involve the animal associating the stimuli that it is
2218 trained to with a behavioural task and this would provide an apt context
2219 to study association related changes in stimulus responses.

2220

2221 In the following sections, we discuss some important protocols that we
2222 tried and tested and a list of the various kinds of behavioural tasks we
2223 employed for head-fixed mice.

2224

2225 For Project I, we tried several variations of operant conditioning
2226 including Stimulus Detection tasks, Delayed Non-Match to Sample
2227 (DNMS), as well as Go/No-Go tasks. Each of these tasks requires

2228 animals to perform licks to the Conditioned Stimuli and for them to be
2229 rewarded (2-3 μ L water) or punished based on the task demands and
2230 protocol design.

2231 **Water delivery and calibration**

2232 The lick port was made from a trimmed and smoothed 16 gauge
2233 syringe, connected to a water reservoir with small diameter tubing. A
2234 solenoid valve clamped onto this tubing, gated by a 12V DC signal.
2235 When this gate was opened, the volume of water could be regulated by
2236 the duration of the 12V DC signal. We calibrated the duration of gate
2237 opening to achieve ~2 μ L per pulse or spurt (Jaramillo & Zador, 2014).
2238 The weight of 100 spurts was measured and then divided by 100 to get
2239 the weight of 1 spurt. 65 ms was found corresponding to 2.5 μ L (this
2240 value is going to be used for behaviour). In the figure below (Figure 2),
2241 the measured volumes/weights are plotted as blue filled diamonds,
2242 error bars are presented as Standard Error and the linear trendline is
2243 shown in black.

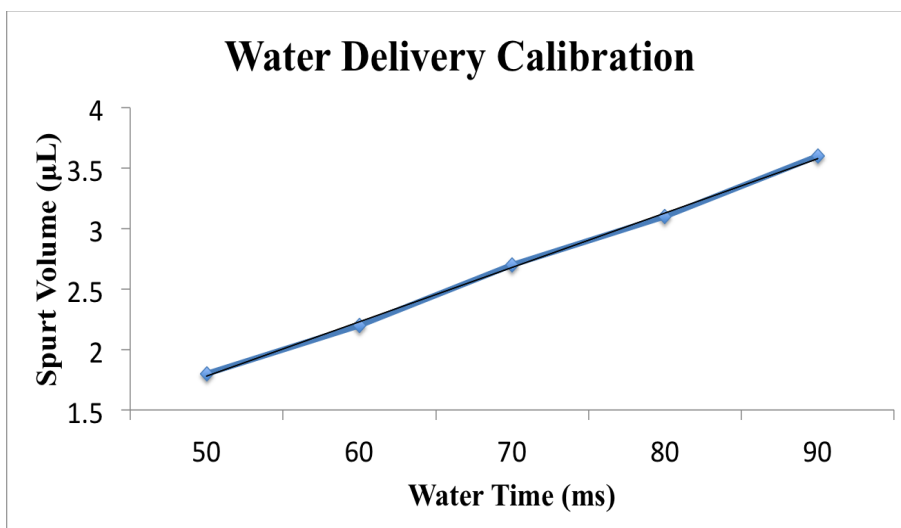


Figure 2: Water delivery calibration to reward the animal consistently with the same volume of water.

2244 **Opto-islator circuit for solenoid control**

2245

2246 To be able to programmatically control the 12V DC line to the solenoid
2247 valve, we used the following circuit (Figure 3), which accepted a 5V
2248 digital input from the DAQ (NI USB-6001) interfacing the lab computer
2249 to the behaviour rig.

2250

2251 **Parts list**

- 2252 1. 470 ohm resistor
- 2253 2. 15 kohm resistor
- 2254 3. MCT2e
- 2255 4. ULN2003
- 2256 5. Bases (adaptors for MCT2e and ULN2003)
- 2257 6. +5V and +12V DC inputs from a Power Supply)
- 2258 7. Source of +5V DC input (DAQ, etc.)
- 2259 8. Connecting wires
- 2260 9. Load Resistance (Solenoid, etc.)

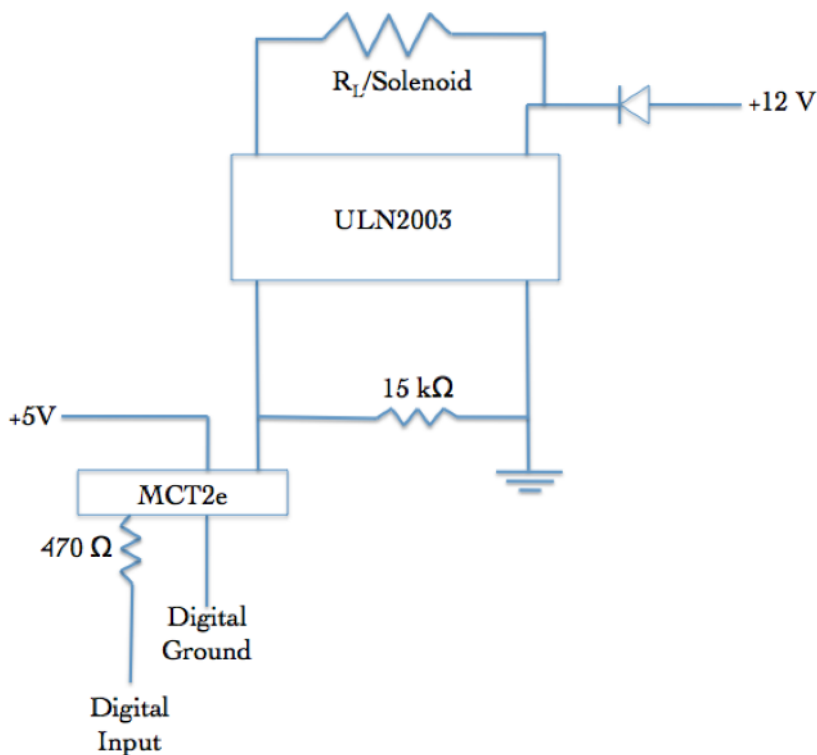


Figure 3: Optoisolator circuit to amplify +5V DC input to +12V DC output.

2262

2263 **Lick detection circuit**

2264

2265 To be able to monitor the presence or absence of licks to the port, the
 2266 conductive part (metal) of the lick port syringe was connected to a
 2267 MOSFET such that a 5V DC voltage could be read out, whenever the
 2268 animal would make contact with the port. This was designed as a
 2269 readout to Stimulus Detection by the animal. The circuit diagram is
 2270 shown below (Figure 4):

2271

2272 **Parts list**

2273 1. +5V Power Supply

2274 2. 4.7 kohm resistor
2275 3. 22 Mohm resistor
2276 4. IN4007 Diode
2277 5. NPN Transistor IRF540N (MOSFET)
2278

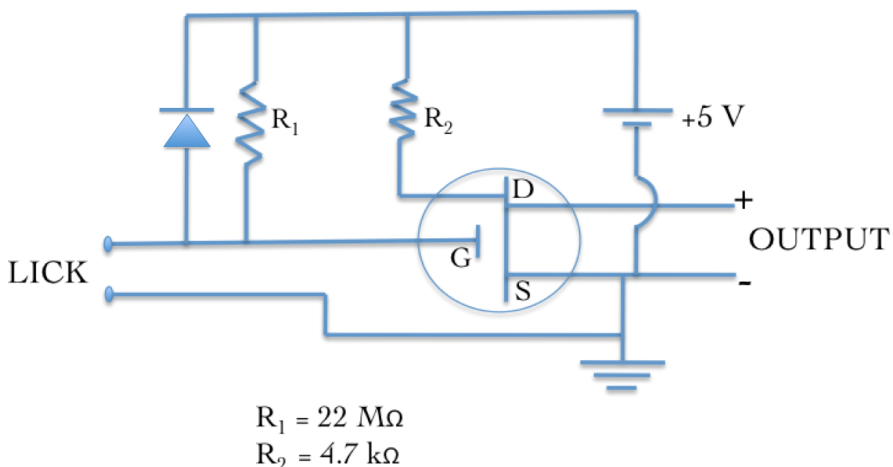


Figure 4: Lick detector circuit based on a MOSFET design.
Whenever the animal performed a lick, a +5V DC Output would be read out.

2280 **Controlling task details and protocol information**

2281
2282 All protocols were controlled using custom scripts written in NI
2283 LabVIEW 8. These scripts were run on a lab desktop which interfaced
2284 with the DAQ (NI USB-6001) via USB. The DAQ,
2285 1. Sent the 5V digital input to switch on the solenoid valve
2286 regulating water delivery, and
2287 2. Received the 5V digital output of the lick detection circuit
2288 whenever a lick was produced by the animal.
2289

2290 **Head-bar implant, Animal Handling, and Water**
2291 **deprivation**

2292

2293 All experiments were planned to be conducted on head-fixed C57Bl/6
2294 mice, with the eventual intention to perform in vivo imaging on these
2295 animals. For this, we surgically implanted metal head-bars on the skull
2296 of the animals while they were maintained on 1-2% Isoflurane, above a
2297 heating pad (35°C). Surgeries would last no longer than 30 mins per
2298 animal.

2299

2300 After 1-7 days of recovery after surgery, we handled the animals gently
2301 for 2 days till the animals would appear comfortable with lifting and
2302 gentle collar grabbing. Next, for 3-4 days, we kept the animals head-
2303 clamped. We restricted our animals to ~1ml of water per day, keeping
2304 check that their body weight did not fall to below 80% of the weight on
2305 day 1.

2306

2307 **PROTOCOL 1.1: Stimulus Detection Task**

2308

2309 We first tried the simplest version of the lick task wherein an auditory
2310 tone was followed by a water reward. The animal would have to
2311 withhold licking till the end of the stimulus presentation, and then
2312 perform the lick for the reward (Figure 5).

2313

2314 **Total number of trials:** 600/session; 1 session/day

2315 **Trial phases:**

2316 1. Stimulus free pre-tone (PT): 1 s

2317 2. Tone: 5 kHz for 1 s
2318 3. Critical timeout (CT): 100 ms
2319 4. Inter-trial Interval (ITI): randomized between 2 s to 5
2320



Figure 5: Typical trial structure with the various phases. Each trial was followed by a randomized Inter-Trial Interval (ITI).

2325

2326 Only licks during the critical timeout (CT) phase immediately after the
2327 Tone phase were rewarded while licks in other phases resulted in a
2328 phase restart. **No aversive stimuli were presented in this particular
2329 protocol.**

2330

**2331 PROTOCOL 1.2: Stimulus Detection Task with aversive
2332 punishment**

2333

2334 **Total number of trials:** 600/session; 1 session/day

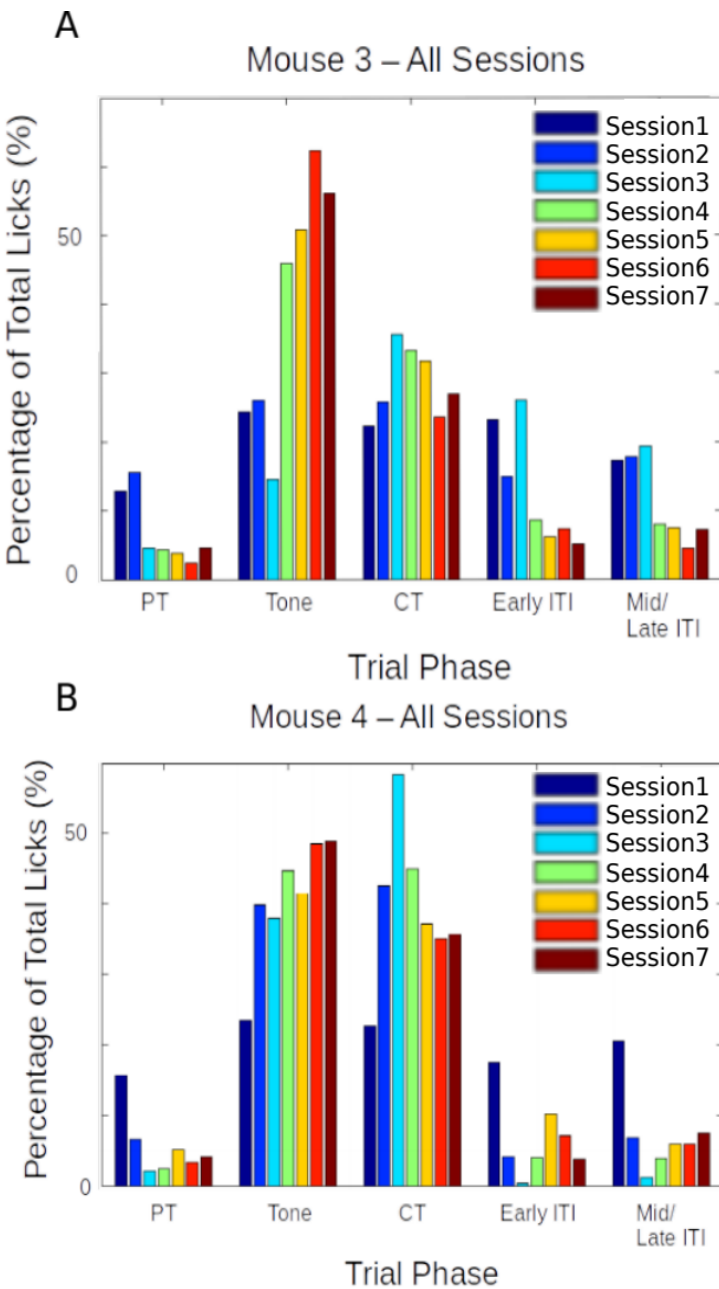


Figure 6: Performance evaluation for two example mice trained to Protocol 1.1 and 1.2. Percentage of total licks in the various trial phases (Pre-Tone, Tone, CT, and ITI), across all sessions of training (coloured bar plots) for A) Mouse 3, and B) Mouse 4.

2339 Only licks during the critical timeout (CT) phase immediately after the
2340 Tone phase were rewarded while licks in other phases resulted in an
2341 aversive punishment, *viz.*, 100 ms air-puff to the body of the animal,
2342 before a phase restart. For Mouse 3 we started Protocol 1.2 from
2343 Session 3 while for Mouse 4 we started Protocol 1.2 from Session 2.

2344 **Results – Protocols 1.1 and 1.2**

2345
2346 The behavioural performance for each of the experiment animals was
2347 evaluated using custom analysis scripts written in MATLAB 2011. Here
2348 are the results from two mice trained based on Protocols 1.1 and 1.2
2349 (Figure 6). In both the examples shown, animals would typically
2350 produce a great percentage of total licks even during the Tone period.
2351 **Each animal was presented with 600 training trials/day (1 session/day).**
2352 **Protocols 1.1 and 1.2 were prototyping experiments by design. Given**
2353 **the nature of our results, we decided to abort these protocols in favour**
2354 **of more structured, less aversive protocols, as described in the next**
2355 **few sections. The inability of our mice to behaviourally discriminate or**
2356 **withhold incorrect or unrewarded licks even for 7-14 sessions was**
2357 **considered, and the task was ultimately deemed unsuccessful.**

2358

2359 **Total animals trained:** 2

2360 **Conclusion:** Aborted

2361

2362 **Protocol 2: Stimulus Detection task with timeout box**

2363

2364 We also tried the same Stimulus Detection protocol, without an air-puff
2365 punishment, but with incorrect licks punished by a trial abort and a

2366 stimulus-free timeout phase, which the animal could escape from if it
2367 withheld licking. We decided to train the animals in blocks, each with a
2368 specific goal that the animal had to achieve.

2369

2370 **Trial phases:**

2371 1 Stimulus-free pre-tone (PT): 1 s

2372 2 Tone: 5 kHz for a variable duration (based on Block)

2373 3 Critical timeout (CT): 1000 ms

2374 4 Inter-trial Interval (ITI): randomized between 2 s to 5 s

2375

2376 Only licks during the critical timeout (CT) phase immediately after the
2377 Tone phase were rewarded while licks in other phases resulted in a
2378 phase restart.

2379

2380 **Block 1:** Unconditional Water to get the animal to associate the tone

2381 - ~20 trials

2382 - 100 or 200 ms Tone duration

2383 - Unconditional water provided at the end of the tone, irrespective of

2384 lick

2385

2386 **Block 2:** Conditional Water to get the animal to learn that licking

2387 with/after tone is going to be rewarded

2388 - 100 or 200 ms Tone duration

2389 - 1000 ms Reward phase

2390 - Lick during/after tone (Reward phase) = reward

2391 - No lick = no reward

2392 - Lick during pre-tone = no reward/abortion of trial

2393 - Lick during ITI = no reward/abortion of trial

2394 - Animals graduate to the next Block of training only after achieving at
2395 least 70-80% success rates

2396

2397 **Block 3:** Training the animal to learn "when" to lick

2398 - 1000 ms pre-tone, 100 or 200 ms Tone, 1000 ms Reward phase, 3-5
2399 s randomized ITI

2400 - Lick during Reward phase = reward

2401 - Any lick during the pre-tone or the tone, aborts the trial and sends the
2402 program to a Timeout phase (lasting, 2-3 s)

2403 - The timeout phase ends only when there is a 2-3 s (specified) interval
2404 of no licking

2405 - If the timeout phase ends, a new trial begins

2406 - Licks during ITI are also "punished" accordingly

2407 - Animals graduate to the next Block of training only after achieving 70-
2408 80% success rates

2409

2410 **Block 4:** Same as Block 3, but with a gradually increasing tone
2411 duration in steps of 50/100 ms

2412 - The tone duration is gradually increased, the increase being tailored
2413 to the performance of the animal

2414 - It will be attempted to get the animals to learn to wait for 500-700 ms

2415 - Animals graduate to the next Block of the experiment only after
2416 achieving 70-80% success rates

2417

2418 **Results – Protocol 2**

2419

2420 The behavioural performance for each of the experiment animals was
2421 evaluated using custom analysis scripts written in MATLAB. Here are
2422 two representative examples of mice trained based on Protocol 2 –
2423 Block 3 (Figure 7).

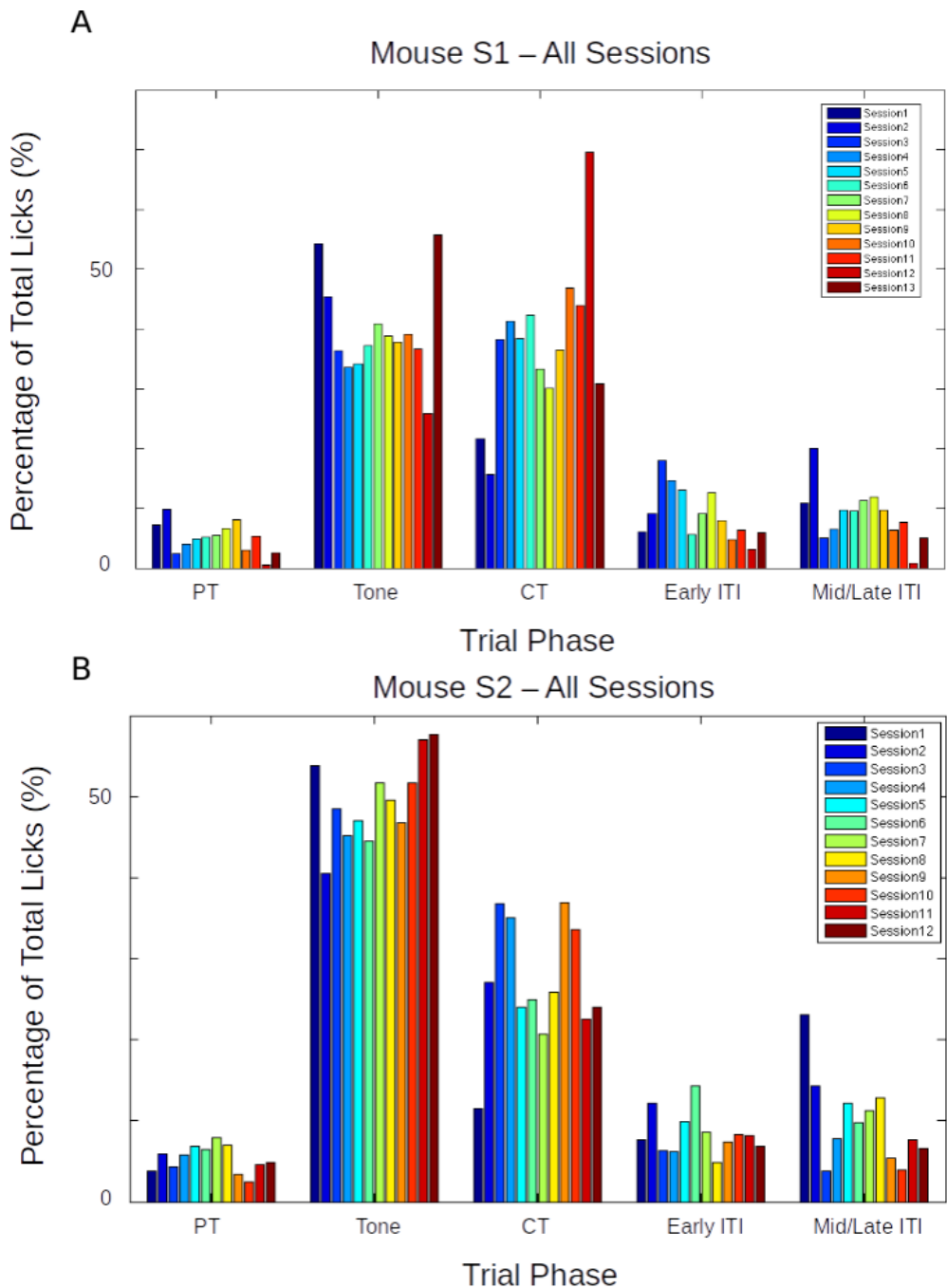


Figure 7: Performance evaluation for two example mice trained to Protocol 2. Percentage of total licks in the various trial phases (Pre-Tone, Tone, CT, and ITI), across all sessions of training (coloured bar plots), for (A) Mouse S1, and (B) Mouse S2.

2425 Again, as is clear from the examples above, that while the mice
2426 eventually produced a decent percentage of total licks in the critical
2427 timeout (CT) phase to get a water reward, they did not learn to
2428 withhold licks during the Tone phase, even after >10 sessions. The
2429 task was ultimately unsuccessful.

2430

2431 **Total animals trained:** 4

2432 **Conclusion:** Fail

2433

2434 **Protocol 3: Delayed Non-Match to Sample (DNMS)**

2435

2436 Delayed Non-Match to Sample (DNMS) is a task that is ideally suited
2437 to study working memory and recognition (Chudasama, 2010), but we
2438 decided to try it. This task involves trial-by-trial presentation of two
2439 stimuli separated by a stimulus-free delay interval. For any given trial,
2440 If the two pseudorandomly chosen pairs of stimuli were identical, then
2441 licks would not be rewarded. However, if the pair of stimuli were
2442 different, then licks would be rewarded with 2 μ L water.

2443

2444 We referenced previously published protocols (Jaramillo & Zador,
2445 2014) for their selection of auditory tone frequencies (3 kHz - 16.3 kHz)
2446 to select frequencies in the audible range. We had designed the
2447 experiment in such a way that the animal could behaviourally express
2448 a response to the perception of the various stimuli presented, as well
2449 as having learnt the overall task. We tried to incorporate more tones, in
2450 the hope that this may improve the chances of the animals focusing on
2451 the task specifics, instead of producing licks to just any stimulus.

2452

2453 **Tones used:** 6000 Hz, 8500 Hz, 10000 Hz, and 11500 Hz

2454 **Trial phases:**

2455 1. Pre-Tone duration (ms): 1000 ms

2456 2. CS 1 duration (ms): 350 ms

2457 3. Delay Interval duration (ms): 250 ms

2458 4. CS 2 duration (ms): 350 ms (unless a correct lick is
2459 elicited)

2460 5. ITI duration (s): randomized from 1 s to 3 s

2461 **Punishment:** Timeout Box (minimum of 3s of no licks to escape)

2462 **Reward:** 2 µL of water

2463

2464 **Results – Protocol 3**

2465

2466 >70-80% of the trials had to be aborted because the animals would not
2467 withhold licking after the 1st of the pair of tones was presented. This
2468 did not change even after 7 days (sessions) of training.

2469

2470 **Total animals trained:** 6

2471 **Conclusion:** Fail

2472

2473 **Protocol 4: Go/No-Go Task**

2474

2475 In an attempt to simplify the behavioural task, we decided to
2476 reconfigure the DNMS task to a simpler Go/No-Go task. Here, we
2477 would again present the animal with two stimuli, but with the only

2478 condition being that the animal would have to lick after the second
2479 stimulus, and not before. This simplifies the behaviour to a certain
2480 extent, because the animals need only use the first stimulus as a cue
2481 for the second. Failure to perform this task could more easily then be
2482 attributed to a lack of attention in that trial. Only the data from the trials
2483 where the animal succeeds to do the task would be considered for
2484 analysis. Training related changes in actual stimulus representations
2485 would be carefully dissected out. Furthermore, such a task would
2486 control for the behavioural state of the animal and help provide
2487 important datasets.

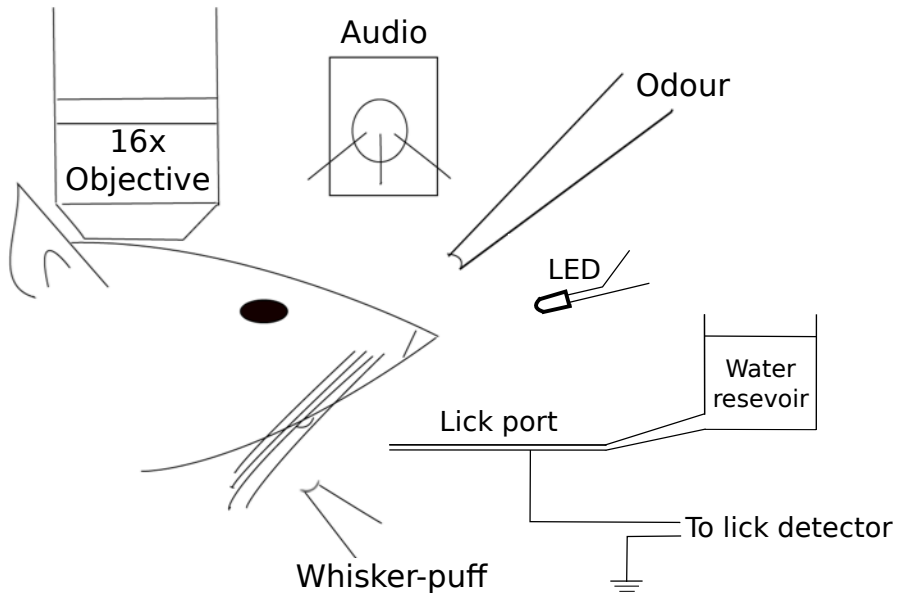


Figure 8: Schematic representation of the experimental setup for a simple detection task where the animal must perform a lick upon correctly detecting the presence of the conditioned stimulus (CS; from a range of modalities).

2492 In terms of imaging, we hoped to use the no-go stimulus to record a
2493 clean stimulus response without the possible contamination of
2494 movement (licking behaviour), and the go stimulus to verify attention
2495 (Figure 8).
2496 Trials were designed to go through the following phases and have the
2497 animal graduate to subsequent phases, only after correctly performing
2498 the behaviour:
2499 1. Pre-tone: Stimulus-free period; no lick
2500 2. No-go tone: 7kHz tone period; no lick
2501 3. Go tone: 10kHz tone period; lick for reward
2502 If the animal would perform an incorrect lick, the particular phase
2503 currently occurring was restarted. Only licks to the Go tone were
2504 rewarded (Figure 9).

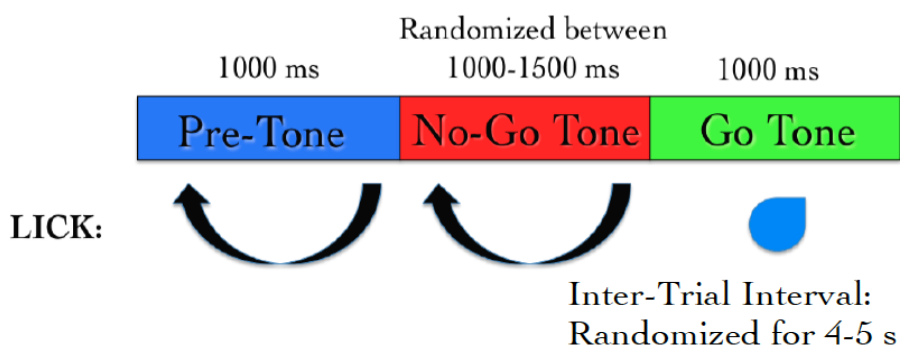


Figure 9: Typical trial structure with the various phases and lick dependent relationships.

2505

2506 **Results – Protocol 4**

2507
2508 The behavioural performance improves only after ~3-4 sessions of
2509 training (Figure 10A). This is primarily due to an increase in the
2510 percentage of trials with a correct Go tone lick, as shown (Figure 10B).

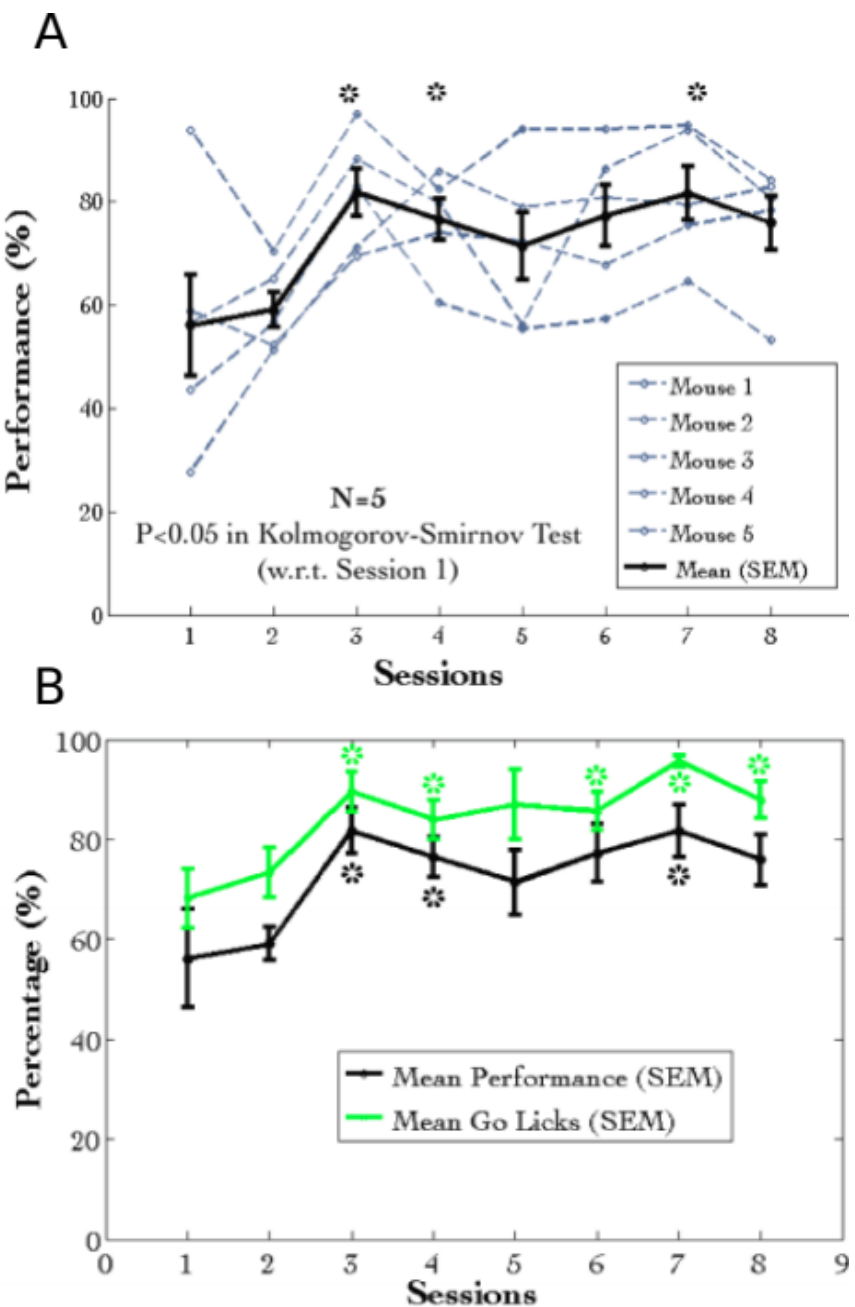


Figure 10: (A) Performance traces for all the animals individually shown in dashed grey lines. Mean + SEM in black. (B) Mean Performance (%) and Mean Go Tone Lick Percentage (%) with Session for the Go/No-Go Task, plotted in black and green, respectively.

2514 A plot of the lick histogram for the various trial phases revealed that
2515 despite reaching the maximum success rate, the animals continued to
2516 lick during the no-go tone phase (incorrect lick) for a long duration of
2517 time (Figure 11). There was no difference in the amounts of time spent
2518 in the pre-tone or no-go tone phases. This suggested that the animals
2519 did not discriminate between the Go and no-go tones. Accordingly, the
2520 current protocol was not being learnt as expected.

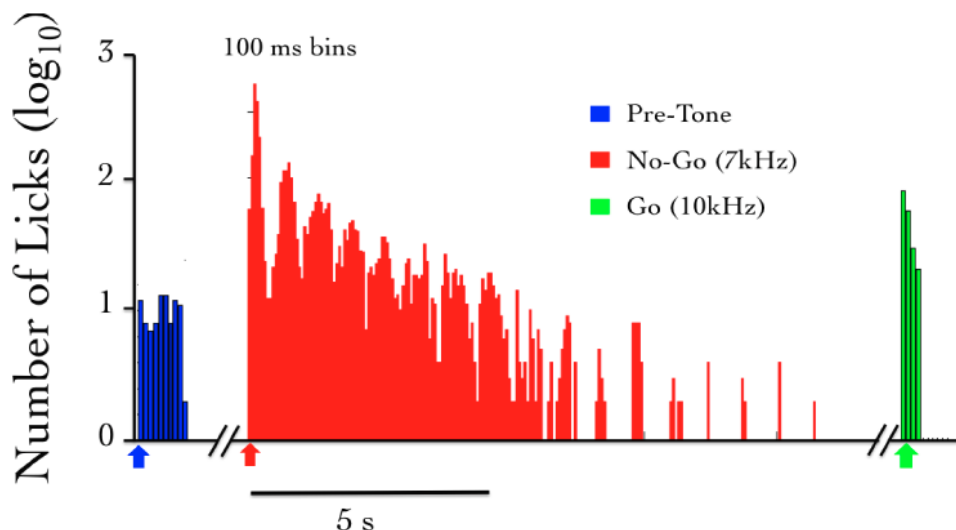


Figure 11: The number of licks in the pre-tone (blue), no-go tone (red), and go tone (green) phases, in a representative animal, in a session with maximum Performance (%).

2521
2522 We were not able to get discriminatory detection. Animals would resort
2523 to performing licks continuously and agnostically, to the go and no-go
2524 stimulus. In a study published many years later, it was determined that
2525 discriminatory tasks such as the one described above, could often
2526 require 3-4 weeks of training (Guo et al., 2014), since the animal was
2527 not punished with anything more than a delay or phase restart.

2528

2529 **Total animals trained:** 5

2530 **Conclusion:** Fail

2531 **Operant conditioning experiments failed to match**
2532 **behavioural requirements**

2533

2534 Operant conditioning tasks have been extensively and successfully
2535 modeled in a variety of laboratories. For our specific experiments, we
2536 required a task that could be learnt within 1-2 weeks. This was
2537 because we were not confident on how many simultaneous days of
2538 chronic imaging, we could achieve with the *in vivo* chronic 2-photon
2539 calcium imaging preparation (see Chapter 3 – “Imaging”). Additionally,
2540 it typically takes 3-4 weeks for head-fixed rodents to acquire sufficient
2541 expertise in behavioural performance for Operant Conditioning tasks,
2542 *viz.*, behavioural discrimination - to lick to the rewarded stimulus and
2543 withhold licks for non-rewarded stimuli or incorrect trial phases (Guo et
2544 al., 2014). Some animals have been reported to learn such tasks within
2545 1 week of training (Guo et al., 2014), but we did not observe this with
2546 our implemented protocols.

2547

2548 One alternative that we could have tried was to train the animals to
2549 expert levels of performance, and subsequently performed the
2550 hippocampus prep. The issue(s) with this is that,
2551 a) We wanted to study the hippocampal CA1 network during the
2552 learning or acquisition phase of behavioural training, as a distinct
2553 experiment from those published in literature.
2554 b) In such a protocol, we would require two separate surgeries, *viz.*, i)
2555 Head-bar implant, and, ii) hippocampus preparations. This, we
2556 believed would increase the technical difficulty of the overall
2557 experiment and could be more stressful for the experiment animals.

2558 c) We suspected that there could be unknown effects on behavioural
2559 performance, post-surgery, complicating the analysis and insights we
2560 aimed to study.

2561

2562 Across all Operant Conditioning protocols attempted, we could not
2563 observe behavioural discrimination (not licking to incorrect phases)
2564 within 1-2 weeks of training. We considered the experiments as
2565 failures, in line with this reasoning.

2566

2567 Eventually, we had to abandon these experiments, to switch to an
2568 aversive conditioning task, *viz.*, Trace Eye-Blink Conditioning (TEC).
2569 With the change in the main behavioural task we also changed the
2570 project goals. The TEC task was standardized with the intention to
2571 work on Project II which is to study how animals make complex
2572 associations between different types of stimuli and how they adapt to
2573 changes to the inter-stimulus interval (ISI).

2574 **Trace Eye-Blink Conditioning [Project II]**

2575

2576 We have introduced the Trace Eye-Blink conditioning paradigm in
2577 Chapter 1 – “Introduction”, but some key definitions and results require
2578 mention. Eye-blink Conditioning is a class of Classical Conditioning
2579 and requires the presentation of a neutral stimulus (Conditioned
2580 Stimulus, CS) along with an eye-blink eliciting, mildly aversive stimulus
2581 (Unconditioned Stimulus, US). Depending on whether the CS
2582 presentation overlaps with the US presentation or if the two stimuli are
2583 separated by a stimulus free interval in between (Trace interval), the
2584 concomitant procedure is called Delay Conditioning or Trace

2585 Conditioning, respectively (Figure 12). In either case, precise timing of
2586 the CS and US is mandated.

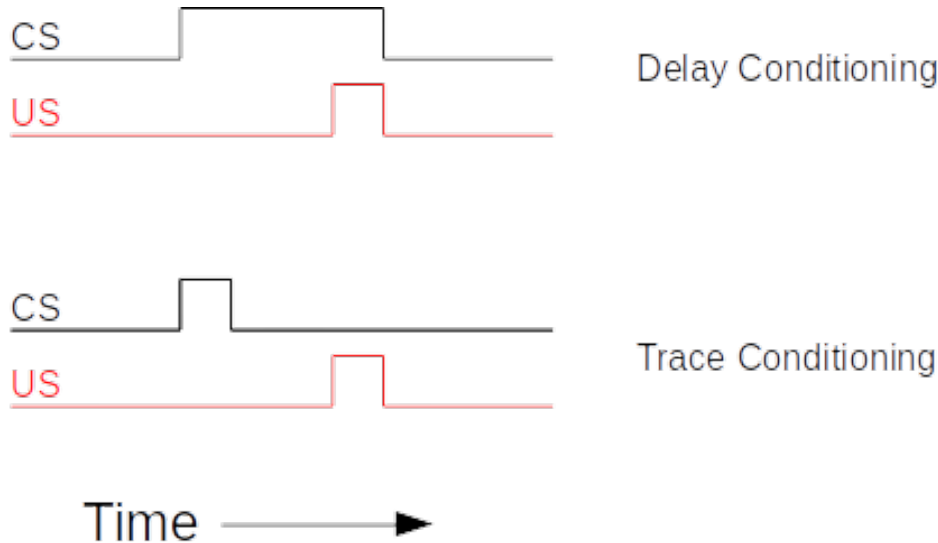


Figure 12: Schematic representation to showcase the two main subtypes of Classical Conditioning (Eye-Blink Conditioning, for our experiments) based on the relative timing and presentation of the CS and US.

2587
2588 The CS is usually an auditory tone or a visual stimulus (e.g.- LED
2589 Flash), while the US is typically a mild air-puff to the cornea, or a
2590 gentle electric shock to the eye-lid. Naive animals (rabbits, rodents,
2591 monkeys, etc.) produce a robust, reflexive eye-blink to the US
2592 (Unconditioned Response or UR) and ignore the CS, in early trials.
2593 However, with repeated pairing of CS and US, the animals are able to
2594 associate the two, and use the CS as a cue to predict the US,
2595 producing a partial, preemptive eye-blink just before the expected time
2596 of the US (Conditioned Response or CR). The CR develops in
2597 amplitude over multiple pairings or training sessions. In well trained
2598 animals, the CR begins at a time point closer and closer to the CS

2599 onset, and usually merges with the UR. The animals produce this CR
2600 in an attempt to avoid the US.

2601

2602 Traditionally, Trace Eye-Blink Conditioning has been an important
2603 hippocampus-dependent behavioural task, and has been adapted to a
2604 variety of different species, spanning rabbits, rats, and mice.

2605

2606 Damage or inhibition of the hippocampus has been shown to limit task
2607 acquisition without affecting other non-hippocampus dependent tasks
2608 such as Delay Conditioning. In an experiment, Ibotenic Acid was used
2609 in a session dependent fashion, to observe both limitations in first
2610 acquiring the Trace Conditioning task, as well as detriments to
2611 behavioural recall, even after animals learn the task to a high degree of
2612 proficiency, suggesting the pivotal role that the hippocampus plays in
2613 temporal tasks of this nature (Tseng et al., 2004).

2614

2615 A single session of Trace Eye-Blink Conditioning, with strong stimuli
2616 (CS and US), has been previously employed (Modi et al., 2014), but
2617 with only upto 50% of the animals learning the task. Typically animals
2618 require around 3-7 sessions (~200-600 trials) to robustly learn the task.
2619 Accordingly, we designed and standardized a multi-session version of
2620 TEC, to allow more animals to learn and acquire the task, based on
2621 previously published work (Siegel et al., 2015).

2622

2623 **Tracking eye-blink responses**

2624

2625 The most foolproof way to track eye-blink responses (especially with
2626 head-fixed animals) chronically (for multiple sessions across days), is

2627 to use a video camera. We used a Point Grey Chameleon3 1.3 MP
2628 Monochrome USB3.0 camera) for this purpose. It is cost effective and
2629 with proper scaling of the resolution and field of view, can achieve
2630 recording rates of >200 frames per second (FPS). An important criteria
2631 for getting faster frame rates is to have better illumination, so that the
2632 camera may be set to lower exposure settings. We used a set of 5-10
2633 Red colour LEDs as the light source, and these are run using a 12V
2634 DC line, with current limited resistors in series. Additionally, we used
2635 an IR-blocking filter to avoid capturing the 2-Photon excitation light
2636 (910-920 nm) when conduction behaviour and imaging experiments
2637 simultaneously. Finally, to focus the light from the eye of the animal
2638 onto the camera sensor, we used a Tamron M118FM16 lens (1/1.8,
2639 16mm F/1.4).

2640 **Treadmill and tracking running speed**

2641

2642 Allowing the head-fixed animals to run on a treadmill was an important
2643 behaviour rig consideration, as this allows the animals to be more
2644 engaged and less stressed **during experiments** (Siegel et al., 2015).
2645 **We considered treadmill tracking as a relevant variable to keep track**
2646 **of, despite the potential complications this could provide to imaging,**
2647 **viz., z-axis drift owing to relative motion between the brain tissue and**
2648 **microscope objective as the head-fixed animals run.** We used a 6 inch
2649 cylindrical massage roller with a stainless steel axle running along the
2650 length. This axle had ball bearings on the two ends, to allow for free
2651 rotation against clamps. Additionally, we used linear actuators to be
2652 able to adjust the height of the treadmill relative to the head-fixing
2653 clamps.

2654

2655 On one side of the treadmill, we used a printed pattern of black
 2656 squares (side length: 1 cm) along the circumference. This allowed an
 2657 IR LED - Photodetector pair to catch the edges of the black printed
 2658 squares. The number of edges detected per unit time, then gave us the
 2659 run speed of the animals being trained. We followed previously
 2660 published routines and protocols (Siegel et al., 2015) for setting up the
 2661 treadmill and run speed tracking (Figure 13), **over 50 ms sized bins**,
 2662 across each trial.

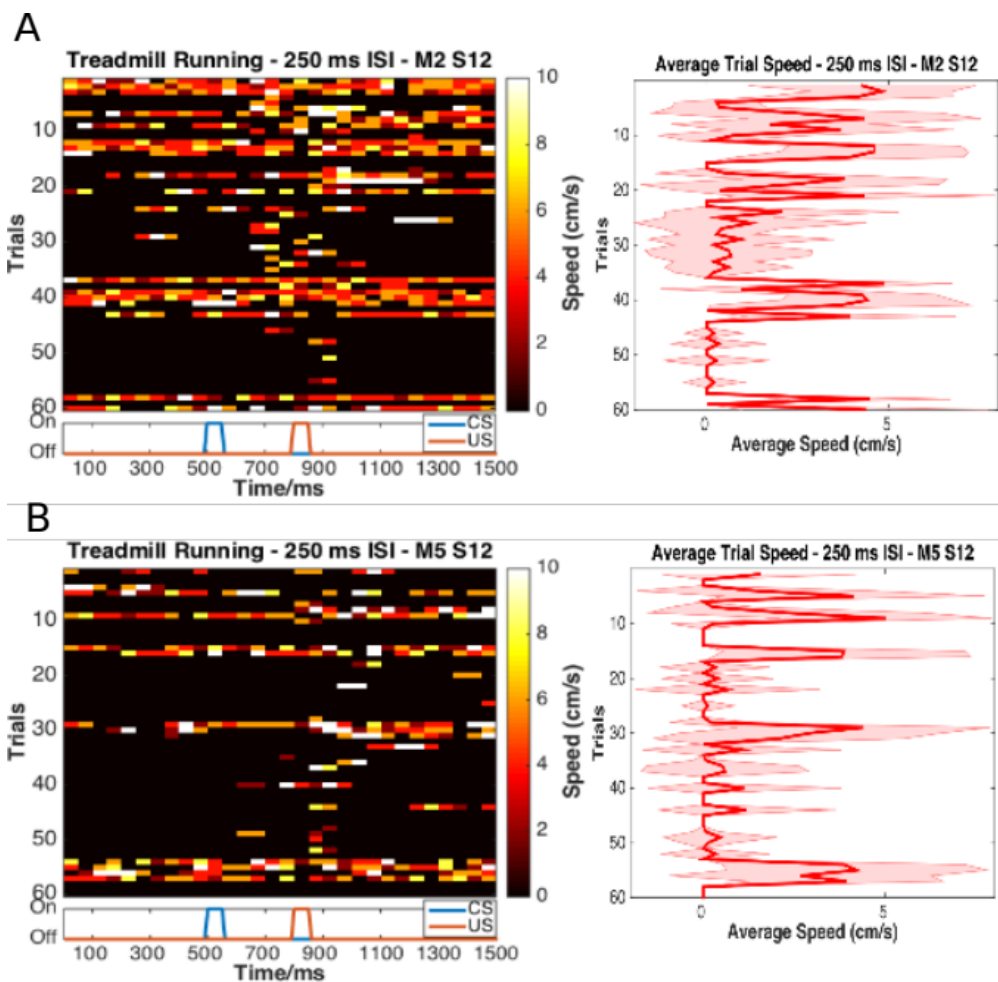


Figure 13: Trial-by-trial (left) and trial-averaged running speed (right) for two example animals, (A) M2 Session 12, and (B) M5 Session 12.

2663

2664 **Behaviour rig and protocol control - Software**

2665

2666 For our initial experiments we used the open-source behaviour

2667 controlling software suite Bonsai (Windows version). Later on, we were

2668 able to implement our own custom codes that allowed integration of

2669 the video camera, Arduino for stimulus delivery and treadmill tracking,

2670 and the software side of the protocols. Dilawar S. Rajput was

2671 instrumental in setting up the camera pipeline and integrating it into the

2672 Arduino code. The Camera server was implemented in C++ with

2673 Spinnaker API (Point Grey) and this fetched frames from the camera.

2674 The camera client was written in Python, and this read the frames to

2675 produce a copy to monitor the video feed live, as well as write the

2676 video frames to disk as .tif files.

2677 With this setup, the maximum memory usage was ~1.3 GB RAM, and

2678 the code (available at <https://github.com/BhallaLab/PointGreyCamera>)

2679 had the following dependencies:

2680 • libopencv-dev, python-opencv

2681 • cmake, g++, gnu-make

2682 • libtiff-dev, python-tifffile, python-numpy

2683 • python-gnuplotlib, gnuplot-x11

2684

2685 An important requirement for our behaviour experiment design was to

2686 be able to train the animals systematically under reproducible

2687 conditions, with the aim to have stable behavioural training and animal

2688 performance. We used a blue LED as the Conditioned Stimulus (CS,

2689 50 ms flash) with an air-puff to the eye serving as the Unconditioned

2690 Stimulus (US, 50 ms pulse). We used an Arduino to orchestrate

2691 stimulus delivery and protocol design. All experiments were performed

2692 on head-fixed C57Bl6 mice, since we planned to use a stationary,

2693 custom-built two-microscope to image hippocampal CA1 activity during
2694 task acquisition and recall (Figure 14; Figure 15).

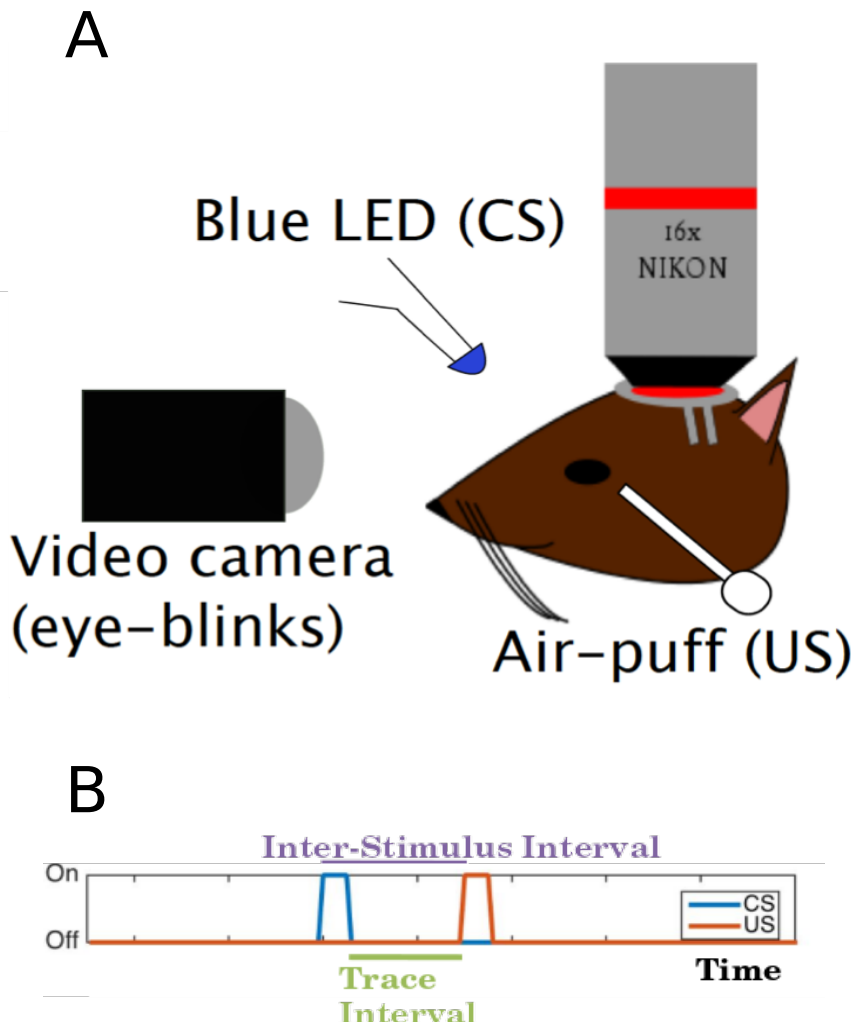


Figure 14: Schematic representation of (A) the behaviour rig with 2-Photon imaging, to train head-fixed mice on a Trace Eye-Blink Conditioning (TEC) task, and (B) relative time intervals between the CS and US.

2709

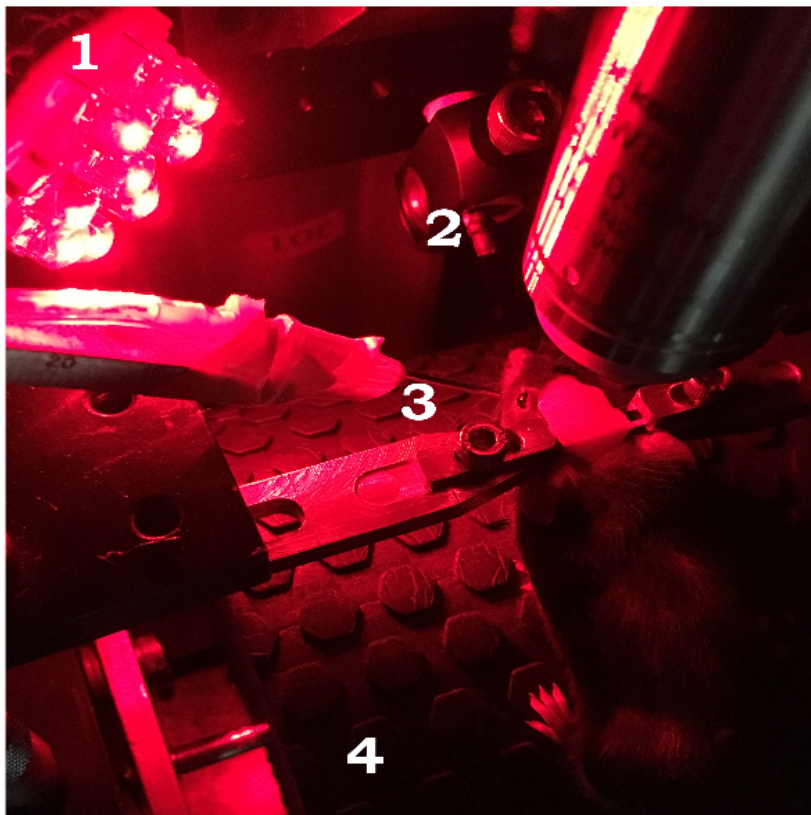


Figure 15: A picture of a head-fixed mouse clamped on the behaviour rig, with key components: 1) Red LED Illumination, 2) Blue LED CS, 3) Air-puff port directed to the left eye, and 4) Height-adjustable Treadmill.

2711 **Analysis - TEC**

2712

2713 Once the .tif movies of the eye of the animal being trained were saved,
2714 they were analyzed by a custom script written in MATLAB, wherein for
2715 every frame we (Figure 16),

- 2716 a) Adjust contrast (optional)
- 2717 b) Apply a median filter (optional)
- 2718 c) Crop out the pixels defining the eye and surrounding (identical
2719 number of pixels for all trials and animals)
- 2720 d) Binarize the image of the eye to get black pixels defining the
2721 visible (opened) portion of the eye
- 2722 e) Count the relative proportion of open vs closed eye pixels in the
2723 cropped image, and
- 2724 f) Assign each frame with a Fraction of Eye Closure (FEC) score.

2725

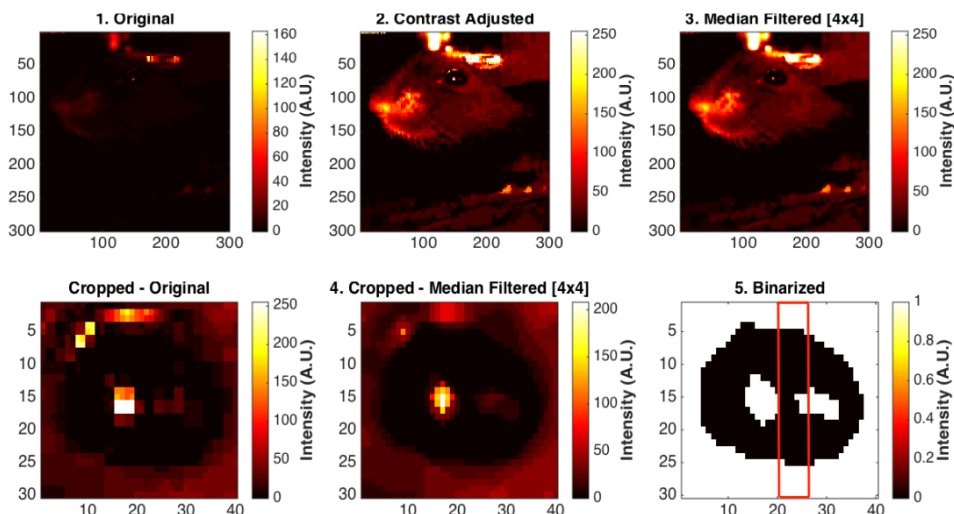


Figure 16: Steps from behaviour video frame to Fraction of Eye-Closed (FEC) analysis.

2726

2727 The FEC score then allowed us to analyse each trial's worth of frames
2728 for eye-blanks. There are many features of the eye-blink that could be

2729 used to gauge the overall performance of the animal in terms of both
2730 the Conditioned Response (CR) as well as the Unconditioned
2731 Response (UR), but for our experiments, we chose to use Eye-Blink
2732 Amplitude (Siegel et al., 2015). Additionally, we studied whether the
2733 animals could produce CRs in the absence of the US, by
2734 pseudorandomly selecting 10% trials to skip the US (Probe Trials).

2735

2736 **Results - TEC**

2737

2738 1. Animals showcase task acquisition by performing Conditioned
2739 Responses (CRs), observed as pre-emptive blinks timed to
2740 avoid the aversive US. The kinetics of the CR (timing,
2741 amplitude, etc.) are dependent on the amount of training, but
2742 are identical across paired and probe trials (Figure 17).

2743

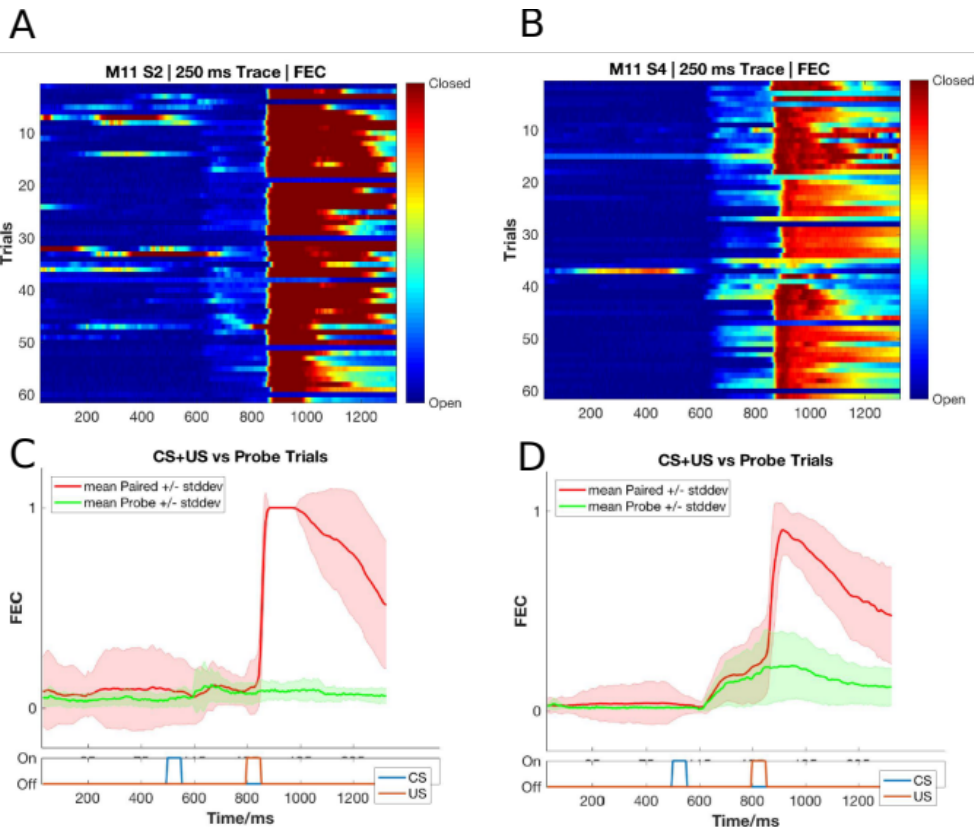


Figure 17: Conditioned Responses (CRs) are small amplitude eye-blanks triggered by the CS, and develop with multiple training sessions, while Unconditioned Responses (URs) are large eye-blanks to the US, typically consistent across sessions. (A,B) Trial-by-trial FEC traces for M11 (A) Session 2, and (B) Session 4. (C,D) Trial-averaged FEC traces for M11 (C) Session 2, and (D) Session 4, with paired (red) and probe (green) trials.

2744

2745 2. Most animals can pick up the task within 4-7 sessions (1
2746 session/day, 60 trials/session), even if on water deprivation.
2747 Animals can also be subsequently trained to different inter-
2748 stimulus intervals. Using the Conditioned Response (CR)
2749 amplitude, each trial can be binarized to whether a CR was
2750 elicited (Hit Trial) or not (Miss Trial), by thresholding at mean
2751 trial FEC + 2*Std. Dev.. Performance for the session is then

estimated as the ratio of Hit Trials to Total Trials (Figure 18). We additionally set a criterion that a performance of >70% be considered “strong learning”, 30-60% be considered “weak learning”, and “0-30%” be considered “non-learning”.

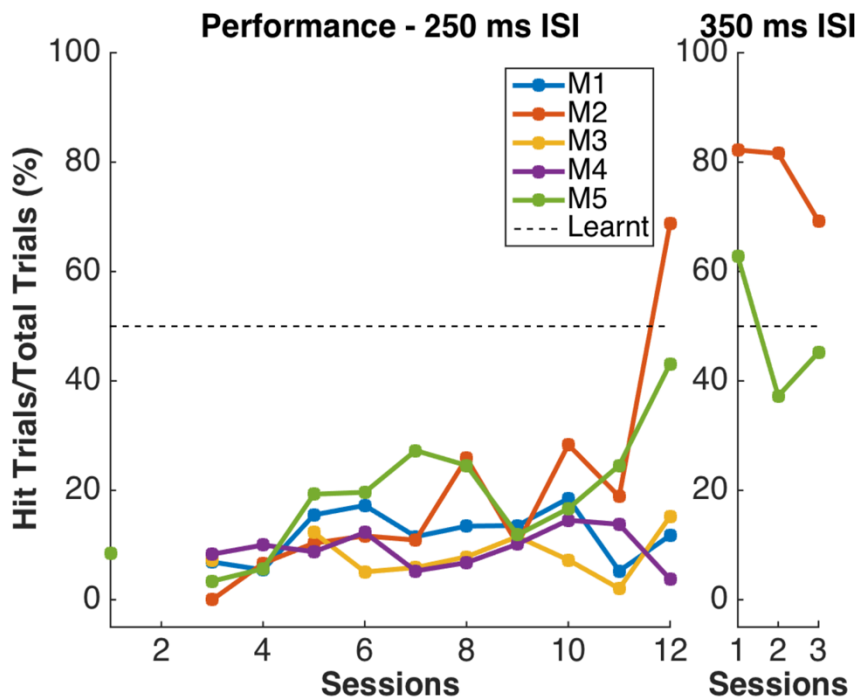


Figure 18: Performance in terms of the percentage of Hit Trials to total trials across sessions, including an ISI switch from 250 ms to 350 ms. Here, M2 is a strong learner (>60% hit trials/session) and M5 is a weak learner (30-60 % hit trials/session). M1, M3, and M4 did not learn the task.

3. Animals that learn multiple ISIs, especially when the second ISI is $\geq 2x$ the first ISI, showcase complex eye-blinks without extinction of the previously learnt CRs. Once an animal showcases the ability to produce Conditioned Responses (CRs) to one inter-stimulus interval (ISI), this interval can be elongated. In the example shown below we first trained the

2763 animal to a 250 ms ISI, and then switched to a 500 ms ISI
2764 (Figure 19).

2765

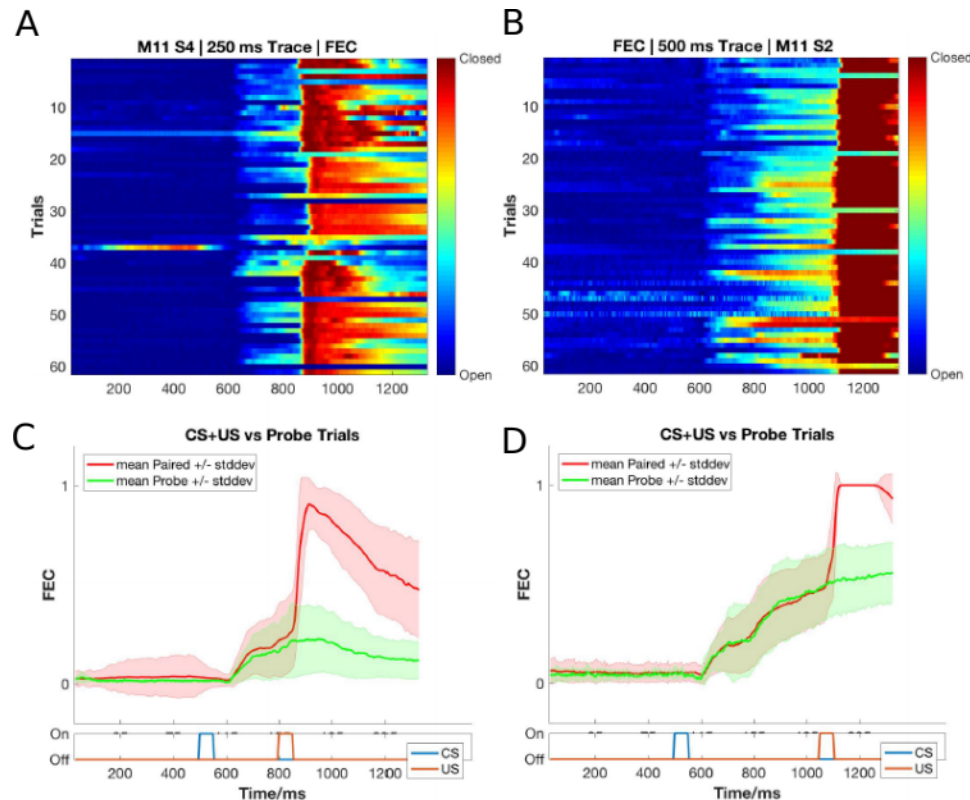


Figure 19: Conditioned Responses (CRs) are preserved for previously learnt ISIs, and switching the ISI to longer intervals results in Complex (multi-CR) eye-blink responses. (A,B) Trial-by-trial FEC scores for (A) 250 ms ISI (left) and (B) 500 ms ISI. (C,D) Trial-averaged FEC traces for (C) 250 ms ISI, and (D) 500 ms ISI, with paired (red) and probe (green) trials.

2766

2767 4. The onset of the Conditioned Response (CR) is not affected by
2768 the ISI switch, irrespective of how strongly the animals learn the
2769 task. CRs during paired and probe trials were near identical,
2770 showcasing that the animal (Figure 20; Figure 21).

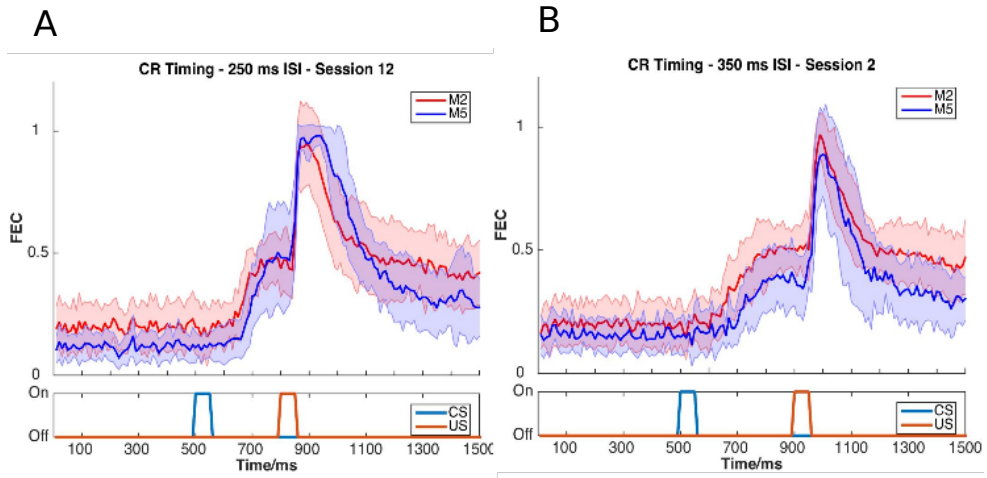


Figure 20: Conditioned Response (CR) onset timing is maintained across ISI switches. Representative examples from a short ISI switch from (A) 250 ms to (B) 350 ms (right).

2771

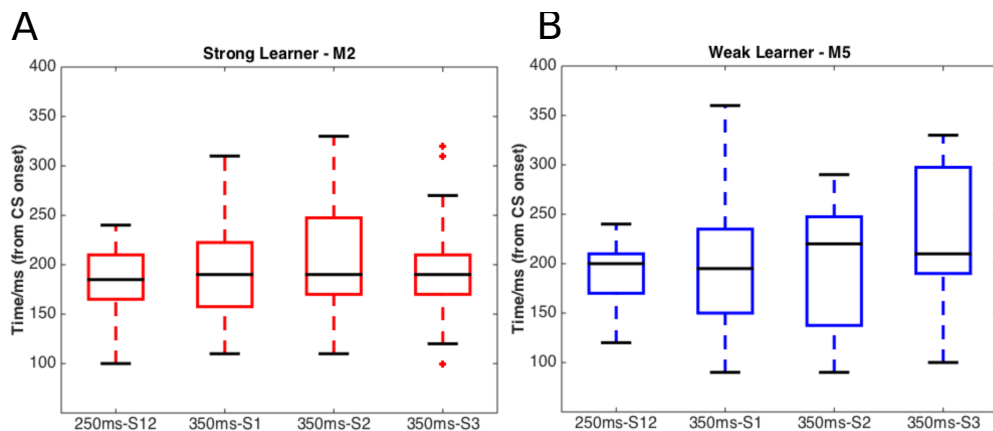


Figure 21: Bar plots for Conditioned Response (CR) onset across multiple sessions of training after ISI switch from 250 ms to 350 ms, irrespective of how strongly the animals learnt the task. (A) red, strong learner, and (B) blue, weak learner.

2772

2773 5. Animals can also be trained to very long ISIs from Session 1,
2774 with acquisition taking <10-14 days. Here we tried to train
2775 animals to either a 550 ms ISI or a 750 ms ISI. Note, however,

2776 that unless multiple ISIs are taught to the same animal, the CR
2777 eye-blink is singular (Figure 22).
2778

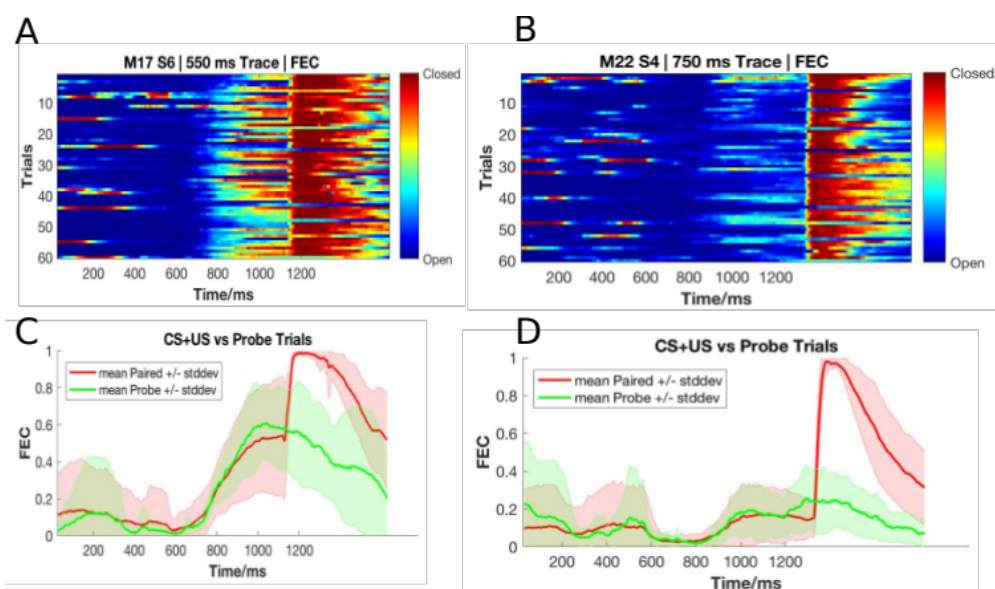


Figure 22: Representative example of mice trained to 550 ms ISI (Session 6) and 750 ms ISI (Session 4). (A,B) Trial-by-trial FEC responses for (A) 550 ms ISI (M17 Session 6), and (B) 750 ms ISI (M22 Session 4). (C,D) Trial-averaged FEC responses for (C) 550 ms ISI (M17 Session 6), and (D) 750 ms ISI (M22 Session 4), with paired (red) and probe trials (green).

2779
2780 **Total animals trained:** 18 [Conditioned Responses visible]

2781 **Conclusion:** Success

2782
2783 Ultimately, we were satisfied with the Trace Eye-Blink Conditioning
2784 paradigm since we could observe stable conditioned responses that
2785 developed over a reasonably short period of training time (<1 week),
2786 and adaptable conditioned responses to behaviour parameter
2787 modulations, in head-fixed mice that could be subjected to
2788 simultaneous 2-Photon calcium imaging.

Table 1: Summary table of behaviour protocols attempted and essential results.

NAME	PUNISHMENT TYPE	REMARKS
Operant Protocol 1.1 (Stimulus Detection)	No water reward for incorrect licks	Lack of water reward for incorrect licks not enough for behavioural discrimination at <1 week of training
Operant Protocol 1.2 (Stimulus Detection)	Air-puff punishment for incorrect licks	Strong punishment for incorrect licks not enough for behavioural discrimination at <1-2 weeks of training.
Operant Protocol 2 (Stimulus Detection)	Timeout (3s) punishment for incorrect licks	Alternate or weaker punishment attempted but not enough for behavioural discrimination at <1 week of training.
Operant Protocol 3 (DNMS)	Timeout (3s) punishment for incorrect licks	Alternate punishment attempted but not enough for behavioural discrimination at <1 week of training No obvious effect of adding delay intervals between stimulus presentations
Operant Protocol 4 (Go/No-Go)	Trial base repeat punishment for incorrect licks	Alternate punishment attempted but not enough for behavioural discrimination at <1 week of training
Aversive Protocol (Trace Eye-Blink Conditioning)	No punishment	Animals learn the task and produce stable, adaptable Conditioned Responses (CRs) within 1 week of training

2789 Bibliography

- 2790 Brown, G. D. (1998). Nonassociative learning processes affecting
2791 swimming probability in the seashell Tritonia diomedea:
2792 habituation, sensitization and inhibition. *Behavioural Brain
2793 Research*, 95(2), 151–165.
2794 [https://doi.org/https://doi.org/10.1016/S0166-4328\(98\)00072-2](https://doi.org/https://doi.org/10.1016/S0166-4328(98)00072-2)
- 2795 Chudasama, Y. (2010). Delayed (Non)Match-to-Sample Task. In I. P.
2796 Stolerman (Ed.), *Encyclopedia of Psychopharmacology* (p. 372).
2797 Springer Berlin Heidelberg. https://doi.org/10.1007/978-3-540-68706-1_1619
- 2798 Deshmukh, S. S., & Bhalla, U. S. (2003). Representation of odor
2799 habituation and timing in the hippocampus. *The Journal of
2800 Neuroscience : The Official Journal of the Society
2801 for Neuroscience*, 23(5), 1903–1915.
2802 <https://doi.org/10.1523/JNEUROSCI.23-05-01903.2003>
- 2803 Fyhn, M., Molden, S., Witter, M. P., Moser, E. I., & Moser, M.-B.
2804 (2004). Spatial representation in the entorhinal cortex. *Science
2805 (New York, N.Y.)*, 305(5688), 1258–1264.
2806 <https://doi.org/10.1126/science.1099901>
- 2807 Guo, Z. V., Hires, S. A., Li, N., O'Connor, D. H., Komiyama, T., Ophir,
2808 E., Huber, D., Bonardi, C., Morandell, K., Gutnisky, D., Peron, S.,
2809 Xu, N., Cox, J., & Svoboda, K. (2014). Procedures for Behavioral
2810 Experiments in Head-Fixed Mice. *PLOS ONE*, 9(2), e88678.
2811 <https://doi.org/10.1371/journal.pone.0088678>
- 2812 Hafting, T., Fyhn, M., Molden, S., Moser, M.-B., & Moser, E. I. (2005).
2813 Microstructure of a spatial map in the entorhinal cortex. *Nature*,
2814 436(7052), 801–806. <https://doi.org/10.1038/nature03721>
- 2815 Hubel, D. H., & Wiesel, T. N. (1962). Receptive fields, binocular
2816 interaction and functional architecture in the cat's visual cortex.
2817 *The Journal of Physiology*, 160(1), 106–154.
2818 <https://doi.org/10.1113/jphysiol.1962.sp006837>
- 2819 Jaramillo, S., & Zador, A. M. (2014). Mice and rats achieve similar
2820 levels of performance in an adaptive decision-making task . In
2821 *Frontiers in Systems Neuroscience* (Vol. 8).
2822 <https://www.frontiersin.org/articles/10.3389/fnsys.2014.00173>
- 2823 Modi, M. N., Dhawale, A. K., & Bhalla, U. S. (2014). CA1 cell activity
2824 sequences emerge after reorganization of network correlation
2825 structure during associative learning. *eLife*, 3, e01982–e01982.
2826 <https://doi.org/10.7554/eLife.01982>
- 2827 O'Keefe, J., & Dostrovsky, J. (1971). The hippocampus as a spatial
2828 map. Preliminary evidence from unit activity in the freely-moving
2829 rat. *Brain Research*, 34(1), 171–175. [https://doi.org/10.1016/0006-8993\(71\)90358-1](https://doi.org/10.1016/0006-8993(71)90358-1)

- 2832 Ranck, J. B. (1973). Studies on single neurons in dorsal hippocampal
2833 formation and septum in unrestrained rats: Part I. Behavioral
2834 correlates and firing repertoires. *Experimental Neurology*, 41(2),
2835 462–531. [https://doi.org/https://doi.org/10.1016/0014-4886\(73\)90290-2](https://doi.org/https://doi.org/10.1016/0014-4886(73)90290-2)
- 2836 Schreurs, B. G. (1989). Classical conditioning of model systems: A
2837 behavioral review. *Psychobiology*, 17(2), 145–155.
2838 <https://doi.org/10.3758/BF03337830>
- 2839 Siegel, J. J., Taylor, W., Gray, R., Kalmbach, B., Zemelman, B. V.,
2840 Desai, N. S., Johnston, D., & Chitwood, R. A. (2015). Trace
2841 Eyeblink Conditioning in Mice Is Dependent upon the Dorsal
2842 Medial Prefrontal Cortex, Cerebellum, and Amygdala: Behavioral
2843 Characterization and Functional Circuitry. *ENeuro*, 2(4),
2844 ENEURO.0051-14.2015. <https://doi.org/10.1523/ENEURO.0051-14.2015>
- 2845 Taube, J. S., Muller, R. U., & Ranck, J. B. J. (1990). Head-direction
2846 cells recorded from the postsubiculum in freely moving rats.
2847 I. Description and quantitative analysis. *The Journal of
2848 Neuroscience : The Official Journal of the Society
2849 for Neuroscience*, 10(2), 420–435.
2850 <https://doi.org/10.1523/JNEUROSCI.10-02-00420.1990>
- 2851 Tseng, W., Guan, R., Disterhoft, J. F., & Weiss, C. (2004). Trace
2852 eyeblink conditioning is hippocampally dependent in mice.
2853 *Hippocampus*, 14(1), 58–65. <https://doi.org/10.1002/hipo.10157>

Chapter 3 – Imaging

2857

2858 The mammalian hippocampus is considered important in the formation
2859 of new memories about experienced events (episodic or
2860 autobiographical memory), general declarative memory (memories that
2861 can be explicitly verbalized), spatial memory and navigation, and
2862 associations between stimuli that are distinct in time, among other
2863 functions. To achieve this, the Hippocampus must integrate information
2864 from different areas of the cortex.

2865

2866 Much of the cortical information that enters the Hippocampus (at the
2867 Dentate Gyrus), comes through the Entorhinal Cortex, along the
2868 Perforant Path (Hjorth-Simonsen & Jeune, 1972). The Dentate Gyrus
2869 cell network then relays this information to the CA3 cell network
2870 through Mossy Fibers, which in turn relays the information to CA1
2871 cells, through the Schaffer Collateral Fibers. This is popularly known as
2872 the Trisynaptic Circuit or Pathway (Figure 1 from Chapter 1 -
2873 "Introduction") and there is scope and evidence for computation and
2874 information processing at every step (MacDonald et al., 2011, 2013;
2875 Modi et al., 2014; Nakashiba et al., 2008; Suh et al., 2011). Finally, the
2876 CA1 cells have their outputs to other brain regions. It is important to
2877 note, however, that regions like the CA1 are known to have access to
2878 information directly from other brain regions, as well (P. Andersen et
2879 al., 2006).

2880

2881 Literature in the field suggests that naïve animals may have some
2882 sensory gating of "Neutral" stimuli at the level of the CA1 (Abe et al.,
2883 2014; Bellistri et al., 2013; Kamondi, 1998). The source of this
2884 inhibition (at least the step before the local interneurons) seems to be

2885 the Medial Septum, through Fimbria-Fornix (Abe et al., 2014). Also,
2886 behavioural relevance allows the CA1 to elicit depolarizations that can
2887 be mapped to brain external stimuli (Dombeck et al., 2010; Harvey et
2888 al., 2009; P. M. Itskov et al., 2011; MacDonald et al., 2011, 2013; Modi
2889 et al., 2014; Pastalkova et al., 2008).

2890

2891 The Hippocampus consists of ventral and dorsal portions both of which
2892 are of similar composition but are parts of different neural circuits
2893 (Moser & Moser, 1998). The dorsal hippocampus performs primarily
2894 cognitive functions and in memory function, while the ventral
2895 hippocampus modulates emotional and affective processes (Fanselow
2896 & Dong, 2010).

2897

2898 **Physiology in the hippocampus**

2899

2900 The Hippocampus is located deep in the medial temporal lobe of
2901 mammals and is defined by several sub-structures, including the
2902 Dentate Gyrus (one site for information input to the hippocampus) and
2903 the Hippocampus Proper constituted by the CA1, CA2, CA3 and CA4
2904 cellular levels.

2905

2906 Using extracellular tungsten microelectrodes in naïve unanesthetized
2907 rabbits serially exposed to multimodal stimuli (Vinogradova, 2001), it
2908 was reported that in the CA1,

2909 1. A major fraction the reactive neurons have unimodal responses
2910 (41-44%)

2911 2. Multimodal neurons are modality-unspecific but have
2912 differentiated responses to stimuli of different modalities and even to
2913 various stimuli within a single modality
2914 3. Many neurons respond by Phasic (evoked responses last for the
2915 duration and as long as the stimulus) and Specific (stimulus-specific
2916 pattern) responses
2917 4. Neurons with inhibitory responses are encountered less
2918 frequently than those with various types of excitatory
2919 5. Habituation (non-responsiveness to repeatedly presented stimuli) is
2920 present though not among all the responsive cells (71-75%) and is
2921 often gradual
2922
2923 Imaging based activity studies have the advantage of being able to
2924 capture many more cells (>100 from the same animal) during
2925 experiments (Dombeck et al., 2010; Pachitariu et al., 2017; Peron et
2926 al., 2015; Sofroniew et al., 2016) as compared to typical
2927 electrophysiological measurements. Imaging provides an unambiguous
2928 method to identify cells that are not active during a period of interest.
2929 Another advantage is that it provides anatomical confirmation to help
2930 track the same cell over multiple days of recording, without ambiguity,
2931 for longitudinal studies. Finally, imaging techniques have gained
2932 momentum in the study of the hippocampal CA1 various spatial scales,
2933 from cellular resolution somatic studies (Dombeck et al., 2010; Modi et
2934 al., 2014), to dendrites (Mizrahi, 2004; Sheffield & Dombeck, 2014),
2935 axonic boutons terminating on the CA1 interneuron populations
2936 (Kaifosh et al., 2013; Lovett-Barron et al., 2014), as well as spines
2937 (Attardo et al., 2015), *in vivo*.
2938

2939 We designed our imaging studies (for this thesis), with the aim to
2940 understand the network and cellular mechanisms of the hippocampal
2941 CA1 that corresponded with behavioral learning induced changes. We
2942 started by looking for CA1 responses to neutral stimuli in naive
2943 animals, *in vivo*. Subsequently, we planned to subject these animals to
2944 behavioural training and study if and how the same cells would
2945 respond.

2946

2947 Depending on the intended duration of the imaging experiments, *viz.*, a
2948 few hours (single session) or a few days and weeks (multiple
2949 sessions), we were able to standardize both an Acute as well as a
2950 Chronic *in vivo* hippocampal preparation. We now discuss the *in vivo*
2951 hippocampal preparation, physiology recordings, and a brief summary
2952 of the results. An important perspective for our experiments was to
2953 study how sensory stimulus responses of hippocampal CA1 develop
2954 with associative learning.

2955

2956 **Methodology – Acute and chronic imaging**

2957 **[Projects I & II]**

2958

2959 The overall experiment deals with optically measuring the activity of
2960 the dorsal CA1 hippocampal neurons when different stimulus
2961 modalities are presented to a male C57BL/6 mouse. The thesis covers
2962 experiments conducted acutely (lasting <10 hours) using OGB-1 as a
2963 calcium sensor), as well as chronically (~7-21 days) using a genetically
2964 encoded calcium indicator, GCaMP6f.

2965

2966 The 2-Photon excitation wavelength for OGB-1 experiments was set to
 2967 810 nm (scattering coefficient: ~3 rad²/mm) and the same for
 2968 GCaMP6f was set to 910 nm (scattering coefficient: ~2 rad²/mm) to
 2969 image cell bodies (Min et al., 2017) in the CA1, *in vivo*. However,
 2970 despite the relatively low scattering of longer wavelengths, the
 2971 hippocampus cannot be imaged directly, through the cortex since the
 2972 layer of cortex is too thick (~1-1.5 mm) to allow proper excitation of the
 2973 sample. These infra-red (IR) photons are expected to be scattered
 2974 almost completely, well before the imaging depth of the CA1 layer.
 2975 These layers of cortex have to accordingly be carefully suctioned out to
 2976 allow the microscope objective to have optical access to the exposed
 2977 tissue (Figure 23).

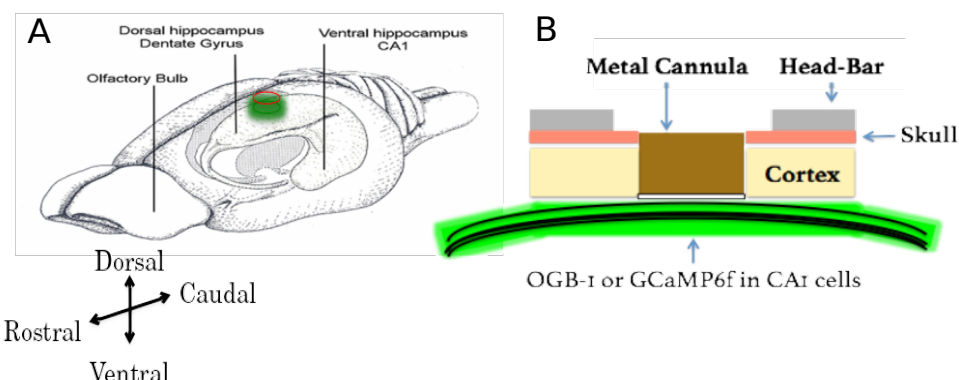


Figure 23: (A) A schematic of the rodent brain, showcasing the two hippocampi, one in each hemisphere. The hippocampi lie ~1 mm (mice) below the cortical surface. (B) The hippocampal preparation allows optical access to the deep lying hippocampal CA1 cells, relative to the skull/cortex. The CA1 cell bodies arrange in a laminar fashion as a tight cell body layer that can be visualized by fluorescence (using either OGB-1 or GCaMP).

2978
 2979 We first put the animal under anesthesia using a vapor chamber
 2980 saturated with 3% isoflurane. Next, the animal was cheek-clamped and
 2981 a light state of anesthesia was maintained using 1-2% isoflurane,

2982 provided directly to the nozzle of the animal, keeping track of ~1 Hz
2983 breathing rate and a body temperature of 35-37 °C (with heating pad).
2984 The animal was given a haircut and a circular incision of ~5 cm
2985 circumference was made on the scalp, revealing the skull below. We
2986 then affixed head-bars and skull screws with the help of dental cement,
2987 to be able to clamp the animal post surgery on the 2-Photon
2988 Microscope.
2989
2990 The left, dorsal hippocampus was targeted with a 3-5 mm circular
2991 craniotomy aimed at 1.5 mm left and 2.0 mm behind bregma, tearing
2992 and peeling out the Dura to reveal the cortex. We then carefully
2993 aspirated out the cortex (part of the somatosensory cortex) under
2994 repeated washes of Cortex Buffer (see table 1 for recipe), until the
2995 horizontal CC fibre layer was visible. Finally, we added a drop of low
2996 gelling agarose and a 5 mm coverslip (for acute preps); Kwik-Sil and
2997 inserted a 3 mm metal cannula with a coverslip attached at the bottom
2998 (for chronic preps). We used different sensors depending on the
2999 requirement for the preparation, *viz.*, acute (OGB-1) or chronic imaging
3000 (GCaMP6f). **We kept track of animals that showcased unusual gait or**
3001 **low/no mobility and avoided their use altogether for production**
3002 **datasets and experiments, in accordance with previously published**
3003 **protocols** (Dombeck et al., 2010). We refer to this series of steps as
3004 the hippocampal preparation.

3005 **Preparation of Cortex Buffer**

3006
3007 We prepared cortex buffer by weighing out the required amount of the
3008 salts, NaCl, KCl, Glucose and HEPES (see table 2 for recipe) and

3009 making up the volume of the solution with Milli Q Water to ~1000 ml.
3010 We then set the pH of the buffer using a calibrated pH meter to 7.35,
3011 using 1M NaOH_(aq). Next, we fill up the volume to 1000 ml and verify
3012 the pH (should not have changed). Finally, we filter the contents
3013 through a 0.22 um membrane using a vacuum filtration, and store at
3014 6 °C.

3015 Recipe for ready-to-use cortex buffer. The buffer is typically prepared
3016 and stored in aliquots to be used each week. The correct pH range of
3017 the buffer was often a crucial factor ensuring the success of the
3018 hippocampal preparation.

3019

Table 2: Recipe for ready-to-use cortex buffer. The buffer is typically prepared and stored in aliquots to be used each week. The correct pH range of the buffer was often a crucial factor ensuring the success of the hippocampal preparation.

INGREDIENT	CONCENTRATION (mM)	AMOUNT (g or ml) for 1000 ml]
NaCl (s)	125	7.31 g
KCl (s)	5	0.373 g
Glucose (s)	10	1.8 g
HEPES (s)	10	2.38 g
CaCl ₂ (aq)	2	1.6 ml of 1.25 M stock solution
MgCl ₂ (aq)	2	1.5 ml of 1.3 M stock solution

3020

3021 **Oregon Green Bapta-1 injections for acute**
 3022 **imaging**

3023

3024 To prepare Oregon Green Bapta-1 (OGB-1) dye for microinjections, we
3025 first dissolve a 50 µg tube of OGB-1 in 5 µl of Pluronic Acid, and vortex
3026 the mix for 5 minutes. Separately, we dilute 20 µl of Phenol Red into
3027 500 µl of cortex buffer, and transfer 45 µl of this solution to the OGB-1
3028 mix. Next, we sonicate the 50 µl solution for 20 mins., followed by
3029 centrifugation at 10000 RPM for 5 seconds. The remaining supernatant
3030 is split into 7 aliquots (7 µl), and stored at -20 C for a maximum of one
3031 week (7 days).

3032

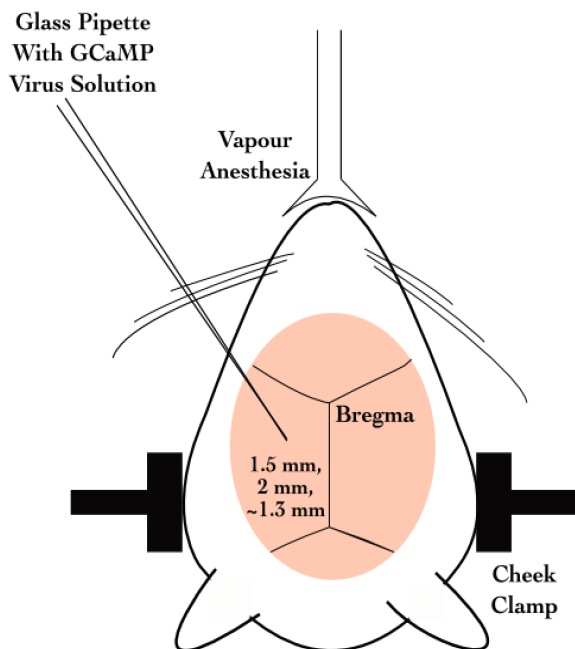
3033 For acute/single-day experiments, we injected OGB-1 using pulled,
3034 dye loaded micropipettes (~2 MΩ resistance, ~2 µm diameter) at a
3035 depth of 100-150 µm (Figure 23) from the topmost layer of exposed
3036 tissue, till a slow but detectable pulse of dye (visualized as a red/pink
3037 solution) may be visible just below the tissue surface. This allows the
3038 dye to be soaked up by the basal dendrites of the CA1 and takes 30-
3039 60 mins for incorporation into the cytoplasm. We typically allow the
3040 animal 1-2 hours of respite before the subsequent imaging session.
3041 High pressure ejection of the dye into the tissue may damage the
3042 neuropil, while very low pressures or clogs in the pipette affect the
3043 spread of the dye across the tissue. We aimed to image ~100 x 100
3044 µm² of the tissue in any particular ROI, and achieved this with 5 minute
3045 injections with each micropipette aiming to load the dye at 2-3, well
3046 separated positions spread across the entire exposed dorsal surface.
3047 We estimated that the dye volume was <1000 nl/injection. After the
3048 injection cycle with any micropipette, we left the tissue undisturbed for
3049 at least 5-10 mins before pulling the micropipette out of the tissue.
3050 Once all the injections were complete, the exposure was sealed using
3051 5% low gelling agarose making sure the temperature was cool enough
3052 to avoid heat-related tissue damage.

3053
3054 OGB-1 is eventually cleared from the cytoplasm but allows for a limited
3055 window for imaging studies (Stosiek et al., 2003). Reopening the
3056 agarose seal and re-injections were never attempted to prevent
3057 unnecessary damage to the underlying tissue. Additionally, the
3058 agarose plug itself was found to be unstable beyond 1-3 days. This
3059 resulted in the imaging possibility being limited to the same day as the
3060 surgery (acute imaging).

3061

3062 **GCaMP and chronic imaging**

3063
3064 For chronic/multi-day experiments, we standardized a stereotaxic viral
3065 injection step, where we inject the gene for GCaMP5 or GCaMP6f into
3066 the dorsal hippocampus at -1.5 mm lateral, 2 mm posterior, and 1.3
3067 mm dorsal from bregma on the skull surface (Figure 24).



3080

Figure 24: Schematic representation for stereotaxic viral injection.

3083

3084 Later on, we switched to directly using GCaMP6f transgenic mice
3085 (background: C56BL/6) which express GCaMP6f in the Hippocampus
3086 [Tg(Thy1-
3087 GCaMP6f)GP5.17Dkim JAX stock #025393]. This helped us
3088 circumvent the dye loading or viral injection steps, aiding in the
3089 potential success of the preparations, by way of tissue health and
3090 recording quality.

3091

3092 **Results - Imaging**

3093

3094 **2-Photon calcium imaging of hippocampal CA1, *in vivo***

3095

3096 The CA1 cell body layer is ~200 µm deep, in through the hippocampal
3097 surface. At these depths, scattering of excitation as well as emission
3098 light is significant. However, we are able to image at these depths with
3099 Two-Photon Imaging LASER Scanning Imaging (810 nm for OGB-1
3100 and 910 nm for GCaMP5/GCaMP6f), where a high intensity pulsed
3101 LASER allows for two photons to near instantaneously excite
3102 fluorophores in a thin z-slice plane which is the focal plane of the
3103 Objective. Our LASER, the Coherent Chameleon Ultra II emits ~3 W at
3104 810 nm, and ~2 W at 910 nm. At these depths, there is scattering of
3105 emitted photons. However, since only the focal plane is excited any
3106 and all emitted photons that we capture are part of the signal. We use
3107 a Nikon 16x water immersion, 0.8 NA, 3 mm working distance
3108 Objective (N16XLWD-PF), to get a large field of view.

3109

3110 **Acute Imaging of OGB-1 loaded hippocampal CA1, *in*
3111 *vivo***

3112

3113 We injected OGB-1 dye into brain tissue for our acute imaging
3114 experiments (see Methodology for details). OGB-1 spreads throughout
3115 the cytoplasm and neuropil, and infiltrates the cell nucleus, giving the
3116 cells the appearance of solid circles (cells). The cell body (soma)

3117 ranges from 10-15 μm depending on the orientation of the imaging
3118 layer in 3D tissue space (Figure 25A).
3119

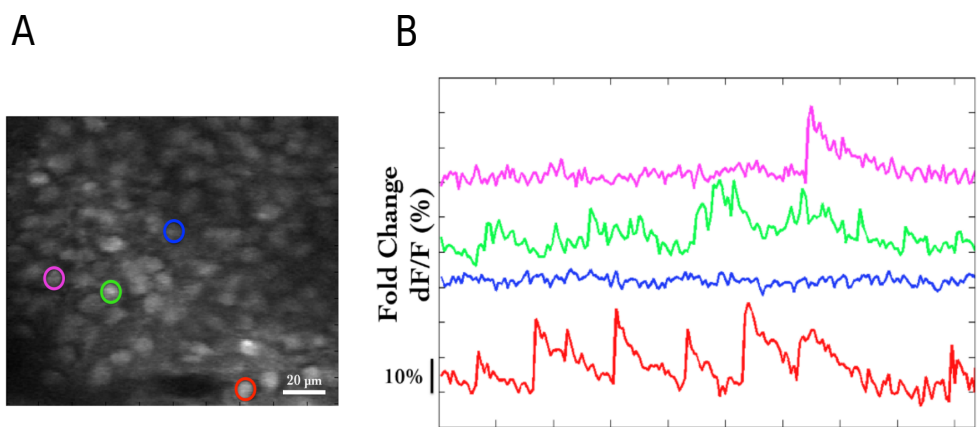


Figure 25: (A) Representative Two-Photon Calcium Image of a plane of Hippocampal CA1 cells, bolus loaded with Oregon Green Bapta-1 (OGB-1), at an instant in time. Example cells marked out post-hoc as pink, green, blue and red. Scale bar 20 μm . (B) Representative dF/F (%) traces for the calcium activity. Recorded in a single 10s video for example cells – pink, green, blue, and red. Scale bar 1 sec; 10% dF/F .

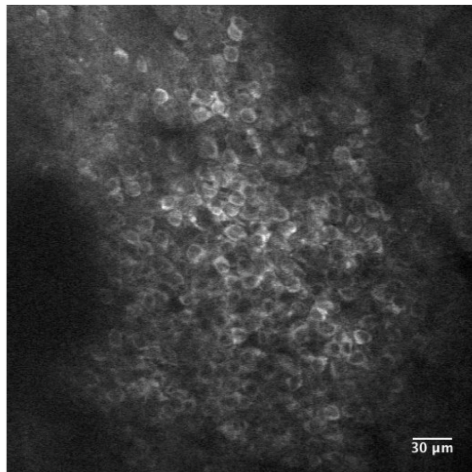
3120 Each cell in the recorded region of interest (ROI), is identified, marked
3121 out (in pixel identity), based on local activity of correlated pixels in the
3122 time series movies. The average intensity of the pixels corresponding
3123 to each cell for each frame in each recording video, is saved as the
3124 raw calcium fluorescence trace. Next, these raw calcium traces are
3125 baseline normalized to equate the baselines for each cell at 0, and
3126 describe the dynamic range of the intensity values as 0 to 1, or 1 to
3127 100%. The corresponding time series of baseline normalized dF/F for
3128 the representative example cells are shown (Figure 25B; Figure 28B).
3129

3130 **Chronic imaging of hippocampal CA1 using GCaMP**

3131

3132 For chronic imaging, tissue health was of paramount concern since it
3133 could easily degrade in time (Figure 26). With practice and
3134 standardization, we were able to get the preparations to survive for 2-4
3135 weeks at very good signal-to-noise. Preparations that resulted in very
3136 poor signal-to-noise were often recorded but have been filtered out of
3137 the data showcased in this thesis. While preparations can sometimes
3138 last even months, typically it is crucial to consider if the ROI for
3139 recording could provide >20 cells, to continue the experiment.
3140 GCaMP is typically designed to be cytosolic and does not typically
3141 cross into the cell nucleus. GCaMP labeled cell bodies appear as
3142 doughnuts in the imaging slice (Figure 26A; Figure 27).

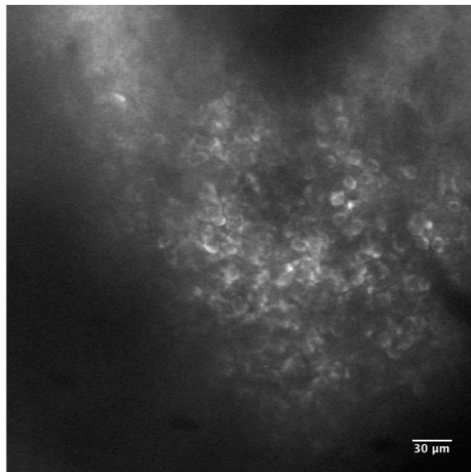
A



DAY 1

Laser Power (at 890 nm): ~50-60 mW
Supply Voltage to PMT: 13.5 V
Control Voltage to PMT: 0.5 V
Preamplifier Sensitivity: 200 nA/V

B



DAY 3

Laser Power (at 890 nm): ~150 mW (!!)
Supply Voltage to PMT: 12-13 V
Control Voltage to PMT: 0.5 V
Preamplifier Sensitivity: 200 nA/V

Figure 26: Tissue Degradation over time. Representative Two-Photon Calcium images of a snapshot in time of the Hippocampal CA1 cell body layer on (A) Day 1 after the surgery and (B) Day 3, after the surgery. Scale bar 30 μm.

3143

3144 Recordings with very good signal-to-noise, where the same chronically
3145 labeled CA1 cells could be anatomically identified on subsequent days
3146 even >2-3 weeks post surgery (Figure 27) were eventually acquired,
3147 and are featured in the data presented in Chapter 4.

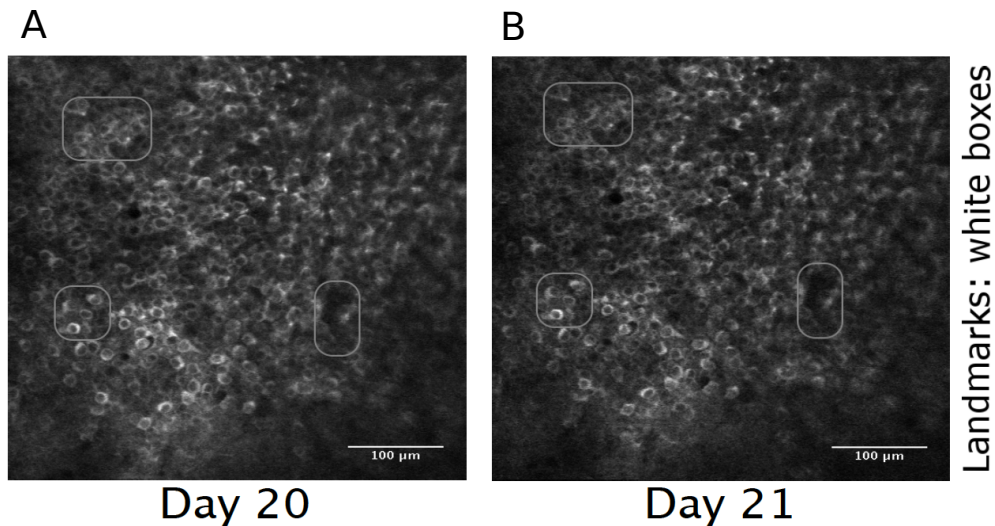


Figure 27: Chronic calcium imaging of the same Hippocampal CA1 cells over weeks. Representative 2-Photon images from (A) Day 20, and (B) Day 21, after surgery. Landmarks have been marked and were used to confirm frame registration and identify cells. Scale bar 100 μm .

3148
 3149 The magnification and resolution of the field of view are important
 3150 parameters to consider when balancing magnification for the resolution
 3151 and the maximization of the number of cells being simultaneously
 3152 recorded from (Figure 25A; Figure 28A).
 3153
 3154 While recording at high frame rates for live imaging, we captured a
 3155 relatively large number of cells (~100) in time-series imaging frames, at
 3156 frame rates of around 10-15 frames per second (FPS). Subsequently,
 3157 we subjected the animal to various stimuli across trials and saved
 3158 these images for analysis.

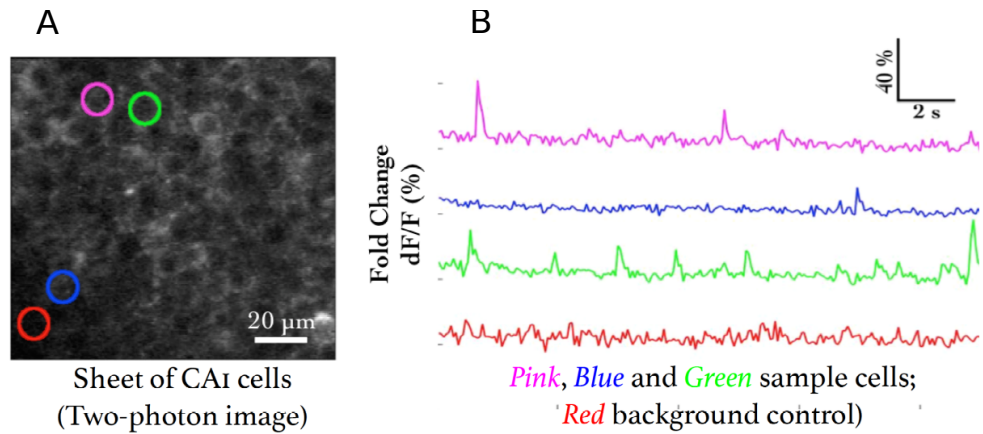


Figure 28: (A) Representative Two-Photon Calcium Image of a plane of Hippocampal CA1 cells expressing GCaMP6f at an instant in time. Example cells marked out post-hoc in pink, blue, and green, with no-cell background in red. Scale bar 20 μ m. (B) Representative dF/F (%) traces for the calcium activity recorded in a single 10s video for example cells – pink, blue, and green, with no-cell background in red. Scale bar 2 sec; 10% dF/F.

3159

3160 Spontaneous activity during non-stimulus periods

3161

3162 We recorded the calcium activity from a large number of hippocampal
 3163 CA1 cell bodies, while presenting various neutral and conditioning
 3164 stimuli, including fairly large periods of time before and after stimulus
 3165 presentation. Activity of cells, typically observed *in vivo*, in these
 3166 periods is termed spontaneous activity. Cells may showcase variable
 3167 rate (number of calcium events per sec) and timing. Given proper
 3168 signal isolation for identified cells in an ROI, each source or “cell” may
 3169 be considered independent, *i.e.* - there is minimized cross talk between
 3170 the fluorescence emitted by each cell body.

3171

3172 **Spatial organization of activity correlated cells during**
3173 **spontaneous activity**

3174

3175 As part of our Acute Imaging experiments using OGB-1, we studied the
3176 Pearson's Correlation Coefficient for the activity traces across all cell
3177 pairs, during bouts of spontaneous activity, viz., all frames from the
3178 beginning of the trial till the presentation of the stimulus, across all
3179 trials. Cell pairs showcased a range of correlation coefficients (Figure
3180 29) and we were able to cluster cells based on activity using Meta-K
3181 Means (unpublished data from Dhawale, 2013; Modi et al., 2014). We
3182 set the initial seed to $k = 3$, with 1000 bootstrap iterations (see Modi et
3183 al., 2014 for sensitivity analysis), distance as specified by pair-wise
3184 correlation coefficient (Figure 29A; Figure 31A; Figure 32A), and a
3185 threshold of 80% to bundle meta-groups.

3186

3187 Correlations were calculated for all frames post the whisker-puff
3188 (stimulus), which corresponds to ~8 s of network activity. It is across
3189 this period that the clustering was performed.

3190

3191 The correlation analysis was performed to check for consistency
3192 across previous recordings in the lab (Modi et al., 2014; Ashesh
3193 Dhawale's Thesis). The idea here is to be able to provide proof-of-
3194 principle results to confirm if the technique was working. Additionally,
3195 although the results are from 1 animal, the session consists of 60 trials
3196 for each of the >100 cells recorded. This very preliminary result has
3197 been studied and described in detail, previously (Modi et al., 2014).

3198

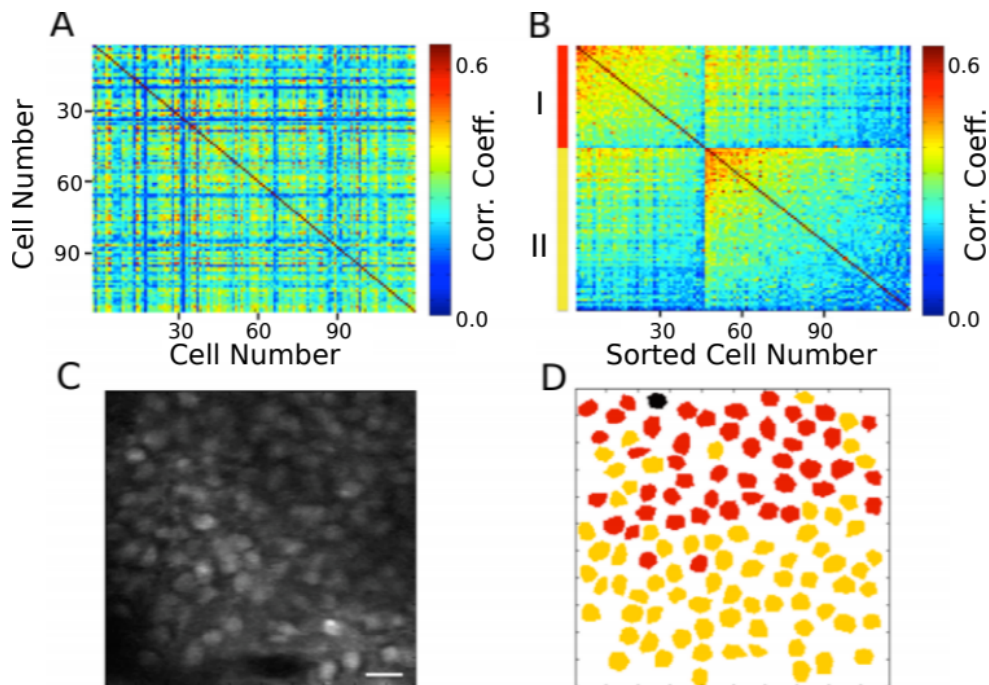


Figure 29: (A) Correlation Coefficients for cell pairs from an example two-photon recording. (B) Meta-K Means clustering with cell pairs using the heuristic that within group pairs would be more similar than between group pairs. In this example, the cells were clustered into two groups, I (red) and II (yellow). (C) Two-Photon image of the field of view of cells; same as Figure 25A. (D) Spatial organization of correlated cell pair groups during spontaneous activity (Modi et al., 2014).

3199 **Stimulus evoked responses**

3200

3201 We also recorded calcium activity from the same cells during
3202 presentation of various neutral stimuli to the animals. Here are the
3203 results of the auditory (tone) and somatosensory (whisker) stimulus
3204 experiments.

3205

3206 A neutral auditory tone at 5000 Hz (for 1 sec) was presented to the
 3207 animals N= 6 animals; 25 trials). We observed no clear signs of cell
 3208 activity modulation by neutral tones. Below, we show an example
 3209 animal with trial-averaged calcium traces as dF/F (%), across all
 3210 recorded cells with a 1 sec tone presentation (Figure 30A). We also
 3211 presented animals to whisker stimulation by playing a 1s long air-puff
 3212 (5 LPM) to the ipsilateral (left) whisker (N = 5 animals; 25 trials). In this
 3213 case, we observed whisker-stimulation based cell activity modulation.
 3214 Below, we show the trial-averaged calcium traces as dF/F (%) of the
 3215 same example animal as above, presented with a 1 sec whisker-puff
 3216 (Figure 30B).

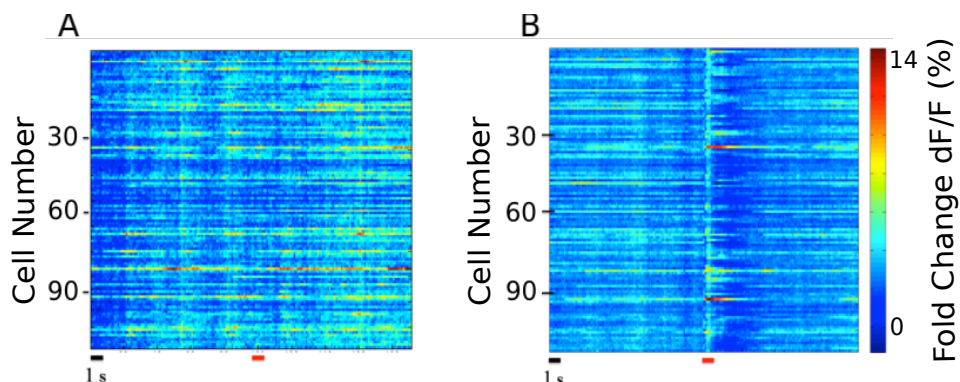


Figure 30: (A) Trial-averaged (25 trials) calcium activity from ~100 CA1 cells in trials where a 5000 Hz tone was presented (red bar). (B) Trial-averaged (18 trials) calcium activity from the same cells in trials where a 5 LPM air-puff to the ipsilateral whiskers was presented (red bar). Scale bar 1 sec (black bar).

3217
 3218 The damage inflicted to the somatosensory cortex was only on one
 3219 hemisphere. We presented somatosensory cortex to the ipsilateral
 3220 whiskers, information that is expected to be processed on the
 3221 contralateral hemisphere. In any case, we observed responses at the
 3222 CA1 timed to the presentation of the whisker-puff, unlike trials with
 3223 tone. We describe tuning modulations across days for the chronically

3224 tracked time cells in the last section of Chapter 3 – “Imaging”. It is very
3225 difficult to isolate and therefore comment on the effect of tissue
3226 recovery, since we did not directly measure this variable.

3227 **Spatial organization of activity correlated cells post whisker-puff
3228 stimulation**

3229

3230 We attempted the same clustering analysis using Meta-K-Means on
3231 the activity profiles of all the cells post presentation of the whisker-puff
3232 till the end of the trial, across all trials (~8 s). These functionally
3233 correlated cell pair groups were found distributed across the imaging
3234 plane with no clear sign of spatial clustering (Figure 31).

3235 Comparing Figure 29D and Figure 31C, we observe that the whisker-
3236 puff stimulation results in a change in the spatial map of correlated
3237 activity, in the same network of cells.

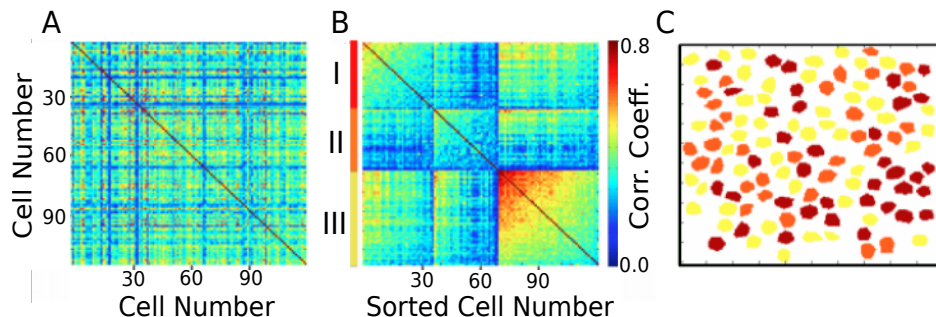


Figure 31: (A) Correlation Coefficients for cell pairs from post whisker-puff stimulation periods. (B) Meta-K Means clustering with cell pairs using the heuristic that within group pairs would be more similar than between group pairs. In this example, the cells were clustered into three groups I (red), II (orange), and III (yellow). (D) No clear spatial organization of correlated cell pair groups post whisker stimulation.

3238

3239 We did not have clear values for the exact duration of the persistence
3240 of the *in vivo*, hippocampal network state post US. This is actually a
3241 very interesting potential experiment, but we did not sub-divide the
3242 post-US period for this analysis. At the time, we only wished to see if
3243 our results were consistent with those previously published (Modi et
3244 al., 2014; Ashesh Dhawale's Thesis), as proof-of-principle for
3245 technique standardization.

3246

3247 As a control, we shuffled the trial time points for each cell
3248 pseudorandomly, to artificially break activity correlations. When we
3249 attempted the Meta-K-Means clustering on this surrogate dataset, we
3250 did not observe functional clustering (Figure 32).

3251

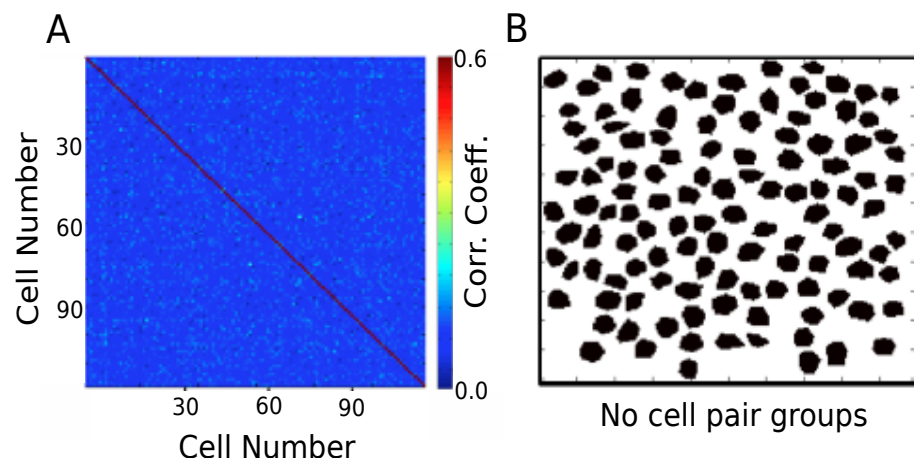


Figure 32: (A) Correlation Coefficients for cell pairs from a trial-shuffle control dataset (B) Meta-K Means clustering revealed that there were no cell pair groups identified.

3255 **Chronic imaging now possible for weeks with the same**
3256 **mouse**

3257

3258 The need for multi-day tracking was mandated for recordings through
3259 behavioural training, since the animals typically only learn Trace Eye-
3260 Blink Conditioning (TEC; Chapter 2) over the course of 3-7 days
3261 (Siegel et al., 2015). A different experiment design would have been to
3262 train animals and then perform the hippocampal preparation to record
3263 CA1 neural activity while the animal(s) exhibit learnt Conditioned
3264 Responses (CRs). However, we argued against this experimental
3265 design, on account of the following.

3266 1. The actual cellular and network mechanisms that allow for the
3267 animal to learn the behavioural task would be very difficult to study
3268 given that the learning period would have passed.

3269 2. The success rate of the hippocampal preparation is typically very
3270 low (estimated at ~33-50% based on the last 200 attempts), given
3271 potential sources of failures such as tissue decay, bleeding into the
3272 imaging window from damaged parts of the hippocampus, implant
3273 instability especially with stressed or unsettled experiment animals,
3274 and photobleaching from the 2-P excitation LASER over multiple
3275 imaging sessions. TEC is typically learnt by >50% animals (Modi et al.,
3276 2014; Siegel et al., 2015). We had argued for exposing the
3277 hippocampus for imaging before behavioural training since any
3278 successful preparations could then be subjected to the relatively more
3279 consistent behavioural training.

3280 3. Having the preparation performed before training minimizes the
3281 number of times the animal would be subjected to surgery (to just the
3282 once), improving chances of animal health through the experiment.

3283

3284 Next, we discuss some preliminary results from the chronic imaging
3285 datasets. A non-overlapping set of results that feature in “Chapter 4 -
3286 Analysis” of this thesis, have been skipped here for brevity.

3287

3288 **Preliminary analysis to identify time cells**

3289

3290 The analysis algorithm pertaining only to the results presented here in
3291 “Chapter 3 - Imaging”, was adapted from William Mau’s Temporal
3292 Information method (Mau et al., 2018; Chapter 4 – “Analysis”). This
3293 version of the algorithm is expected to be subject to some degree of
3294 Type I (false positives) and Type II (false negative) errors.

3295 Subsequently, the algorithm was developed to the extent of the
3296 Python/C++ implementation featured in “Chapter 4 – Analysis”, with
3297 much superior prediction performance.

3298

3299 1. We applied a filter to select for cells that had activity in >25% of
3300 trials (irrespective of tuning)
3301 2. We then develop Peri-stimulus Time Histograms (PSTH), using
3302 Area Under the Curve for a binsize of 3 frames, centering the “0
3303 ms” to the onset of the Conditioned Stimulus for visualization.
3304 3. Next, we estimate Temporal Information (TI), using

$$3305 \quad TI = 1/\lambda * \sum_j \lambda_j \log_2 (\lambda_j / \lambda) P_j$$

3306 where,

3307 λ : Average Transient rate for each cell

3308 λ_j : Average transient rate for each cell in bin “j”

3309 P_j : Probability that the mouse was in time bin “j”

3310 For every trial, we also random shuffled the frame points to develop a
3311 random activity model (1000 times) and ensure that $\lambda > \lambda_{\text{rand}}$ in more
3312 than 99% of the models. Filtering for cells active in >25% trials with a
3313 $\lambda > \lambda_{\text{rand}}$ in >99% shuffles along with the estimation of TI, provided us a
3314 handle on reliability.

3315

3316 We define time cells as cells with a higher probability of eliciting
3317 activation (tuning fields) to specific temporal landmarks across trials,
3318 rather than uniformly over the whole trial. For the results described in
3319 this chapter (Chapter 3 – “Imaging”), our temporal information
3320 calculation was used as a functional definition for time cells.

3321

3322 **Time Cells**

3323

3324 During the experience of temporally organized events or stimuli, in this
3325 case post training to Trace Eye-Blink Conditioning, a rough contingent
3326 of ~20% of the total cells recorded, were observed to showcase time-
3327 locked calcium activity mapping the Blue LED or Conditioned Stimulus
3328 (CS) to the air-puff or Unconditioned Stimulus (US). These cells were
3329 classified as time cells. Here are some example time cells (Figure 33).

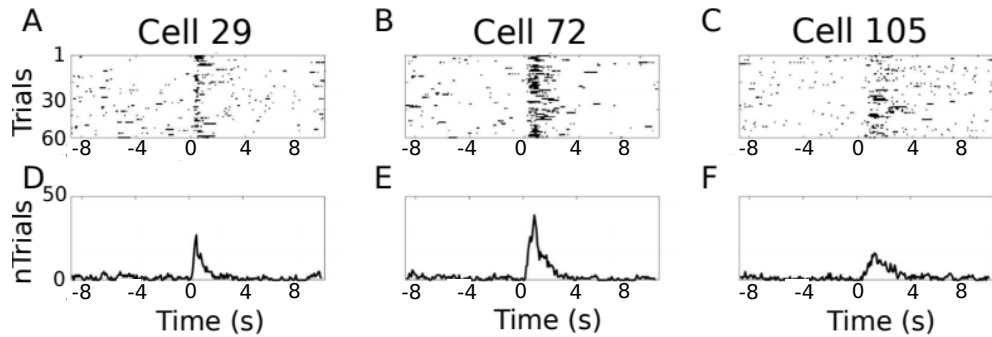


Figure 33: Example Time Cells visualized as event raster plots (A, B, C), along with the trial-summed activity profiles (D, E, F) suggesting ~50% hit trials, for cells 29 and 72 from Session 1 (session type 5) with mouse M26, and slightly lower reliability (~25% hit trials) from cell 105. **The Conditioned Stimulus (CS; blue LED) is presented at time 0 ms.**

3330

3331

3332 Other Cells

3333

3334 On the other hand, most cells did not clear our analysis algorithm

3335 checkpoints and were classified as other cells. Here are some example

3336 Other Cells (Figure 34) from the same session with mouse M26

3337 (Session 1; session type 5).

3338

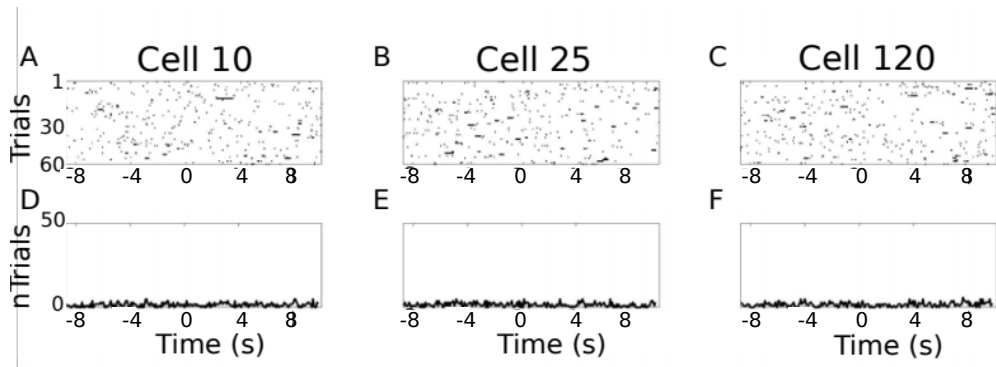


Figure 34: Example Other Cells visualized as event raster plots (A, B, C), along with the trial-summed activity profiles (D, E, F) for cells 10, 25, and 120 from Session 1 (session type 5) with mouse M26. **The Conditioned Stimulus (CS; blue LED) is presented at time 0 ms.**

3339

3340 Considering only the classified time cells, we sorted cells based on the
 3341 time of the peak of the trial-average activity and a spatiotemporal
 3342 sequence was visualized (Figure 35; also see “Chapter 4 - Analysis
 3343 Figure 7H”). **Peri-stimulus time histograms (PSTH) or event time**
 3344 **histograms (ETH)** were developed by summing the number of
 3345 threshold crossing activity events per bin (bin size = 3 frames/bin or
 3346 ~200 ms/bin at 14.5 Hz) across trials. Different cells showcase different
 3347 widths for ETH or tuning curves (Figure 35A; Figure 35B).

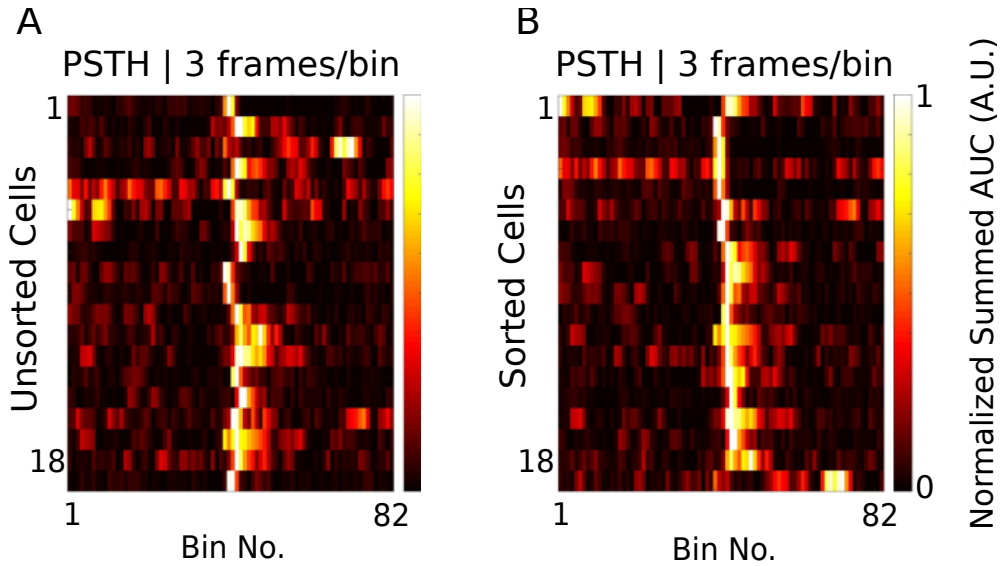


Figure 35: Event Time Histograms or tuning curves for Identified Time-Locked Cells with trial-summed peaks in session 4 of training (session type 5) with mouse M26. (A) Unsorted list of Time cells. (B) Peak-sorted list of the same cells. Here, 1 bin = 3 frames = ~210 ms (sampling rate 14.5 Hz without binning; ~5 Hz with binning). As per the (legacy) session type 5 protocol, the CS (50 ms Blue LED flash) was presented in frame bin 39, followed by a stimulus-free trace interval during frame bins 40 and 41, and then the US (50 ms airpuff to ipsilateral eye) was presented in frame bin 42.

3348

3349

3350 We did not observe any obvious trend in the temporal information of
3351 time cells with peak times. For the same cells (as in Figure 35), we
3352 now look at the actual Temporal Information estimates plotted against
3353 sorted time cells (Figure 36).

3354

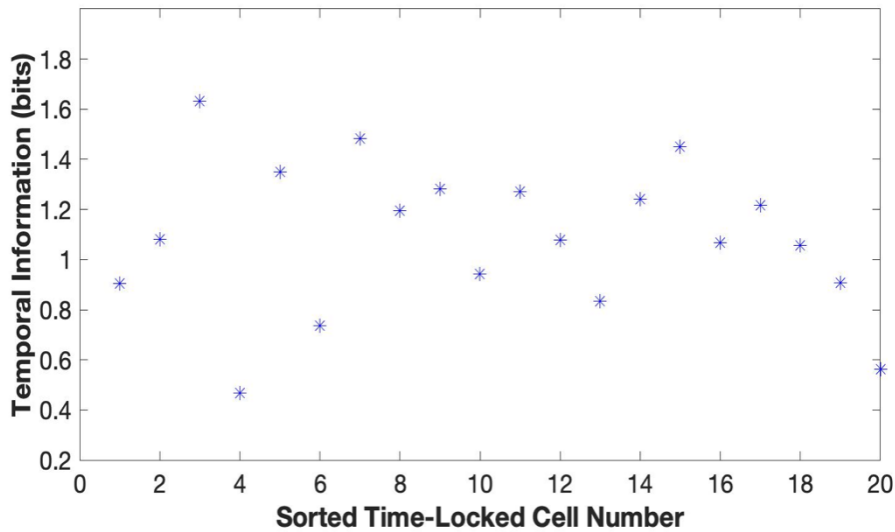


Figure 36: Temporal Information (bits) vs Sorted time cell number from the analytically identified Time Cells in Session 4 (session type 5) with mouse M26. No clear trend was observed.

3371 It has been observed in time cell literature as well as in our real
3372 physiology recordings that time cells with tuning to later time points in a
3373 trial, tend to have wider tuning curves (B. J. Kraus et al., 2015;
3374 MacDonald et al., 2011, 2013; Mau et al., 2018; Pastalkova et al.,
3375 2008). This is why no obvious trend in a graph of Temporal Information
3376 vs time of peak sorted time cells, seemed curious enough to mention in
3377 the thesis. However, while we report the observation, we made no
3378 attempts to delineate further detail, given a limited number of
3379 observations. This legacy adaptation of the temporal information
3380 calculation had not been benchmarked and thus the result was not
3381 certain, at the time. Subsequently, we have observed similar results in
3382 other lab colleague's recordings, and avoided further discussion, with
3383 regard to the scope of this thesis.

3384 **Tuning, re-tuning, and de-tuning of time cells across**
3385 **sessions**

3386
3387 A crucial advantage of the chronic preparation was that many
3388 anatomically aligned and classified cells (as cell ROIs), could be
3389 recorded from over several days and sessions, to look for possible
3390 changes in calcium activity profiles across sessions in the same set of
3391 cells.

3392
3393 We noticed some evidence for an expansion of the set of identified
3394 time cells with sessions, up to a reliable pool of ~20% time cells.
3395 Altogether, from the pool of chronically aligned cells (across sessions),
3396 there was an increase from 7.7% to 23.1% of time cells. Considering
3397 the full cohort cells (irrespective of tracking across multiple training
3398 sessions) the increase was from 7.2% to 21.1% time cells. Here are

3399 the classified time cells between two independent recording sessions,
3400 early in training (Figure 37).

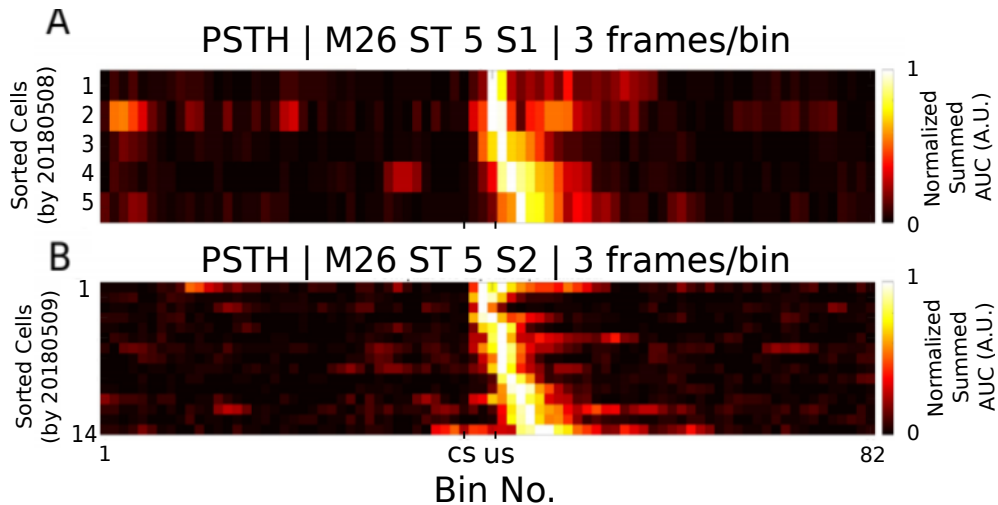


Figure 37: More time cells observed to attain tuning as training sessions. Event Time Histograms of the identified set of time cells between A) Sessions 1 and (B) Session 2, with mouse M26 (session type 5).

3401
3402 The same may also be visualized as trial-averaged calcium activity
3403 profiles for all recorded cells across independent recording sessions
3404 (Figure 38).

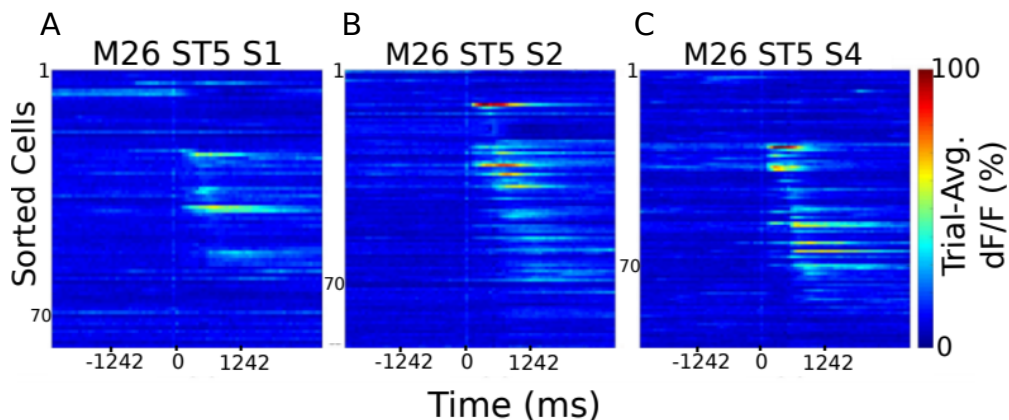


Figure 38: Sorted Time Cells form Sequences that develop with learning. Trial-Averaged calcium activity traces for all recorded cells across A) Session 1, B) Session 2, and C) Session 4, with mouse M26 (sessiontype 5). Time 0 ms was aligned to the CS. The CS + Trace + US interval lasted from 0-600 ms, here.

3405

3406 Chronically tracked time cells that showed reliable tuning across
 3407 sessions were then compared to look for any shifts in the peak tuning
 3408 bin. We observed examples of cells that maintained their tuning across
 3409 pairs of sessions (Figure 39).

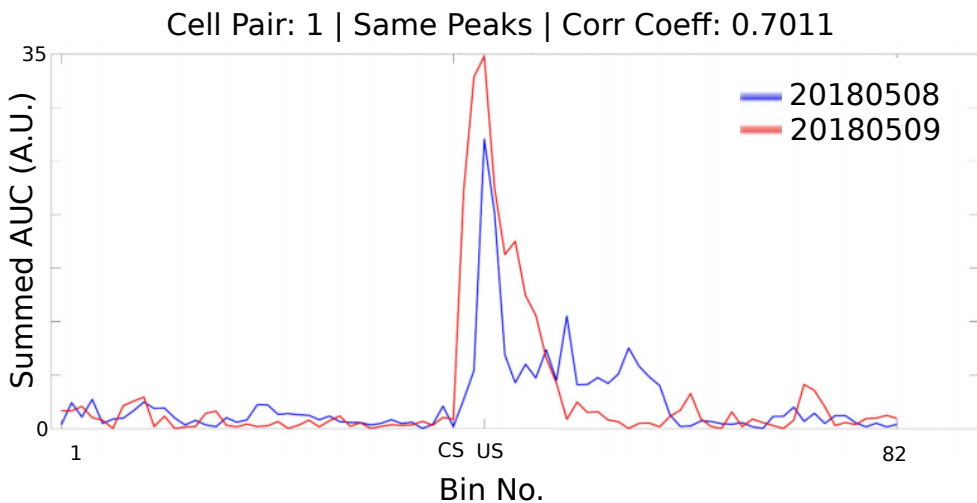


Figure 39: Same/similar tuning across session 1 and session 2 for this example time cell. Blue Event Time Histograms represent the tuning curve for the cell for session 1 (date: 20180508) and Red represent the same but for session 2 (date: 20180509). Pearson's correlation coefficient between the two session pairs was 0.7011.

3410

3411 Here are examples wherein the tuning curve peaks shift to earlier time
 3412 points, across sessions (Figure 40) for Mouse M26, session type 5,
 3413 session 1 vs 2.

3414

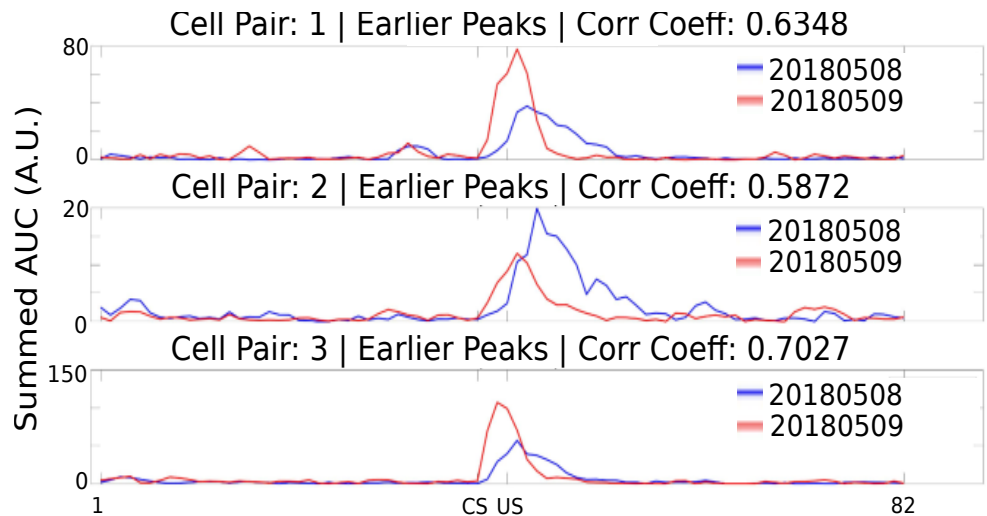


Figure 40: Three example chronically tracked cell pairs with tuning peaks arriving earlier with training sessions (rows). Blue Event Time Histograms represent the tuning curve for any cell for session 1 (date: 20180508) and Red represent the same but for session 2 (date: 20180509). Pearson's correlation coefficient between the session pairs was 0.6.348, 0.5872 and 0.7027 for A) cell pair 1, B) cell pair 2, and C) cell pair3, respectively.

3416 Here is an example of a cell showcasing de-tuning for the CS-US
3417 interval, across sessions (Figure 41), potentially with a new, delayed
3418 peak almost 100 frames later.

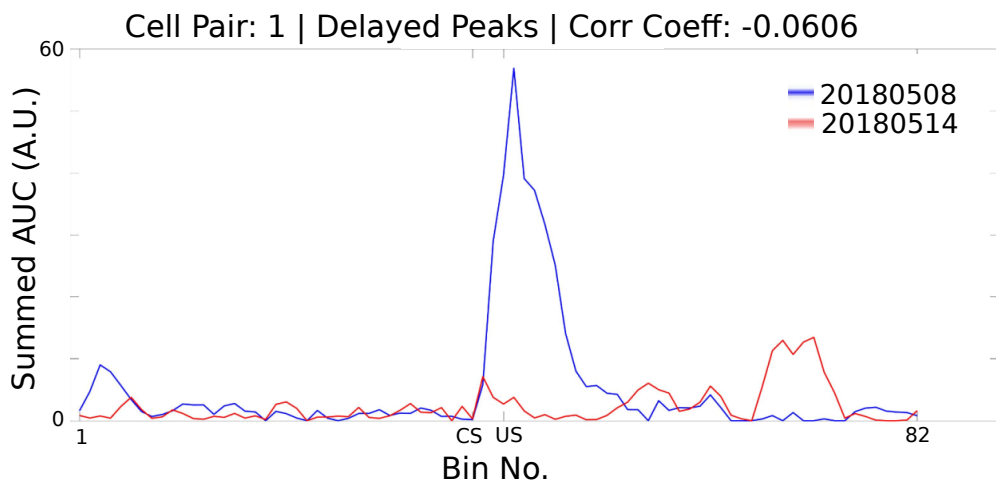


Figure 41: Example chronically tracked cell pair with de-tuning between session 1 and 4. Blue Event Time Histograms represent the tuning curve for the example cell for session 1 (date: 20180508) and Red represent the same but for session 4 (date: 20180514). Pearson's correlation coefficient between the two curves was -0.0606.

3419
3420 A full summary of the correlation based peak timing analysis for
3421 chronically identified time cells with mouse M26 is shown (Figure 42).
3422 Across all same cell pairs (~60% of all session-wise cells tracked; ~80
3423 cells), there was positive correlation (>0.2) in 71% of Time Cells
3424 (Figure 42A). Typically, we observed only at best a correlation
3425 coefficient of ~0.6-0.8 across cell pairs (see Figures 29 and 31). We
3426 chose 0.2 as the threshold, accordingly.
3427
3428 Also a comparison of the tuning curve peaks between the same time
3429 cell pairs (Figure 42B) revealed that a majority of the re-tuned peaks
3430 occurred earlier in time, going across sessions (71%), with an equal

3431 proportion of cells without much re-tuning (14%) or de-tuning to later
3432 time points (14%).

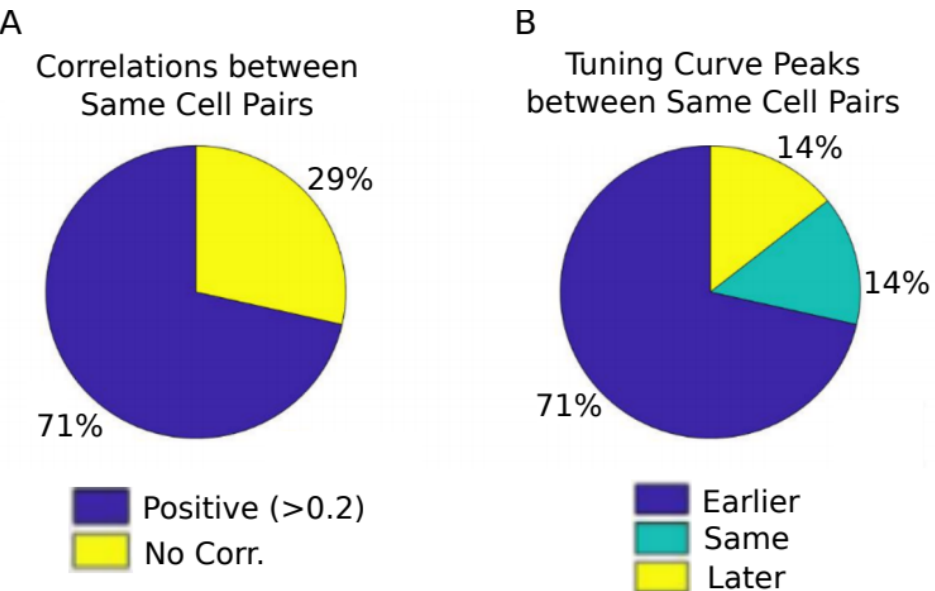


Figure 42: Comparing chronically tracked time cells across sessions for all matched cell pairs by (A) Correlation Analysis, and (B) Timing of peaks.

3433

3434 A summary of the key preliminary results observed using real
3435 physiology data is as follows.

3436 1. Time cell tuning curve peaks typically began only after the
3437 presentation of the CS.

3438 2. The width of the tuning curve peaks for time cells increased with
3439 tuning to later frame bins. This was consistent with the recordings
3440 presented in literature under physiological conditions (B. Kraus et al.,
3441 2013; B. J. Kraus et al., 2015; MacDonald et al., 2011, 2013; Mau et
3442 al., 2018; Pastalkova et al., 2008).

3443 3. Pairwise time cell tuning curves for different time cells may have
3444 some overlap in timing, but peaks were observed in all frame bins
3445 between the CS and the US. This particular observation is confounded

3446 by the short number of Trace period frames recorded and the
3447 requirement to consider 3 recording frames to every bin (Mau et al.,
3448 2018), decreasing the effective sampling rate even further (14.5 Hz
3449 without binning, to ~5 Hz with binning). However, the observation is still
3450 consistent with previous literature (B. Kraus et al., 2013; B. J. Kraus et
3451 al., 2015; MacDonald et al., 2011, 2013; Mau et al., 2018; Modi et al.,
3452 2014; Pastalkova et al., 2008).

3453 4. A surprisingly large number of time cells could be identified with
3454 tuning peaks for frame bins occurring after the termination of the US.
3455 Single cell measurements tend to define responses up to 200-1000 ms
3456 post US. Our own correlation-based clustering analysis was across the
3457 whole post US phase (vs pre-stim phase), which corresponded to ~8s.
3458 It was surprising to us, that such a wide window post-US period could
3459 still reveal distinctly different spatial clustering to a comparable ~8s
3460 window pre-CS.

3461 5. Considering all chronically tracked cells, the classified and sorted
3462 time cells formed sequences that were dynamic across learning
3463 sessions. Many time cells developed tuning curves with sessions while
3464 some time cells lost their tuning.

3465 6. For the majority of time cells, re-tuning occurred with initial tuning to
3466 the timing of the US in earlier sessions, followed by a shift to earlier
3467 time points for the tuning peak, as training progressed through
3468 sessions.

3469
3470 Our preliminary imaging and behaviour results describe neuronal
3471 sequence activations based on the emergence or re-tuning dynamics
3472 of temporal tuning by time cells, during early phases of behavioural
3473 acquisition, in a chronically tracked fashion. Future directions to be
3474 explored in the lab include studying the reliability of a larger pool of

3475 chronically tracked cells with switches in the inter-stimulus interval (ISI)
3476 between the CS and the US as well as with a larger palette of different
3477 stimuli testing out a battery of Conditioned Stimuli (CS1, CS2, etc.) and
3478 Unconditioned Stimuli (US1, US2, etc.). The goal is to understand how
3479 well the internal neural spatiotemporal CA1 sequence maps to the
3480 external behavioural protocol parameters, *in vivo*.

3481 **Bibliography**

- 3482 Abe, R., Sakaguchi, T., Matsumoto, N., Matsuki, N., & Ikegaya, Y.
3483 (2014). Sound-induced hyperpolarization of hippocampal neurons.
3484 *Neuroreport*, 25(13), 1013–1017.
3485 <https://doi.org/10.1097/WNR.0000000000000206>
- 3486 Andersen, P., Morris, R., Amaral, D., Bliss, T., & O'Keefe, J. (Eds.).
3487 (2006). *The Hippocampus Book*. Oxford University Press.
3488 <https://doi.org/10.1093/acprof:oso/9780195100273.001.0001>
- 3489 Attardo, A., Fitzgerald, J. E., & Schnitzer, M. J. (2015). Impermanence
3490 of dendritic spines in live adult CA1 hippocampus. *Nature*,
3491 523(7562), 592–596. <https://doi.org/10.1038/nature14467>
- 3492 Bellistri, E., Aguilar, J., Brotons-Mas, J. R., Foffani, G., & de la Prida, L.
3493 M. (2013). Basic properties of somatosensory-evoked responses
3494 in the dorsal hippocampus of the rat. *The Journal of Physiology*,
3495 591(10), 2667–2686. <https://doi.org/10.1113/jphysiol.2013.251892>
- 3496 Dhawale, A. K. (2013). *Temporal and spatial features of sensory
3497 coding in the olfactory bulb and hippocampus*. Tata Institute of
3498 Fundamental Research.
- 3499 Dombeck, D. A., Harvey, C. D., Tian, L., Looger, L. L., & Tank, D. W.
3500 (2010). Functional imaging of hippocampal place cells at cellular
3501 resolution during virtual navigation. *Nature Neuroscience*, 13(11),
3502 1433–1440. <https://doi.org/10.1038/nn.2648>
- 3503 Fanselow, M. S., & Dong, H.-W. (2010). Are the dorsal and ventral
3504 hippocampus functionally distinct structures? *Neuron*, 65(1), 7–19.
3505 <https://doi.org/10.1016/j.neuron.2009.11.031>
- 3506 Harvey, C. D., Collman, F., Dombeck, D. A., & Tank, D. W. (2009).
3507 Intracellular dynamics of hippocampal place cells during virtual
3508 navigation. *Nature*, 461(7266), 941–946.
3509 <https://doi.org/10.1038/nature08499>
- 3510 Hjorth-Simonsen, A., & Jeune, B. (1972). Origin and termination of the
3511 hippocampal perforant path in the rat studied by silver

- 3512 impregnation. *The Journal of Comparative Neurology*, 144(2),
3513 215–232. <https://doi.org/10.1002/cne.901440206>
- 3514 Itskov, P. M., Vinnik, E., & Diamond, M. E. (2011). Hippocampal
3515 representation of touch-guided behavior in rats: persistent and
3516 independent traces of stimulus and reward location. *PLoS One*,
3517 6(1), e16462. <https://doi.org/10.1371/journal.pone.0016462>
- 3518 Kaifosh, P., Lovett-Barron, M., Turi, G. F., Reardon, T. R., & Losonczy,
3519 A. (2013). Septo-hippocampal GABAergic signaling across
3520 multiple modalities in awake mice. *Nature Neuroscience*, 16(9),
3521 1182–1184. <https://doi.org/10.1038/nn.3482>
- 3522 Kamondi, A. (1998). *Theta Oscillations in Somata and Dendrites of*
3523 *Hippocampal Pyramidal Cells In Vivo: Activity-Dependent Phase-*
3524 *Precession of Action Potentials*. 261(March), 244–261.
- 3525 Kraus, B. J., Brandon, M. P., Robinson, R. J., Connerney, M. A.,
3526 Hasselmo, M. E., & Eichenbaum, H. (2015). During Running in
3527 Place, Grid Cells Integrate Elapsed Time and Distance Run.
3528 *Neuron*, 88(3), 578–589.
3529 <https://doi.org/10.1016/j.neuron.2015.09.031>
- 3530 Kraus, B., Robinson, R., White, J., Eichenbaum, H., & Hasselmo, M.
3531 (2013). Hippocampal “Time Cells”: Time versus Path Integration.
3532 *Neuron*, 78(6), 1090–1101.
3533 <https://doi.org/10.1016/j.neuron.2013.04.015>
- 3534 Lovett-Barron, M., Kaifosh, P., Kheirbek, M. A., Danielson, N.,
3535 Zaremba, J. D., Reardon, T. R., Turi, G. F., Hen, R., Zemelman, B.
3536 V, & Losonczy, A. (2014). Dendritic inhibition in the hippocampus
3537 supports fear learning. *Science (New York, N.Y.)*, 343(6173), 857–
3538 863. <https://doi.org/10.1126/science.1247485>
- 3539 MacDonald, C. J., Carrow, S., Place, R., & Eichenbaum, H. (2013).
3540 Distinct hippocampal time cell sequences represent odor
3541 memories in immobilized rats. *The Journal of Neuroscience : The*
3542 *Official Journal of the Society for Neuroscience*, 33(36), 14607–
3543 14616. <https://doi.org/10.1523/JNEUROSCI.1537-13.2013>
- 3544 MacDonald, C. J., Lepage, K. Q., Eden, U. T., & Eichenbaum, H.
3545 (2011). Hippocampal “time cells” bridge the gap in memory for
3546 discontiguous events. *Neuron*, 71(4), 737–749.
3547 <https://doi.org/10.1016/j.neuron.2011.07.012>
- 3548 Mau, W., Sullivan, D. W., Kinsky, N. R., Hasselmo, M. E., Howard, M.
3549 W., & Eichenbaum, H. (2018). The Same Hippocampal CA1
3550 Population Simultaneously Codes Temporal Information over
3551 Multiple Timescales. *Current Biology*, 28(10), 1499-1508.e4.
3552 <https://doi.org/10.1016/j.cub.2018.03.051>
- 3553 Modi, M. N., Dhawale, A. K., & Bhalla, U. S. (2014). CA1 cell activity
3554 sequences emerge after reorganization of network correlation

- 3555 structure during associative learning. *eLife*, 3, e01982–e01982.
3556 <https://doi.org/10.7554/eLife.01982>
- 3557 Moser, M.-B., & Moser, E. I. (1998). Distributed encoding and retrieval
3558 of spatial memory in the hippocampus. In *The Journal of*
3559 *Neuroscience* (Vol. 18, pp. 7535–7542). Society for Neuroscience.
- 3560 Nakashiba, T., Young, J. Z., McHugh, T. J., Buhl, D. L., & Tonegawa,
3561 S. (2008). Transgenic inhibition of synaptic transmission reveals
3562 role of CA3 output in hippocampal learning. *Science (New York,*
3563 *N.Y.*), 319(5867), 1260–1264.
3564 <https://doi.org/10.1126/science.1151120>
- 3565 Pachitariu, M., Stringer, C., Dipoppa, M., Schröder, S., Rossi, L. F.,
3566 Dalgleish, H., Carandini, M., & Harris, K. D. (2017). Suite2p:
3567 beyond 10,000 neurons with standard two-photon microscopy.
3568 *BioRxiv*, 61507. <https://doi.org/10.1101/061507>
- 3569 Pastalkova, E., Itskov, V., Amarasingham, A., & Buzsaki, G. (2008).
3570 Internally Generated Cell Assembly Sequences in the Rat
3571 Hippocampus. *Science*, 321(5894), 1322–1327.
3572 <https://doi.org/10.1126/science.1159775>
- 3573 Peron, S. P., Freeman, J., Iyer, V., Guo, C., & Svoboda, K. (2015). A
3574 Cellular Resolution Map of Barrel Cortex Activity during Tactile
3575 Behavior. *Neuron*, 86(3), 783–799.
3576 <https://doi.org/10.1016/j.neuron.2015.03.027>
- 3577 Siegel, J. J., Taylor, W., Gray, R., Kalmbach, B., Zemelman, B. V.,
3578 Desai, N. S., Johnston, D., & Chitwood, R. A. (2015). Trace
3579 Eyeblink Conditioning in Mice Is Dependent upon the Dorsal
3580 Medial Prefrontal Cortex, Cerebellum, and Amygdala: Behavioral
3581 Characterization and Functional Circuitry. *ENeuro*, 2(4),
3582 ENEURO.0051-14.2015. <https://doi.org/10.1523/ENEURO.0051-14.2015>
- 3584 Sofroniew, N. J., Flickinger, D., King, J., & Svoboda, K. (2016). A large
3585 field of view two-photon mesoscope with subcellular resolution for
3586 in vivo imaging. *eLife*, 5(JUN2016), 1–20.
3587 <https://doi.org/10.7554/eLife.14472>
- 3588 Stosiek, C., Garaschuk, O., Holthoff, K., & Konnerth, A. (2003). In vivo
3589 two-photon calcium imaging of neuronal networks. *Proceedings of*
3590 *the National Academy of Sciences of the United States of*
3591 *America*, 100(12), 7319–7324.
3592 <https://doi.org/10.1073/pnas.1232232100>
- 3593 Suh, J., Rivest, A. J., Nakashiba, T., Tominaga, T., & Tonegawa, S.
3594 (2011). Entorhinal cortex layer III input to the hippocampus is
3595 crucial for temporal association memory. *Science (New York,*
3596 *N.Y.*), 334(6061), 1415–1420.
3597 <https://doi.org/10.1126/science.1210125>

3598 Vinogradova, O. S. (2001). Hippocampus as comparator: Role of the
3599 two input and two output systems of the hippocampus in selection
3600 and registration of information. *Hippocampus*, 11(5), 578–598.
3601 <https://doi.org/https://doi.org/10.1002/hipo.1073>

3602

3603 **Chapter 4 – Analysis**

3604

3605

3606 Our efforts to identify the best use cases for the various implemented
3607 time cell analysis algorithms on the basis of a testbed of user-defined,
3608 categorically labeled synthetic data with known ground truth (Project
3609 III), have been consolidated into a publication. The early access
3610 version of our paper (along with supplementary figures) has been
3611 attached.

3612

Novel Tools and Methods

Synthetic Data Resource and Benchmarks for Time Cell Analysis and Detection Algorithms

Kambadur G. Ananthamurthy and Upinder S. Bhalla

<https://doi.org/10.1523/ENEURO.0007-22.2023>

National Centre for Biological Sciences - Tata Institute of Fundamental Research, Bellary Road, Bengaluru - 560065, Karnataka, India

Abstract

Hippocampal CA1 cells take part in reliable, time-locked activity sequences in tasks that involve an association between temporally separated stimuli, in a manner that tiles the interval between the stimuli. Such cells have been termed time cells. Here, we adopt a first-principles approach to comparing diverse analysis and detection algorithms for identifying time cells. We generated synthetic activity datasets using calcium signals recorded *in vivo* from the mouse hippocampus using two-photon (2-P) imaging, as template response waveforms. We assigned known, ground truth values to perturbations applied to perfect activity signals, including noise, calcium event width, timing imprecision, hit trial ratio and background (untuned) activity. We tested a range of published and new algorithms and their variants on this dataset. We find that most algorithms correctly classify over 80% of cells, but have different balances between true and false positives, and different sensitivity to the five categories of perturbation. Reassuringly, most methods are reasonably robust to perturbations, including background activity, and show good concordance in classification of time cells. The same algorithms were also used to analyze and identify time cells in experimental physiology datasets recorded *in vivo* and most show good concordance.

Significance Statement

Numerous approaches have been developed to analyze time cells and neuronal activity sequences, but it is not clear whether their classifications match, nor how sensitive they are to various sources of data variability. We provide two main contributions to address this: (1) a resource to generate ground truth labeled synthetic two-photon (2-P) calcium activity data with defined distributions for confounds such as noise and background activity, and (2) a survey of several methods for analyzing time cell data using our synthetic data as ground truth. As a further resource, we provide a library of efficient C++ implementations of several algorithms with a Python interface. The synthetic dataset and its generation code are useful for profiling future methods, testing analysis toolchains, and as input to computational and experimental models of sequence detection.

Introduction

The mammalian hippocampus is important for the formation of several kinds of memory, one of which is the association between stimuli occurring separately in time. Time cells were originally described using tuning curves from single-unit recordings of cellular activity when rats ran on a running wheel in between behavioral decisions (Pastalkova et al., 2008). These cells exhibited time tuning of the order of seconds. Several further studies have shown that small populations of hippocampal CA1 cells

fire in time-locked sequences, “bridging” the time gap between stimulus and response in temporal delay tasks lasting several seconds (Pastalkova et al., 2008; MacDonald et al., 2011, 2013; Kraus et al., 2013). Cellular calcium imaging studies have also been used to report time cells, albeit at slower sampling rate (Modi et al., 2014; Mau et al., 2018). For example, similar interval tiling properties of hippocampal CA1 neurons were observed on much shorter, 500 ms timescales in a Trace Eyeblink Conditioning (TEC) task (Modi et al., 2014). Spontaneous sequential activity

Received January 2, 2022; accepted February 9, 2023; First published February 23, 2023.

The authors declare no competing financial interests.

Author contributions: K.G.A. and U.S.B. designed research; K.G.A. performed research; K.G.A. and U.S.B. analyzed data; K.G.A. and U.S.B. wrote the paper.

has also been reported in free-running animals (Villette et al., 2015). Such cells with a well-defined temporal firing field are commonly termed time cells (MacDonald et al., 2011; Eichenbaum, 2017). However, there is a wide diversity of methods used to detect and characterize time cells, and it is not clear how consistent these methods are in classifying cells as time cells. It is also unclear how sensitive each method may be to a range of physiological sources of variability and noise. A consistent set of benchmarks of classification performance is necessary to draw accurate and comparable conclusions from real physiology data across different methods and different laboratories. Our approach in the current study is not prescriptive, but pragmatic: we ask how existing methods work when we already know exactly which cells are time cells, and we determine how well each method deals with imperfect data.

The major approaches used to identifying time cells are tuning curves (peristimulus time histograms), temporal information (TI), principal component analysis with time offset, support vector machines, and bootstrap analysis of activity peaks. Several studies have used a temporal delay task lasting several seconds, in which a rat runs on a treadmill during the delay period. A temporal information metric (Mau et al., 2018) has been used to find individual time cells in such tasks. A distinct task involves monitoring recurrent sequences of activity during free-running treadmill recordings. Such datasets have been analyzed using offset principal component analysis (Kaifosh et al., 2013; Villette et al., 2015; Malvache et al., 2016), to first denoise two-photon (2-P) data, establish correlation coefficients, and detect hippocampal CA1 sequences. Time cells have also been reported for much shorter duration tasks (~500 ms) such as hippocampus-dependent trace conditioning (Tseng et al., 2004; Modi et al., 2014). Time cells in these 2-P datasets were identified using yet another method, in which bootstrapping was used to determine whether peak activity at a given time was different from chance. This method was termed ratio of ridge/background (Modi et al., 2014). Yet other methods have utilized support vector machines to categorize time cells (Ahmed et al., 2020). Additionally, while the applicability of a variety of algorithms for place cell detection has been previously compared (Souza et al., 2018), we have

K.G.A. and the experiments received support from the Department of Biotechnology Grant BT/PR12255/MED/122/8/2016 (to U.S.B.). National Centre for Biological Sciences-Tata Institute of Fundamental Research (NCBS-TIFR) provided resources for analysis equipment and support to U.S.B. through intramural funds supported by the Department of Atomic Energy, Government of India, Project Identification No. TRI 4006.

Acknowledgments: We thank Daniel Dombeck for help with the chronic preparation for physiological 2-P calcium recording of hippocampal CA1 cells and William Mau for his Temporal Information calculation code. We also thank Vinu Varghese and Bhanu Priya Somashekhar for helpful comments on this manuscript.

Correspondence should be addressed to Upinder S. Bhalla at bhalla@ncbs.res.in.

<https://doi.org/10.1523/ENEURO.0007-22.2023>

Copyright © 2023 Ananthamurthy and Bhalla

This is an open-access article distributed under the terms of the Creative Commons Attribution 4.0 International license, which permits unrestricted use, distribution and reproduction in any medium provided that the original work is properly attributed.

focused on methods which are fully automatable and which scale well to large datasets, specifically comparing algorithms to detect time cells.

Time cell detection is closely related to sequence detection, which has been fraught with statistical challenges. For example, detection of synfire chains has been the subject of some debate (Ikegaya et al., 2004; Lee and Wilson, 2004; Mokeichev et al., 2007; Schrader et al., 2008). Time cell detection is usually easier, in that in most experiments there is a well-defined initiating stimulus and a known delay or trace phase (however, see Villette et al., 2015). For any cell identified as a time cell, it is desirable to define a score to measure quality or reliability along with decodable time. Hence it is also valuable to be able to compare the score of a time cell across recordings and even between groups, using well defined, analog measures. Each algorithm currently used in the literature implements a different scoring method and it is as yet unclear whether comparable results would be observed with other metrics.

In the current study, we compare these diverse methods by estimating their performance on synthetic test datasets where we controlled all features of the data, including the identity and timing of each time cell. The development of a synthetic dataset serves two purposes. First, it facilitates principled comparison of different methods, since the ground truth is known. Second, it facilitates an analysis over many dimensions of input variance, corresponding to very different experimental and neural circuit contexts. Richness in variety of input data allows for better sampling of the performance of the analyses under many potential conditions. We have explored variance along the key dimensions of noise, timing imprecision, signal widths, frequency of occurrence, as well as several others. To strengthen the applicability of this synthetic data resource to real data, our generated output uses sampled experimental data.

Our experimental data, synthetic dataset, and code base are intended to be a resource for algorithm testing and optimization.

Materials and Methods

Animals, chronic implants, and behavioral training

All animal procedures were performed in accordance with the National Centre for 114 Biological Sciences Institutional Animal Ethics Committee (project ID NCBS115 IAE-2016/20(M)), in accordance with the guidelines of the Government of India (Animal Facility CPCSEA registration number 109/1999/CPCSEA) and equivalent guidelines of the Society for Neuroscience.

To chronically monitor the activity of the same population of hippocampal CA1 cells, we implanted two- to four-month-old male and female GCaMP6f mice [Tg(Thy1-GCaMP6f)GP5.17Dkim JAX stock #025393] with an optical window and head-bar using a protocol adapted from previously published methods (Dombeck et al., 2010). Briefly, anesthesia was induced with 2–3% isoflurane in a chamber, and subsequently maintained (breathing rate of ~1 Hz) with 1–2% isoflurane, directly to the mouse's nose using an inverted pipette tip. Surgery was performed on a

temperature-controlled table, maintained at 36.5°C, while the anaesthetized animal was cheek-clamped. After a haircut, a ~5 cm piece of scalp was cut open to reveal the skull. A ~3 mm circular craniotomy was then performed at a position 2 mm caudal and ~1.5 mm lateral to bregma, on the left hemisphere. After gently tearing off the dura, the underlying cortex was carefully aspirated till the corpus callosum (CC) layer, clearing out any blood using repeated washes of cortex buffer (Modi et al., 2014). A small thickness of corpus callosum fibers were then carefully aspirated till horizontal CC fibers were sparse but visible. The cortex buffer was then carefully suctioned out to dry the exposure till tacky. The exposure was then quickly sealed using a thin layer of Kwik-Sil and a coverslip attached to the bottom of a 3 mm steel cannula. This preparation left the CA1 cell body layer ~200 μm below the most exposed tissue. Finally, an imaging head-bar was surgically implanted and fixed to the scalp, using dental cement and skull screws, before the animal was brought out of anesthesia.

The animals were allowed to recover for 1–5 d after implantation, with a further 3–4 d of habituation to the rig. Following this simultaneous behavioral training and 2-P *in vivo* imaging was conducted.

Trace Eyeblink Conditioning (TEC)

We standardized a multi-session Trace Eyeblink Conditioning (TEC) paradigm to train head-fixed mice, based on previous literature (Siegel et al., 2015). TEC involves an association between a previously neutral conditioned stimulus (CS) with an eyeblink inducing unconditioned stimulus (US), across an intervening, stimulus-free, trace interval. Training involved 60 trials per session, one session a day, for approximately two weeks. The CS was a 50 ms blue LED flash while the US was a 50 ms air-puff to the left eye. The stimulus-free trace interval was 250–750 ms long, depending on the session. Additionally, a pseudorandom 10% of the trials were CS-only probe trials (no US) to test for learning. All behavior routines were controlled by programmed Arduinos. Eyeblinks were measured for every trial, by video camera (Point Gray Chameleon3 1.3 MP Monochrome USB3.0) based detection.

The conditioned response (CR) is observed as a preemptive blink before the US is delivered, in animals that learn the task. The analysis of the behavioral data was performed using custom written MATLAB scripts. In brief, each frame for every trial was:

1. Cropped to get the eye;
2. Binarized to get the pixels defining just the eye, and finally;
3. Given an FEC score from 0 to 1 (see below).

Every trial was then scored as a hit or miss, using the result of a two-sample Kolmogorov-Smirnov test between the FEC during the trace and pre-CS period (1% significance). The performance of an animal for a session was then established as the percentage of hit trials/total trials.

Definitions:

FEC: The fraction of eye-closed is estimated by counting the pixels defining the eye in every image of a time series, normalized by the maximum number of pixels defining the eye, in that session. Thus, every frame was given an analog score from 0 to 1, where,

- 0: fully opened eye
- 1: fully closed eye

CR: The conditioned response is the eye-closing transition during the trace period.

UR: The unconditioned response is the eye-closing transition when the US is delivered.

Performance: Percentage of hit trials/total trials. This allowed us to observe how the animals perform during and across sessions.

Two-photon imaging

We used a custom-built two photon laser-scanning microscope (Modi et al., 2014) to record calcium activity from 100–150 hippocampal CA1 cell bodies *in vivo*, at cellular resolution. We performed galvo-scans through the imaging window, over a field of view of ~100 × 100 μm², at 14.5 Hz, during TEC (Fig. 1A). An Arduino microcontroller was used to control the behavior routines, and it additionally sent a TTL trigger to initiate the imaging trials. The behavior and imaging were conducted simultaneously to record calcium activity when the animal was learning the task.

Time-series fluorescence data for various cells was extracted using Suite2P (Pachitariu et al., 2017). All further analysis and code development was done on MATLAB R2017b and batch analysis runs were performed on MATLAB R2021a. The average of the fluorescence values for cell specific pixels is then converted into the fold change relative to the baseline (dF/F₀; F₀ as 10th percentile), for every marked cell, in every trial (Fig. 1B). These dF/F traces were used for the rest of the analysis.

Curating a library of calcium events

For all synthetic data experiments, we used one good quality 2-P recording session's worth of data from one animal. We mapped our imaging dataset into a matrix of dF/F values for all cells, trials, and frames. We then identified calcium events as signal deviations that were above a threshold (mean ± 2*SD) for more than four consecutive frames (frame rate: 14.5 Hz or ~70 ms per frame). Once identified, we curated a library for each event by a cell, and saved the respective start indices and widths. Using this library, we generated synthetic data by inserting experimental calcium events into the time series for each simulated cell. This approach just uses a time series of signal bins and amplitudes, hence is signal-agnostic and could be applied to other imaging and recording modalities. In the interests of data integrity, our synthetic datasets were watermarked to be distinguishable from real physiology datasets.

Generating synthetic data

Synthetic data were generated using a custom-written MATLAB function script “generateSyntheticData()” in the provided code repository. We preallocated and set up a 3-D matrix of zeros (as cells, trials, frames), and added

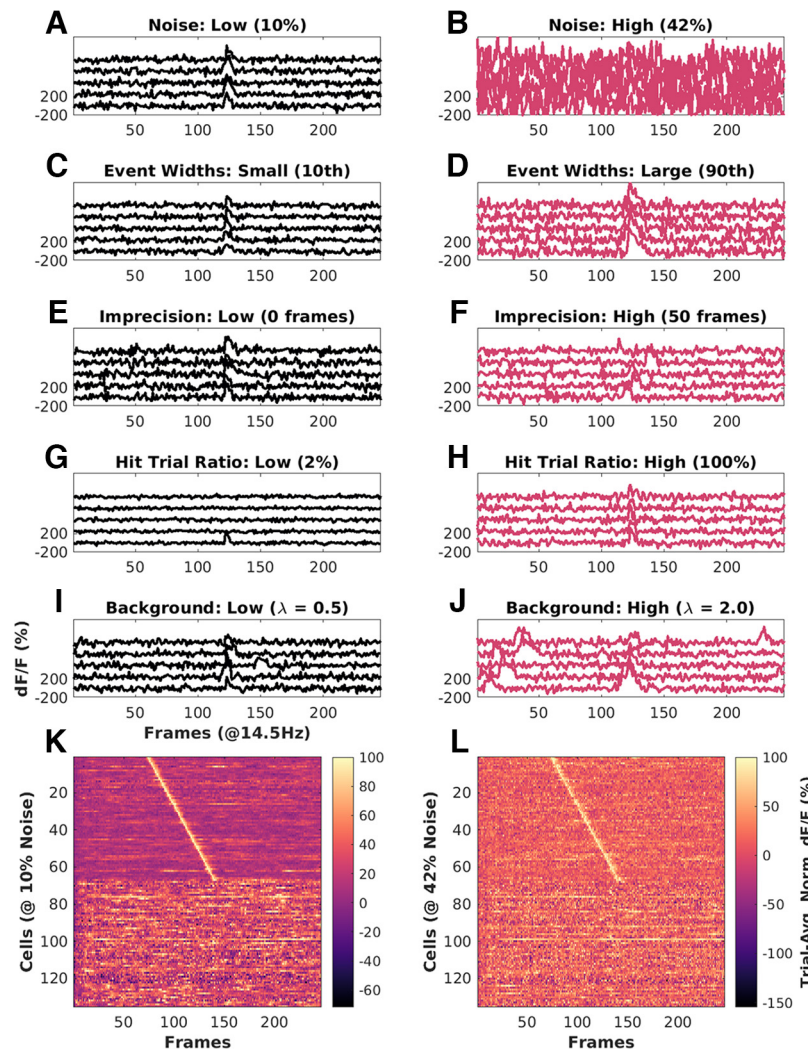


Figure 1. Key features of synthetic datasets. Left, Black panels, Low range of features. Right, Red panels, High range of features. **A**, Noise = 10%. **B**, Noise = 42%. **C**, Event width: 10th percentile ± 1 SD. **D**, Event width 90th percentile ± 1 SD. **E**, Imprecision at 0 frames FWHM. **F**, Imprecision at 50 frames FWHM. **G**, Hit trial ratio from 0% to 2%. **H**, Hit trial ratio from 0% to 100%. **I**, **J**, Background activity with the number of background spikes per background sampled from a Poisson distribution for with mean (λ), for **I**: $\lambda = 0.5$ (low), and **J**: $\lambda = 2.0$ (high). **K**, **L**, Trial-averaged Calcium traces from example synthetic datasets of 135 neurons, displayed as heatmap sorted by time of peak Ca signal. **K**, Baseline physiology synthetic data trial-average with 10% noise (low) and high background activity ($\lambda = 2$ to 3 events/trial). **L**, Same as **K** with 42% noise (high) and comparable background activity ($\lambda = 2$ to 3 events/trial). In both cases, 50% of the cells (top 67) are time cells and the remainder are not. Extended Data Figure 1-1 describes the most important parameters modulated for datasets in each of the three parameter regimes, “Unphysiological,” “Canonical,” and “Physiological,” along with the false positives and false negatives, for each of the 10 implemented algorithms.

calcium events sampled from the Calcium Event Library at frames (time) determined by the synthesis algorithm. The input parameters to this algorithm included timing, noise, imprecision, event width selection, hit trial ratio, background activity, and several others. We aimed to cover the most likely conditions to affect timing and other experiment design properties. In more detail, we generated synthetic datasets using the following control parameters:

- Time cell percent

Value: Number between 0 and 100. This sets the number of cells that are assigned tuned calcium activity as a

percentage of total cells, and controls the number of positive and negative class cells in the dataset.

- Cell order

Value: ‘basic’ or ‘random.’ In ‘basic’ mode, time cells are indexed lower than other cells. In ‘random’ mode, the indices of time cells and other cells are randomly selected. This should have no impact on algorithm detection but is useful for visualization.

- Max hit trial percent

Value: Number between 0 and 100. This sets the maximum possible fraction of total trials, during which a Time Cell will exhibit tuned calcium activity.

- Hit trial percent assignment

Value: ‘fixed’ or ‘random.’ In ‘fixed’ mode, the number of hit trials is set as defined by max hit trial percent. In ‘random’ mode, the number of hit trials is calculated by randomly picking a value from a range ($\frac{1}{2} \times \text{max hit trials}$, max hit trials).

- Trial order

Value: ‘basic’ or ‘random.’ In ‘basic’ mode, the hit trials are indexed lower than miss trials. In ‘random’ mode, the indices of hit and miss trials are randomly selected. Specific patterns of hit and miss trials for a session have not been reported in physiology, so this feature is not implemented.

- Event width

Value: {0–100 percentile value, Integer N}. For each cell, this defines the selection of events based on width in frames. The percentile value is estimated from the histogram of all event widths. The variance of this selection is set by “N,” which adds N^*SD to the selection. All synthetic cells exhibit a range of different calcium events. This is considered an important parameter.

- Event amplification factor

Value: Number from 0 to $+\infty$. This allows additional control to multiplicatively amplify any chosen calcium event, before incorporation. Our library was curated from physiologically recorded signals. The default value is 1.

- Event timing

Value: ‘sequential’ or ‘random.’ In ‘sequential’ mode, the time of peak calcium activity is reflected by the indexing of the time cells. In ‘random’ mode, the time of peak calcium activity is randomly dispersed over the trial frame points.

- Start frame

Value: Number from 0 to total number of frames. This sets the timing of the first cell in a time cell sequence.

- End frame

Value: Number from 0 to total number of frames. This sets the timing of the last cell in a time cell sequence.

- Imprecision full width at half max (FWHM)

Value: Number from 0 to total number of frames. This sets the lower and upper bounds for the difference in timing of calcium activity across trial pairs for a time cell. We use this parameter to model trial to trial variability and is considered an important parameter to test.

- Imprecision type

Value: ‘none,’ ‘uniform,’ or ‘normal.’ In ‘uniform’ and ‘normal’ modes, the trial pair Imprecision is picked from a normal and uniform distribution, respectively. In ‘none’ mode, the trial pair Imprecision defaults to 0.

- Noise

Value: ‘Gaussian’ or ‘none.’ In ‘Gaussian’ mode, the noise is sampled as a time-series vector with points from

a Gaussian distribution. In ‘none’ mode, the noise percent defaults to 0.

- Noise percent

Value: Number from 0 to 100. This allows scaling for any sample noise point, based on the max signal value for any cell.

- Add background spikes for time cells

Value: Boolean 0 or 1. This switch controls the incorporation of background (untuned) activity for putative time cells.

- Add background spikes for other cells

Value: Boolean 0 or 1. This switch controls the incorporation of background (untuned) activity for other (nontime) cells.

- Background distribution mean

Value: Number from 0 to $+\infty$. This sets the mean (λ) of the Poisson distribution to sample from when selecting how many background events to add per trial, for any given cell.

Implementation of a reference quality measure, Q

In order to compare the readouts from the various time-cell detection methods, we implemented a reference measure of quality (Q) of synthetic time cells that used the known inputs to the generation algorithm.

Based on preliminary analysis, we selected following five parameters as the most likely to affect the behavior and detection of time cells:

1. Noise
2. Event width
3. Imprecision
4. Hit trial ratio
5. Background activity

Accordingly, we were able to calculate a reference quality measure, using the following equation:

$$\text{RefQ} = \text{HTR} \times \exp\left(-\{\alpha \times \text{MNP}/100 \times \text{EAF} + \beta \times \text{std. dev. EW}/\text{meanEW} + \gamma \times \text{std. dev. Imp}/\text{Stim Win}\}\right), \quad (1)$$

where HTR: hit trial ratio

MNP: max noise percent (%)

EAF: event amplification factor

EW: event widths (frames)

Imp: imprecision (frames)

Stim Win: stimulus window (frames)

α : 1

β : 1

γ : 10

The values of α , β , and γ , were set to have comparable effects of each of the terms inside the exponent. This reference Q was useful for debugging code and was the basis for a further metric for time cell classification discussed below. A representative synthetic activity trace for ‘low’ and ‘high’ values of each of these five parameters is shown in Figure 1.

All modulations for the datasets in this study along with the estimates for false positives and false negatives, across all algorithms are shown in Extended Data Figure 1-1.

Separate analysis modules were developed for three categories of analysis

We implemented three analysis modules: *ti*, *r2b*, and *peq*, shorthand for temporal information, ridge-to-background, and parametric equations. The *ti* module implements three algorithms from Mau et al. (2018). The *r2b* module implements two algorithms from Modi et al. (2014). The *peq* module computes estimates for noise, hit trial ratio, event width and imprecision, and estimates a Q score as above. All three methods were implemented in C++ with a PyBind11 interface to Python. This combination is fast and efficient in memory use, and also has the ease-of-use of Python. Thanks to the native MATLAB interface to Python, all three methods can also be called from MATLAB.

Synthetic datasets generated and analyzed in batch mode

We generated datasets pertaining to parameter sensitivity analysis by modulating one of the four main parameters and setting the others to noninterference levels. In this manner, we devised 99 cases to study in which one of the main parameters was varied. Note that in these cases the resultant activity was in an unphysiological regime because other sources of variation were kept to low levels so as not to interfere with the parameter of interest. With three randomized shuffles, we generated 297 unique datasets.

We wanted to use more realistic datasets, where we would modulate one of the four parameters while keeping the others to ranges typical of physiological data. We devised 12 canonical cases. With 10 randomized shuffles each, we generated 120 additional unique datasets in the canonical regime. Finally, we devised 12 physiological regime cases, identical to those in the canonical regime, with the addition of background (untuned) activity. This yielded another 150 datasets, with randomization.

Altogether, we had 567 unique datasets for our tests, each with 135 cells (total: 76,545 cells), 60 trials, and 246 frames/trial. Except when the percent time cells were modulated, all datasets featured 50% time cells.

We next implemented an analysis pipeline to run all the datasets through the time cell detection algorithms, yielding scores and predictions for each case. Finally, all the scores and predictions were collated for comparison and benchmarks as shown in the schematic (Fig. 2).

Metrics for time cell classification performance

Recall is inversely proportional to the number of false negatives (Type II error) and is the fraction of true positive class predictions over all positive class ground labels.

$$\text{Recall} = \text{TPR}/(\text{TPR} + \text{FNR}) \quad (2)$$

Precision is inversely proportional to the number of false positives (Type I error) and is the fraction of true positive class predictions over all positive class predictions.

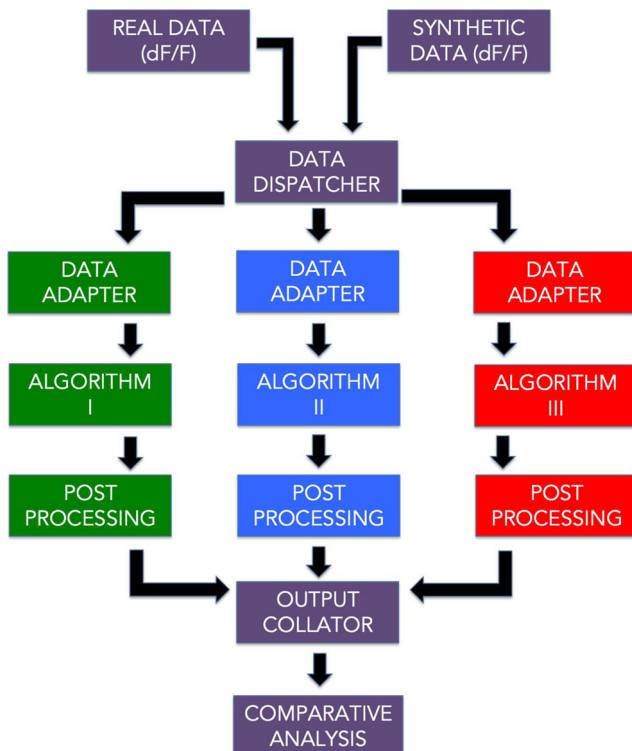


Figure 2. A schematic representation of the analysis pipeline. Physiology data as well as synthetic data were analyzed by 10 different implemented algorithms and the output was collated for comparative benchmarks.

$$\text{Precision} = \text{TPR}/(\text{TPR} + \text{FPR}). \quad (3)$$

F1 Score is the harmonic mean of recall and precision.

$$\text{F1 Score} = 2 * \text{Precision} * \text{Recall}/(\text{Precision} + \text{Recall}), \quad (4)$$

where

TPR: true positive rate

FNR: false negative rate

FPR: false positive rate

Here are the definitions for predictive/classification performance evaluation (Table 1).

Here are the important functions provided in the code base (Table 2).

Here are the MATLAB scripts running the comparative analysis and figure generation (Table 3).

Code and resource availability

The code/software described in the paper is freely available online at <https://github.com/BhallaLab/TimeCellAnalysis>. The code is available as Extended Data 1.

Results

We developed a pipeline (Fig. 2) with 10 different algorithm implementations for time cell detection, which involve scoring and then classifying cells.

Here, we describe the implementation of each of the methods.

Table 1: Definitions for predictive/classification performance evaluation

Ground truth	Prediction/classification	Remark
0/false/other cell	0/false	True negative (TN)
0/false/other cell	1/true	False positive (FP)
1/true/time cell	0/false	False negative (FN)
1/true/time cell	1/true	True positive (TP)

For each detection algorithm, the classification results were compared with known ground truth values to get the total number of true positive (TP), true negative (TN), false positive (FP), and false negative (FN) cases.

Time cell scoring methods and classification

Temporal information: *tiBoot*, *tiMean*, *tiBoth*, *tiMean-O*, *tiBase-O* (Mau et al., 2018)

Here, we used the algorithm from Mau et al. (2018) as follows. There was an initial criterion of cells to have activity in at least 25% of trials. Their activity was summed into event time histograms with a bin size of three frames. The temporal information (TI) was estimated using Equation 5,

$$TI = 1 \times \lambda j \times \log_2 \lambda j \times P_j, \quad (5)$$

where, λ is the average transient rate for each cell;

λj is the average transient rate for each cell in bin “j”; P_j is the probability that the mouse was in time bin “j.”

Bootstrapping was used to determine whether each cell had a TI greater than chance. We circularly randomized the frame points to develop a random activity model (1000 iterations) and classified cells as time cells if $\lambda > \lambda_{rand}$ in >99% of the models for at least two consecutive bins. We implemented the activity filter from Mau et al. (2018); by considering the trial-averaged peak of the calcium traces for each of the cells, and testing for significance using bootstrapping (*tiMean*). A logical AND operation between the prediction lists for *tiBoot* and *tiMean*, provided us with the full Mau et al., 2018 Temporal Information based detection algorithm (*tiBoth*).

Additionally, we used Otsu’s threshold (Otsu, 1979) on the temporal information scores as well as the trial-averaged peaks to get *tiBase-O* and *tiMean-O* using the MATLAB function “graythresh()” (<https://in.mathworks.com/help/images/ref/graythresh.html>). The purpose of adding the Otsu’s threshold-based classification step was to study how well the scores could be classified with a fast thresholding method, rather than the computationally expensive bootstrap.

Table 2: List of important functions provided in the code base

Name	Description	Command line	Location	Language
synthesis Demo.m	Command line demo, output to file: “synthData-demo.mat”. Generates a synthetic 2-P time cell dataset file	\$ cd TimeCellAnalysis/rho-matlab/demos && matlab -nodisplay -nosplash -r “synthesisDemo; quit”	rho-matlab/demos	MATLAB
ti_demo.py	Command-line demo, output to console.	\$ python TcPy(ti_demo.py sampleData/sample_synth_data.mat	TcPy	Python interface and C++ numerics
r2b_demo.py	Command-line demo, output to console. Runs Ridge-to-Background analysis from Modi et al. (2014). Reports R2B Mean and R2B Bootstrap classifications	\$ python TcPy(r2b_demo.py sampleData/sample_synth_data.mat	TcPy	Python interface and C++ numerics
peq_demo.py	Command-line demo, output to console. Runs parametric equation analysis from current study. Reports PEQ threshold classification, and estimates for noise, event width, imprecision, and hit trial ratio for dataset	\$ python TcPy(peq_demo.py sampleData/sample_synth_data.mat	TcPy	Python interface and C++ numerics
ground_truth_check.py	Command-line demo, output to console. Uses synthetic data files to assess accuracy of classification by the various Mau and Modi algorithms	\$ python TcPy/ground-truth_check.py sampleData/sample_synth_data.mat	TcPy	Python interface and C++ numerics
Benchmark.py	Command-line demo, output to console. Simple time and memory benchmarks for the Mau, Modi, or PEQ algorithms	\$ python TcPy/run_batch_analysis.py sampleData/sample_synth_data.mat	TcPy	Python interface and C++ numerics
run_batch_analysis.py	Command-line production script, output to CSV files. Runs a batch analysis using all methods on a data file. Generates .csv files for TI, R2B, PEQ, and ground truth classifications	\$ python TcPy(ti_demo.py sampleData/sample_synth_data.mat	TcPy	Python interface and C++ numerics
pyBindMap.py	Provides an interface for MATLAB programmers, to the python/C__ fuctions using two wrapper functions: runTlAnalysis and runR2Banalysis	Utility function, not run from command line	TcPy	Python
dodFbF.m	Utility function to convert experimental raw 2p calcium activity data from Suite2P to df/F form.	Utility function, not run from command line	rho-matlab/CustomFunctions	MATLAB

All these functions should be run from the cloned repository, TimeCellAnalysis.

Table 3: List of paper figure generating scripts

Name	Description	Command line
paperFigures	Plots all figures estimating algorithm performance for synthetic data analysis (paper Figs. 1, 4–6, and 8)	\$ matlab -r "paperFiguresSynth"
Synth.m		
paperFigures	Plots all figures estimating algorithm performance for real physiology data analysis (paper Fig. 7)	\$ matlab -r "paperFiguresReal"
Real.m		
paperFigures	For diagnostics; plots figures estimating algorithm performance over all the regimes (unphysiological, canonical, and physiologic)	\$ cd .. /src && matlab -r "paperFiguresSplits"
Splits.m		

All these functions should be run from the cloned repository, TimeCellAnalysis/p-matlab/paperFigures.

Ratio of ridge/background, *r2bMean*, *r2bBoot*, *r2bBase-O* (Modi et al., 2014)

Here, we re-implemented the algorithm from Modi et al., 2014. The time of peak response for each cell was identified in averaged, nonoverlapping trials' worth of $\Delta F/F$ traces, in the CS-onset to US-onset period, or as specified. The rest of the trials were averaged and the summed area under the time of peak was estimated. The ridge was then defined to be a 200 ms window centered at the peak. Next, we calculated the summed area in the ridge window as well as the background (non-ridge frames) to get the ridge to background ratio. As a control condition, these traces were given random time-offsets and then averaged. An independent time of peak was identified for each random-offset, averaged trace and ridge to background ratio calculated for it. This bootstrapping was repeated 1000 times for each cell's data and averaged. The reliability score was then calculated individually, for each cell, as the ratio of the ridge to background ratio for aligned traces to the mean of that of the random-offset traces (*r2bMean*).

We also studied the significance of each cell's raw *r2b* values by comparing them to each of the *r2b* values of the randomized datasets, thresholding significance at the 99th percentile (*r2bBoot*). Finally, the raw *r2b* values were also thresholding using Otsu's Thresholding (*r2bBase-O*; Otsu 1979).

Parametric equations, *peqBase* and *peqBase-O* (in-house)

We developed this method to score cells in a manner similar to the reference quality, which uses the known ground truth of the input parameters given to the generator functions for the synthetic dataset. Rather than using the known inputs, this method computes the corresponding parameters read out or estimated from the dataset, whether synthetic or real. It is applicable to labeled or unlabeled datasets. It is defined as:

$$Q = \text{HTR} \times \exp - \{\alpha \times N/S + \beta \times \text{std. dev. EW} / \text{mean EW} + \gamma \times \text{std. dev. Imp/Stim Win}\}, \quad (6)$$

where HTR: hit trial ratio

N/S: estimated noise/signal

EW: read out event widths (frames)

Imp: estimated imprecision (frames)

Stim Wind: stimulus window (frames)

$\alpha: 10$

$\beta: 1$

$\gamma: 10$

While $10 \times \alpha$ was required, β , and γ , were inspired by the same used for reference Q. Classification was then performed using Bootstrapping (as described above) as well as Otsu's threshold.

All of these implemented algorithms can handle unlabeled (real) or ground truth labeled (synthetic) data.

A schematic to describe the steps involved in each algorithm is shown (Fig. 3). We were then able to run all our synthetically generated datasets through each of the 10 implemented algorithms and perform comparative benchmarks.

Good predictive power in time cell quality scores despite different distributions

We ran each of the analysis methods on our synthetic datasets to assess how they scored the (known) time cells. There were four methods that provided a scoring function for time-cell classification: *tIMean*, *tIBase*, *r2bBase*, and *peqBase* (Fig. 4A–D). By inspection, these methods appeared to have distinct distributions. Below we describe how we compare the distributions using correlation analysis. In subsequent sections we describe other methods in our study that used these scores to generate a categorization through thresholding or bootstrap.

In these synthetic experiments, time cells were generated with a single calcium event per hit trial. Event insertions into the synthetic datasets were subject to noise, variable selection of event widths, trial-pair or timing imprecision, and hit trial ratio. We generated 99 unique unphysiological combinations (3 \times randomized shuffles) 12 unique canonical regime combinations (10 \times randomized shuffles), as well as 15 unique physiological regime combinations featuring background activity (10 \times randomized shuffles). In all, we performed our comparative analysis studies using 567 datasets, each with 135 cells, 60 trials/session, and 246 frames/trial at 14.5 Hz). We found that only *tIMean* and *tIBase* had a correlation coefficient of ~ 0.6 , whereas other pairs were correlated below 0.4 (Fig. 4E).

Generalized linear regression (GLM) models were generated to look for the ideal thresholding value for the best classification predictions by each method. We used the MATLAB implementation of GLMs (*fitglm*); <https://in.mathworks.com/help/stats/fitglm.html>). This is a linear model assuming a binomial distribution of categories (0 or 1, i.e., other cell or time cell; Collett, 2002). We obtained good predictive power for the four methods that provided a scoring function for time-cell classification. We generated Receiver Operating Characteristic (ROC) curves by going over the full range of thresholds for the range of scores for each method

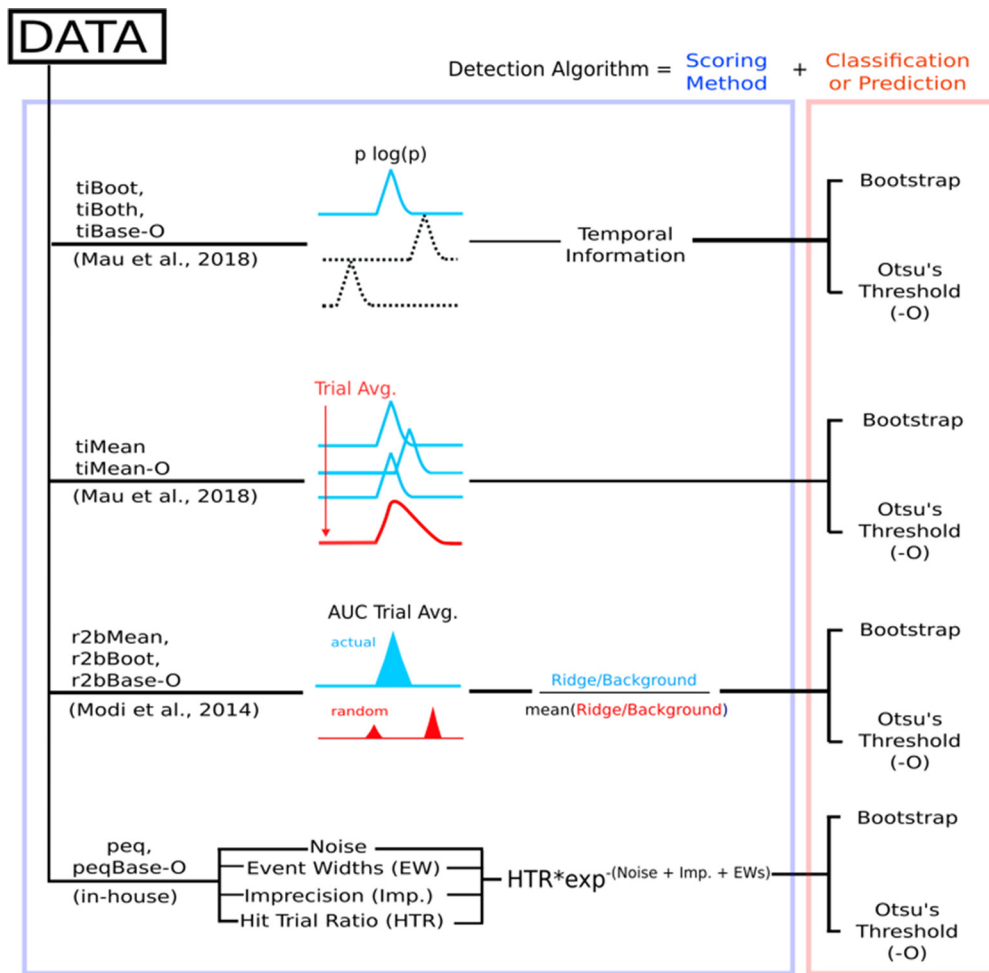


Figure 3. Schematic representation of the implemented algorithms, involving four different scoring methods followed by a classification step (bootstrapping or Otsu's automatic threshold) to have 10 complete time cell detection algorithms.

(ROC curves; Fig. 4F). We found that each distribution of scores had good predictive power, since ideal thresholds could be found to maximize TPR/FPR in all cases. We used the *tiBoth* categorization to distinguish time cells (Fig. 4G) from other cells (Fig. 4H), and plotted trial-averaged calcium traces to visually assess quality of classification as seen from raw data. Overall, each of our methods had distinct distributions of their base scores, but all had good predictive power for classification. The outcome of the classification steps is described in the next sections.

All algorithms exhibit near perfect precision with good recall

Next, we used the scores to classify the cells in our synthetic datasets, compared the predictions to ground truth, and established summaries for true and false cases. Confusion matrices were estimated to compare the predictions (classifications) for each algorithm, with reference to ground truth, and are shown (Fig. 5A,B). All methods exhibit very good precision (true positive classifications over the sum of all positive classifications), suggesting low false positive rates (Type I error; Fig. 5C). Most algorithms also generate good values for recall (true positive

classifications over ground-truth positives). We observed F1 scores (harmonic mean of recall and precision) >0.75 , all the way to 1 (perfect score), for most of the algorithms, as shown (Fig. 5C), suggesting overall usability.

We noticed moderate to strong correlation (>0.8) between the Boolean prediction lists for *tiMean*, *tiBoot*, *tiBoth*, *r2bMean*, and *r2bBoot* (Fig. 5D), but only weak to moderate correlation (<0.6) between the other pairs of predictions. The *tiMean-O* method does slightly better (correlation ~ 0.7 with the first five methods).

Algorithms differ in memory use and speed

Hardware and runtime requirements are a secondary, but practical concern when designing analysis of large datasets, and are specially relevant for experiment designs that require online analysis. We therefore looked at how memory use and runtime scaled on a per dataset basis when considering 67 or 135 cells per dataset ($2\times$).

We ran the memory usage and runtime experiments on a gaming laptop (Lenovo Ideapad 3 Gaming) with a 6 core AMD Ryzen 5 4600H, 16 GB DDR4 RAM (3200 MHz) running MATLAB R2021a on Ubuntu 20.04. Note, however, that we have implemented all the time cell algorithms in

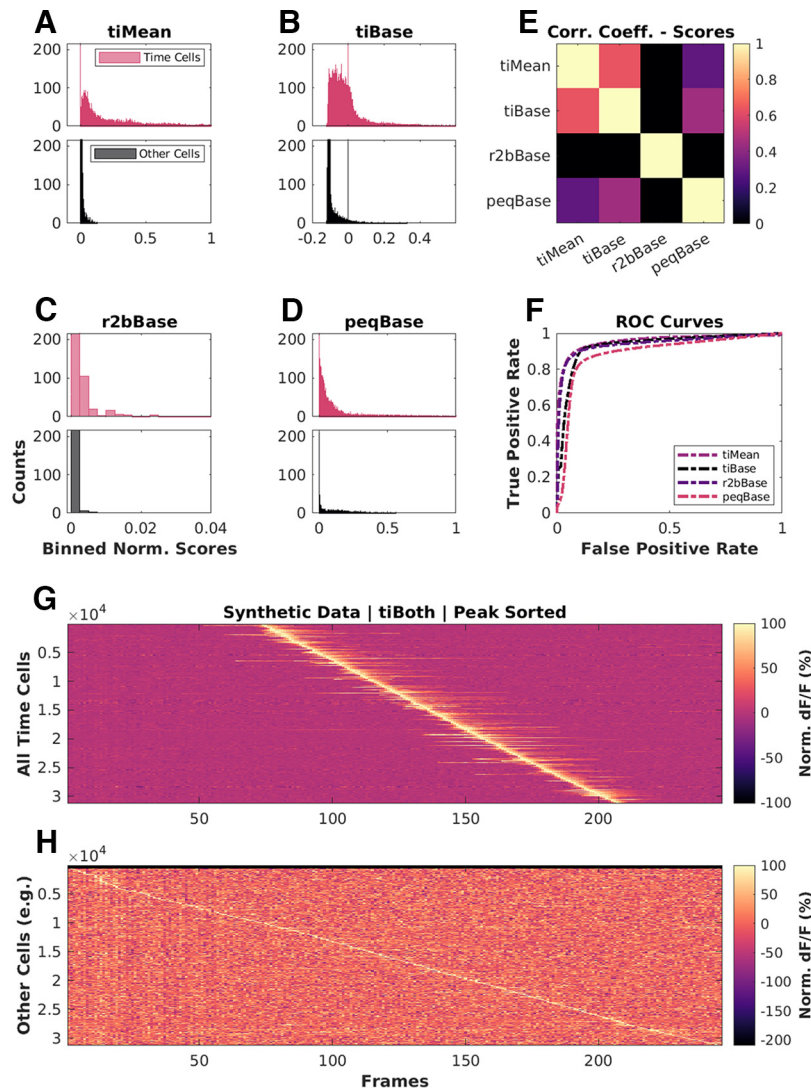


Figure 4. Base scores for different methods differ in their distributions but all have good predictive power. Scores for top (blue): time cells; bottom (red): other cells, across **A**, **tiMean**; **B**, **tiBase**; **C**, **r2bBase**; **D**, **peqBase**. **E**, Pairwise correlation coefficients between the distributions of analog scores (pooling time cells and other cells) by each of the four scoring methods. **F**, Receiver-operator characteristic (ROC) curves after generalized linear regression using the respective distributions of scores and comparisons with known ground truth. **G, H**, Trial-averaged calcium activity traces for cells classified as **G**, time cells; **H**, other cells.

serial and these do not use the additional cores. We found that most algorithms ran to completion requiring ~15 MB/dataset at a rate of ~1–4 s/dataset (135 cells/dataset). With 67 cells/dataset, the memory requirement and runtimes are approximately halved, suggesting that computational costs in memory and time were roughly linear with dataset size. We note that the analysis algorithms work independently for each cell. Thus, in principle, the analysis could be run in an embarrassingly parallel manner and should scale well on multicore architectures.

The synthesis of the main benchmarking datasets ($N=567$ datasets or 76,545 total cells) required a more powerful analysis machine, running a 6 core AMD Ryzen 5 3600, 32GB of DDR4 RAM, running MATLAB R2021a on Ubuntu 20.04. Dataset batches up to ~30 datasets ($N=40,500$ cells), however, could be easily handled by a less powerful laptop. The memory usage and runtime for

135 cells per dataset were accordingly, ~30 MB/dataset requiring ~1 s to complete. Thus, the methods scale readily to handle large datasets on modern hardware.

Physiologic range tests show sensitivity to noise but not to other features of the dataset

We next set out to see how these methods would work in estimated physiological ranges of signal confounds. Given our categorical labels on the synthetic data, we were able to split the datasets to look for the effects of the five main parameters: noise, event widths, imprecision, hit trial ratio, and background activity. We first computed the baseline physiology readouts keeping noise to 10%, event widths to the 60th percentile (± 1 SD), imprecision to 0 frames, hit trial ratios to a range of 33–66%, and background activity to 0.9–1.2 events/trial for time cells

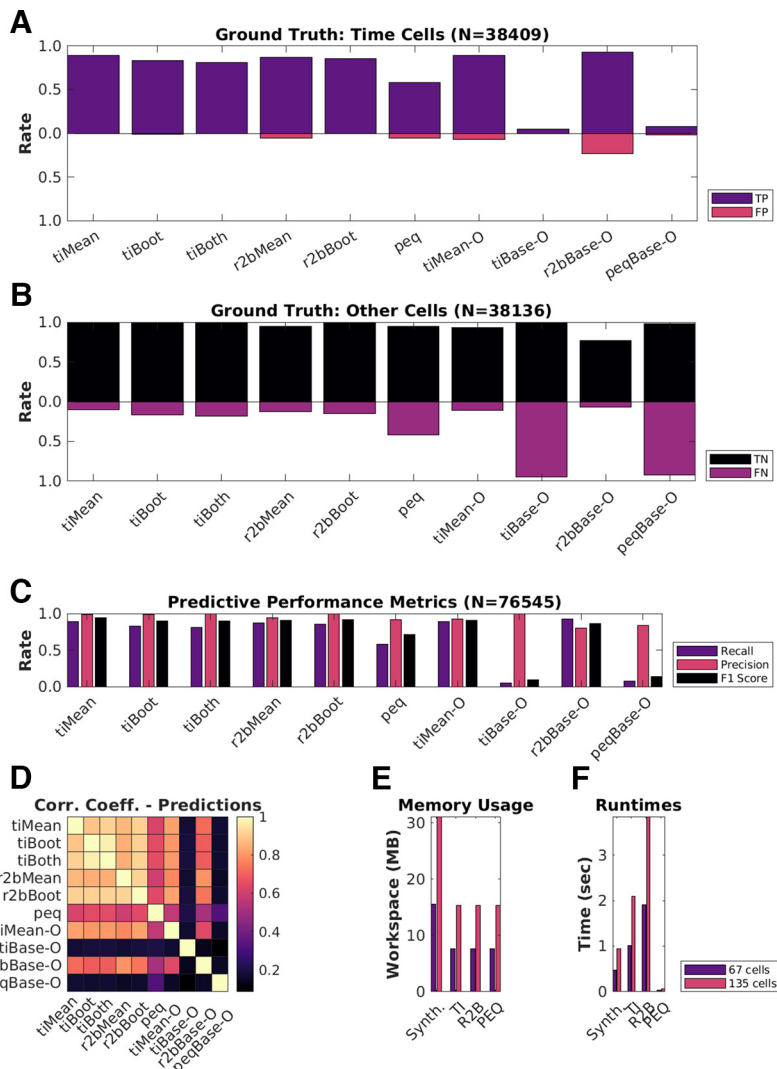


Figure 5. Good predictive performance by all algorithms. **A, B**, Classification performance of each of the 10 implemented detection algorithms. **A**, True positives (TP; purple), false positives (FP; red). **B**, True negatives (TN; black), false negatives (FN; purple). **C**, Predictive performance metrics [Recall = TP/(TP + FN), Precision = TP/(TP + FP), and F1 Score = Harmonic mean of Recall and Precision] to consolidate the confusion matrices. **D**, Pairwise correlation coefficients between the Boolean prediction lists by each of the 10 detection algorithms. Note that the first six methods correlate strongly. **E**, Average memory usage per dataset by the implemented algorithms on datasets with either 67 cells (purple) or 135 cells (red). **F**, Average runtimes per dataset by the implemented algorithms on datasets with either 67 cells (purple) or 135 cells (red).

(~50% of all synthetically generated cells, $N=50$ baseline datasets, 135 cells/dataset, 60 trials/dataset). Next, we established dependency slopes for each of the algorithms, based on their predictions ($N=10$ randomized shuffles for each case; Fig. 6B–F; Extended Data Figs. 6-1, 6-2).

Most methods exhibited a negative dependence of noise (range: 10% to 70%) on prediction F1 score (Fig. 6B). Although many methods are designed with some form of denoising strategy (trial-averaging, etc.), as expected all algorithms ran into classification difficulties at higher Noise levels. This reinforces the value of relatively high signal-to-noise recordings.

The relative insensitivity to event widths (Fig. 6C) is potentially useful for calcium imaging datasets where events may be slow, and in cases where slower tuning curves are

expected. However, this criterion may need to be stringent for analyses that need to precisely identify fine differences in cell responses.

We observed that most algorithms were insensitive to how frequently time cells were active across trials in a session (HTR). This is possibly the reason for the potential confusion among physiologists with regard to how many time cells were expected in a recorded dataset.

We found that the first six algorithms (*tiMean*, *tiBoot*, *tiBoth*, *r2bMean*, *r2bBoot*, and *peq*) gave equivalent predictions in ~66% of cases (Extended Data Fig. 6-1A). Next, we considered the various prediction lists across these top six algorithms and looked for consensus in time cell predictions from the most lenient threshold (“ ≥ 1 ” algorithm), incrementally through the most stringent threshold (“ $=10$ ” algorithms). We thus established a

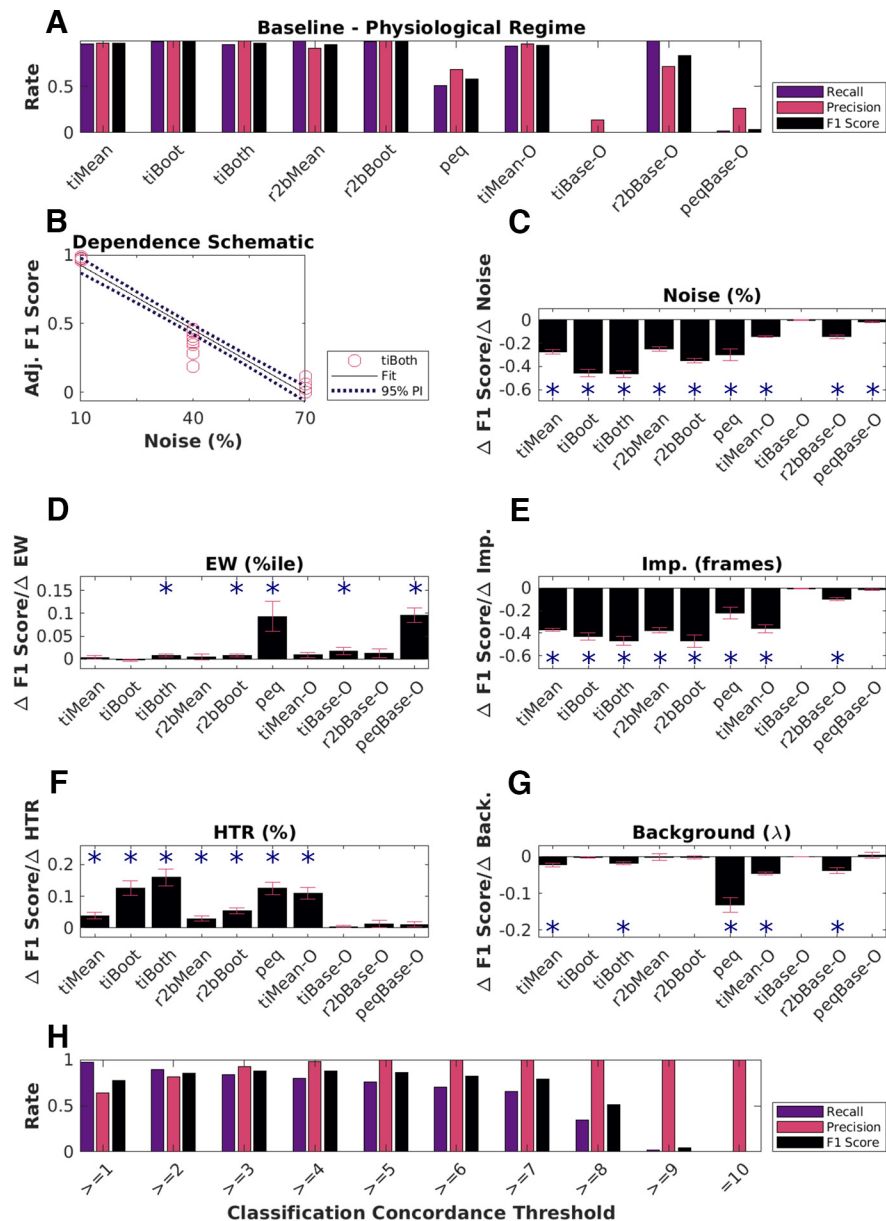


Figure 6. Physiological sensitivity analysis and concordance. **A**, Classification performance scores for all algorithms with the baseline physiology synthetic datasets ($N=6750$ cells). The first five methods perform well. Peq does poorly by all measures when confronted with physiology-range activity variability. Otsu's threshold method for score classification also does not work well for any method under physiological conditions. **B**, Dependence of F1 score on noise as a schematic. This has an overall negative slope (dashed line) which was used for panel **C**, TI-both. A similar calculation was performed for each method. Panels **C–G**, Parameters were systematically modulated one at a time with respect to baseline and the impact on classification score for each algorithm was estimated by computing the slope, using repeats over 10 datasets each with an independent random seed. Significant dependence on the perturbing parameter was determined by testing whether the slope differed from 0 at $p < 0.01$, indicated by asterisks using the MATLAB function `coeffTest()`. Plotted here are bar graphs with mean and error as RMSE normalized by the square root of N ($N=10$ datasets). **C**, Dependence on noise %. **D**, Dependence on event width percentiles. **E**, Dependence on imprecision frames. **F**, Dependence on hit trial ratio (HTR; %). **G**, Background activity (Poisson distribution mean, λ). **H**, Classification performance using concordance for a range of classification thresholds. Extended Data Figure 6-1 describes the three-point line plot dependency curves for the F1 score for each of the implemented algorithms against each of the five main parameters modulated, as the mean of $N=10$ datasets for each case, with error bars as SD. Extended Data Figure 6-2 showcases the linear regression fits for the same, with 95% prediction intervals (PIs), used to estimate the slopes of the various dependency curves.

Concordance based metric for time cell classification. We tested the predictive power of this Concordance based metric, which considers time cells based on consensus among the predictions from all the 10 implemented algorithms.

We identified differences in the classification performance, across the full range of concordance thresholds (Fig. 6H). With lower threshold values (“ $>=4$ ” and below), we notice a slight drop in the Precision, indicating an

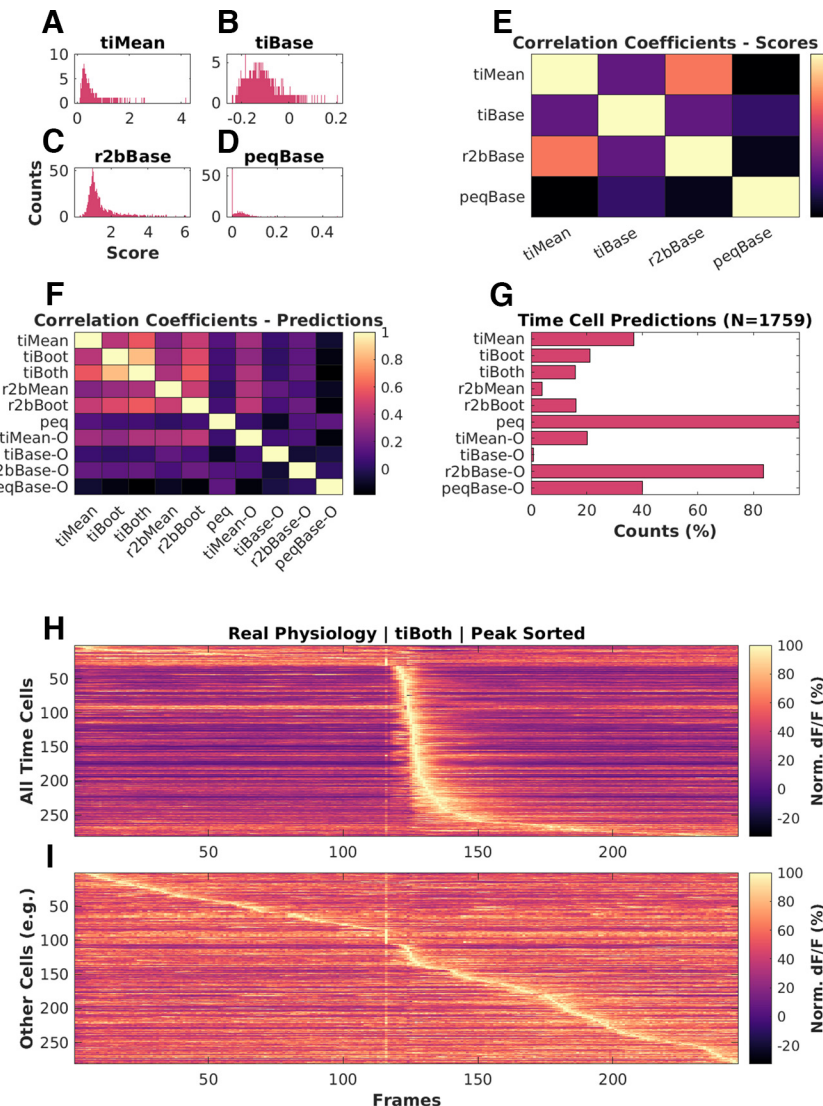


Figure 7. Analysis of experimental 2-P recordings of Ca^{2+} signals. **A–D**, Histograms of scores for physiologically recorded *in vivo* calcium activity from hippocampal CA1 cells (total $N = 1759$), by (A) tiMean, (B) tiBase, (C) r2bBase, and (D) peqBase. **E**, Pairwise correlation coefficients between the distributions of analog scores by the four scoring methods. **F**, Pairwise correlation coefficients between the Boolean prediction lists by the 10 detection algorithms. **G**, Numbers of positive class (time cell) predictions by each of the detection algorithms. **H, I**, Trial-averaged calcium activity traces for (**H**) time cells and (**I**) other cells. LED conditioned stimulus (CS) is presented at frame number 116, as seen by the bright band of the stimulus artifact. Most cells classified as time cells are active just after the stimulus. There is a characteristic broadening of the activity peak for classified time cells at longer intervals after the stimulus. Some of the cells at the top of panel **H** may be false positives because their tuning curve is very wide or because of picking up the stimulus transient. Similarly, some of the cells in the middle of panel **I** may be false negatives because of stringent cutoffs, although they appear to be responsive to the stimulus.

increase in false positive rate (Type I error). On the other hand, with increasing threshold values it is the Recall that drops, suggesting a higher false negative rate (Type II error). We find that a concordance threshold of “ $>=4$ ” achieves the best recall, precision, and F1 scores, for time cell prediction (Fig. 6F). The utility of this approach is subject to the availability of resources to apply multiple algorithms to each dataset.

Time cells identified in real physiology recordings

We used the 10 different implemented algorithms on *in vivo* 2-P calcium recordings ($N = 13$ datasets, namely,

1759 isolated cells from three animals across chronically recorded datasets), to compare time cell classification between the algorithms. As we observed for the synthetic data, experimental 2-P Ca traces also yielded different base scores from the four different methods (Fig. 7A–D). Again, consistent with the synthetic data, the pairwise correlation was weak to moderate (Fig. 7E). When we consider the boolean prediction lists (Fig. 7F), we observed moderate pairwise correlation between tiMean, tiBoot, tiBoth, r2bMean, and r2bBoot (>0.5), and low or weak correlation between the other pairs (<0.5). This was consistent with observations for the synthetic data but the correlations were overall slightly

weaker. The total number of time cells predicted were also different across the implemented algorithms (Fig. 7G). Algorithms such as *r2bBase-O* and *peq*, which had more false positives (Fig. 5B) also had more cells classified as time cells. The converse was not true. *r2bMean*, which had moderate false negatives as well as false positives on the synthetic dataset, classified very few of the experimental set as time cells. The trial-averaged activity of the detected time cells (Fig. 7H; including false positives) and other cells (Fig. 7I), based on the predictions by *tiBoth*, are shown. The experimentally recorded time cells exhibited a characteristic widening of tuning curves (Pastalkova et al., 2008; MacDonald et al., 2011, 2013; Kraus et al., 2013; Mau et al., 2018) with tuning to later time points (Fig. 7H).

Overall, four of the algorithms from the literature seemed consistent in their classifications as well as having reasonable numbers of classified time cells. These were the three algorithms from Mau et al. (2018; *tiMean*, *tiBoot*, and *tiBoth*), and the *r2bBoot* method derived from Modi et al. (2014). This is broadly in agreement with their performance on the synthetic datasets.

Discussion

We have developed a full pipeline for comparing time cell detection algorithms. This starts with synthetic datasets for benchmarking, in which we program in the ground truth of cell identity and timed activity, and a range of perturbations characteristic of experiments. These include noise, event widths, trial-pair timing imprecision, hit trial ratio, and background activity. This resource is, in itself, a key outcome of the current study, and though it is designed for 2-P calcium imaging data it can be extended to rate-averaged single-unit recordings. We built a pipeline for running and comparing the outcome from five methods derived from two previous studies, and one from the current work. These algorithms were applied to synthetic and experimental datasets and compared against each other and, where possible, against ground truth. We observed that most algorithms perform well and substantially agree in their time cell classification, but there were different degrees of sensitivity to different forms of signal variability, notably noise and imprecision.

The value of synthetic data in experimental science

Synthetic neural activity datasets are valuable in at least two main ways: evaluating algorithms for detection of important activity features, and for delivering stimuli to *in vitro* and simulated neurons, so as to provide a more physiological context in which to study input-output properties (Abbasi et al., 2020). While we have deployed our synthetic dataset for the specific purpose of comparing time cell detection algorithms, we suggest that it could also be useful for evaluating sequence analysis algorithms (Ikegaya et al., 2004; Foster and Wilson, 2006; Villette et al., 2015). Beyond the domain of neuronal data analysis, such synthetic datasets act as a test-bed for critique and development of analysis algorithms meant for deployment on real-world or typical use case data. They have been used previously to benchmark unsupervised outlier detection

(Steinbuss and Bohm, 2020), explainable machine learning (Liu et al., 2021), intrusion detection systems (Iannucci et al., 2017), 3D reconstruction algorithms (Koch et al., 2021), among several others. We report the first use of synthetic data pertaining to cellular physiology in the context of identifying time cells from network recordings. Moreover, our experiments study important operational differences across several previously published and new detection algorithms.

Our dataset may also be valuable for the second use case, stimulus delivery. There is a growing body of work on network detection of sequences (Ikegaya et al., 2004; Foster and Wilson, 2006; Csicsvari et al., 2007; Jadhav et al., 2012; Villette et al., 2015; Malvache et al., 2016) or even single-neuron sequence selectivity (Branco et al., 2010; Bhalla, 2017). More realistic input activity patterns with a range of physiological perturbations may be useful probes for such experimental and theoretical studies. Further, experimenter-defined neural activity inputs through optogenetic stimulation has already begun to use more complex temporal patterns than static or periodic illumination (Schrader et al., 2008; Dhawale et al., 2010; Bhatia et al., 2021). Our approaches to synthetic sequential neuronal activity generation may be useful to add more physiological dimensions to the sequential activity employed in such studies.

Further dimensions of time cell modulation

Our experiments allowed us to probe for parametric dependence systematically across published and new algorithms. We observed little or no dependence of the predictive performance (F1 score) of the various algorithms to event widths, hit trial ratios, and background activity. We did observe the F1 scores for most algorithms to be negatively dependent on noise and imprecision. On the one hand, this is a useful outcome in that different methods yield similar time-cell classification. It is a limitation, however, if the network uses such response features for coding, since it means that these methods are insensitive to relevant response changes. Further potential coding dimensions were not explored. Thus, several potential behavioral correlates of tuned cells (Ranck, 1973), could not be studied in our experiments. Such correlates include but are not limited to measurements of spatial navigation (O'Keefe and Dostrovsky, 1971; O'Keefe and Nadel, 1978; Wilson and McNaughton, 1993) and decision-making (Foster and Wilson, 2006; Csicsvari et al., 2007; Diba and Buzsáki, 2007; Davidson et al., 2009; Karlsson and Frank, 2009; Gupta et al., 2010; MacDonald et al., 2013; Villette et al., 2015), as well as navigation across tone frequencies (Aronov and Tank, 2014). While each of these further inputs would be interesting to incorporate into synthetic datasets, this requires that the time cell generation algorithm itself incorporate some form of simulation of the neural context. This is beyond the scope of the current study.

A specific limitation of our dataset is that it assumes that time is encoded by individual neurons. This leaves out population encoding schemes in which no one cell responds with the level of precision or consistency that would clear the criteria we use. For example, many of the same studies that use the methods tested here also use

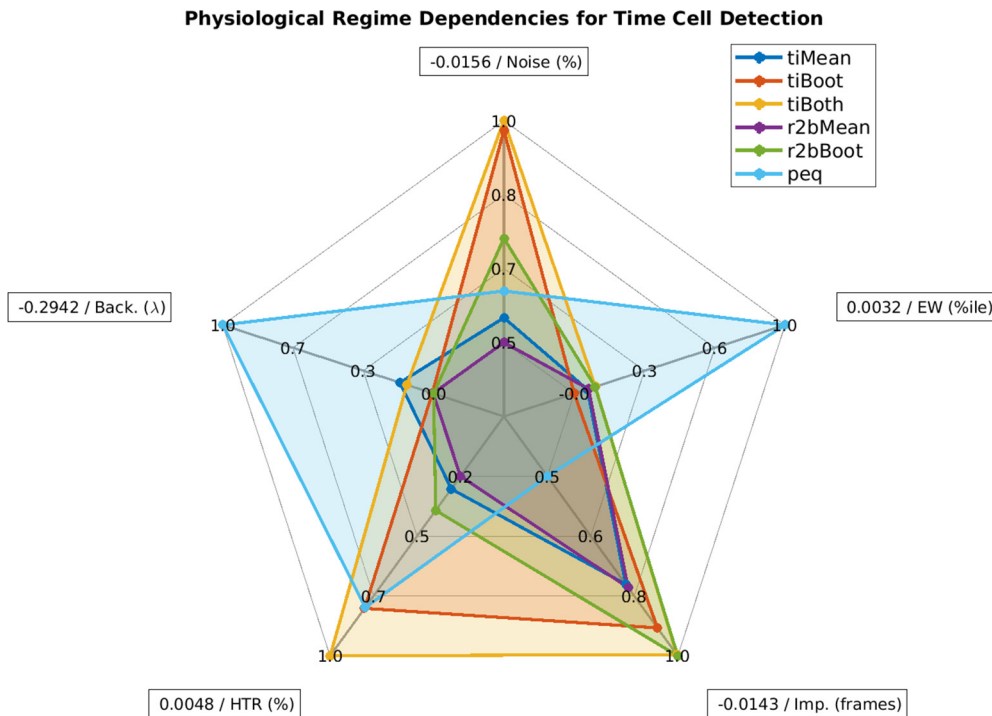


Figure 8. Spider plot summary. Relative sensitivity of the six best detection algorithms (*tiMean*, *tiBoot*, *tiBoth*, *r2bMean*, *r2bBoth*, and *peq*) to the five main parameters for data variability, noise (%), event widths (%ile), imprecision (frames), hit trial ratio (%), and background activity (λ). A perfect algorithm would have very small values (i.e., low sensitivity) for each of the parameters and, thus, occupy only the smallest pentagon in the middle. Note that even the maximal absolute value of sensitivity for most parameters (outer perimeter) is quite small, indicated in boxes at the points of the spider plot.

neural network decoders to report time (Mau et al., 2018). Such decoders might detect time encoding without time cells. A similar situation of individual versus network coding appears for the closely related problem of sequence representation. Place cell replay sequences have been shown to be modulated by the prevalence of location specific aversive (Wu et al., 2017) as well as appetitive stimuli (Bhattarai et al., 2020). Such physiological findings have been the subject of theoretical models of behavior planning (Foster, 2017; Mattar and Daw, 2018), and have been reported to improve performance on multiple Atari games by artificial neural networks (Mnih et al., 2015) featuring salience detection and experience mapping. We suggest that synthetic data for such higher-order encoding schemes might be a useful tool, and could draw on the approaches in the current study.

Comparative analysis benchmarks and concordance

A particularly challenging time cell classification problem is when the same cells may play different timing roles, such as forward and reverse replay. This is made more difficult because of the relative rarity of forward replay sequences over the more typical reverse replay (Diba and Buzsáki, 2007; Foster, 2017). Preplay is also a topic of some debate (Dragoi and Tonegawa, 2013; Foster, 2017). At least one possible problem in such debates is the degree of consistency between time cell or sequence classifiers. Our pipeline allows for (1) error correction in case of nonconcordant classifications, (2) suggest candidate algorithms

with a dependence on dataset features like event widths, imprecision, and hit trial ratio, as well as (3) the possibility to expand the detection regime in more realistic physiological datasets using concordance.

Which algorithms to use?

We did not set out to rank algorithms, but our analysis does yield suggestions for possible use domains based on sensitivity to experimental perturbations (Fig. 8). In cases where runtime and compute resource use is a concern, we recommend using the temporal information method with Bootstrap along with the activity filter (*tiBoth*). Combinations of *tiBoth* with *r2bBoth* may be useful where there are rare and potentially multimodally tuned time cells (Pastalkova et al., 2008; Villette et al., 2015), either to combine their classification for stringent time cell identification, or to pool their classified cells. While it is tempting to use Otsu's threshold as a very fast alternative to bootstrapping, we found that none of the Otsu variants of these methods did a good job of classification. Ultimately, five of our algorithms *tiMean*, *tiBoot*, *tiBoth*, *r2bMean*, and *r2bBoth*: all based on either Mau et al. (2018) or Modi et al. (2014), have very good Precision, and classify with very few false positives (low Type I error). Many methods are susceptible to classification errors if the dataset has high noise.

Here we also implemented the parametric equation (*peq*) algorithm. It is not very good for time cell classification per se, as it is prone to false positives and is susceptible to noise and low hit trial ratios. However, it generates useful

additional estimates of the four key parameters of real data, namely, noise, hit trial ratio, event width and imprecision. This is useful for a first-pass characterization of the properties of the dataset.

Sequence detection in large-scale recordings and scaling of analysis runs

The discovery of replay over the past two decades, has benefitted from the technological advances made in increasing the cellular yield of network recordings and has been reviewed previously (Foster, 2017). Further advances such as with the large scale recordings of $\sim 10^3$ single units by electrical recording using Neuropixels (Jun et al., 2017), fast volumetric fluorescence scanning with up to $\sim 10^4$ cells using resonant electro-optic imaging (Poort et al., 2015; Pachitariu et al., 2017; Bowman and Kasevich, 2021), $\sim 10^3$ mesoscopes (Sofroniew et al., 2016), as well as advances in automated cell region of interest (ROI) detection, denoising, and neuropil subtraction (Pachitariu et al., 2017; Pnevmatikakis et al., 2016) only increase the scale and size of datasets, likely leading to longer analysis runtimes. In addition to our recommendations above for the temporal information/boot method for scalable time-cell analysis, our C++/Python implementations may also be useful in further optimizing these methods. Our implementations allow for relatively fast analysis of the same datasets with multiple algorithms.

References

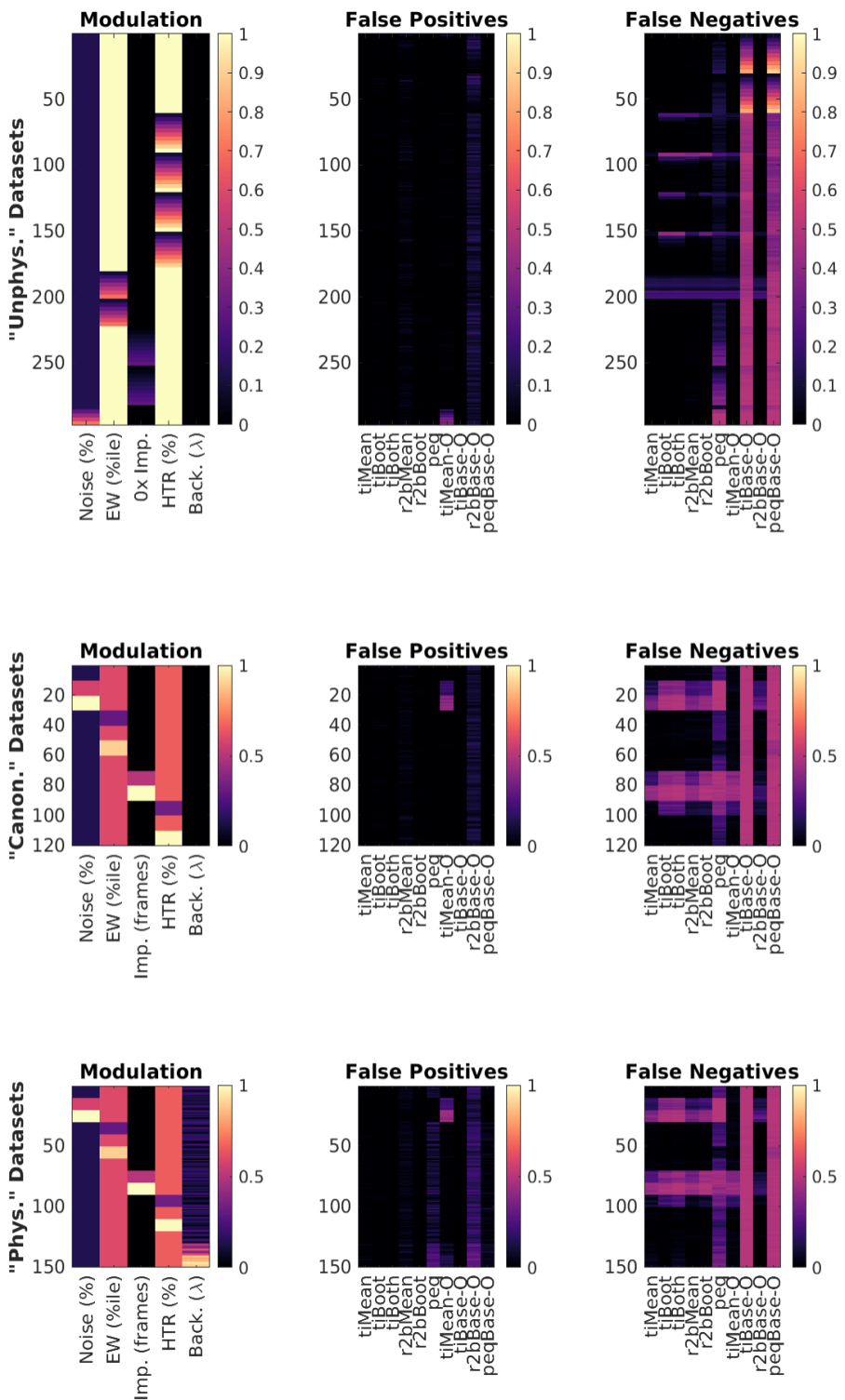
- Abbasi S, Maran S, Jaeger D (2020) A general method to generate artificial spike train populations matching recorded neurons. *J Comput Neurosci* 48:47–63.
- Ahmed MS, Priestley JB, Castro A, Stefanini F, Solis Canales AS, Balough EM, Lavoie E, Mazzucato L, Fusi S, Losonczy A (2020) Hippocampal network reorganization underlies the formation of a temporal association memory. *Neuron* 107:283–291.e6.
- Aronov D, Tank DW (2014) Engagement of neural circuits underlying 2D spatial navigation in a rodent virtual reality system. *Neuron* 84:442–456.
- Bhalla US (2017) Synaptic input sequence discrimination on behavioral timescales mediated by reaction-diffusion chemistry in dendrites. *Elife* 6:e25827.
- Bhatia A, Moza S, Bhalla US (2021) Patterned optogenetic stimulation using a DMD projector. *Methods Mol Biol* 2191:173–188.
- Bhattarai B, Lee JW, Jung MW (2020) Distinct effects of reward and navigation history on hippocampal forward and reverse replays. *Proc Natl Acad Sci U S A* 117:689–697.
- Bowman AJ, Kasevich MA (2021) Resonant electro-optic imaging for microscopy at nanosecond resolution. *ACS Nano* 15:16043–16054.
- Branco T, Clark BA, Häusser M (2010) Dendritic discrimination of temporal input sequences in cortical neurons. *Science* 329:1671–1675.
- Collett D (2002) Modeling binary data. London: Chapman and Hall.
- Csicsvari J, O'Neill J, Allen K, Senior T (2007) Place-selective firing contributes to the reverse-order reactivation of CA1 pyramidal cells during sharp waves in open-field exploration. *Eur J Neurosci* 26:704–716.
- Davidson TJ, Kloosterman F, Wilson MA (2009) Hippocampal replay of extended experience. *Neuron* 63:497–507.
- Dhawale AK, Hagiwara A, Bhalla US, Murthy VN, Albeau DF (2010) Non-redundant odor coding by sister mitral cells revealed by light addressable glomeruli in the mouse. *Nat Neurosci* 13:1404–1412.
- Diba K, Buzsáki G (2007) Forward and reverse hippocampal place-cell sequences during ripples. *Nat Neurosci* 10:1241–1242.
- Dombeck DA, Harvey CD, Tian L, Looger LL, Tank DW (2010) Functional imaging of hippocampal place cells at cellular resolution during virtual navigation. *Nat Neurosci* 13:1433–1440.
- Dragoi G, Tonegawa S (2013) Distinct preplay of multiple novel spatial experiences in the rat. *Proc Natl Acad Sci U S A* 110:9100–9105.
- Eichenbaum H (2017) On the integration of space, time, and memory. *Neuron* 95:1007–1018.
- Foster DJ (2017) Replay comes of age. *Annu Rev Neurosci* 40:581–602.
- Foster DJ, Wilson MA (2006) Reverse replay of behavioural sequences in hippocampal place cells during the awake state. *Nature* 440:680–683.
- Gupta AS, van der Meer MAA, Touretzky DS, Redish AD (2010) Hippocampal replay is not a simple function of experience. *Neuron* 65:695–705.
- Iannucci S, Kholidy HA, Ghimire AD, Jia R, Abdelwahed S, Banicescu I (2017) A comparison of graph-based synthetic data generators for benchmarking next-generation intrusion detection systems. 2017 IEEE International Conference on Cluster Computing (CLUSTER), Honolulu, HI, pp. 278–289, <https://doi.org/10.1109/CLUSTER.2017.54>.
- Ikegaya Y, Aaron G, Cossart R, Aronov D, Lampl I, Ferster D, Yuste R (2004) Synfire chains and cortical songs: temporal modules of cortical activity. *Science* 304:559–564.
- Jadhav SP, Kemere C, German PW, Frank LM (2012) Awake hippocampal sharp-wave ripples support spatial memory. *Science* 336:1454–1458.
- Jun JJ, et al. (2017) Fully integrated silicon probes for high-density recording of neural activity. *Nature* 551:232–236.
- Kaifosh P, Lovett-Barron M, Turi GF, Reardon TR, Losonczy A (2013) Septo-hippocampal GABAergic signaling across multiple modalities in awake mice. *Nat Neurosci* 16:1182–1184.
- Karlsson MP, Frank LM (2009) Awake replay of remote experiences in the hippocampus. *Nat Neurosci* 12:913–918.
- Koch S, Worcel M, Silva C, Alexa M (2021) Hardware Design and Accurate Simulation of Structured-Light Scanning for Benchmarking of 3D Reconstruction Algorithms (Vol. 2021). Proceedings of the Neural Information Processing Systems Track on Datasets and Benchmarks 1 (NeurIPS Datasets and Benchmarks 2021). Retrieved from <https://openreview.net/forum?id=bNL5VfTe3p>.
- Kraus B, Robinson R, White J, Eichenbaum H, Hasselmo M (2013) Hippocampal “time cells”: time versus path integration. *Neuron* 78:1090–1101.
- Lee AK, Wilson MA (2004) A combinatorial method for analyzing sequential firing patterns involving an arbitrary number of neurons based on relative time order. *J Neurophysiol* 92:2555–2573.
- Liu Y, Khandagale S, White C, Neiswanger W (2021) Synthetic benchmarks for scientific research in explainable machine learning. <https://github.com/abacusai/xai-bench>.
- MacDonald CJ, Lepage KQ, Eden UT, Eichenbaum H (2011) Hippocampal “time cells” bridge the gap in memory for discontinuous events. *Neuron* 71:737–749.
- MacDonald CJ, Carrow S, Place R, Eichenbaum H (2013) Distinct hippocampal time cell sequences represent odor memories in immobilized rats. *J Neurosci* 33:14607–14616.
- Malvache A, Reichinnek S, Villette V, Haimerl C (2016) Awake hippocampal reactivations project onto orthogonal neuronal assemblies. *353:1280–1283*.
- Mattar MG, Daw ND (2018) Prioritized memory access explains planning and hippocampal replay. *Nat Neurosci* 21:1609–1617.
- Mau W, Sullivan DW, Kinsky NR, Hasselmo ME, Howard MW, Eichenbaum H (2018) The same hippocampal CA1 population simultaneously codes temporal information over multiple time-scales. *Curr Biol* 28:1499–1508.e4.
- Mnih V, Kavukcuoglu K, Silver D, Rusu AA, Veness J, Bellemare MG, Graves A, Riedmiller M, Fidjeland AK, Ostrovski G, Petersen S, Beattie C, Sadik A, Antonoglou I, King H, Kumaran D, Wierstra D,

- Legg S, Hassabis D (2015) Human-level control through deep reinforcement learning. *Nature* 518:529–533.
- Modi MN, Dhawale AK, Bhalla US (2014) CA1 cell activity sequences emerge after reorganization of network correlation structure during associative learning. *Elife* 3:e01982.
- Mokeichev A, Okun M, Barak O, Katz Y, Ben-Shahar O, Lampl I (2007) Stochastic emergence of repeating cortical motifs in spontaneous membrane potential fluctuations in vivo. *Neuron* 53:413–425.
- O'Keefe J, Dostrovsky J (1971) The hippocampus as a spatial map. Preliminary evidence from unit activity in the freely-moving rat. *Brain Res* 34:171–175.
- O'Keefe J, Nadel L (1978) The hippocampus as a cognitive map. Oxford: Clarendon Press.
- Otsu N (1979) A threshold selection method from gray level histograms. *IEEE Trans Syst Man Cyber* 9:62–66.
- Pachitariu M, Stringer C, Dipoppa M, Schröder S, Rossi LF (2017) Suite2p: beyond 10,000 neurons with standard two-photon microscopy. *BioRxiv* 061507. <https://doi.org/https://doi.org/10.1101/061507>.
- Pastalkova E, Itskov V, Amarasingham A, Buzsáki G (2008) Internally generated cell assembly sequences in the rat hippocampus. *Science* 321:1322–1327.
- Pnevmatikakis EA, Soudry D, Gao Y, Machado TA, Merel J, Pfau D, Reardon T, Mu Y, Lacefield C, Yang W, Ahrens M, Bruno R, Jessell TM, Peterka DS, Yuste R, Paninski L (2016) Simultaneous denoising, deconvolution, and demixing of calcium imaging data. *Neuron* 89:285–299.
- Poort J, Khan AG, Pachitariu M, Nemri A, Orsolic I, Krupic J, Bauza M, Sahani M, Keller GB, Mrsic-Flogel TD, Hofer SB (2015) Learning enhances sensory and multiple non-sensory representations in primary visual cortex. *Neuron* 86:1478–1490.
- Ranck JB, J (1973) Studies on single neurons in dorsal hippocampal formation and septum in unrestrained rats. I. Behavioral correlates and firing repertoires. *Exp Neurol* 41:461–531.
- Schrader S, Grün S, Diesmann M, Gerstein GL (2008) Detecting synfire chain activity using massively parallel spike train recording. *J Neurophysiol* 100:2165–2176.
- Siegel JJ, Taylor W, Gray R, Kalmbach B, Zemelman BV, Desai NS, Johnston D, Chitwood RA (2015) Trace eyeblink conditioning in mice is dependent upon the dorsal medial prefrontal cortex, cerebellum, and amygdala: behavioral characterization and functional circuitry. *eNeuro* 2:ENEURO.0051-14.2015.
- Sofroniew NJ, Flickinger D, King J, Svoboda K (2016) A large field of view two-photon mesoscope with subcellular resolution for in vivo imaging. *Elife* 5:e14472.
- Souza BC, Pavão R, Belchior H, Tort ABL (2018) On information metrics for spatial coding. *Neuroscience* 375:62–73.
- Steinbuss G, Bohm K (2020) Generating artificial outliers in the absence of genuine ones—a survey. *arXiv*. <https://doi.org/10.48550/arXiv.2006.03646>.
- Tseng W, Guan R, Disterhoft JF, Weiss C (2004) Trace eyeblink conditioning is hippocampally dependent in mice. *Hippocampus* 14:58–65.
- Villette V, Malvache A, Tressard T, Dupuy N, Cossart R (2015) Internally recurring hippocampal sequences as a population template of spatiotemporal information. *Neuron* 88:357–366.
- Wilson MA, McNaughton BL (1993) Dynamics of the hippocampal ensemble code for space. *Science* 261:1055–1058.
- Wu CT, Haggerty D, Kemere C, Ji D (2017) Hippocampal awake replay in fear memory retrieval. *Nat Neurosci* 20:571–580.

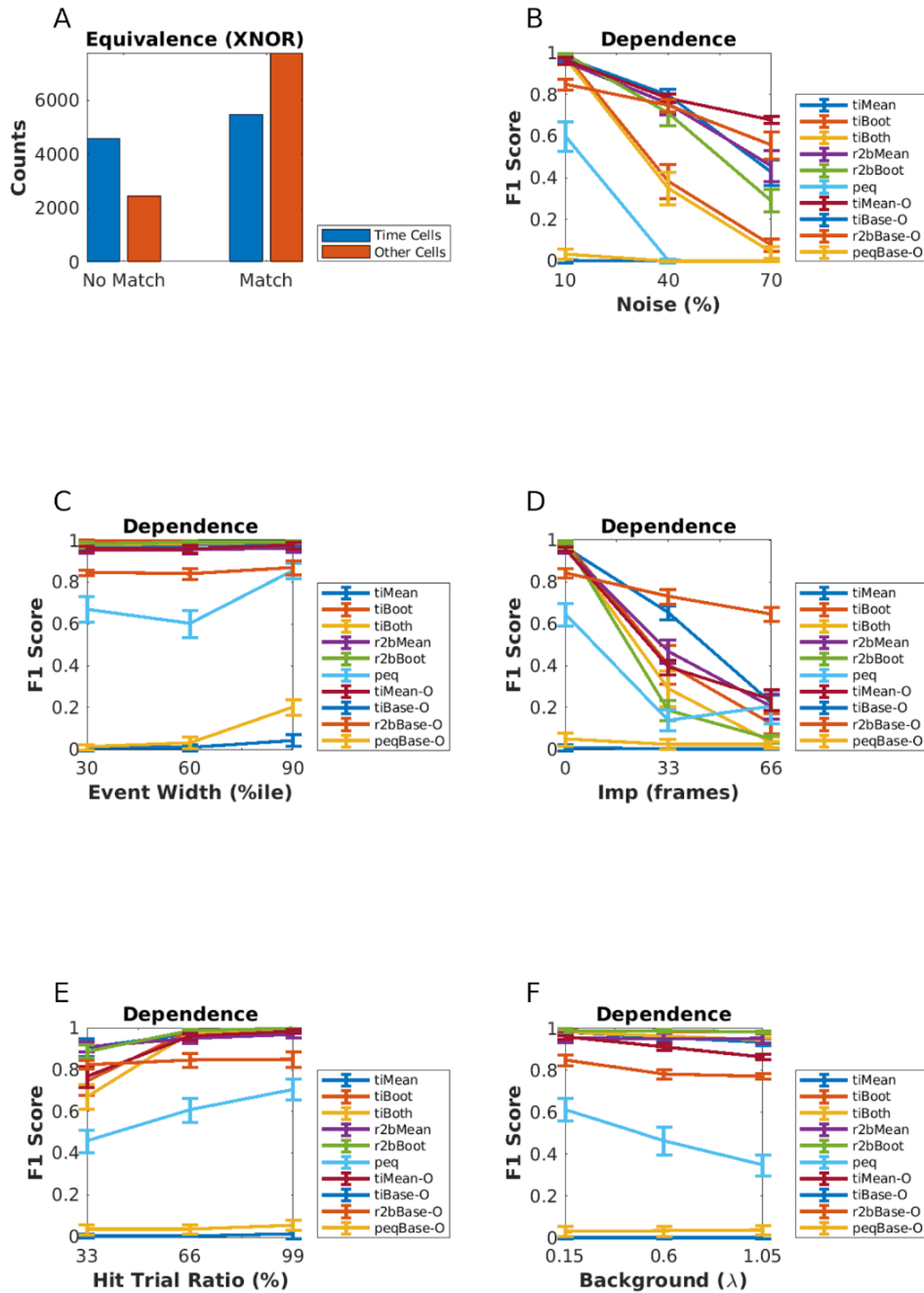
3613 **Extended Data Figures (Supplementary)**

3614

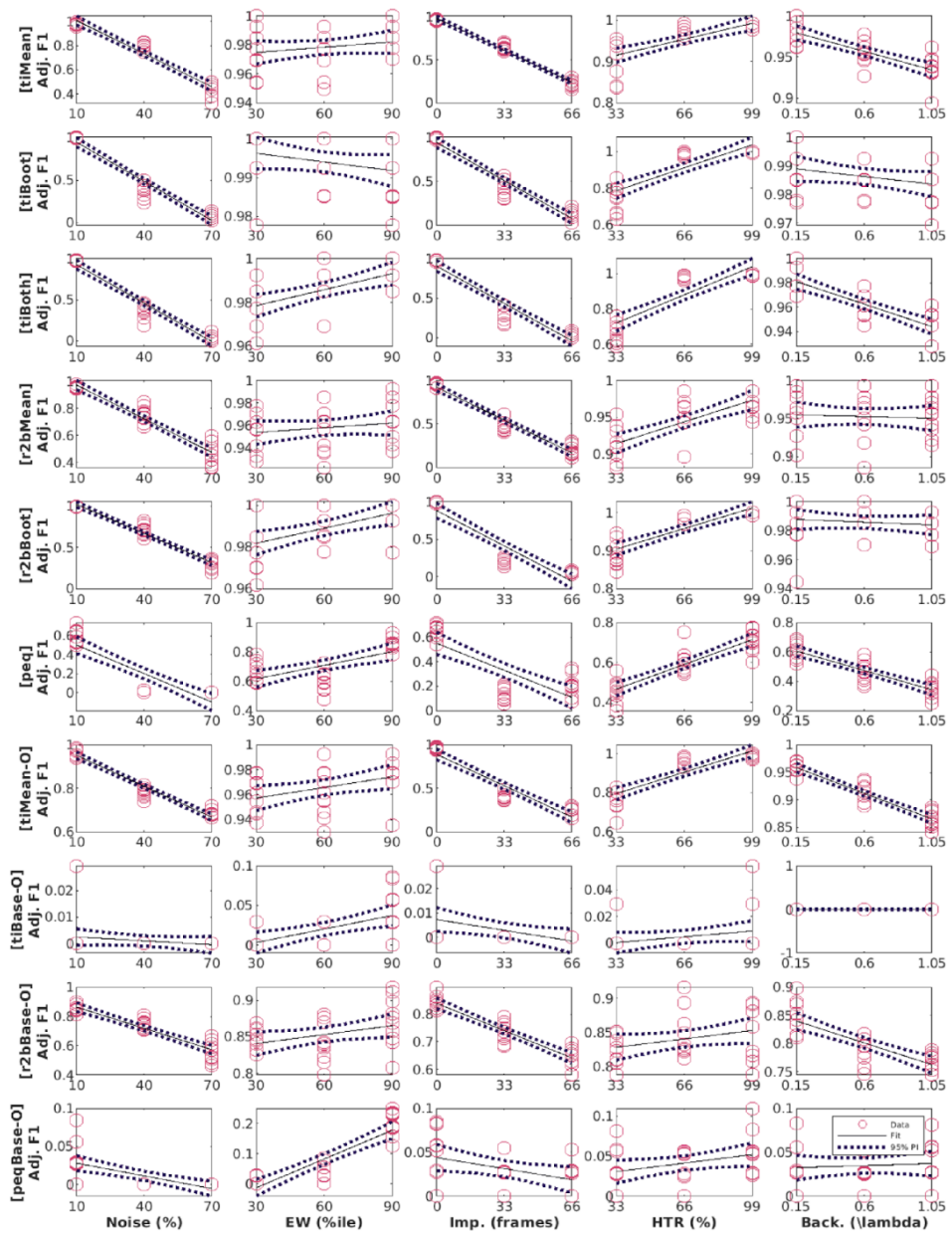
3615 **Extended Figure 1-1.** Modulation profile along with the False Positive and
3616 False Negative rates per dataset, for important parameters configured in
3617 each of the 567 synthetic datasets generated. A-C: “Unphysiological
3618 Regime”, D-F: “Canonical Regime”, G-I: “Physiological Regime”.



3620 **Extended Figure 6-1.** A: Equivalence by XNOR matching the prediction lists
3621 from the top six detection algorithms (Blue: Time Cells; Red: Other Cells). B-
3622 F: Dependence of the predictive performance (F1 Score) on the various
3623 important synthetic dataset configuration parameters, B: Noise (%), C: Event
3624 Width (%ile), D: Imprecision (frames), E: Hit Trial Ratio (%), and F:
3625 Background Activity (λ).



3628 **Extended Figure 6-2:** Linear Regression fits for all algorithm parameter
3629 dependence curves with data points (red circles), best fit line (black), and the
3630 95% prediction interval (PI; dotted black lines). The columns represent the
3631 physiology regime modulation parameter (out of the 5 main parameters
3632 tested), and the rows represent the various implemented algorithms for time
3633 cell detection.



3635 **Chapter 5 – Discussion**

3636 **The study of hippocampal CA1 sequences**

3637

3638 The standardized protocols described in the thesis are expected to aid
3639 in future experiments studying hippocampal CA1 sequences. Our
3640 simultaneous 2-photon calcium imaging recordings and behavioural
3641 training provided us the platform to study neural activity from ~100-150
3642 cells/animal at behaviourally relevant timescales (~70 ms per frame).

3643

3644 We standardized a multi-day Trace Eye-Blink Conditioning or TEC
3645 ("Chapter 2 - Behaviour") training system for mice based on previous
3646 literature (Siegel et al., 2015) and could demonstrate several types of
3647 behavioural adaptations that experimental animals could learn under a
3648 variety of experiment conditions and modulations. Notably,
3649 1. The animals typically learnt the tasks quickly, within 1-2 weeks of
3650 training.

3651 2. Modulating the inter-stimulus interval (ISI) between the CS and US
3652 results affected the expression of the conditioned response (CR).

3653 3. A wide palette of stimuli may now be incorporated into existing
3654 protocols as either of the presented stimuli (data not shown). TEC
3655 experiments with multiple CS, viz., blue LED and Tone, have been
3656 tried in the lab. They form the primary behavioural modulation being
3657 investigated by a lab colleague. These experiments are now directly
3658 possible due to the standardization efforts.

3659 4. In our experiments where we extended the Trace Duration, animals
3660 show retention of previously learnt CR times (Figures 19-21),
3661 showcase complex blinks (Figure 19) without change to CR onset
3662 (Figure 20).

3663 5. We could also train animals on very long Trace durations (550 ms,
3664 and 750 ms), which have previously not been reported for head-fixed
3665 mice.

3666 6. Across all the single interval training experiments, the animals only
3667 produce one conditioned response, with time of peak adjusted relative
3668 to the timing of the US.

3669 7. Complex blinks were only observed in animals trained to more than
3670 one trace interval.

3671

3672 Simultaneous large-scale recordings have been fundamental to the
3673 discovery of long spatiotemporal activity patterns with several
3674 participant CA1 neurons (Davidson et al., 2009; Foster, 2017).

3675 Electrical recordings provide many orders of magnitude better temporal
3676 resolution, not to mention being a direct readout of action potentials.

3677 However at the time of the design of the thesis, imaging based
3678 approaches could yield more recorded neurons per experiment animal.

3679 We standardized 2-photon fluorescence based chronic imaging of
3680 hippocampal CA1 neurons to allow calcium imaging based recording of
3681 the spatiotemporal sequences across multiple days ("Chapter 3 -
3682 Imaging"). This gave us the ability to

3683 1. Record neurophysiology over a large population of neurons
3684 (~100), in conjunction with temporally relevant behavioural contexts
3685 and modulations, albeit at ~100 ms temporal resolution.

3686 2. Chronically track cells across various behaviour sessions without
3687 ambiguity.

3688 3. Allow for scalability in the per animal yield of recording neurons with
3689 the use of faster and modern 2-photon microscope hardware utilizing
3690 Resonant Scanning instead of galvo-scanning, as well as multi-
3691 channel imaging.

3692

3693 We could identify time cells with the ability to retain, de-tune, or even
3694 re-tune, over the course of multiple sessions. Given no change in the
3695 behaviour protocol variables, it is unlikely we would have found such
3696 adaptations without scaling up the yield of cells or improving our
3697 temporal resolution while recording each individual session. Since the
3698 behaviour task is typically learnt to ~70-80% performance levels over
3699 the course of multiple sessions, our methodology gives us the ability to
3700 look into learning mechanisms utilized by the CA1 in the interim.

3701 Production quality datasets were quickly obtained by colleagues in the
3702 lab, following the protocols standardized and described here.

3703

3704 From our preliminary data, the largest proportion of re-tuned cells had
3705 tuning peaks shift to earlier time points (Chapter 3 – “Imaging”, Figure
3706 37), with subsequent sessions. Early in training, the timing of tuning
3707 peaks would typically occur near the time of the Unconditioned
3708 Stimulus (US; air-puff to eye). Our experiments presenting stimuli to
3709 naive animals (in accordance with Dhawale, 2013) suggested that
3710 somatosensory stimuli may be able to modulate CA1 responses, while
3711 many neutral stimuli may not (Chapter 3 – “Imaging”, Figure 29),
3712 without training. These results do allow for speculation on how initially
3713 neutral Conditioned Stimuli (CS; Light LED pulse) could develop
3714 behavioural valence for the animal, viz., the selective suppression of
3715 Response Inhibition to the previously neutral CS. An as yet unknown
3716 fraction of time cells may initially be triggered by the Unconditioned
3717 Stimulus (US; air-puff), but over the course of multiple training
3718 sessions, shift tuning fields to respond to the CS at the level of the CA1
3719 network. However, many more datasets would be required to firmly
3720 establish any mechanistic insight into the phenomenon.

3721

3722 **Standardizing combined behaviour and**
3723 **recording experiments**

3724

3725 Hippocampal CA1 time cells had been previously described to fire in
3726 reliable sequences, as observed in animals that learnt a single-session
3727 version of the TEC paradigm (Modi et al., 2014). We wished to further
3728 develop the paradigm and more fully study time cells, especially during
3729 the early or acquisition phase of training (sessions 1-7). It was not
3730 considered trivial to bundle behaviour and recording in a non-
3731 interfering way. For instance, we needed to study time cells
3732 longitudinally or chronically, and this is likely achieved by ensuring that
3733 the experimental animals were not overtly stressed, but rather, were
3734 reasonably compliant to the experiment in terms of motivation.

3735 Towards this,

3736 1) We focused on performing only one surgery, viz., head-bar implant
3737 and hippocampus to minimize surgery-induced trauma, rather than
3738 multiple surgery strategies.

3739 2) We incorporated a treadmill for the animals to run on during the
3740 experiments, at the potential cost of observing z-axis drift in the
3741 imaging.

3742 3) Imaging requires that the sample (experimental animals) be
3743 illuminated only by the excitation laser and that the sensor systems for
3744 the emitted photons receive only the photons from the excited sample.
3745 We considered and designed the filter sets before our photomultiplier
3746 tube (PMT) in the emission path, to reject all IR and partially red
3747 frequencies, not just to protect the sensor from the excitation 2-photon

3748 laser, but also the red/short IR illumination on the animal's eye for the
3749 behaviour camera.

3750

3751 Through our experiments, we were able to provide some evidence that
3752 somatosensory stimuli, but not other neutral stimuli, could trigger CA1
3753 responses but the effect of behavioural training results in the
3754 development of CA1 responses to the CS, now triggering a whole
3755 spatiotemporal sequence of activation. Altogether, we were able to
3756 observe preliminary results regarding the tuning, de-tuning, and re-
3757 tuning of time cells to temporal fields during learning, as described in
3758 Chapter 3 – “Imaging”.

3759 **Mapping sequences to abstract variables**

3760

3761 Visual cues are typically considered important to place cell activity and
3762 tuning. The specific requirement of vision, however, was tested in a
3763 study published in 2015. Experimenters switched off the lights as their
3764 animals navigated a maze. The animals were provided only olfactory
3765 cues at specific locations in the maze, yet place cell activity and tuning
3766 could be recorded. This suggested that the hippocampus could use
3767 non-visuospatial resources to generate spatial representations, when
3768 vision was compromised (Zhang & Manahan-Vaughan, 2015).

3769

3770 In a sound manipulation task (SMT) rats changed the frequency of
3771 auditory tones in their environment, by self-initiated joystick control,
3772 ramping logarithmic sweeps of frequency space. The rate of change in
3773 frequency could be manipulated either by the animal or
3774 pseudorandomly by the experimenter. This study describes neural

3775 activity recorded from the medial entorhinal cortex (MEC) as well as
3776 the hippocampal CA1 with sub-populations that were found tuned to
3777 specific frequency “landmarks” during the auditory sequence (Aronov
3778 et al., 2017). The CA1 were, thus, argued to be capable of tuning to
3779 abstract variables and were designed to map out sequences of
3780 events/stimuli in their own spatiotemporal patterns of activity.

3781

3782 The ubiquity of neural sequences in a wide variety of systems has
3783 been discussed previously (Bhalla, 2019; Conen & Desrochers, 2022;
3784 S. Zhou et al., 2020) and over a century of research has discovered
3785 remarkable physiological features that may be used to identify neurons
3786 that participate in these sequences. However, research is still required
3787 to carefully dissect out the contribution that each participant neuron
3788 has to behaviour, an important goal in neuroscience (Ranck, 1973,
3789 1975).

3790

3791 The use of user-configurable, categorically labeled synthetic calcium
3792 activity profiles allowed us to probe and compare a range of different
3793 time cell detection algorithms, identifying strategies to best classify
3794 time cells. We were able to identify Temporal Information as a strong
3795 contender for the choice of algorithm for such classification
3796 (Ananthamurthy & Bhalla, 2023). The algorithms developed along the
3797 way were tested within the time scales of ~100 ms, that correspond to
3798 Replay Sequences or other behaviour timescale sequences. We
3799 expect the analysis routines to be useful in a variety of different
3800 experiments that could potentially help describe the neural code in
3801 more detail.

3802 **Better temporal resolution requires new
3803 techniques**

3804
3805 There are many other techniques that experimenters in the field have
3806 employed to record activity. Many of these techniques do, in fact,
3807 achieve much better temporal resolution. Here are some examples:

3808 1) Resonant Scanning based 2p calcium imaging can achieve even up
3809 to 30 Hz for 4x larger fields of view, or more frame rates for smaller
3810 fields of view (Bonin et al., 2011; Leybaert et al., 2005; Nguyen et al.,
3811 2001; Rochefort et al., 2009). At the time when we started the
3812 experiments for the thesis, Resonant scanning microscopes required a
3813 lot of additional, expensive components to be purchased. Towards this,
3814 we co-wrote a sanctioned DBT grant application
3815 (BT/PR12255/MED/122/8/2016) and began setting up the new
3816 microscope. However, we did not have this technology available for
3817 experiments before 2020.

3818 2) High-density tetrodes can be used to perform electrical recordings
3819 at ≥ 20 kHz, as compared to ~ 14.5 Hz for our galvo-scanning 2p
3820 calcium imaging experiments. This technique typically achieves yields
3821 of ~ 40 cells for hippocampal recordings, and we argued that we could
3822 achieve a higher yield (>100 cells) with galvo-scanning 2p calcium
3823 imaging. The relative sparsity of the hippocampal neural code in terms
3824 of cells participating in any engram, mandates high-yield recordings to
3825 identify the full temporal sequence of CA1 activations (Foster, 2017).

3826 3) Neuropixels (Jun et al., 2017) can be used to perform electrical
3827 recordings at ≥ 20 kHz. At the time when we started the experiments
3828 for the thesis, these sorts of electrical probes had yet to be
3829 successfully deployed in published literature.

3830

3831 We discuss all these techniques while comparing electrical- vs.
3832 imaging-based recording strategies in Chapter 1 – “Introduction”.
3833 Fundamentally, given the technological constraints at the time, we had
3834 devised combined behaviour with galvo-scanning 2p calcium imaging
3835 as the principle for the experiments described in this thesis.

3836 Does the brain create or predict?

3837 An important direction to neuroscience research is to understand the
3838 brain and nervous system, in how these structures allow animals to
3839 interact meaningfully with their environment. More conservatively,
3840 however, the goal of this thesis was to help provide a multi-disciplinary
3841 toolkit to study time cells in the hippocampus. Predictive coding has
3842 been considered as a way for the brain to ultimately use external
3843 sensory information to minimize prediction errors during tasks (Doya et
3844 al., 2007; Rao & Ballard, 1999). One of the core ideas of Bayesian
3845 approaches to neurophysiology and behaviour is that the brain could
3846 be modeled as a prediction machine that is constantly modeling the
3847 change of variables. These variables may be external or internal yet
3848 salient concepts to any experimental animal, arguably expressed in
3849 neurophysiology as the dynamics of engrams. The ability of the
3850 mammalian hippocampus to bind both information streams to create
3851 new, more elaborate engrams, is likely crucial to the learning of new
3852 concepts behaviourally (N. J. Cohen & Eichenbaum, 1993;
3853 Eichenbaum, 2017).

3854

3855 Attentional states have been shown to have a bidirectional relationship
3856 with the expression of memory and learning (Chun & Johnson, 2011;

3857 Hutchinson & Turk-Browne, 2012; Uncapher et al., 2011). Specifically,
3858 Trace Eye-Blink Conditioning (TEC) performance has been suggested
3859 to be positively correlated with attention (Manns et al., 2000). The
3860 question of the effect of attentional states on the dynamics of the
3861 associated engram motivated an important milestone for the Thesis,
3862 *viz.*, to combine stable, adaptable behaviour studies with large-scale
3863 neurophysiology.

3864

3865 We were able to train head-fixed mice to TEC and confirm adaptable
3866 conditioned responses to task variables. We were also able to
3867 simultaneous record from ~100 hippocampal CA1 cell bodies as the
3868 animals acquired top behavioural performance. We observed in our
3869 preliminary results that many identified time cells showcased the ability
3870 to tune to different time points across sessions or days, as has been
3871 previously reported (Mau et al., 2018). This standardization of
3872 simultaneous behaviour and imaging ensured that colleagues from our
3873 lab were able to generate production quality data, quickly.

3874

3875 Several more high quality recordings and behaviour modulations would
3876 be required to conclusively describe time cells physiology and engram
3877 dynamics, at least at the level of a sub-population of hippocampal CA1.
3878 However, progress has been made to suggest the best time cell
3879 detection algorithm(s) based on their sensitivity to different recording
3880 parameters (Ananthamurthy & Bhalla, 2023). We hope that the Thesis
3881 is of aid to future research on the neural mechanisms of Learning and
3882 Memory by the nervous system.

3883

3884 Bibliography

- 3885 Ananthamurthy, K. G., & Bhalla, U. S. (2023). Synthetic Data Resource
3886 and Benchmarks for Time Cell Analysis and Detection Algorithms.
3887 *ENeuro*, ENEURO.0007-22.2023.
3888 <https://doi.org/10.1523/ENEURO.0007-22.2023>
- 3889 Aronov, D., Nevers, R., & Tank, D. W. (2017). Mapping of a non-spatial
3890 dimension by the hippocampal-entorhinal circuit. *Nature*,
3891 543(7647), 719–722. <https://doi.org/10.1038/nature21692>
- 3892 Bhalla, U. S. (2019). Dendrites, deep learning, and sequences in the
3893 hippocampus. *Hippocampus*, 29(3), 239–251.
3894 <https://doi.org/https://doi.org/10.1002/hipo.22806>
- 3895 Bonin, V., Histed, M. H., Yurgenson, S., & Reid, R. C. (2011). Local
3896 Diversity and Fine-Scale Organization of Receptive Fields in
3897 Mouse Visual Cortex. *The Journal of Neuroscience*, 31(50),
3898 18506. <https://doi.org/10.1523/JNEUROSCI.2974-11.2011>
- 3899 Chun, M. M., & Johnson, M. K. (2011). Memory: enduring traces of
3900 perceptual and reflective attention. *Neuron*, 72(4), 520–535.
3901 <https://doi.org/10.1016/j.neuron.2011.10.026>
- 3902 Cohen, N. J., & Eichenbaum, H. (1993). *Memory, amnesia, and the
3903 hippocampal system*.
- 3904 Conen, K. E., & Desrochers, T. M. (2022). *The Neural Basis of
3905 Behavioral Sequences in Cortical and Subcortical Circuits*. Oxford
3906 University Press.
3907 <https://doi.org/10.1093/acrefore/9780190264086.013.421>
- 3908 Davidson, T. J., Kloosterman, F., & Wilson, M. A. (2009). Hippocampal
3909 replay of extended experience. *Neuron*, 63(4), 497–507.
3910 <https://doi.org/10.1016/j.neuron.2009.07.027>
- 3911 Dhawale, A. K. (2013). *Temporal and spatial features of sensory
3912 coding in the olfactory bulb and hippocampus*. Tata Institute of
3913 Fundamental Research.
- 3914 Doya, K., Ishii, S., Pouget, A., & Rao, R. P. N. (2007). Bayesian brain:
3915 Probabilistic approaches to neural coding. In K. Doya, S. Ishii, A.
3916 Pouget, & R. P. N. Rao (Eds.), *Bayesian brain: Probabilistic
3917 approaches to neural coding*. MIT Press.
- 3918 Eichenbaum, H. (2017). On the Integration of Space, Time, and
3919 Memory. *Neuron*, 95(5), 1007–1018.
3920 <https://doi.org/10.1016/j.neuron.2017.06.036>
- 3921 Foster, D. J. (2017). Replay Comes of Age. *Annual Review of
3922 Neuroscience*, 40, 581–602. <https://doi.org/10.1146/annurev-neuro-072116-031538>
- 3924 Hutchinson, J. B., & Turk-Browne, N. B. (2012). Memory-guided
3925 attention: control from multiple memory systems. *Trends in*

- 3926 *Cognitive Sciences*, 16(12), 576–579.
3927 <https://doi.org/10.1016/j.tics.2012.10.003>
- 3928 Jun, J. J., Steinmetz, N. A., Siegle, J. H., Denman, D. J., Bauza, M.,
3929 Barbarits, B., Lee, A. K., Anastassiou, C. A., Andrei, A., Aydin, Ç.,
3930 Barbic, M., Blanche, T. J., Bonin, V., Couto, J., Dutta, B., Gratiy,
3931 S. L., Gutnisky, D. A., Häusser, M., Karsh, B., ... Harris, T. D.
3932 (2017). Fully integrated silicon probes for high-density recording of
3933 neural activity. *Nature*, 551(7679), 232–236.
3934 <https://doi.org/10.1038/nature24636>
- 3935 Leybaert, L., de Meyer, A., Mabilde, C., & Sanderson, M. J. (2005). A
3936 simple and practical method to acquire geometrically correct
3937 images with resonant scanning-based line scanning in a custom-
3938 built video-rate laser scanning microscope. *Journal of Microscopy*,
3939 219(3), 133–140. [https://doi.org/https://doi.org/10.1111/j.1365-2818.2005.01502.x](https://doi.org/10.1111/j.1365-2818.2005.01502.x)
- 3940 Manns, J. R., Clark, R. E., & Squire, L. R. (2000). Parallel acquisition
3941 of awareness and trace eyeblink classical conditioning. *Learning &*
3942 *Memory (Cold Spring Harbor, N.Y.)*, 7(5), 267–272.
3943 <https://doi.org/10.1101/lm.33400>
- 3944 Mau, W., Sullivan, D. W., Kinsky, N. R., Hasselmo, M. E., Howard, M.
3945 W., & Eichenbaum, H. (2018). The Same Hippocampal CA1
3946 Population Simultaneously Codes Temporal Information over
3947 Multiple Timescales. *Current Biology*, 28(10), 1499-1508.e4.
3948 <https://doi.org/10.1016/j.cub.2018.03.051>
- 3949 Modi, M. N., Dhawale, A. K., & Bhalla, U. S. (2014). CA1 cell activity
3950 sequences emerge after reorganization of network correlation
3951 structure during associative learning. *eLife*, 3, e01982–e01982.
3952 <https://doi.org/10.7554/eLife.01982>
- 3953 Nguyen, Q.-T., Callamaras, N., Hsieh, C., & Parker, I. (2001).
3954 Construction of a two-photon microscope for video-rate Ca²⁺
3955 imaging. *Cell Calcium*, 30(6), 383–393.
3956 <https://doi.org/https://doi.org/10.1054/ceca.2001.0246>
- 3957 Ranck, J. B. (1973). Studies on single neurons in dorsal hippocampal
3958 formation and septum in unrestrained rats: Part I. Behavioral
3959 correlates and firing repertoires. *Experimental Neurology*, 41(2),
3960 462–531. [https://doi.org/https://doi.org/10.1016/0014-4886\(73\)90290-2](https://doi.org/https://doi.org/10.1016/0014-4886(73)90290-2)
- 3961 Ranck, J. B. (1975). *Behavioral Correlates and Firing Repertoires of*
3962 *Neurons in the Dorsal Hippocampal Formation and Septum of*
3963 *Unrestrained Rats BT - The Hippocampus: Volume 2:*
3964 *Neurophysiology and Behavior* (R. L. Isaacson & K. H. Pribram,
3965 Eds.; pp. 207–244). Springer US. https://doi.org/10.1007/978-1-4684-2979-4_7

- 3969 Rao, R. P. N., & Ballard, D. H. (1999). Predictive coding in the visual
3970 cortex: a functional interpretation of some extra-classical
3971 receptive-field effects. *Nature Neuroscience*, 2(1), 79–87.
3972 <https://doi.org/10.1038/4580>
- 3973 Rochefort, N. L., Garaschuk, O., Milos, R.-I., Narushima, M., Marandi,
3974 N., Pichler, B., Kovalchuk, Y., & Konnerth, A. (2009).
3975 Sparsification of neuronal activity in the visual cortex at eye-
3976 opening. *Proceedings of the National Academy of Sciences of the*
3977 *United States of America*, 106(35), 15049–15054.
3978 <https://doi.org/10.1073/pnas.0907660106>
- 3979 Siegel, J. J., Taylor, W., Gray, R., Kalmbach, B., Zemelman, B. V.,
3980 Desai, N. S., Johnston, D., & Chitwood, R. A. (2015). Trace
3981 Eyeblink Conditioning in Mice Is Dependent upon the Dorsal
3982 Medial Prefrontal Cortex, Cerebellum, and Amygdala: Behavioral
3983 Characterization and Functional Circuitry. *ENeuro*, 2(4),
3984 ENEURO.0051-14.2015. <https://doi.org/10.1523/ENEURO.0051-14.2015>
- 3985 3986 Uncapher, M. R., Hutchinson, J. B., & Wagner, A. D. (2011).
3987 Dissociable effects of top-down and bottom-up attention during
3988 episodic encoding. *The Journal of Neuroscience : The Official*
3989 *Journal of the Society for Neuroscience*, 31(35), 12613–12628.
3990 <https://doi.org/10.1523/JNEUROSCI.0152-11.2011>
- 3991 Zhang, S., & Manahan-Vaughan, D. (2015). Spatial olfactory learning
3992 contributes to place field formation in the hippocampus. *Cerebral*
3993 *Cortex (New York, N.Y. : 1991)*, 25(2), 423–432.
3994 <https://doi.org/10.1093/cercor/bht239>
- 3995 Zhou, S., Masmanidis, S. C., & Buonomano, D. V. (2020). Neural
3996 Sequences as an Optimal Dynamical Regime for the Readout of
3997 Time. *Neuron*, 108(4), 651-658.e5.
3998 <https://doi.org/https://doi.org/10.1016/j.neuron.2020.08.020>
- 3999

All Bibliography

- 4001 Abe, R., Sakaguchi, T., Matsumoto, N., Matsuki, N., & Ikegaya, Y.
4002 (2014). Sound-induced hyperpolarization of hippocampal neurons.
4003 *Neuroreport*, 25(13), 1013–1017.
4004 <https://doi.org/10.1097/WNR.0000000000000206>
- 4005 Abeles, M. (1982). *Local Cortical Circuits: An Electrophysiological Study*. Springer-Verlag.
4006 <https://books.google.co.in/books?id=s25lwwEACAAJ>
- 4008 Abeles, M. (1991). *Corticonics: Neural Circuits of the Cerebral Cortex*.
4009 Cambridge University Press. <https://doi.org/DOI:10.1017/CBO9780511574566>
- 4011 Abeles, M. (2004). Time Is Precious. *Science*, 304(5670), 523–524.
4012 <https://doi.org/10.1126/science.1097725>
- 4013 Abeles, M. (2009). *Synfire Chains* (L. R. B. T.-E. of N. Squire, Ed.; pp. 829–832). Academic Press.
4014 <https://doi.org/https://doi.org/10.1016/B978-008045046-9.01437-6>
- 4016 Abeles, M., Hayon, G., & Lehmann, D. (2004). Modeling
4017 compositionality by dynamic binding of synfire chains. *Journal of Computational Neuroscience*, 17(2), 179–201.
4018 <https://doi.org/10.1023/B:JCNS.0000037682.18051.5f>
- 4020 Ananthamurthy, K. G., & Bhalla, U. S. (2023). Synthetic Data Resource
4021 and Benchmarks for Time Cell Analysis and Detection Algorithms.
4022 *ENeuro*, ENEURO.0007-22.2023.
4023 <https://doi.org/10.1523/ENEURO.0007-22.2023>
- 4024 Andermann, M. L., Gilfoy, N. B., Goldey, G. J., Sachdev, R. N. S.,
4025 Wölfel, M., McCormick, D. A., Reid, R. C., & Levene, M. J. (2013).
4026 Chronic Cellular Imaging of Entire Cortical Columns in Awake
4027 Mice Using Microprisms. *Neuron*, 80(4), 900–913.
4028 <https://doi.org/10.1016/j.neuron.2013.07.052>
- 4029 Andersen, P., Morris, R., Amaral, D., Bliss, T., & O'Keefe, J. (Eds.).
4030 (2006). *The Hippocampus Book*. Oxford University Press.
4031 <https://doi.org/10.1093/acprof:oso/9780195100273.001.0001>
- 4032 Andersen, R. A., Snyder, L. H., Li, C.-S., & Stricanne, B. (1993).
4033 Coordinate transformations in the representation of spatial
4034 information. *Current Opinion in Neurobiology*, 3(2), 171–176.
4035 [https://doi.org/https://doi.org/10.1016/0959-4388\(93\)90206-E](https://doi.org/https://doi.org/10.1016/0959-4388(93)90206-E)
- 4036 Aronov, D., Nevers, R., & Tank, D. W. (2017). Mapping of a non-spatial
4037 dimension by the hippocampal-entorhinal circuit. *Nature*,
4038 543(7647), 719–722. <https://doi.org/10.1038/nature21692>
- 4039 Attardo, A., Fitzgerald, J. E., & Schnitzer, M. J. (2015). Impermanence
4040 of dendritic spines in live adult CA1 hippocampus. *Nature*,
4041 523(7562), 592–596. <https://doi.org/10.1038/nature14467>

- 4042 Ballard, I. C., Wagner, A. D., & McClure, S. M. (2019). Hippocampal
4043 pattern separation supports reinforcement learning. *Nature
4044 Communications*, 10(1), 1073. <https://doi.org/10.1038/s41467-019-08998-1>
- 4045 Barreto, R. P. J., Messerschmidt, B., & Schnitzer, M. J. (2009). In vivo
4046 fluorescence imaging with high-resolution microlenses. *Nature
4047 Methods*, 6(7), 511–512. <https://doi.org/10.1038/nmeth.1339>
- 4048 Barreto, R. P. J., & Schnitzer, M. J. (2012). In vivo optical
4049 microendoscopy for imaging cells lying deep within live tissue.
4050 *Cold Spring Harbor Protocols*, 2012(10), 1029–1034.
4051 <https://doi.org/10.1101/pdb.top071464>
- 4052 Baudry, M., & Lynch, G. (1981). Hippocampal glutamate receptors.
4053 *Molecular and Cellular Biochemistry*, 38(1), 5–18.
4054 <https://doi.org/10.1007/BF00235685>
- 4055 Bellistri, E., Aguilar, J., Brotons-Mas, J. R., Foffani, G., & de la Prida, L.
4056 M. (2013). Basic properties of somatosensory-evoked responses
4057 in the dorsal hippocampus of the rat. *The Journal of Physiology*,
4058 591(10), 2667–2686. <https://doi.org/10.1113/jphysiol.2013.251892>
- 4059 Bhalla, U. S. (2019). Dendrites, deep learning, and sequences in the
4060 hippocampus. *Hippocampus*, 29(3), 239–251.
4061 <https://doi.org/https://doi.org/10.1002/hipo.22806>
- 4062 Bialek, W., Callan, C. G., & Strong, S. P. (1996). Field Theories for
4063 Learning Probability Distributions. *Physical Review Letters*,
4064 77(23), 4693–4697. <https://doi.org/10.1103/physrevlett.77.4693>
- 4065 Bialek, W., Nemenman, I., & Tishby, N. (2001). Predictability,
4066 Complexity, and Learning. *Neural Comput.*, 13(11), 2409–2463.
4067 <https://doi.org/10.1162/089976601753195969>
- 4068 Bienenstock, E. (1995). A model of neocortex. *Network: Computation
4069 in Neural Systems*, 6(2), 179–224. https://doi.org/10.1088/0954-898X_6_2_004
- 4070 Bjerknes, T. L., Moser, E. I., & Moser, M.-B. (2014). Representation of
4071 Geometric Borders in the Developing Rat. *Neuron*, 82(1), 71–78.
4072 <https://doi.org/10.1016/j.neuron.2014.02.014>
- 4073 Bonin, V., Histed, M. H., Yurgenson, S., & Reid, R. C. (2011). Local
4074 Diversity and Fine-Scale Organization of Receptive Fields in
4075 Mouse Visual Cortex. *The Journal of Neuroscience*, 31(50),
4076 18506. <https://doi.org/10.1523/JNEUROSCI.2974-11.2011>
- 4077 Brown, G. D. (1998). Nonassociative learning processes affecting
4078 swimming probability in the seashell Tritonia diomedea:
4079 habituation, sensitization and inhibition. *Behavioural Brain
4080 Research*, 95(2), 151–165.
4081 [https://doi.org/https://doi.org/10.1016/S0166-4328\(98\)00072-2](https://doi.org/https://doi.org/10.1016/S0166-4328(98)00072-2)
- 4082 Buccino, A. P., Garcia, S., & Yger, P. (2022). Spike sorting: new trends
4083
- 4084

- 4085 and challenges of the era of high-density probes. *Progress in*
4086 *Biomedical Engineering*, 4(2), 022005.
4087 <https://doi.org/10.1088/2516-1091/ac6b96>
- 4088 Burgess, N. (2008). Spatial Cognition and the Brain. *Annals of the New*
4089 *York Academy of Sciences*, 1124(1), 77–97.
4090 <https://doi.org/https://doi.org/10.1196/annals.1440.002>
- 4091 Buzsáki, G., & Llinás, R. (2017). Space and time in the brain. *Science*
4092 (*New York, N.Y.*), 358(6362), 482–485.
4093 <https://doi.org/10.1126/science.aan8869>
- 4094 Cai, D. J., Aharoni, D., Shuman, T., Shobe, J., Biane, J., Song, W.,
4095 Wei, B., Veshkini, M., La-Vu, M., Lou, J., Flores, S. E., Kim, I.,
4096 Sano, Y., Zhou, M., Baumgaertel, K., Lavi, A., Kamata, M.,
4097 Tuszyński, M., Mayford, M., ... Silva, A. J. (2016). A shared neural
4098 ensemble links distinct contextual memories encoded close in
4099 time. *Nature*, 534(7605), 115–118.
4100 <https://doi.org/10.1038/nature17955>
- 4101 Caporale, N., & Dan, Y. (2008). Spike timing-dependent plasticity: a
4102 Hebbian learning rule. *Annual Review of Neuroscience*, 31, 25–
4103 46. <https://doi.org/10.1146/annurev.neuro.31.060407.125639>
- 4104 Carew, T. J., Castellucci, V. F., & Kandel, E. R. (1971). An Analysis of
4105 Dishabituation and Sensitization of The Gill-Withdrawal Reflex In
4106 Aplysia. *International Journal of Neuroscience*, 2(2), 79–98.
4107 <https://doi.org/10.3109/00207457109146995>
- 4108 Chen, T.-W., Wardill, T. J., Sun, Y., Pulver, S. R., Renninger, S. L.,
4109 Baohan, A., Schreiter, E. R., Kerr, R. A., Orger, M. B., Jayaraman,
4110 V., Looger, L. L., Svoboda, K., & Kim, D. S. (2013). Ultrasensitive
4111 fluorescent proteins for imaging neuronal activity. *Nature*,
4112 499(7458), 295–300. <https://doi.org/10.1038/nature12354>
- 4113 Chigirev, D., & Bialek, W. (2004, January). Optimal manifold
4114 representation of data: An information theoretic approach.
4115 *Advances in Neural Information Processing Systems 16 -*
4116 *Proceedings of the 2003 Conference, NIPS 2003*.
- 4117 Chudasama, Y. (2010). Delayed (Non)Match-to-Sample Task. In I. P.
4118 Stolerman (Ed.), *Encyclopedia of Psychopharmacology* (p. 372).
4119 Springer Berlin Heidelberg. https://doi.org/10.1007/978-3-540-68706-1_1619
- 4121 Chun, M. M., & Johnson, M. K. (2011). Memory: enduring traces of
4122 perceptual and reflective attention. *Neuron*, 72(4), 520–535.
4123 <https://doi.org/10.1016/j.neuron.2011.10.026>
- 4124 Clayton, N. S., Salwiczek, L. H., & Dickinson, A. (2007). Episodic
4125 memory. *Current Biology*, 17(6), R189–R191.
4126 <https://doi.org/10.1016/j.cub.2007.01.011>
- 4127 Cohen, M. R., & Kohn, A. (2011). Measuring and interpreting neuronal

- 4128 correlations. *Nature Neuroscience*, 14(7), 811–819.
4129 <https://doi.org/10.1038/nn.2842>
- 4130 Cohen, N. J., & Eichenbaum, H. (1993). *Memory, amnesia, and the*
4131 *hippocampal system*.
- 4132 Conen, K. E., & Desrochers, T. M. (2022). *The Neural Basis of*
4133 *Behavioral Sequences in Cortical and Subcortical Circuits*. Oxford
4134 University Press.
4135 <https://doi.org/10.1093/acrefore/9780190264086.013.421>
- 4136 Conway, M. A. (2009). Episodic memories. *Neuropsychologia*, 47(11),
4137 2305–2313.
4138 <https://doi.org/https://doi.org/10.1016/j.neuropsychologia.2009.02.003>
- 4139 Csicsvari, J., O'Neill, J., Allen, K., & Senior, T. (2007). Place-selective
4140 firing contributes to the reverse-order reactivation of
4141 CA1 pyramidal cells during sharp waves in open-field exploration.
4142 *The European Journal of Neuroscience*, 26(3), 704–716.
4143 <https://doi.org/10.1111/j.1460-9568.2007.05684.x>
- 4144 Davidson, T. J., Kloosterman, F., & Wilson, M. A. (2009). Hippocampal
4145 replay of extended experience. *Neuron*, 63(4), 497–507.
4146 <https://doi.org/10.1016/j.neuron.2009.07.027>
- 4147 Denk, W., Strickler, J. H., & Webb, W. W. (1990). Two-photon laser
4148 scanning fluorescence microscopy. *Science (New York, N.Y.)*,
4149 248(4951), 73–76. <https://doi.org/10.1126/science.2321027>
- 4150 Deshmukh, S. S., & Bhalla, U. S. (2003). Representation of odor
4151 habituation and timing in the hippocampus. *The Journal of*
4152 *Neuroscience : The Official Journal of the Society*
4153 *for Neuroscience*, 23(5), 1903–1915.
4154 <https://doi.org/10.1523/JNEUROSCI.23-05-01903.2003>
- 4155 Dhawale, A. K. (2013). *Temporal and spatial features of sensory*
4156 *coding in the olfactory bulb and hippocampus*. Tata Institute of
4157 Fundamental Research.
- 4158 Dhawale, A. K., Poddar, R., Wolff, S. B. E., Normand, V. A.,
4159 Kopelowitz, E., & Ölveczky, B. P. (2017). Automated long-term
4160 recording and analysis of neural activity in behaving animals.
4161 *eLife*, 6, e27702. <https://doi.org/10.7554/eLife.27702>
- 4162 Diamond, A. (2013). Executive Functions. *Annual Review of*
4163 *Psychology*, 64(1), 135–168. <https://doi.org/10.1146/annurev-psych-113011-143750>
- 4164 Diba, K., & Buzsáki, G. (2007). Forward and reverse hippocampal
4165 place-cell sequences during ripples. *Nature Neuroscience*, 10(10),
4166 1241–1242. <https://doi.org/10.1038/nn1961>
- 4167 Dickinson, A., Nicholas, D. J., & Mackintosh, N. J. (1983). A re-
4168 examination of one-trial blocking in conditioned suppression. *The*
4169
- 4170

- 4171 *Quarterly Journal of Experimental Psychology B: Comparative and*
4172 *Physiological Psychology*, 35, 67–79.
4173 <https://doi.org/10.1080/14640748308400914>
- 4174 Disterhoft, J. F., & Weiss, C. (2017). Eyeblink Conditioning – A
4175 Behavioral Model of Procedural and Declarative Learning. In J. H.
4176 Byrne (Ed.), *Learning and Memory: A Comprehensive Reference*
4177 (Second Edition) (pp. 327–355). Academic Press.
4178 <https://doi.org/https://doi.org/10.1016/B978-0-12-809324-5.21087-0>
- 4179 Dombeck, D. A., Graziano, M. S., & Tank, D. W. (2009). Functional
4180 Clustering of Neurons in Motor Cortex Determined by Cellular
4181 Resolution Imaging in Awake Behaving Mice. *The Journal of*
4182 *Neuroscience*, 29(44), 13751 LP – 13760.
4183 <https://doi.org/10.1523/JNEUROSCI.2985-09.2009>
- 4184 Dombeck, D. A., Harvey, C. D., Tian, L., Looger, L. L., & Tank, D. W.
4185 (2010). Functional imaging of hippocampal place cells at cellular
4186 resolution during virtual navigation. *Nature Neuroscience*, 13(11),
4187 1433–1440. <https://doi.org/10.1038/nn.2648>
- 4188 Doya, K., Ishii, S., Pouget, A., & Rao, R. P. N. (2007). Bayesian brain:
4189 Probabilistic approaches to neural coding. In K. Doya, S. Ishii, A.
4190 Pouget, & R. P. N. Rao (Eds.), *Bayesian brain: Probabilistic*
4191 *approaches to neural coding*. MIT Press.
- 4192 Dragoi, G. (2013). Internal operations in the hippocampus: single cell
4193 and ensemble temporal coding. *Frontiers in Systems*
4194 *Neuroscience*, 7, 46. <https://doi.org/10.3389/fnsys.2013.00046>
- 4195 Dragoi, G., & Buzsáki, G. (2006). Temporal encoding of place
4196 sequences by hippocampal cell assemblies. *Neuron*, 50(1), 145–
4197 157. <https://doi.org/10.1016/j.neuron.2006.02.023>
- 4198 Dragoi, G., Carpi, D., Recce, M., Csicsvari, J., & Buzsáki, G. (1999).
4199 Interactions between hippocampus and medial septum during
4200 sharp waves and theta oscillation in the behaving rat. *The Journal of*
4201 *Neuroscience : The Official Journal of the Society for*
4202 *Neuroscience*, 19(14), 6191–6199.
4203 <http://www.ncbi.nlm.nih.gov/pubmed/10407055>
- 4204 Dragoi, G., & Tonegawa, S. (2011). Preplay of future place cell
4205 sequences by hippocampal cellular assemblies. *Nature*,
4206 469(7330), 397–401. <https://doi.org/10.1038/nature09633>
- 4207 Eichenbaum, H. (2004). Hippocampus: Cognitive processes and
4208 neural representations that underlie declarative memory. *Neuron*,
4209 44(1), 109–120. <https://doi.org/10.1016/j.neuron.2004.08.028>
- 4210 Eichenbaum, H. (2017). On the Integration of Space, Time, and
4211 Memory. *Neuron*, 95(5), 1007–1018.
4212 <https://doi.org/10.1016/j.neuron.2017.06.036>

- 4214 Ekstrom, A. D., & Ranganath, C. (2018). Space, time, and episodic
4215 memory: The hippocampus is all over the cognitive map.
4216 *Hippocampus*, 28(9), 680–687.
4217 <https://doi.org/https://doi.org/10.1002/hipo.22750>
- 4218 Fanselow, M. S., & Dong, H.-W. (2010). Are the dorsal and ventral
4219 hippocampus functionally distinct structures? *Neuron*, 65(1), 7–19.
4220 <https://doi.org/10.1016/j.neuron.2009.11.031>
- 4221 Fassihi, A., Akrami, A., Pulecchi, F., Schönfelder, V., & Diamond, M. E.
4222 (2017). Transformation of Perception from Sensory to Motor
4223 Cortex. *Current Biology : CB*, 27(11), 1585-1596.e6.
4224 <https://doi.org/10.1016/j.cub.2017.05.011>
- 4225 Ferbinteanu, J., & Shapiro, M. L. (2003). Prospective and retrospective
4226 memory coding in the hippocampus. *Neuron*, 40(6), 1227–1239.
4227 [https://doi.org/10.1016/s0896-6273\(03\)00752-9](https://doi.org/10.1016/s0896-6273(03)00752-9)
- 4228 Ferbinteanu, J., Shirvalkar, P., & Shapiro, M. L. (2011). Memory
4229 Modulates Journey-Dependent Coding in the Rat Hippocampus.
4230 *The Journal of Neuroscience*, 31(25), 9135 LP – 9146.
4231 <https://doi.org/10.1523/JNEUROSCI.1241-11.2011>
- 4232 Focus on spatial cognition. (2017). *Nature Neuroscience*, 20(11), 1431.
4233 <https://doi.org/10.1038/nn.4666>
- 4234 Foster, D. J. (2017). Replay Comes of Age. *Annual Review of
4235 Neuroscience*, 40, 581–602. <https://doi.org/10.1146/annurev-neuro-072116-031538>
- 4237 Foster, D. J., & Wilson, M. A. (2006). Reverse replay of behavioural
4238 sequences in hippocampal place cells during the awake state.
4239 *Nature*, 440(7084), 680–683. <https://doi.org/10.1038/nature04587>
- 4240 Foster, D. J., & Wilson, M. A. (2007). Hippocampal theta sequences.
4241 *Hippocampus*, 17(11), 1093–1099.
4242 <https://doi.org/10.1002/hipo.20345>
- 4243 Francis, M., Qian, X., Charbel, C., Ledoux, J., Parker, J. C., & Taylor,
4244 M. S. (2012). Automated region of interest analysis of dynamic
4245 Ca²⁺ signals in image sequences. *American Journal of
4246 Physiology. Cell Physiology*, 303(3), C236-43.
4247 <https://doi.org/10.1152/ajpcell.00016.2012>
- 4248 Frank, L. M., Brown, E. N., & Wilson, M. (2000). Trajectory encoding in
4249 the hippocampus and entorhinal cortex. *Neuron*, 27(1), 169–178.
4250 [https://doi.org/10.1016/s0896-6273\(00\)00018-0](https://doi.org/10.1016/s0896-6273(00)00018-0)
- 4251 Fyhn, M., Molden, S., Witter, M. P., Moser, E. I., & Moser, M.-B.
4252 (2004). Spatial representation in the entorhinal cortex. *Science
4253 (New York, N.Y.)*, 305(5688), 1258–1264.
4254 <https://doi.org/10.1126/science.1099901>
- 4255 Giovannucci, A., Badura, A., Deverett, B., Najafi, F., Pereira, T. D.,
4256 Gao, Z., Ozden, I., Kloth, A. D., Pnevmatikakis, E., Paninski, L.,

- 4257 De Zeeuw, C. I., Medina, J. F., & Wang, S. S.-H. (2017).
4258 Cerebellar granule cells acquire a widespread predictive feedback
4259 signal during motor learning. *Nature Neuroscience*, 20(5), 727–
4260 734. <https://doi.org/10.1038/nn.4531>
- 4261 Grün, S. (2009). Data-Driven Significance Estimation for Precise Spike
4262 Correlation. *Journal of Neurophysiology*, 101(3), 1126–1140.
4263 <https://doi.org/10.1152/jn.00093.2008>
- 4264 Guo, Z. V., Hires, S. A., Li, N., O'Connor, D. H., Komiyama, T., Ophir,
4265 E., Huber, D., Bonardi, C., Morandell, K., Gutinsky, D., Peron, S.,
4266 Xu, N., Cox, J., & Svoboda, K. (2014). Procedures for Behavioral
4267 Experiments in Head-Fixed Mice. *PLOS ONE*, 9(2), e88678.
4268 <https://doi.org/10.1371/journal.pone.0088678>
- 4269 Gupta, A. S., van der Meer, M. A. A., Touretzky, D. S., & Redish, A. D.
4270 (2010). Hippocampal Replay Is Not a Simple Function of
4271 Experience. *Neuron*, 65(5), 695–705.
4272 <https://doi.org/https://doi.org/10.1016/j.neuron.2010.01.034>
- 4273 Hafting, T., Fyhn, M., Molden, S., Moser, M.-B., & Moser, E. I. (2005).
4274 Microstructure of a spatial map in the entorhinal cortex. *Nature*,
4275 436(7052), 801–806. <https://doi.org/10.1038/nature03721>
- 4276 Hamme, L. J. Van, & Wasserman, E. A. (1993). Cue Competition in
4277 Causality Judgments: The Role of Manner of Information
4278 Presentation. *Bulletin of the Psychonomic Society*, 31(5), 457–
4279 460. <https://doi.org/10.3758/bf03334962>
- 4280 Han, J.-H., Kushner, S. A., Yiu, A. P., Hsiang, H.-L. L., Buch, T.,
4281 Waisman, A., Bontempi, B., Neve, R. L., Frankland, P. W., &
4282 Josselyn, S. A. (2009). Selective erasure of a fear memory.
4283 *Science (New York, N.Y.)*, 323(5920), 1492–1496.
4284 <https://doi.org/10.1126/science.1164139>
- 4285 Hartley, T., Lever, C., Burgess, N., & O'Keefe, J. (2014). Space in the
4286 brain: how the hippocampal formation supports spatial cognition.
4287 *Philosophical Transactions of the Royal Society B: Biological
4288 Sciences*, 369(1635), 20120510.
4289 <https://doi.org/10.1098/rstb.2012.0510>
- 4290 Harvey, C. D., Collman, F., Dombeck, D. A., & Tank, D. W. (2009).
4291 Intracellular dynamics of hippocampal place cells during virtual
4292 navigation. *Nature*, 461(7266), 941–946.
4293 <https://doi.org/10.1038/nature08499>
- 4294 Hebb, D. O. (1949). The organization of behavior; a
4295 neuropsychological theory. In *The organization of behavior; a
4296 neuropsychological theory*. Wiley.
- 4297 Helmchen, F., & Denk, W. (2005). Deep tissue two-photon microscopy.
4298 2(12), 9. <https://doi.org/10.1038/nmeth818>
- 4299 Heys, J. G., Rangarajan, K. V., & Dombeck, D. A. (2014). The

- 4300 Functional Micro-organization of Grid Cells Revealed by Cellular-
4301 Resolution Imaging. *Neuron*, 84(5), 1079–1090.
4302 <https://doi.org/10.1016/j.neuron.2014.10.048>
- 4303 Hjorth-Simonsen, A., & Jeune, B. (1972). Origin and termination of the
4304 hippocampal perforant path in the rat studied by silver
4305 impregnation. *The Journal of Comparative Neurology*, 144(2),
4306 215–232. <https://doi.org/10.1002/cne.901440206>
- 4307 Hubel, D. H., & Wiesel, T. N. (1962). Receptive fields, binocular
4308 interaction and functional architecture in the cat's visual cortex.
4309 *The Journal of Physiology*, 160(1), 106–154.
4310 <https://doi.org/10.1113/jphysiol.1962.sp006837>
- 4311 Hutchinson, J. B., & Turk-Browne, N. B. (2012). Memory-guided
4312 attention: control from multiple memory systems. *Trends in*
4313 *Cognitive Sciences*, 16(12), 576–579.
4314 <https://doi.org/10.1016/j.tics.2012.10.003>
- 4315 Hyde, R. A., & Strowbridge, B. W. (2012). Mnemonic representations
4316 of transient stimuli and temporal sequences in the rodent
4317 hippocampus in vitro. *Nature Neuroscience*, 15(10), 1430–1438.
4318 <https://doi.org/10.1038/nn.3208>
- 4319 Ikegaya, Y., Aaron, G., Cossart, R., Aronov, D., Lampl, I., Ferster, D.,
4320 & Yuste, R. (2004). Synfire chains and cortical songs: temporal
4321 modules of cortical activity. *Science (New York, N.Y.)*, 304(5670),
4322 559–564. <https://doi.org/10.1126/science.1093173>
- 4323 Itskov, P. M., Vinnik, E., & Diamond, M. E. (2011). Hippocampal
4324 representation of touch-guided behavior in rats: persistent and
4325 independent traces of stimulus and reward location. *PloS One*,
4326 6(1), e16462. <https://doi.org/10.1371/journal.pone.0016462>
- 4327 Itskov, V., Pastalkova, E., Mizuseki, K., Buzsaki, G., & Harris, K. D.
4328 (2008). Theta-mediated dynamics of spatial information in
4329 hippocampus. *The Journal of Neuroscience : The Official Journal*
4330 *of the Society for Neuroscience*, 28(23), 5959–5964.
4331 <https://doi.org/10.1523/JNEUROSCI.5262-07.2008>
- 4332 Jadhav, S. P., Kemere, C., German, P. W., & Frank, L. M. (2012).
4333 Awake hippocampal sharp-wave ripples support spatial memory.
4334 *Science (New York, N.Y.)*, 336(6087), 1454–1458.
4335 <https://doi.org/10.1126/science.1217230>
- 4336 Jaramillo, S., & Zador, A. M. (2014). Mice and rats achieve similar
4337 levels of performance in an adaptive decision-making task . In
4338 *Frontiers in Systems Neuroscience* (Vol. 8).
4339 <https://www.frontiersin.org/articles/10.3389/fnsys.2014.00173>
- 4340 Josselyn, S. A., & Tonegawa, S. (2020). Memory engrams: Recalling
4341 the past and imagining the future. *Science (New York, N.Y.)*,
4342 367(6473). <https://doi.org/10.1126/science.aaw4325>

- 4343 Jun, J. J., Steinmetz, N. A., Siegle, J. H., Denman, D. J., Bauza, M.,
4344 Barbarits, B., Lee, A. K., Anastassiou, C. A., Andrei, A., Aydin, Ç.,
4345 Barbic, M., Blanche, T. J., Bonin, V., Couto, J., Dutta, B., Gratiy,
4346 S. L., Gutnisky, D. A., Häusser, M., Karsh, B., ... Harris, T. D.
4347 (2017). Fully integrated silicon probes for high-density recording of
4348 neural activity. *Nature*, 551(7679), 232–236.
4349 <https://doi.org/10.1038/nature24636>
- 4350 Kaifosh, P., Lovett-Barron, M., Turi, G. F., Reardon, T. R., & Losonczy,
4351 A. (2013). Septo-hippocampal GABAergic signaling across
4352 multiple modalities in awake mice. *Nature Neuroscience*, 16(9),
4353 1182–1184. <https://doi.org/10.1038/nn.3482>
- 4354 Kalmbach, B. E., Davis, T., Ohyama, T., Riusech, F., Nores, W. L., &
4355 Mauk, M. D. (2010). Cerebellar Cortex Contributions to the
4356 Expression and Timing of Conditioned Eyelid Responses. *Journal
4357 of Neurophysiology*, 103(4), 2039–2049.
4358 <https://doi.org/10.1152/jn.00033.2010>
- 4359 Kalmbach, B. E., Ohyama, T., & Mauk, M. D. (2010). Temporal
4360 Patterns of Inputs to Cerebellum Necessary and Sufficient for
4361 Trace Eyelid Conditioning. *Journal of Neurophysiology*, 104(2),
4362 627–640. <https://doi.org/10.1152/jn.00169.2010>
- 4363 Kamondi, A. (1998). *Theta Oscillations in Somata and Dendrites of
4364 Hippocampal Pyramidal Cells In Vivo: Activity-Dependent Phase-
4365 Precession of Action Potentials*. 261(March), 244–261.
- 4366 Khan, A. G., Parthasarathy, K., & Bhalla, U. S. (2010). Odor
4367 representations in the mammalian olfactory bulb. *Wiley
4368 Interdisciplinary Reviews. Systems Biology and Medicine*, 2(5),
4369 603–611. <https://doi.org/10.1002/wsbm.85>
- 4370 Kim, S., & Lee, I. (2012). The hippocampus is required for visually
4371 cued contextual response selection, but not for visual
4372 discrimination of contexts. *Frontiers in Behavioral Neuroscience*,
4373 6. <https://doi.org/10.3389/fnbeh.2012.00066>
- 4374 Kraus, B. J., Brandon, M. P., Robinson, R. J., Connerney, M. A.,
4375 Hasselmo, M. E., & Eichenbaum, H. (2015). During Running in
4376 Place, Grid Cells Integrate Elapsed Time and Distance Run.
4377 *Neuron*, 88(3), 578–589.
4378 <https://doi.org/10.1016/j.neuron.2015.09.031>
- 4379 Kraus, B., Robinson, R., White, J., Eichenbaum, H., & Hasselmo, M.
4380 (2013). Hippocampal “Time Cells”: Time versus Path Integration.
4381 *Neuron*, 78(6), 1090–1101.
4382 <https://doi.org/10.1016/j.neuron.2013.04.015>
- 4383 Kropff, E., Carmichael, J. E., Moser, M.-B., & Moser, E. I. (2015).
4384 Speed cells in the medial entorhinal cortex. *Nature*, 523(7561),
4385 419–424. <https://doi.org/10.1038/nature14622>

- 4386 Krupa, D., & Thompson, R. (2003). Inhibiting the Expression of a
4387 Classically Conditioned Behavior Prevents Its Extinction. *The
4388 Journal of Neuroscience : The Official Journal of the Society for
4389 Neuroscience*, 23, 10577–10584.
4390 <https://doi.org/10.1523/JNEUROSCI.23-33-10577.2003>
- 4391 Lever, C., Burton, S., Jeewajee, A., O'Keefe, J., & Burgess, N.
4392 (2009). Boundary Vector Cells in the Subiculum of the
4393 Hippocampal Formation. *The Journal of Neuroscience*, 29(31),
4394 9771 LP – 9777. <https://doi.org/10.1523/JNEUROSCI.1319-09.2009>
- 4395 Leybaert, L., de Meyer, A., Mabilde, C., & Sanderson, M. J. (2005). A
4396 simple and practical method to acquire geometrically correct
4397 images with resonant scanning-based line scanning in a custom-
4398 built video-rate laser scanning microscope. *Journal of Microscopy*,
4399 219(3), 133–140. <https://doi.org/https://doi.org/10.1111/j.1365-2818.2005.01502.x>
- 4400 Lovett-Barron, M., Kaifosh, P., Kheirbek, M. A., Danielson, N.,
4401 Zaremba, J. D., Reardon, T. R., Turi, G. F., Hen, R., Zemelman,
4402 B. V., & Losonczy, A. (2014). Dendritic inhibition in the
4403 hippocampus supports fear learning. *Science (New York, N.Y.)*,
4404 343(6173), 857–863. <https://doi.org/10.1126/science.1247485>
- 4405 Luo, L., Callaway, E. M., & Svoboda, K. (2018). Genetic Dissection of
4406 Neural Circuits: A Decade of Progress. *Neuron*, 98(2), 256–281.
4407 <https://doi.org/https://doi.org/10.1016/j.neuron.2018.03.040>
- 4408 MacDonald, C. J., Carrow, S., Place, R., & Eichenbaum, H. (2013).
4409 Distinct hippocampal time cell sequences represent odor
4410 memories in immobilized rats. *The Journal of Neuroscience : The
4411 Official Journal of the Society for Neuroscience*, 33(36), 14607–
4412 14616. <https://doi.org/10.1523/JNEUROSCI.1537-13.2013>
- 4413 MacDonald, C. J., Lepage, K. Q., Eden, U. T., & Eichenbaum, H.
4414 (2011). Hippocampal “time cells” bridge the gap in memory for
4415 discontiguous events. *Neuron*, 71(4), 737–749.
4416 <https://doi.org/10.1016/j.neuron.2011.07.012>
- 4417 Manns, J. R., Clark, R. E., & Squire, L. R. (2000). Parallel acquisition
4418 of awareness and trace eyeblink classical conditioning. *Learning &
4419 Memory (Cold Spring Harbor, N.Y.)*, 7(5), 267–272.
4420 <https://doi.org/10.1101/lm.33400>
- 4421 Maruyama, R., Maeda, K., Moroda, H., Kato, I., Inoue, M., Miyakawa,
4422 H., & Aonishi, T. (2014). Detecting cells using non-negative matrix
4423 factorization on calcium imaging data. *Neural Networks : The
4424 Official Journal of the International Neural Network Society*, 55,
4425 11–19. <https://doi.org/10.1016/j.neunet.2014.03.007>
- 4426 Mau, W., Sullivan, D. W., Kinsky, N. R., Hasselmo, M. E., Howard, M.

- 4429 W., & Eichenbaum, H. (2018). The Same Hippocampal CA1
4430 Population Simultaneously Codes Temporal Information over
4431 Multiple Timescales. *Current Biology*, 28(10), 1499-1508.e4.
4432 <https://doi.org/10.1016/j.cub.2018.03.051>
- 4433 McLelland, D., & Paulsen, O. (2007). Cortical Songs Revisited: A
4434 Lesson in Statistics. *Neuron*, 53(3), 319–321.
4435 <https://doi.org/https://doi.org/10.1016/j.neuron.2007.01.020>
- 4436 McNaughton, N., & Gray, J. A. (2000). Anxiolytic action on the
4437 behavioural inhibition system implies multiple types of arousal
4438 contribute to anxiety. *Journal of Affective Disorders*, 61(3), 161–
4439 176. [https://doi.org/10.1016/s0165-0327\(00\)00344-x](https://doi.org/10.1016/s0165-0327(00)00344-x)
- 4440 Medina, J. F., Garcia, K. S., Nores, W. L., Taylor, N. M., & Mauk, M. D.
4441 (2000). Timing mechanisms in the cerebellum: testing predictions
4442 of a large-scale computer simulation. *The Journal of
4443 Neuroscience : The Official Journal of the Society
4444 for Neuroscience*, 20(14), 5516–5525.
4445 <https://doi.org/10.1523/JNEUROSCI.20-14-05516.2000>
- 4446 Meeks, J. P., Arnson, H. A., & Holy, T. E. (2010). Representation and
4447 transformation of sensory information in the mouse
4448 accessory olfactory system. *Nature Neuroscience*, 13(6), 723–
4449 730. <https://doi.org/10.1038/nn.2546>
- 4450 Miller, A. M. P., Jacob, A. D., Ramsaran, A. I., De Snoo, M. L.,
4451 Josselyn, S. A., & Frankland, P. W. (2023). Emergence of a
4452 predictive model in the hippocampus. *Neuron*.
4453 <https://doi.org/10.1016/j.neuron.2023.03.011>
- 4454 Modi, M. N., Dhawale, A. K., & Bhalla, U. S. (2014). CA1 cell activity
4455 sequences emerge after reorganization of network correlation
4456 structure during associative learning. *eLife*, 3, e01982–e01982.
4457 <https://doi.org/10.7554/eLife.01982>
- 4458 Mokeichev, A., Okun, M., Barak, O., Katz, Y., Ben-Shahar, O., &
4459 Lampl, I. (2007). Stochastic Emergence of Repeating Cortical
4460 Motifs in Spontaneous Membrane Potential Fluctuations In Vivo.
4461 *Neuron*, 53, 413–425.
4462 <https://doi.org/10.1016/j.neuron.2007.01.017>
- 4463 Mollinedo-Gajate, I., Song, C., & Knöpfel, T. (2021). Genetically
4464 Encoded Voltage Indicators. *Advances in Experimental Medicine
4465 and Biology*, 1293, 209–224. https://doi.org/10.1007/978-981-15-8763-4_12
- 4466 Morris, R. G. M., Garrud, P., Rawlins, J. N. P., & O'Keefe, J. (1982).
4467 Place navigation impaired in rats with hippocampal lesions.
4468 *Nature*, 297(5868), 681–683. <https://doi.org/10.1038/297681a0>
- 4469 Moscovitch, M., Cabeza, R., Winocur, G., & Nadel, L. (2016). Episodic
4470 Memory and Beyond: The Hippocampus and Neocortex in
4471

- 4472 Transformation. *Annual Review of Psychology*, 67(1), 105–134.
4473 <https://doi.org/10.1146/annurev-psych-113011-143733>
- 4474 Moser, M.-B., & Moser, E. I. (1998). Distributed encoding and retrieval
4475 of spatial memory in the hippocampus. In *The Journal of*
4476 *Neuroscience* (Vol. 18, pp. 7535–7542). Society for Neuroscience.
- 4477 Moyer, J. R. J., Thompson, L. T., & Disterhoft, J. F. (1996). Trace
4478 eyeblink conditioning increases CA1 excitability in a transient
4479 and learning-specific manner. *The Journal of Neuroscience : The*
4480 *Official Journal of the Society for Neuroscience*, 16(17), 5536–
4481 5546. <https://doi.org/10.1523/JNEUROSCI.16-17-05536.1996>
- 4482 Mukamel, E. A., Nimmerjahn, A., & Schnitzer, M. J. (2009). Automated
4483 analysis of cellular signals from large-scale calcium imaging data.
4484 *Neuron*, 63(6), 747–760.
4485 <https://doi.org/10.1016/j.neuron.2009.08.009>
- 4486 Muller, R. U., & Kubie, J. L. (1989). The firing of hippocampal place
4487 cells predicts the future position of freely moving rats. *The Journal*
4488 *of Neuroscience : The Official Journal of the Society*
4489 *for Neuroscience*, 9(12), 4101–4110.
4490 <https://doi.org/10.1523/JNEUROSCI.09-12-04101.1989>
- 4491 Murray, T. A., & Levene, M. J. (2012). Singlet gradient index lens for
4492 deep in vivo multiphoton microscopy. *Journal of Biomedical*
4493 *Optics*, 17(2), 021106. <https://doi.org/10.1117/1.JBO.17.2.021106>
- 4494 Nakashiba, T., Young, J. Z., McHugh, T. J., Buhl, D. L., & Tonegawa,
4495 S. (2008). Transgenic inhibition of synaptic transmission reveals
4496 role of CA3 output in hippocampal learning. *Science (New York,*
4497 *N.Y.*), 319(5867), 1260–1264.
4498 <https://doi.org/10.1126/science.1151120>
- 4499 Nestler, E. J., Hyman, S. E., Holtzman, D. M., & Malenka, R. C. (2015).
4500 Higher Cognitive Function and Behavioral Control. In *Molecular*
4501 *Neuropharmacology: A Foundation for Clinical Neuroscience*, 3e.
4502 McGraw-Hill Education.
4503 neurology.mhmedical.com/content.aspx?aid=1105916482
- 4504 Nguyen, Q.-T., Callamaras, N., Hsieh, C., & Parker, I. (2001).
4505 Construction of a two-photon microscope for video-rate Ca²⁺
4506 imaging. *Cell Calcium*, 30(6), 383–393.
4507 <https://doi.org/https://doi.org/10.1054/ceca.2001.0246>
- 4508 Ohyama, T., Nores, W. L., Murphy, M., & Mauk, M. D. (2003). What
4509 the cerebellum computes. *Trends in Neurosciences*, 26(4), 222–
4510 227. [https://doi.org/10.1016/S0166-2236\(03\)00054-7](https://doi.org/10.1016/S0166-2236(03)00054-7)
- 4511 O'Keefe, J., & Burgess, N. (1996). Geometric determinants of the
4512 place fields of hippocampal neurons. *Nature*, 381(6581), 425–428.
4513 <https://doi.org/10.1038/381425a0>
- 4514 O'Keefe, J., & Dostrovsky, J. (1971). The hippocampus as a spatial

- 4515 map. Preliminary evidence from unit activity in the freely-moving
4516 rat. *Brain Research*, 34(1), 171–175. [https://doi.org/10.1016/0006-8993\(71\)90358-1](https://doi.org/10.1016/0006-8993(71)90358-1)
- 4517
- 4518 O'Keefe, J., & Nadel, L. (1978). The Hippocampus as a Cognitive Map.
4519 In *Philosophical Studies* (Vol. 27).
4520 <https://doi.org/10.5840/philstudies19802725>
- 4521 O'Keefe, J., & Recce, M. L. (1993). Phase relationship between
4522 hippocampal place units and the EEG theta rhythm.
4523 *Hippocampus*, 3(3), 317–330.
4524 <https://doi.org/10.1002/hipo.450030307>
- 4525 Ozden, I., Lee, H. M., Sullivan, M. R., & Wang, S. S.-H. (2008).
4526 Identification and Clustering of Event Patterns From In Vivo
4527 Multiphoton Optical Recordings of Neuronal Ensembles. *Journal
4528 of Neurophysiology*, 100(1), 495–503.
4529 <https://doi.org/10.1152/jn.01310.2007>
- 4530 Pachitariu, M., Stringer, C., Dipoppa, M., Schröder, S., Rossi, L. F.,
4531 Dalgleish, H., Carandini, M., & Harris, K. D. (2017). Suite2p:
4532 beyond 10,000 neurons with standard two-photon microscopy.
4533 *BioRxiv*, 61507. <https://doi.org/10.1101/061507>
- 4534 Paredes, R. M., Etzler, J. C., Watts, L. T., Zheng, W., & Lechleiter, J.
4535 D. (2008). Chemical calcium indicators. *Methods (San Diego,
4536 Calif.)*, 46(3), 143–151.
4537 <https://doi.org/10.1016/j.ymeth.2008.09.025>
- 4538 Pastalkova, E., Itskov, V., Amarasingham, A., & Buzsaki, G. (2008).
4539 Internally Generated Cell Assembly Sequences in the Rat
4540 Hippocampus. *Science*, 321(5894), 1322–1327.
4541 <https://doi.org/10.1126/science.1159775>
- 4542 Pavlov, I. P. (1927). Conditioned reflexes: an investigation of the
4543 physiological activity of the cerebral cortex. In *Conditioned
4544 reflexes: an investigation of the physiological activity of the
4545 cerebral cortex*. Oxford Univ. Press.
- 4546 Peron, S. P., Freeman, J., Iyer, V., Guo, C., & Svoboda, K. (2015). A
4547 Cellular Resolution Map of Barrel Cortex Activity during Tactile
4548 Behavior. *Neuron*, 86(3), 783–799.
4549 <https://doi.org/10.1016/j.neuron.2015.03.027>
- 4550 Petersen, C. C. H. (2019). Sensorimotor processing in the rodent
4551 barrel cortex. *Nature Reviews. Neuroscience*, 20(9), 533–546.
4552 <https://doi.org/10.1038/s41583-019-0200-y>
- 4553 Pfeiffer, B. E., & Foster, D. J. (2013). Hippocampal place-cell
4554 sequences depict future paths to remembered goals. *Nature*,
4555 497(7447), 74–79. <https://doi.org/10.1038/nature12112>
- 4556 Pnevmatikakis, E. A., Soudry, D., Gao, Y., Machado, T. A., Merel, J.,
4557 Pfau, D., Reardon, T., Mu, Y., Lacefield, C., Yang, W., Ahrens, M.,

- 4558 Bruno, R., Jessell, T. M., Peterka, D. S., Yuste, R., & Paninski, L.
4559 (2016). Simultaneous Denoising, Deconvolution, and Demixing of
4560 Calcium Imaging Data. *Neuron*, 89(2), 285–299.
4561 <https://doi.org/https://doi.org/10.1016/j.neuron.2015.11.037>
- 4562 Poort, J., Khan, A. G., Pachitariu, M., Nemri, A., Orsolic, I., Krupic, J.,
4563 Bauza, M., Sahani, M., Keller, G. B., Mrsic-Flogel, T. D., & Hofer,
4564 S. B. (2015). Learning Enhances Sensory and Multiple Non-
4565 sensory Representations in Primary Visual Cortex. *Neuron*, 86(6),
4566 1478–1490. <https://doi.org/10.1016/j.neuron.2015.05.037>
- 4567 Poppenk, J., Evensmoen, H. R., Moscovitch, M., & Nadel, L. (2013).
4568 Long-axis specialization of the human hippocampus. *Trends in
4569 Cognitive Sciences*, 17(5), 230–240.
4570 <https://doi.org/10.1016/j.tics.2013.03.005>
- 4571 Pudil, P., & Novovičová, J. (1998). Novel Methods for Feature Subset
4572 Selection with Respect to Problem Knowledge. In H. Liu & H.
4573 Motoda (Eds.), *Feature Extraction, Construction and Selection: A
4574 Data Mining Perspective* (pp. 101–116). Springer US.
4575 https://doi.org/10.1007/978-1-4615-5725-8_7
- 4576 Ranck, J. B. (1973). Studies on single neurons in dorsal hippocampal
4577 formation and septum in unrestrained rats: Part I. Behavioral
4578 correlates and firing repertoires. *Experimental Neurology*, 41(2),
4579 462–531. [https://doi.org/https://doi.org/10.1016/0014-4886\(73\)90290-2](https://doi.org/https://doi.org/10.1016/0014-4886(73)90290-2)
- 4580 Ranck, J. B. (1975). *Behavioral Correlates and Firing Repertoires of
4581 Neurons in the Dorsal Hippocampal Formation and Septum of
4582 Unrestrained Rats BT - The Hippocampus: Volume 2:
4583 Neurophysiology and Behavior* (R. L. Isaacson & K. H. Pribram,
4584 Eds.; pp. 207–244). Springer US. https://doi.org/10.1007/978-1-4684-2979-4_7
- 4585 Rao, R. P. N., & Ballard, D. H. (1999). Predictive coding in the visual
4586 cortex: a functional interpretation of some extra-classical
4587 receptive-field effects. *Nature Neuroscience*, 2(1), 79–87.
4588 <https://doi.org/10.1038/4580>
- 4589 Rescorla, R. A., & Wagner, A. (1972). A theory of Pavlovian
4590 conditioning: Variations in the effectiveness of reinforcement and
4591 nonreinforcement. In *Classical Conditioning II: Current Research
4592 and Theory: Vol. Vol. 2*.
- 4593 Reyes, A. D. (2003). Synchrony-dependent propagation of firing rate in
4594 iteratively constructed networks in vitro. *Nature Neuroscience*,
4595 6(6), 593–599. <https://doi.org/10.1038/nn1056>
- 4596 Robbins, M., Christensen, C. N., Kaminski, C. F., & Zlatic, M. (2021).
4597 Calcium imaging analysis - how far have we come?
4598 *F1000Research*, 10, 258.
- 4600

- 4601 Rochefort, N. L., Garaschuk, O., Milos, R.-I., Narushima, M., Marandi,
4602 N., Pichler, B., Kovalchuk, Y., & Konnerth, A. (2009).
4603 Sparsification of neuronal activity in the visual cortex at eye-
4604 opening. *Proceedings of the National Academy of Sciences of the*
4605 *United States of America*, 106(35), 15049–15054.
4606 <https://doi.org/10.1073/pnas.0907660106>
- 4607 Rogerson, T., Cai, D. J., Frank, A., Sano, Y., Shobe, J., Lopez-Aranda,
4608 M. F., & Silva, A. J. (2014). Synaptic tagging during memory
4609 allocation. *Nature Reviews Neuroscience*, 15(3), 157–169.
4610 <https://doi.org/10.1038/nrn3667>
- 4611 Savelli, F., Yoganarasimha, D., & Knierim, J. J. (2008). Influence of
4612 boundary removal on the spatial representations of the
4613 medial entorhinal cortex. *Hippocampus*, 18(12), 1270–1282.
4614 <https://doi.org/10.1002/hipo.20511>
- 4615 Schreurs, B. G. (1989). Classical conditioning of model systems: A
4616 behavioral review. *Psychobiology*, 17(2), 145–155.
4617 <https://doi.org/10.3758/BF03337830>
- 4618 Scoville, W. B., & Milner, B. (1957). Loss of recent memory after
4619 bilateral hippocampal lesions. In *Journal of Neurology,*
4620 *Neurosurgery & Psychiatry* (Vol. 20, pp. 11–21). BMJ Publishing
4621 Group. <https://doi.org/10.1136/jnnp.20.1.11>
- 4622 Shadlen, M. N., & Shohamy, D. (2016). Decision making and
4623 sequential sampling from memory. *Neuron*, 90(5), 927–939.
- 4624 Shannon, C. E. (1948). A Mathematical Theory of Communication. *Bell*
4625 *System Technical Journal*, 27(3), 379–423.
<https://doi.org/https://doi.org/10.1002/j.1538-7305.1948.tb01338.x>
- 4627 Siegel, J. J., & Mauk, M. D. (2013). Persistent Activity in Prefrontal
4628 Cortex during Trace Eyelid Conditioning: Dissociating Responses
4629 That Reflect Cerebellar Output from Those That Do Not. *The*
4630 *Journal of Neuroscience*, 33(38), 15272 LP – 15284.
4631 <https://doi.org/10.1523/JNEUROSCI.1238-13.2013>
- 4632 Siegel, J. J., Taylor, W., Gray, R., Kalmbach, B., Zemelman, B. V.,
4633 Desai, N. S., Johnston, D., & Chitwood, R. A. (2015). Trace
4634 Eyeblink Conditioning in Mice Is Dependent upon the Dorsal
4635 Medial Prefrontal Cortex, Cerebellum, and Amygdala: Behavioral
4636 Characterization and Functional Circuitry. *ENeuro*, 2(4),
4637 ENEURO.0051-14.2015. <https://doi.org/10.1523/ENEURO.0051-14.2015>
- 4639 Silva, A. J., Zhou, Y., Rogerson, T., Shobe, J., & Balaji, J. (2009).
4640 Molecular and cellular approaches to memory allocation in neural
4641 circuits. *Science (New York, N.Y.)*, 326(5951), 391–395.
4642 <https://doi.org/10.1126/science.1174519>
- 4643 Skaggs, W., McNaughton, B., Gothard, K., & Markus, E. (1996). An

- 4644 Information-Theoretic Approach to Deciphering the Hippocampal
4645 Code. *Neural Inf. Process Syst.*, 5.
- 4646 Sofroniew, N. J., Flickinger, D., King, J., & Svoboda, K. (2016). A large
4647 field of view two-photon mesoscope with subcellular resolution for
4648 in vivo imaging. *eLife*, 5(JUN2016), 1–20.
4649 <https://doi.org/10.7554/eLife.14472>
- 4650 Solstad, T., Boccara, C. N., Kropff, E., Moser, M.-B., & Moser, E. I.
4651 (2008). Representation of Geometric Borders in the Entorhinal
4652 Cortex. *Science*, 322(5909), 1865–1868.
4653 <https://doi.org/10.1126/science.1166466>
- 4654 Souza, B. C., Pavão, R., Belchior, H., & Tort, A. B. L. (2018). On
4655 Information Metrics for Spatial Coding. *Neuroscience*, 375, 62–73.
4656 <https://doi.org/10.1016/j.neuroscience.2018.01.066>
- 4657 Stosiek, C., Garaschuk, O., Holthoff, K., & Konnerth, A. (2003). In vivo
4658 two-photon calcium imaging of neuronal networks. *Proceedings of
4659 the National Academy of Sciences of the United States of
4660 America*, 100(12), 7319–7324.
4661 <https://doi.org/10.1073/pnas.1232232100>
- 4662 Suh, J., Rivest, A. J., Nakashiba, T., Tominaga, T., & Tonegawa, S.
4663 (2011). Entorhinal cortex layer III input to the hippocampus is
4664 crucial for temporal association memory. *Science (New York,
4665 N.Y.)*, 334(6061), 1415–1420.
4666 <https://doi.org/10.1126/science.1210125>
- 4667 Takehara, K., Kawahara, S., Takatsuki, K., & Kirino, Y. (2002). Time-
4668 limited role of the hippocampus in the memory for trace eyeblink
4669 conditioning in mice. *Brain Research*, 951(2), 183–190.
4670 [https://doi.org/10.1016/s0006-8993\(02\)03159-1](https://doi.org/10.1016/s0006-8993(02)03159-1)
- 4671 Tao, S., Wang, Y., Peng, J., Zhao, Y., He, X., Yu, X., Liu, Q., Jin, S., &
4672 Xu, F. (2021). Whole-Brain Mapping the Direct Inputs of Dorsal
4673 and Ventral CA1 Projection Neurons. *Frontiers in Neural Circuits*,
4674 15. <https://doi.org/10.3389/fncir.2021.643230>
- 4675 Taube, J. S., Muller, R. U., & Ranck, J. B. J. (1990). Head-direction
4676 cells recorded from the postsubiculum in freely moving rats.
4677 I. Description and quantitative analysis. *The Journal of
4678 Neuroscience : The Official Journal of the Society
4679 for Neuroscience*, 10(2), 420–435.
4680 <https://doi.org/10.1523/JNEUROSCI.10-02-00420.1990>
- 4681 Thompson, R. F. (2004). In Search of Memory Traces. *Annual Review
4682 of Psychology*, 56(1), 1–23.
4683 <https://doi.org/10.1146/annurev.psych.56.091103.070239>
- 4684 Tishby, N., Pereira, F. C., & Bialek, W. (1999). The information
4685 bottleneck method. *Proc. of the 37-Th Annual Allerton Conference
4686 on Communication, Control and Computing*, 368–377.

- 4687 <https://arxiv.org/abs/physics/0004057>
- 4688 Tseng, W., Guan, R., Disterhoft, J. F., & Weiss, C. (2004). Trace
4689 eyeblink conditioning is hippocampally dependent in mice.
4690 *Hippocampus*, 14(1), 58–65. <https://doi.org/10.1002/hipo.10157>
- 4691 Uncapher, M. R., Hutchinson, J. B., & Wagner, A. D. (2011).
4692 Dissociable effects of top-down and bottom-up attention during
4693 episodic encoding. *The Journal of Neuroscience : The Official
4694 Journal of the Society for Neuroscience*, 31(35), 12613–12628.
4695 <https://doi.org/10.1523/JNEUROSCI.0152-11.2011>
- 4696 Vaidya, A. R., Pujara, M. S., Petrides, M., Murray, E. A., & Fellows, L.
4697 K. (2019). Lesion Studies in Contemporary Neuroscience. *Trends
4698 in Cognitive Sciences*, 23(8), 653–671.
4699 <https://doi.org/https://doi.org/10.1016/j.tics.2019.05.009>
- 4700 Valero, M., Cid, E., Averkin, R. G., Aguilar, J., Sanchez-Aguilera, A.,
4701 Viney, T. J., Gomez-Dominguez, D., Bellistri, E., & de la Prida, L.
4702 M. (2015). Determinants of different deep and superficial CA1
4703 pyramidal cell dynamics during sharp-wave ripples. *Nature
4704 Neuroscience*. <https://doi.org/10.1038/nn.4074>
- 4705 van der Maaten, L., Postma, E., & van den Herik, H. (2009).
4706 Dimensionality reduction: a comparative review. *Journal of
4707 Machine Learning Research*, 66–71.
- 4708 Velasco, M. G. M., & Levene, M. J. (2014). In vivo two-photon
4709 microscopy of the hippocampus using glass plugs. *Biomedical
4710 Optics Express*, 5(6), 1700–1708.
4711 <https://doi.org/10.1364/BOE.5.001700>
- 4712 Vinogradova, O. S. (2001). Hippocampus as comparator: Role of the
4713 two input and two output systems of the hippocampus in selection
4714 and registration of information. *Hippocampus*, 11(5), 578–598.
4715 <https://doi.org/https://doi.org/10.1002/hipo.1073>
- 4716 Voelcker, B., Pancholi, R., & Peron, S. (2022). Transformation of
4717 primary sensory cortical representations from layer 4 to layer 2.
4718 *Nature Communications*, 13(1), 5484.
4719 <https://doi.org/10.1038/s41467-022-33249-1>
- 4720 Wood, E. R., Dudchenko, P. A., Robitsek, R. J., & Eichenbaum, H.
4721 (2000). Hippocampal Neurons Encode Information about Different
4722 Types of Memory Episodes Occurring in the Same Location.
4723 *Neuron*, 27(3), 623–633.
4724 [https://doi.org/https://doi.org/10.1016/S0896-6273\(00\)00071-4](https://doi.org/https://doi.org/10.1016/S0896-6273(00)00071-4)
- 4725 Yiu, A. P., Mercaldo, V., Yan, C., Richards, B., Rashid, A. J., Hsiang,
4726 H.-L. L., Pressey, J., Mahadevan, V., Tran, M. M., Kushner, S. A.,
4727 Woodin, M. A., Frankland, P. W., & Josselyn, S. A. (2014).
4728 Neurons are recruited to a memory trace based on relative
4729 neuronal excitability immediately before training. *Neuron*, 83(3),

- 4730 722–735. <https://doi.org/10.1016/j.neuron.2014.07.017>
- 4731 Zhang, S., & Manahan-Vaughan, D. (2015). Spatial olfactory learning
4732 contributes to place field formation in the hippocampus. *Cerebral
4733 Cortex (New York, N.Y.: 1991)*, 25(2), 423–432.
4734 <https://doi.org/10.1093/cercor/bht239>
- 4735 Zhou, S., Masmanidis, S. C., & Buonomano, D. V. (2020). Neural
4736 Sequences as an Optimal Dynamical Regime for the Readout of
4737 Time. *Neuron*, 108(4), 651-658.e5.
4738 <https://doi.org/https://doi.org/10.1016/j.neuron.2020.08.020>
- 4739 Zhou, Y., Won, J., Karlsson, M. G., Zhou, M., Rogerson, T., Balaji, J.,
4740 Neve, R., Poirazi, P., & Silva, A. J. (2009). CREB regulates
4741 excitability and the allocation of memory to subsets of neurons
4742 in the amygdala. *Nature Neuroscience*, 12(11), 1438–1443.
4743 <https://doi.org/10.1038/nn.2405>
- 4744 Ziv, Y., Burns, L. D., Cocker, E. D., Hamel, E. O., Ghosh, K. K., Kitch,
4745 L. J., El Gamal, A., & Schnitzer, M. J. (2013). Long-term dynamics
4746 of CA1 hippocampal place codes. *Nature Neuroscience*, 16(3),
4747 264–266. <https://doi.org/10.1038/nn.3329>
- 4748